Serotonin Signaling in the Neural Development and Function of the Lower Urinary Tract

By

Karen Elaine Ritter

Dissertation
Submitted to the Faculty of the
Graduate School of Vanderbilt University
in partial fulfillment of the requirements
for the degree of

DOCTOR OF PHILOSOPHY
in

Neuroscience
January 31, 2018
Nashville, Tennessee

Approved:

E. Michelle Southard-Smith, Ph.D.

Rebecca A. Ihrie, Ph.D.

Randy R. Blakely, Ph.D.

Roger R. Dmochowski, M.D.

To my parents, David and Jill Ritter, who fostered my love of science

To Jonathan, always my boo

ACKNOWLEDGEMENTS

First, I must acknowledge that I have been fortunate to have had abundant funding to pursue my research goals and have tuition/stipend support for my time at Vanderbilt. My work was supported by the following grants from the National Institutes of Health: U01 DK101038, R56 DK078158, R01 DK078158, and U01 DK110804, P50 MH096972 (Vanderbilt Conte Center Pilot Grant), awarded to Michelle Southard-Smith, and F31 DK097938 awarded to myself.

My list of people to acknowledge is very long – I have been extraordinarily #blessed by many wonderful, helpful people over the course of my education. My undergraduate research advisor, Dr. David M. Gilbert, treated me like one of his own PhD students and let me design my own research project, instead of having me fill tip boxes and doing other mundane lab chores. He helped me figure out that my heart was really in research and was incredibly supportive through the entire graduate school application process, and even later on in my NRSA F31 fellowship application. The people I worked with in his lab, Kristina Poduch and Elaine Haddock, taught me so much and showed me how important perseverance is in research.

One of the main reasons I came to Vanderbilt was the collaborative and supportive environment, particularly for the developmental biology community. With the critical scientific discussions in weekly journal club, the helpful and honest trouble-shooting dbRIC sessions with fellow graduate students, and of course the riotously fun annual retreats, the Program in Developmental Biology has been one of my favorite and most valuable parts of my graduate education. I especially want to thank Dr. Chris Wright for his visionary leadership of PDB and for always providing thoughtful feedback on my science.

The neuroscience community at Vanderbilt has been immensely supportive of my graduate education and training. Dr. Mark Wallace was always an approachable director (and still is as the Dean of the graduate school), and Dr. Ron Emeson has gone above and beyond the call of duty in his role of interim director. Ron has always been invested in the support and success of trainees – his devoted mentorship means more than he knows. Dr. Doug McMahon and Dr. Bruce Carter have served as the neuroscience Director of Graduate Studies in my time at Vanderbilt. I thank them both for their dedication to graduate education, particularly Dr. Carter for always providing insightful feedback on my work. I also want to thank the administrative staff of the VBI, particularly Roz Johnson and Beth Sims, who always manage to get everything taken care of with a cheery disposition. Interacting with Roz and Beth always seems to put me in a better mood, no matter what kind of day I've had.

I owe much of my professional development to the BRET office at Vanderbilt. The staff of the Office of Career Development work tirelessly to create new opportunities for trainees of all career stages to learn more about future jobs and foster the development of skills that go beyond the bench. I especially want to acknowledge the Vanderbilt BRET Editors' Club – not only for all the writing and editing experience I gained, but also the friendships as well.

My research has benefitted greatly from several extramural collaborations. I was fortunate to have the opportunity to learn how to conduct retrograde tracing surgery in the laboratory of Dr. Janet Keast at the University of Melbourne, Australia. A postdoctoral fellow in her lab, Adam Wallace, provided incredibly thorough training and was kind enough to host me in his own home for part of my stay. Other members of the Keast lab and Heather Young's lab, including Sophie Payne, Agnes Wong, and Lincon Stamp, showed me a wonderful time in Melbourne and made me feel a sense of belonging in the autonomic neuroscience community. I

have the highest respect for Dr. Keast, not only as a leader in her field and supplier of seemingly endless knowledge, but as a role model for women in science. I hope that I will have the chance to cross paths with her again in the future. My project also benefitted greatly from the opportunity to collaborate with Dr. Chad Vezina and Dr. Dale Bjorling at the University of Wisconsin, Madison, for the anesthetized cystometry experiments. These studies were conducted by a research fellow, Dr. Zunyi Wang, and I am grateful for his care and expertise in conducting these procedures. Chad and Dale have always been pleasant to work with and provided so much valuable feedback on many other aspects of my work, not just cystometry. I look forward to staying in touch with them and hope our paths cross frequently.

The completion of my dissertation would not have been possible without the incredible research facilities available at Vanderbilt. My many, many, MANY, ***MANY*** hours of imaging were conducted in the Vanderbilt Cell Imaging Shared Resource. I thank Dr. Bob Matthews, Dr. Jenny Schafer, and the late Carol Ann Bonner for their careful instruction and helpful troubleshooting. I thank the staff of the Vanderbilt Division of Animal Care for their superior level of care for all of our animals used in research. The technicians who took care of my mice, Jenny Taylor, Mollie Lynn Pilkinton, and Caroline Spencer, were especially accommodating of my unusual void spot assay experiments. Despite the difficult and tedious nature of their jobs, they always went above and beyond to make sure I had everything I needed. Their kindness and devotion to our animals are not lost on me.

I am thankful for my wonderfully supportive thesis committee. Dr. Roger Dmochowski has always been so approachable and his urological expertise has greatly benefitted my project. I thank him for taking the time out of his incredibly busy schedule to advise me in my research endeavors. I thank Dr. Randy Blakely for his willingness to serve as my committee chair, and

his continued support on my committee after his move to FAU. I cannot thank him enough for co-sponsoring my NRSA F31 fellowship and welcoming me into his "SERT Squad" lab meetings. Being the first person in the Southard-Smith lab to study serotonin biology, those meetings were critical for helping me get my project off the ground. I thank Dr. Rebecca Ihrie for stepping in as the chair of my committee and all of her guidance. I can always count on Rebecca to ask thoughtful questions and help me think about my project from different angles. I am grateful for all her guidance not just in my project, but also for my career development. Her dedication to trainees is apparent in all she does for me, her own students, and for the PDB. I hope that we will get to cross paths frequently in the future.

I have many previous and current Southard-Smith lab members to thank. Honestly, I feel like I could write an additional 190 pages about how much I love my co-workers, many of whom I have come to cherish as some of my best friends. Tsering Stobdan and Nicole Fleming were in the lab when I rotated way back in 2010. I regret that our time in the MS^2 lab didn't overlap more, but I appreciate the help and training they provided. Noah Lawler, Carrie Wiese (soon to be Dr. Wiese!), and Jean-Marc Dekeyser (a.k.a. Jean-Fart DerpKeyser) were research assistants whose company I enjoyed immensely. I could always count on Noah for a good break in between experiments, particularly in our quest to find New and Interesting Snacks at the various gift shops around the medical center. I thank Carrie for her patience when I first joined the lab – I bombarded her relentlessly with questions (mostly rooted in my own feelings of insecurity) and she taught me how to "Suck it up and make it work." I can't thank her enough for teaching me that it's ok to make mistakes at the bench, as long as you learn something from them. I'm so proud of her hard work in graduate school and wish her the best of luck in her future endeavors – she has enough skill that she doesn't need much luck. As for JMDK, where do I even start?

When it felt like my life was falling apart (in some ways, it was), Jean-Marc gave me friendship and humor when I needed it the most. He and his wife, Stephanie, welcomed me to their home on weekends for goofy movie and pizza nights and helped me forget about all my problems for a few hours. He even helped me move my apartment – several times! A washer and dryer down the steepest flight of stairs I have ever seen! People like him are exceptionally rare and I hope he knows how much his friendship means to me.

Meena "Meatball" Halaka and Jessica "Muball" Do are two previous research assistants who only very recently departed the MS^2 lab. If everybody worked as hard as Meatball, we would probably have a cure for cancer by now. I thank Meatball for his helpful attitude and always going above and beyond to help everyone else in lab, no matter how much it might have inconvenienced himself. I love his sense of humor and will miss our "Relationship Roundups" immensely. I wish him the best of luck in all his future endeavors and hope that the next chapter of his life will provide him satisfaction and a sense of purpose. I'm going to be honest here and say I'm angry that Muball left the lab before my defense, but I'm so proud of her and how hard she's worked to get to this point in her life. She's going to be an amazing doctor and she's the sort of person that makes her dream a reality, no matter what the dream is. When Muss graduated and left the lab (more on Muss below), I wasn't sure I would ever have as close a friend in lab again…and then Muball showed up and became my honorary "Bay Two Bae." After a particular instance of luminal stasis, it was like the heavens parted and declared that we would become #besties. I can't count how many times we have laughed so hard, to the point of literally crying in laughter, and I hope she knows how grateful I am for her and our friendship.

Double-Dr. Melissa "Muss" Musser, a previous MSTP student in the MS^2 lab, is my original Bay Two Bae and one of my best friends in the whole world. I don't think I could ever

express accurately in writing how important her friendship is to me. Muss is the sort of person who is impossible to not love – she goes out of her way to help everyone and anyone, and even when life feels like it couldn't possibly get worse, she finds a way to look on the bright side anyway. We spent so many late nights and weekends in Bay Two together, and to be honest I'm not sure I would have survived some parts of grad school without Muss. Even though we don't get to see each other in person as much anymore, I love how when we do we just pick right back up where we left off. I'm so proud of her and the amazing physician scientist she has become, and I know that no matter where our careers take us we will be lifelong friends.

I have many current members of the Southard-Smith lab to thank! Jenna Brown is our newest addition and I wish she had joined sooner. She's one of the sweetest people and has already brought so much sunshine to lab. The same goes for our new graduate student, Justin Avila – I know he's going to have tons of success in graduate school and I hope our paths will cross again in the future. Dr. Aaron "Ay-Ay-Ron" May-Zhang is an incredibly talented postdoc that I know will be an A-May-Zhang PI in the future. His ability to keep a light-hearted demeanor while working his butt off is an inspiration for how I should work in my own postdoctoral fellowship. I thank Dr. Karen Deal for all her support that she has given me, in matters of lab and life. She is the fountain of knowledge, expertise, incredible stories, and humor I need to get through frustrating days. I didn't realize how much we needed a "Lab Mom" until Karen arrived, and I'm so thankful that she did. I want to thank our previous and current undergraduate students: Katherine Taylor Jones, Makenzie Beaman, Victoria Mityul, and Anoop Chandrashekar. The Southard-Smith lab has been incredibly fortunate to have such talented students and I know they'll go on to be amazing in any career path they follow. I want to give an extra special shout-out to Makenzie, who has become a dear friend and Bay Two Bae. She is

one of the smartest students I've ever known and I admire her ability to juggle lab with all her other obligations. I can't wait to see where her career takes her and hope we can stay friends, even when she's busy in her MSTP program.

My final MS^2 lab member to thank is the extraordinarily talented research assistant, Dennis Buehler. As a true Pee Group Original Gangster, he and I have worked on many projects together over the years. Dennis taught me nearly everything I know – how to handle mice, doing dissections, cell culture, IHC, microscopy, etc. He has a natural gift for teaching and always paid careful attention to what I was doing so he could provide feedback and help me improve. I think he might also be some type of sorcerer, because if anything in lab doesn't want to cooperate all Dennis has to do is *press a single button* and it magically works again. I look up to Dennis for all his countless hours of work and the attention to detail he devotes to everything he does. I wouldn't be the scientist I am today without him.

My adviser, Dr. Michelle Southard-Smith, is an amazing mentor and my list of things to thank her for could go on for pages. Michelle is exceptionally well-connected and has introduced me to so many colleagues and allowed me to attend multiple conferences and workshops to broaden my professional skills. I thank her for including me in other opportunities that many graduate students don't get to experience, such as reviewing multiple manuscripts, crafting grant proposals, and mentoring undergraduate students. I am grateful for how she let me start a brand new project in a subject no one in her lab had delved into before – even though this meant that my dissertation took longer to complete than most, I am grateful for her patience and continued mentorship through the whole process. Even more than all of those things, I am grateful for how our relationship has morphed into a wonderful friendship. I will miss our coffee

breaks and laughing about life together. I thank her for all the ways she has cared for me, not just as her student but as a fellow sister in Christ.

I have many non-lab friends to thank. Several of my IGP classmates have become some of my dearest friends and I'm thankful that I got to go through grad school with them. I thank Kate "Dr. Kittendorf" Mittendorf for being an amazing inspiration for how to keep your chin up, even when life sucks, and I admire her ability to find humor in pretty much everything. Lizzie Ferrick-Kiddie was my roommate for nearly two years, and in that time we both experienced major life events that would have been much harder to face without each other. Lizzie has more optimism than anyone I have ever known, and I hope she never loses it. I am especially grateful to Michelle Krakowiak, because she recognized the deep spiritual trench I was in and (almost literally) dragged me to church with her. She has been one of my strongest spiritual pillars and will forever be one of my most cherished friends. The church she brought me to, Midtown Fellowship, has also been a great source of support for me. The friends I've made there have helped me remember that the most important things in life aren't in the lab, and that God lets bad things happen for good reasons.

I have the best family and I can't express how much they mean to me. I thank my siblings, Paul Ritter, Chris & Linda DeBroeck, Ivy & Bert Carter, Michael & Louise Ritter, and Cindy & Doug Moffett for always being supportive of me. I especially thank my parents, David and Jill Ritter, who have never doubted for second that I could do whatever I set my mind to. They fostered my love of science from a very young age and sacrificed so much to make sure I had the best possible education I could get. There aren't enough words to describe my gratitude for their love and support. Mom, thank you for loving me unconditionally. Dad, I am proud to be your daughter and the next Dr. Ritter.

I also have the best family by marriage. I thank David and Renae Harrison, Jennifer and Russell Sturgeon, and Nita and Chris Hill for welcoming me into their family and always understanding when I have to say "I can't, I have lab." I will be forever grateful to them for raising Jonathan to be the man he is today.

And that finally brings me to my last acknowledgement, Jonathan "Boo" Harrison. Even when I felt unlovable, he looked past all my problems and gave me a chance. I have done nothing to deserve his sacrificial, selfless love and I don't understand how I got so lucky to have him as my husband. Through all the long days and late nights in lab, countless weekends and everything else, I am eternally grateful that I got to come home to my favorite person in the whole world. Where ever life may lead, at least I will always have my boo.

TABLE OF CONTENTS

Page

DEDICATION iii

ACKNOWLEDGEMENTS iv

LIST OF TABLES xvii

LIST OF FIGURES xix

LIST OF ABBREVIATIONS xxii

Chapter

I. Introduction 1

Anatomy of lower urinary tract innervation 1
Development of lower urinary tract innervation 5
Rationale and importance 5
Origins from the neural crest 7
Dorsal root ganglia 9
Pelvic ganglia and bladder intramural ganglia 10
Summary 12
References 14

II. Effects of Targeting Serotonin Receptors in Sacral Neural Crest Progenitors 18

Introduction 18
Materials and Methods 20
Isolation of mRNA from fetal mouse lower urinary tract 20
Immunohistochemistry 20
Microarray hybridizations and data analysis 21
Reverse Transcription Polymerase Chain Reaction (RT-PCR) 22
Assessment of developmental potential in cultures of sacral neural crest 23
Pelvic ganglia explant cultures 24
Sholl analysis 25
Statistical analysis 26
Results 26
Population of pelvic ganglia anlagen by *Sox10+* sacral neural crest precursors 26
Identification of serotonin receptors up-regulated in differentiating pelvic ganglia 27
Multiple serotonin receptors are expressed in sacral neural crest and differentiating lower urinary tract neurons 29
Perturbing serotonin receptor signaling alters differentiation outcomes of *Sox10+*

sacral neural crest progenitors *in vitro* 31
Over-stimulating 5-HT3A in pelvic ganglia explants attenuates neurite outgrowth *in vitro* .33
Discussion 34
Acknowledgements 38
References 38

III. Dynamic Expression of Serotonin Receptor 5-HT3A in Developing Sensory Innervation of the Lower Urinary Tract 42

Introduction 42
Materials and Methods 44
Animals 44
Tissue dissection 44
Immunohistochemistry staining 45
Retrograde tracing surgery 47
Cell counting 48
Data analysis 48
Results 49
Htr3a-EGFP is expressed early in sensory nervous system development 49
Htr3a-EGFP co-localizes with neuropeptides CGRP and Substance P in a subset of DRG neurons 51
The majority of TRPV1+ neurons co-express *Htr3a*-EGFP 55
Htr3a-EGFP does not co-localize with TRPV4 57
Htr3a-EGFP is expressed in a subset of myelinated sensory neurons 57
Htr3a-EGFP is expressed in the majority of bladder-innervating afferent neurons 60
Discussion 65
Acknowledgements 69
References 70

IV. Serotonin receptor 5-HT3A Affects Development of Bladder Innervation and Urinary Bladder Function 75

Introduction 75
Materials and Methods 77
Animals 77
Tissue collection 78
Immunohistochemistry 78
Spontaneous void spot assay 80
Anesthetized bladder cystometry 82
Analysis of bladder innervation density 83
Statistical analysis 84
Results 85
Serotonin receptor 5-HT3A is expressed in mouse fetal and adult major pelvic ganglia 85
Htr3a-/- males, but not females, exhibit increased urinary voiding frequency 85
Male *Htr3a-/-* bladder contractility is impaired 89
Loss of 5-HT3A disrupts autonomic neuronal marker expression patterns in fetal pelvic

ganglia 93
Htr3a mutant bladder detrusor is more densely innervated compared to wildtype 96
Discussion 104
Acknowledgements 110
References 111

V. Summary and Future Directions 115

Roles for serotonin receptors in developing pelvic ganglia and bladder function 115
Downstream effectors of 5-HT3A mediating neural development 117
Htr3a lineage analysis 121
Clinical implications of perturbing 5-HT3A in development 124
Roles for *Htr3a* in bladder inflammation and interstitial cystitis 126
Conclusions 127
References 127

VI. Extended Methods and Short Studies 132

Animals 132
Genotyping 132
Embryo collection and processing 134
Dorsal root ganglia collection, processing, and analysis 135
P2 dorsal root ganglia collection and processing 135
Adult dorsal root ganglia collection and processing 136
Immunohistochemistry on dorsal root ganglia cryo-sections 138
Confocal imaging 141
Cell counting 142
Pelvic ganglia collection, processing, and analysis 143
Immunohistochemistry on fetal cryo-sections 143
Adult pelvic ganglia collection and processing 146
Immunohistochemistry on adult pelvic ganglia cryo-sections 147
Immunohistochemistry on whole mount postnatal and adult pelvic ganglia 149
Retrograde tracing surgery 150
Preparing tools and equipment for surgery 151
Preoperative preparation of animals for surgery 158
Performing surgery: abdominal incisions and exposing the bladder 159
Performing surgery: injecting Fast Blue retrograde tracing dye 160
Suturing muscle and skin 161
Recovery from anesthesia and post-operative monitoring 163
Hematoxylin & Eosin staining of fetal tissue and adult bladder 164
Paraffin embedding and microtome sectioning 164
Hematoxylin & Eosin staining 166
Immunohistochemistry on adult bladder via DAB colorimetric staining 168
Transcardial perfusion 168
Flat-mount fixation of whole adult bladder 169
Immunohistochemistry via DAB staining 171

Spontaneous void spot assay 175
Experimental design 175
Preparing the animals 177
Preparing filter paper 177
Preparing assay cages 178
Conducting the assay 180
Visualizing urine by Ninhydrin staining 181
Quantification of voiding frequency 182
Analysis of urine specific gravity in *Htr3a* mutant mice 183
Analysis of *Htr3a*-EGFP; *Htr3a*-KO phenotypes 186
Characterization of *Htr3a*-Cre reporter mouse line 189
References 192

LIST OF TABLES

Table Page

2.1 Primary antibodies used in immunohistochemistry experiments 21

2.2 Secondary antibodies used in immunohistochemistry experiments 21

2.3 Primers used to detect serotonin receptor expression in reverse-transcription PCR experiments 23

2.4 Effects of serotonergic drugs on sacral neural crest developmental potential.....32

3.1 Primary antibodies used in immunohistochemistry experiments 46

3.2 Secondary antibodies used in immunohistochemistry experiments 46

3.3 Proportions of total neurons (Hu+) expressing *Htr3a*-EGFP and projecting to the bladder (Fast Blue+) 62

3.4 Proportions of bladder-projecting (Fast Blue+) neuronal subtypes in lumbar (L1, L2) and sacral (L6, S1) axial levels.....62

4.1 Primary antibodies used in immunohistochemistry experiments 80

4.2 Secondary antibodies used in immunohistochemistry experiments 80

4.3 Summary of anesthetized bladder cystometry measurements 91

4.4 Measurements of 18.5 dpc bladder smooth muscle innervation density 97

4.5 Measurements of adult bladder smooth muscle innervation density.....101

6.1 Primers and PCR buffers used for mouse genotyping.....133

6.2 Primary antibodies used in analysis of dorsal root ganglia neuronal subtypes.....140

6.3 Secondary antibodies used to detect primary antibodies in DRG immunohistochemistry....141

6.4 Primary antibodies used in the analysis of fetal pelvic ganglia neuronal subtypes.....145

6.5 Secondary antibodies used in fetal pelvic ganglia immunohistochemistry 145

6.6 Tools and equipment required for retrograde tracing surgery 152

6.7 Disposable items required for retrograde tracing surgery.....153

6.8 Strategy for tying musculature and skin sutures 163

6.9 Recipes for phosphate buffer solutions used in colorimetric DAB staining.....171

6.10 Summary of urine specific gravity in *Htr3a*-KO adult mice 184

LIST OF FIGURES

Figure Page

1.1 Anatomy of lower urinary tract autonomic and sensory innervation 2

1.2 Neural crest segmentation.....8

1.3 Dorsal root ganglia development.....10

1.4 Migration of *Sox10*+ neural crest cells into the lower urinary tract 11

2.1 Distribution of *Sox10*-H2BVenus+ neural crest-derived progenitors and neurons in developing pelvic ganglia 28

2.2 Expression of serotonin receptor genes in neural crest-derived progenitors and pelvic ganglia neuronal precursors.....30

2.3 Pharmacologically perturbing serotonin signaling alters differentiation outcomes of sacral neural crest progenitors *in vitro* 33

2.4 Over-stimulating 5-HT3 in cultured fetal pelvic ganglia explants diminishes neurite arbor complexity.....35

3.1 *Htr3a*-EGFP is expressed early in fetal development of sensory neurons 50

3.2 *Htr3a*-EGFP and Calcitonin Gene Related Peptide (CGRP) are co-expressed in a subset of neurons through development and adulthood.....52

3.3 Some, but not all, *Htr3a*-EGFP neurons express Substance P neuropeptide.....54

3.4 The majority of adult TRPV1+ neurons also express *Htr3a*-EGFP 56

3.5 *Htr3a*-EGFP does not co-localize with TRPV4 in lumbosacral DRG 58

3.6 A subset of *Htr3a*-EGFP neurons express Neurofilament 200.....59

3.7 L1, L2 and L6, S1 axial levels harbor bladder-projecting neurons 61

3.8 Distinct expression patterns of 5-HT3A in subclasses of bladder-projecting neurons.....63

3.9 Summary of developmental expression patterns in lumbosacral *Htr3a*-EGFP+ dorsal root ganglia neurons.....65

4.1 Serotonin receptor *Htr3a* is expressed in many neurons within fetal and adult major pelvic ganglia....86

4.2 Male *Htr3a-/-* mice, but not females, exhibit increased urinary voiding frequency in a spontaneous void spot assay....88

4.3 Male, but not female, *Htr3a-/-* mice demonstrate decreased bladder voiding efficiency compared to wild type mice....92

4.4 Loss of serotonin receptor *Htr3a* increases expression of tyrosine hydroxylase in fetal pelvic ganglia....94

4.5 Autonomic marker expression patterns are normal in adult *Htr3a* mutant pelvic ganglia....95

4.6 Loss of serotonin receptor *Htr3a* leads to increased density of autonomic innervation in late fetal bladder smooth muscle....98

4.7 Loss of serotonin receptor *Htr3a* lead to increased density of both autonomic and sensory innervation in adult bladder smooth muscle....102

5.1 Mechanisms of calcium signaling in neuronal development....119

6.1 Dissection strategy for removal of DRG from animals age P14 and older....137

6.2 Wash buckets used for DRG processing....138

6.3 Strategy for embedding DRG and alternating DRG cryo-sections on slides....139

6.4 Embedding fetal sample in cryo-mold for optimal PG sectioning....143

6.5 Tools and equipment for retrograde tracing surgery....156

6.6 Assembly of Hamilton syringe and 33GA removable needle....157

6.7 Disinfection of lower abdominal skin prior to surgery....159

6.8 Lower abdominal incisions in retrograde tracing surgery....160

6.9 Injection of retrograde tracer into bladder....161

6.10 Suturing musculature and skin in retrograde tracing surgery....162

6.11 Hematoxylin & Eosin staining of wild type fetal and adult mouse bladder....168

6.12 Flat-mount fixation of whole adult urinary bladder....170

6.13 Immunohistochemistry via DAB colorimetric staining in adult bladder.....174

6.14 Template for cutting sheets of filter paper for void spot assays 178

6.15 Preparation and analysis of void spot assays 179

6.16 Assessment of urine specific gravity in *Htr3a* mutant adult mice.....185

6.17 Breeding strategy for *Htr3a*-EGFP; *Htr3a*-KO animals.....186

6.18 Representative 10.5 dpc embryos from *Htr3a*-EGFP; *Htr3a*-KO crosses 187

6.19 Autonomic neuronal subtype proportions in 14.5dpc *Htr3a*-EGFP; *Htr3a*-KO mice.....188

6.20 Distribution of *Htr3a*-Cre;Rosa-tdTomato lineages in postnatal mice.....190

6.21 Distribution of *Htr3a*+ cells in the bladder.....191

LIST OF ABBREVIATIONS

3-APES	3-aminopropyltriethoxysilane treated slides
5-HT	5-hydroxytryptamine (serotonin)
5-HTR	5-hydroxytryptamine receptor
ANOVA	analysis of variance statistical test
ASD	Autism Spectrum Disorder
BAC	bacterial artificial chromosome
bp	base pair(s)
BSA	bovine serum albumin
C57BL/6J	C57BL/6J mouse strain
Ca^{2+}	calcium
Cat#	catalog number
cDNA	copied deoxyribonucleic acid
CGRP	calcitonin gene related peptide
ChAT	choline acetyltransferase
CISR	Cell Imaging Shared Resource at Vanderbilt University
CNS	central nervous system
Cre	Cre recombinase
DAB	3,3’-diaminobenzidine
DMEM	Dulbecco’s Modified Eagle Medium
DNA	deoxyribonucleic acid
dNTPs	deoxynucleotide triphosphates

dpc	days post coitus
DRG	dorsal root ganglion/ganglia
E	embryonic day (age)
EDTA	ethylenediaminetetraacetic acid
EGFP	enhanced/emerald green fluorescent protein
ENS	enteric nervous system
EtOH	ethanol
F-actin	filamentous actin
FACS	fluorescence-activated cell sorting
FB	Fast Blue retrograde tracing fluorescent dye
GFAP	Glial Fibrillary Acidic Protein
h	hour(s)
H&E	hematoxylin & eosin staining
HSD	Honest Significant Difference (Tukey's *post-hoc* statistical test)
HT	heterozygous
Htr2a/5-HT2A	serotonin receptor type 2A
Htr3a/5-HT3A	serotonin receptor type 3A
Htr3a-Cre	Tg(*Htr3a*-Cre)NO152Gsat transgenic mouse line
Htr3a-EGFP	Tg(*Htr3a*-EGFP)DH30Gsat transgenic mouse line
*Htr3a*KO/*Htr3a-/-*	B6.129x1-*Htr3a*^{tm1Jul}/J mouse line
Htr3b/5-HT3B	serotonin receptor type 3B
Hu C/D	ELAV (Embryonic lethal, abnormal vision, Drosophila)-like protein 4
IACUC	Institutional Animal Care and Use Committee

IC	interstitial cystitis
IHC	immunohistochemistry
KO	knockout
L1, L2	spinal column axial levels lumbar-1 and lumbar-2
L3-L5	spinal column axial levels encompassing lumbar-3, lumbar-4, and lumbar-5
L6, S1	spinal column axial levels lumbar-6 and sacral-1
LUT	lower urinary tract
LUTS	lower urinary tract symptoms
min	minute(s)
mRNA	messenger RNA (ribonucleic acid)
NBF	neutral buffered formalin
NC	neural crest
NCPCs	neural crest progenitor cells
NDS	normal donkey serum
NF200	neurofilament 200
NGF	nerve growth factor
NIH	National Institutes of Health
O/N	overnight
P	postnatal day (age)
PB	phosphate buffer
PBS	phosphate buffered saline
PCR	polymerase chain reaction
PFA	paraformaldehyde

PG	pelvic ganglion/ganglia
PNS	peripheral nervous system
Prph	peripherin
RNA	ribonucleic acid
Rosa-tdTomato	B6.Cg-*Gt(ROSA)26Sor*$^{tm9(CAG\text{-}tdTomato)Hze}$/J transgenic mouse line
RRID	Research Resource Identifier
RT	room temperature
SDS	sodium dodecyl sulfate
SEM	standard error of the mean
SERT	serotonin transporter
SMA	Smooth Muscle Actin
Sox10	SRY (sex determining region Y)-box 10
Sox10-H2BVenus	Tg(*Sox10*-HIST2H2BE/Venus)^{ASout} transgenic mouse line
SSRI	selective serotonin reuptake inhibitor
SubsP/SP	substance p neuropeptide
SW	Swiss Webster mouse strain
Taq	*Thermus aquaticus* DNA polymerase
TBE	tris borate ethylenediaminetetraacetic acid buffer
tdTom	tdTomato fluorophore
TE	tris ethylenediaminetetraacetic acid buffer
TH	tyrosine hydroxylase
Tph1	tryptophan hydroxylase 1 (non-neuronal)
Tph2	tryptophan hydroxylase 2 (neuronal)

TRPV1	transient receptor potential cation channel subfamily V member 1
TRPV4	transient receptor potential cation channel subfamily V member 4
Tuj1	β-III tubulin
TX-100	triton x-100 detergent
Uchl1	gene encoding Protein Product 9.5 (PGP9.5)
vAChT	vesicular acetylcholine transporter
VSA	void spot assay
WM	whole-mount
WT	wildtype
YFP	yellow fluorescent protein
μL	microliter
μm	micron

CHAPTER I

INTRODUCTION

The physiological functions of visceral organs are regulated by involuntary, autonomic nervous control and thus are often taken for granted. The importance of normal visceral function becomes apparent in cases of dysfunction, particularly when quality of life is greatly dampened. This is especially true of the lower urinary tract (LUT, bladder and urethra), as urinary incontinence is often associated with social embarrassment. Despite the wide prevalence of incontinence, effective therapeutics targeting bladder innervation are limited. A better understanding of the development of bladder innervation could inform novel therapeutic strategies to treat bladder dysfunction.

This chapter aims to summarize what is currently known about the development of bladder innervation, and set the stage for the work in this dissertation on the role of serotonin receptor signaling in the neural development and function of the mouse lower urinary tract.

Anatomy of lower urinary tract innervation

The lower urinary tract (LUT), comprised of the bladder and urethra, functions to store and expel urine (Figure 1.1). The collection and storage of urine occurs during the filling phase of the micturition cycle. As urine filters from the kidneys into the bladder, the bladder smooth muscle (detrusor) relaxes to accommodate the increase in urine volume. Sympathetic neurons, which are primarily adrenergic, actively suppress detrusor contraction during this filling phase while also stimulating the concurrent contraction of the internal urethral sphincter. Sensory

afferent fibers from lumbosacral dorsal root ganglia (DRG) relay information regarding stretch of the detrusor and the contents of the bladder. The expulsion phase of micturition occurs once maximal bladder capacity has been reached, in which parasympathetic neurons (primarily cholinergic) stimulate detrusor contraction while the internal urethral sphincter relaxes to allow urine flow. These aspects of micturition require precisely coordinated activity of the sensory nervous system and the sympathetic and parasympathetic components of the autonomic nervous system. The voluntary component of micturition involves the external urethral sphincter, or urethral rhabdosphincter, which is comprised of skeletal muscle and is controlled by motor neurons from the ventral horn of the spinal cord.

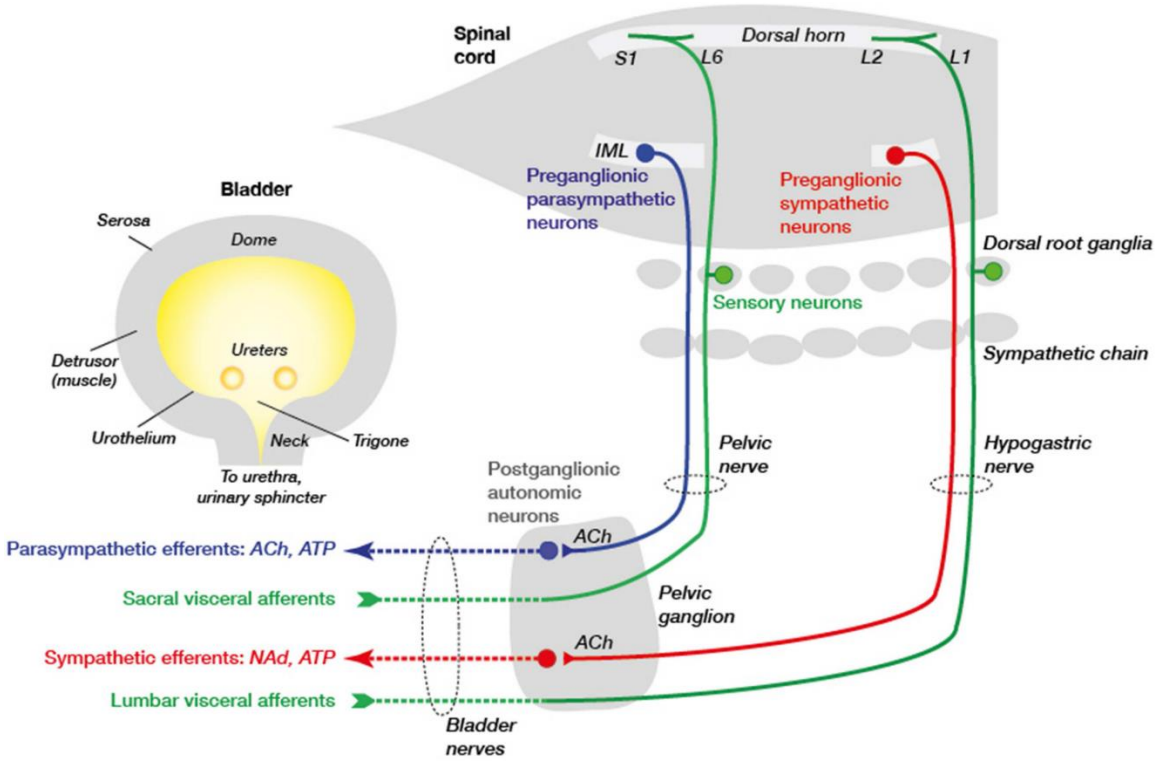

Figure 1.1 Anatomy of lower urinary tract autonomic and sensory innervation, as diagrammed in Keast et al. 2015. Sensory neurons (green) are located in the dorsal root ganglia that flank the spinal cord and project afferent fibers to the bladder smooth muscle and urothelium. Preganglionic autonomic neurons (parasympathetic, blue; sympathetic, red) are housed in the autonomic nuclei of the spinal cord and project to the mixed parasympathetic/sympathetic postganglionic pelvic ganglia. The coordinated activity of the sensory and autonomic nervous systems, in conjunction with somatic motor innervation of the external urethral sphincter (not shown), underlies normal function of the lower urinary tract.

There are several aspects of the LUT that are unique compared to other visceral organ systems. First, LUT function is dependent on the coordination of autonomic and sensory neural components with voluntary, conscious control of voiding behavior. While the activity of other visceral organs are entirely independent of behavioral influence, the voluntary control of voiding is a learned behavior that develops over the postnatal period (Girard et al., 2016). Second, the neural circuits underlying LUT function operate in a switch-like fashion (bladder filling or bladder emptying), rather than in tonic patterns that are characteristic of other visceral organs (de Groat, 1975;de Groat and Wickens, 2013). Third, the autonomic innervation of the LUT in mice is provided by the major pelvic ganglia (PG), which are comprised of both sympathetic and parasympathetic neurons (Wanigasekara et al., 2003). All other autonomic innervation in the body is supplied by anatomically distinct sympathetic and parasympathetic ganglia.

The complexity of LUT innervation makes treating urinary tract disorders similarly complex. Despite extensive characterization of neuronal classes and their involvement in normal adult LUT function, many pharmaceuticals marketed as therapeutics for urinary incontinence or overactive bladder also affect other neural circuits and thus have adverse side effects. To counteract this issue, there is great interest in deciphering the molecular subtypes of sensory and autonomic neurons that supply the LUT in order to devise more specific therapeutics that target these populations. Over the course of four decades, numerous research groups have made substantial progress in identifying sensory neuronal subtypes in adult model animals, particularly cats and rats. This progress has been recently reviewed in great detail (de Groat et al., 2015).

Dorsal root ganglia sensory neurons innervate many target tissues based on the axial level of the DRG. Lower urinary tract sensory innervation is derived from thoracolumbar DRG (L1 and L2 in rodents) and lumbosacral DRG (L6 and S1 in rodents); the latter population comprises

the majority of detrusor and urothelial innervation while the former primarily supplies the bladder serosa (Xu and Gebhart, 2008). Because appropriate functioning of the bladder relies heavily on sensation of bladder fullness, the detrusor and lining of the bladder lumen (urothelium) are densely innervated by sensory fibers (Gabella and Davis 1998). Bladder afferent neurons can be classified by chemical, electrical, and receptor properties (de Groat et al., 2015), but can generally be divided into two categories: small, myelinated Aδ and unmyelinated C-fiber neurons. Aδ fibers act as low-threshold mechanoreceptors that respond to both passive distension of the bladder during filling and active contraction during urine expulsion (Kanai and Andersson, 2010), while C-fibers are generally regarded as high-threshold nociceptive (pain-sensing) neurons that are primarily active only in the context of pathological conditions, such as tissue damage, the presence of irritants in urine, or inflammation (Kanai, 2011). Within the C-fiber class, there is great diversity in the expression of ion channels and neuropeptides that mediate responses to the aforementioned pathologies, including members of the transient receptor potential family TRPV1 and TRPV4 (Birder et al., 2002;Cenac et al., 2008;Arms and Vizzard, 2011;Yoshiyama et al., 2015), and neuropeptides Substance P, and Calcitonin Gene Related Peptide (CGRP) (Laird et al., 2000;Saban et al., 2000;Kiss et al., 2001;Lagerstrom et al., 2011;Russell et al., 2014). The markers that have been identified in C-fiber neuronal populations play important functional roles – for example, SP and CGRP are key mediators of neurogenic inflammation, especially in the context of interstitial cystitis (Saban et al., 2000;Russell et al., 2014). Despite the extensive body of work devoted to determining the composition of afferent neurons innervating the LUT, much remains to be known about co-expressed factors in these neuronal populations that can be readily pharmaceutically targeted.

Autonomic innervation of the LUT is supplied by the mixed sympathetic/parasympathetic pelvic ganglia (Wanigasekara et al., 2003) that control bladder smooth muscle contractility and relaxation, as well as bladder vascular tone (De Groat, 2009;Michel and Igawa, 2015). Contrary to a recent publication (Espinosa-Medina et al., 2016), parasympathetic and sympathetic neurons supplying the lower urinary tract can be readily distinguished by anatomy, neurochemical profile, and physiological function. Parasympathetic neurons, primarily cholinergic (Wanigasekara et al., 2003), comprise the majority of pelvic ganglia neurons (de Groat and Yoshimura, 2015) and function primarily in detrusor contraction. Sympathetic neurons, which are primarily adrenergic (Wanigasekara et al., 2003), represent a much smaller proportion of pelvic ganglia neurons (Forrest et al., 2014) and are principally involved in constriction of blood vessels, as in other autonomic systems (Gabella, 1999;Forrest et al., 2014). Adenosine triphosphate (ATP) has been demonstrated to be a co-transmitter in both parasympathetic and sympathetic pelvic ganglia neurons, but the degree of conservation of these transmitter systems across species is not well understood (de Groat et al., 2015). Anterograde tracing studies of LUT autonomic innervation have demonstrated that spinal preganglionic parasympathetic and sympathetic ganglia make synaptic contacts in the major pelvic ganglia (Keast, 1995; 1999;Kanjhan et al., 2003;Jobling and Lim, 2008).

Development of lower urinary tract innervation

Rationale and importance

Despite years of study of adult lower urinary innervation, the development of this system remains only partially understood (Keast et al., 2015). A more thorough understanding of the

development of autonomic and sensory innervation of the LUT has important clinical implications.

First, pelvic innervation is frequently damaged in various types of abdominal pelvic surgery, including prostatectomy (Cornu et al., 2014) and hysterectomy (Laterza et al., 2015), as well as in child birth. While surgeons have had moderate success in repairing functional somatic innervation of the bladder and the external urethral sphincter (EUS) (Gomez-Amaya et al., 2015), restoration of autonomic innervation has remained more challenging. This may be due, at least in part, to the inability (or long delay) of autonomic neurons to regenerate following axotomy, in contrast to somatic motor and sensory afferent nerves that demonstrate regrowth 4 weeks after transection (Payne et al., 2015). A better understanding of the development of autonomic pelvic innervation would provide significant advancement in regenerative efforts (Kim et al., 2013).

Second, chronic interstitial cystitis (IC) is a prevalent inflammatory condition of the bladder that is characterized by intense pain and discomfort, which may be caused by an excess of sensory and sympathetic innervation to the bladder (Dickson et al., 2006;Boudes et al., 2013). First line treatments for interstitial cystitis are primarily physical therapy and pain-relieving medications (Davis et al., 2014;Hanno et al., 2015). However, the application of neuronal inhibitory growth factors and growth cone repulsive cues could reduce bladder hyperinnervation and become a much more effective means to ameliorate pain and dysfunction in IC patients (Keast et al., 2015). A more thorough comprehension of these molecular growth and repulsive cues in LUT neural development is required in order for these treatment options to be pursued.

Third, very little is known about how exposure to various pharmacological agents *in utero* affects autonomic nervous system development. One of the most common medical

conditions afflicting pregnant women is depression (Gavin et al., 2005;Shakeel et al., 2015) which is commonly treated using drugs with unknown effects on the developing peripheral nervous system. Of particular interest is the increased risk of autism spectrum disorder (ASD) in children who were exposed to serotonin-targeting anti-depressants *in utero* (Rai et al., 2013;Velasquez et al., 2013), as ASD children have increased incidence of urinary incontinence and other lower urinary tract symptoms compared to typically developing children (von Gontard, 2013;Niemczyk et al., 2017). Clearly, there are molecular components common to both central and autonomic nervous system development, and further research is needed to determine how perturbing these pathways in development ultimately leads to urinary tract dysfunction later in life. An improved knowledge base of these fundamental developmental mechanisms would encourage more careful consideration of the risks of *in utero* drug exposure and could help lower fetal risk for neurodevelopmental disorders and associated autonomic dysfunction.

Even though strong rationale exists for studying the development of lower urinary tract innervation, this topic is surprisingly understudied (Keast et al., 2015). The following sections provide a brief summary of the field and highlight open research questions.

Origins from the neural crest

The autonomic and sensory neural components of the lower urinary tract are derived from the neural crest, which is a transient cell population arising from the process of neurulation in early embryonic development (Figure 1.2, Panel A) (Le Douarin and Smith, 1988;Martik and Bronner, 2017). Neural crest progenitor cells (NCPCs) migrate out from the dorsal edges of the nascent neural tube into the periphery and differentiate into a wide variety of cell types, including the dorsal root ganglia of the sensory nervous system and the sympathetic and

parasympathetic ganglia of the autonomic nervous system. The dorsal root ganglia arise from trunk neural crest, while the autonomic pelvic ganglia of the LUT are derived from sacral neural crest (Figure 1.2) (Martik and Bronner, 2017). Prior work using chick-quail chimeric embryos has established that NCPCs are partially limited in their developmental potential by their axial level of origin (Le Lievre et al., 1980). Cranial, vagal, and trunk neural crest lineages have been studied extensively - however, very few studies have focused specifically on sacral NC lineages, and the majority of these works have been in the context of the hindgut portion of the developing enteric nervous system (Kapur, 2000;Anderson et al., 2006;Erickson et al., 2012;Mundell et al., 2012).

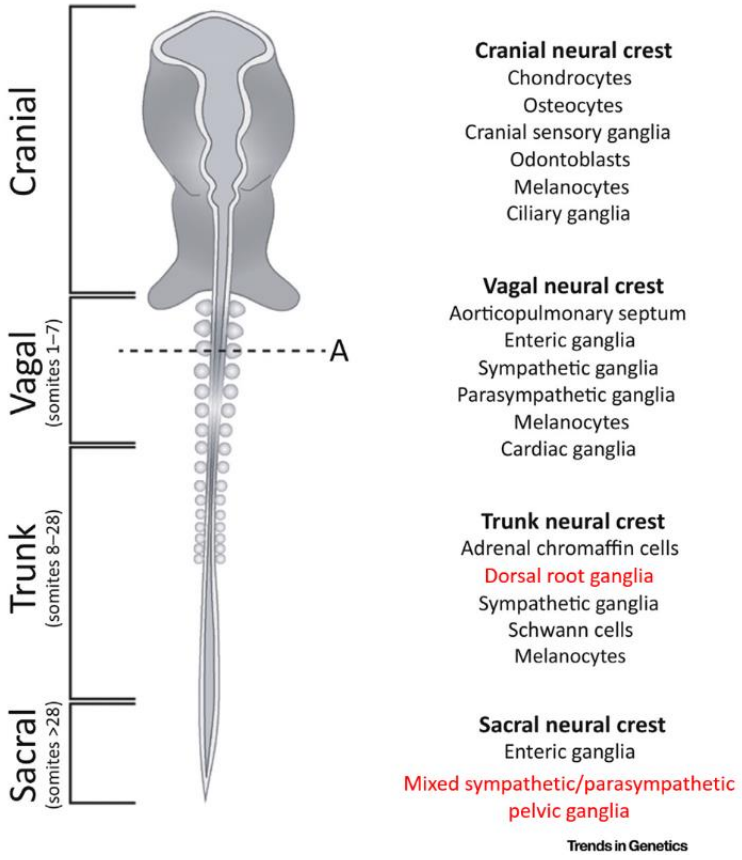

Figure 1.2 Neural crest segmentation, modified from Martik and Bronner 2017. Dorsal root ganglia arise from trunk neural crest, while pelvic ganglia arise from sacral neural crest.

Dorsal root ganglia

Upon delamination from the neural tube, trunk neural crest cells migrate in a chain-like formation to form the dorsal root ganglia, with the most ventral DRG cells arriving first, followed by the most dorsal (Kasemeier-Kulesa et al., 2005). Sensory neurogenesis occurs in three successive "waves" as neural crest cells migrate to form the dorsal root ganglia at approximately 9.5-11.5 dpc in the mouse (Figure 1.3). Interestingly, the neurons born within these neurogenic waves exhibit defined morphological features and varying abilities to proliferate. Extensive genetic analysis of DRG sensory neurogenesis has revealed combinatorial transcription factor "codes" that underlie the generation of specific sensory neuronal subtypes, which have been extensively reviewed (Marmigere and Ernfors, 2007).

Specifically in the context of the LUT, sensory innervation has been less well characterized (Keast et al., 2015). Immunostaining studies conducted in human fetal bladder demonstrates neuropeptidergic innervation of bladder smooth muscle by gestational week 13, with increasing innervation density through fetal and postnatal development (Kimmel and Mc, 1958;Jen et al., 1995). In rodent models, extensive immunohistochemical and genetic labeling of both sensory and autonomic innervation in the developing LUT has been conducted as part of the GUDMAP consortium (Harding et al., 2011). These efforts have identified parasympathetic, sympathetic, and sensory axonal projections in 18.5 dpc mouse fetal bladder. However, the dynamic nature of the characteristic genetic markers of these neuronal populations through fetal and postnatal development is largely unknown. Particularly for sensory neurons of the DRG, tracing these lineages through development is technically challenging. Neurons supplying the LUT are a small minority of the total neuronal population of a given dorsal root ganglion, and injectable

dye tracing studies are only feasible in adult animals. The identification of novel markers of bladder-innervating sensory neurons is a high priority for interrogating the development of bladder sensory innervation further.

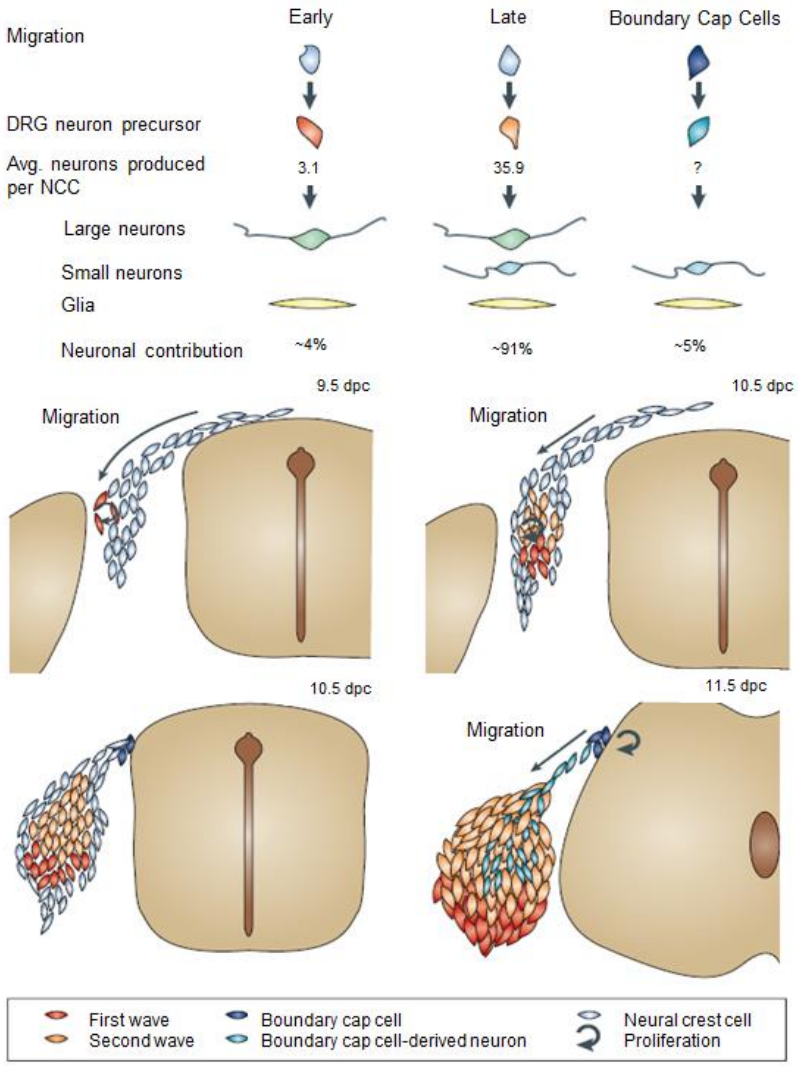

Figure 1.3 Dorsal root ganglia development, modified from Marmigere and Ernfors, 2007. Dorsal root ganglia formation occurs by three successive rounds of neurogenesis – the first two by neural crest cells, and the third by neural crest "boundary cap" cells that migrate from the neural tube later than the first and second waves of neural crest progenitors. Each wave of progenitors exhibits characteristic proliferative and developmental potentials.

Pelvic ganglia and bladder intramural ganglia

Despite the unusual characteristics of the pelvic ganglia described above, only a handful of research groups have sought to characterize pelvic ganglia neuronal development. In a recent

study from the Southard-Smith laboratory, sacral neural crest contributions to the lower urinary tract were investigated using a *Sox10*-H2BVenus transgenic reporter mouse line (Wiese and Deal et al 2017). Sacral NCPCs, identified by their expression of *Sox10*, follow primarily ventromedial migratory routes from the neural tube to the cloaca and are present by 11.0 dpc. Over the next several days in development, these *Sox10+* progenitors continue to migrate into the neck of the bladder and eventually coalesce into a pair of pelvic ganglia (Figure 1.4).

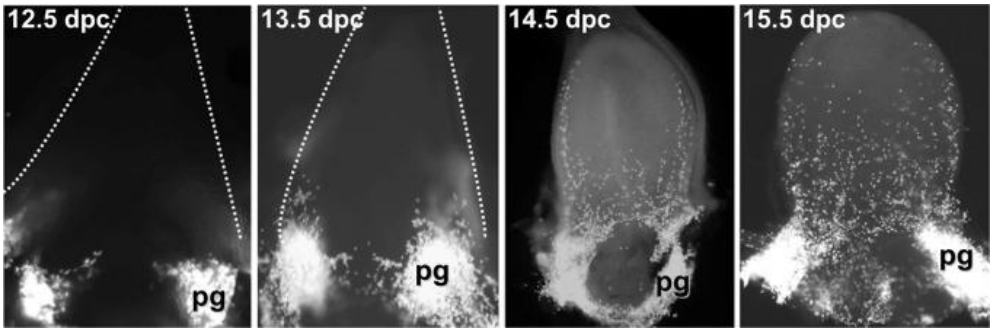

Figure 1.4 Migration of *Sox10+* neural crest cells into the lower urinary tract, from Wiese and Deal et al. 2017. Neural crest progenitors are labeled by *Sox10*-H2BVenus transgene expression. The majority of neural crest cells coalesce at the neck of the bladder and form the major pelvic ganglia (pg), while some continue to migrate in streams to form the intramural ganglia throughout the wall of the bladder dome.

Sacral neural crest progenitor cells arrive at the bladder neck at varying stages of neuronal differentiation. While some cells do not begin neuronal differentiation until after their arrival at the bladder neck, others already express Hu C/D (a marker indicative of neuronal differentiation (Clayton et al., 1998)) by the time they reach the metanephric mesenchyme. Subsequent acquisition of either a sympathetic or parasympathetic fate occur via mechanisms that are poorly understood. Prior work has shown that autonomic neurons may transiently express markers of the sympathetic lineage (i.e., expression of adrenergic neurotransmitter components such as tyrosine hydroxylase) but ultimately commit to a cholinergic parasympathetic fate (Rohrer, 2011). Very little is known about how pelvic ganglia neurons

ultimately become either sympathetic or parasympathetic. Researchers from the laboratory of Heather Young have demonstrated differences in the response to several growth factors between developing sympathetic and parasympathetic neurons (Stewart et al., 2008). Rat sympathetic neurons in late embryonic and early postnatal development respond to exposure to Nerve Growth Factor (NGF) with increased neurite outgrowth, while parasympathetic neurons do not respond to NGF in this time period. In contrast, only parasympathetic neurons exhibit increased neuronal process growth in response to neurturin. While this study contributes to our knowledge of pelvic ganglia development, the drivers of autonomic neuronal subtype lineage commitment in developing pelvic ganglia remain elusive. Many other stages of development of LUT innervation evade our understanding – aside from NGF, how do neural crest progenitors respond to the plethora of other signaling factors circulating in the embryonic environment? How do projections from newly born pelvic ganglia neurons find their appropriate targets within the bladder smooth muscle? In what way do any potential signaling mechanisms ultimately affect the physiological function of the urinary tract?

Summary

Innervation of the lower urinary tract is unique and complex, which contributes to difficulty in treating disorders of urinary tract function. A more thorough understanding of the development of LUT innervation, especially key signaling pathways that can be targeted pharmacologically, could inform novel therapeutic strategies focused on restoration of normal LUT innervation and function. Serotonin signaling has been shown by other groups to play key roles in adult LUT function (Schwen et al., 2013) and development of the CNS (Engel et al., 2013), but has not been studied in the development of urinary tract innervation. The following

chapters of this dissertation demonstrate a critical role for serotonin receptor signaling in the neural development and function of the lower urinary tract. In Chapter II I describe a transcriptome profiling study undertaken to characterize the genetic landscape of sacral neural crest progenitors that give rise to autonomic innervation of the bladder, in which 5-HT receptors were initially identified in developing pelvic ganglia. Targeting these receptors, especially the type 3A receptor (5-HT3A, *Htr3a*) altered the developmental potential and morphological maturation of pelvic ganglia autonomic neurons. In subsequent chapters my studies honed in on the 5-HT3A receptor. Chapter III describes thorough characterization of *Htr3a* gene expression in developing sensory dorsal root ganglia that supply the LUT and report the contribution of *Htr3a*+ populations to this system. In Chapter IV I describe histological, physiological, and behavioral experiments that collectively demonstrate the requirement of 5-HT3A in the development of both autonomic and sensory LUT innervation and normal urinary voiding function in a sex-specific manner. In Chapter V I discuss future directions for research, the implications of my work in a clinical context, and how my discoveries contribute to our understanding of the developmental neurobiology of serotonin. Finally, in Chapter VI I outline additional short studies and extended methodology that will aid future researchers in their work on LUT neural development. Overall this body of work extends our knowledge of serotonin receptor biology, reveals a previously unknown role of 5-HT3 receptors in sacral neural crest development, and has important clinical implications for the treatment of widely prevalent disorders of the urinary tract.

References

Anderson, R.B., Stewart, A.L., and Young, H.M. (2006). Phenotypes of neural-crest-derived cells in vagal and sacral pathways. *Cell Tissue Res* 323**,** 11-25.

Arms, L., and Vizzard, M.A. (2011). Neuropeptides in lower urinary tract function. *Handb Exp Pharmacol***,** 395-423. doi: 10.1007/978-3-642-16499-6_19.

Birder, L.A., Nakamura, Y., Kiss, S., Nealen, M.L., Barrick, S., Kanai, A.J., Wang, E., Ruiz, G., De Groat, W.C., Apodaca, G., Watkins, S., and Caterina, M.J. (2002). Altered urinary bladder function in mice lacking the vanilloid receptor TRPV1. *Nat Neurosci* 5**,** 856-860. doi: 10.1038/nn902.

Boudes, M., Uvin, P., Pinto, S., Freichel, M., Birnbaumer, L., Voets, T., De Ridder, D., and Vennekens, R. (2013). Crucial role of TRPC1 and TRPC4 in cystitis-induced neuronal sprouting and bladder overactivity. *PLoS One* 8**,** e69550. doi: 10.1371/journal.pone.0069550.

Cenac, N., Altier, C., Chapman, K., Liedtke, W., Zamponi, G., and Vergnolle, N. (2008). Transient receptor potential vanilloid-4 has a major role in visceral hypersensitivity symptoms. *Gastroenterology* 135**,** 937-946, 946 e931-932. doi: 10.1053/j.gastro.2008.05.024.

Clayton, G.H., Perez, G.M., Smith, R.L., and Owens, G.C. (1998). Expression of mRNA for the elav-like neural-specific RNA binding protein, HuD, during nervous system development. *Brain Res Dev Brain Res* 109**,** 271-280.

Cornu, J.N., Melot, C., and Haab, F. (2014). A pragmatic approach to the characterization and effective treatment of male patients with postprostatectomy incontinence. *Curr Opin Urol* 24**,** 566-570.

Davis, N.F., Brady, C.M., and Creagh, T. (2014). Interstitial cystitis/painful bladder syndrome: epidemiology, pathophysiology and evidence-based treatment options. *Eur J Obstet Gynecol Reprod Biol* 175**,** 30-37.

De Groat, W. (2009). "Autonomic Nervous System: Urogenital Control", in: *Encyclopedia of Neuroscience.* (ed.) L.R. Squire. 2 ed.: Elsevier).

De Groat, W., and Yoshimura, N. (2015). "Anatomy and physiology of the lower urinary tract," in *Handbook of Clinical Neurology,* eds. D.B. Vodusek & F. Boller. Elsevier), 61-108.

De Groat, W.C. (1975). Nervous control of the urinary bladder of the cat. *Brain Res* 87**,** 201-211.

De Groat, W.C., Griffiths, D., and Yoshimura, N. (2015). Neural control of the lower urinary tract. *Compr Physiol* 5**,** 327-396. doi: 10.1002/cphy.c130056.

De Groat, W.C., and Wickens, C. (2013). Organization of the neural switching circuitry underlying reflex micturition. *Acta Physiol (Oxf)* 207**,** 66-84. doi: 10.1111/apha.12014.

Dickson, A., Avelino, A., Cruz, F., and Ribeiro-Da-Silva, A. (2006). Peptidergic sensory and parasympathetic fiber sprouting in the mucosa of the rat urinary bladder in a chronic model of cyclophosphamide-induced cystitis. *Neuroscience* 141**,** 1633-1647. doi: 10.1016/j.neuroscience.2006.06.007.

Engel, M., Smidt, M.P., and Van Hooft, J.A. (2013). The serotonin 5-HT3 receptor: a novel neurodevelopmental target. *Front Cell Neurosci* 7**,** 76. doi: 10.3389/fncel.2013.00076.

Erickson, C.S., Zaitoun, I., Haberman, K.M., Gosain, A., Druckenbrod, N.R., and Epstein, M.L. (2012). Sacral neural crest-derived cells enter the aganglionic colon of Ednrb-/- mice along extrinsic nerve fibers. *J Comp Neurol* 520**,** 620-632. doi: 10.1002/cne.22755.

Espinosa-Medina, I., Saha, O., Boismoreau, F., Chettouh, Z., Rossi, F., Richardson, W.D., and Brunet, J.F. (2016). The sacral autonomic outflow is sympathetic. *Science* 354**,** 893-897. doi: 10.1126/science.aah5454.

Forrest, S.L., Osborne, P.B., and Keast, J.R. (2014). Characterization of axons expressing the artemin receptor in the female rat urinary bladder: a comparison with other major neuronal populations. *J Comp Neurol* 522**,** 3900-3927. doi: 10.1002/cne.23648.

Gabella, G. (1999). Structure of the intramural nerves of the rat bladder. *J Neurocytol* 28**,** 615-637.

Gavin, N.I., Gaynes, B.N., Lohr, K.N., Meltzer-Brody, S., Gartlehner, G., and Swinson, T. (2005). Perinatal depression: a systematic review of prevalence and incidence. *Obstet Gynecol* 106**,** 1071-1083.

Girard, B.M., Peterson, A., Malley, S., and Vizzard, M.A. (2016). Accelerated onset of the vesicovesical reflex in postnatal NGF-OE mice and the role of neuropeptides. *Exp Neurol* 285**,** 110-125.

Gomez-Amaya, S.M., Barbe, M.F., De Groat, W.C., Brown, J.M., Tuite, G.F., Corcos, J., Fecho, S.B., Braverman, A.S., and Ruggieri, M.R., Sr. (2015). Neural reconstruction methods of restoring bladder function. *Nat Rev Urol* 12**,** 100-118. doi: 10.1038/nrurol.2015.4.

Hanno, P.M., Erickson, D., Moldwin, R., Faraday, M.M., and Association, A.U. (2015). Diagnosis and treatment of interstitial cystitis/bladder pain syndrome: AUA guideline amendment. *J Urol* 193**,** 1545-1553.

Harding, S.D., Armit, C., Armstrong, J., Brennan, J., Cheng, Y., Haggarty, B., Houghton, D., Lloyd-Macgilp, S., Pi, X., Roochun, Y., Sharghi, M., Tindal, C., Mcmahon, A.P., Gottesman, B., Little, M.H., Georgas, K., Aronow, B.J., Potter, S.S., Brunskill, E.W., Southard-Smith, E.M., Mendelsohn, C., Baldock, R.A., Davies, J.A., and Davidson, D. (2011). The GUDMAP database--an online resource for genitourinary research. *Development* 138**,** 2845-2853.

Jen, P.Y., Dixon, J.S., and Gosling, J.A. (1995). Immunohistochemical localization of neuromarkers and neuropeptides in human fetal neonatal urinary bladder. *Br J Urol* 75.

Jobling, P., and Lim, R. (2008). Anatomical and physiological properties of pelvic ganglion neurons in female mice. *Auton Neurosci* 140**,** 30-39. doi: 10.1016/j.autneu.2008.03.001.

Kanai, A., and Andersson, K.E. (2010). Bladder afferent signaling: recent findings. *J Urol* 183**,** 1288-1295. doi: 10.1016/j.juro.2009.12.060.

Kanai, A.J. (2011). Afferent mechanism in the urinary tract. *Handb Exp Pharmacol***,** 171-205. doi: 10.1007/978-3-642-16499-6_9.

Kanjhan, R., Osborne, P.B., Ouyang, M., and Keast, J.R. (2003). Postnatal maturational changes in rat pelvic autonomic ganglion cells: a mixture of steroid-dependent and -independent effects. *J Neurophysiol* 89**,** 315-323. doi: 10.1152/jn.00479.2002.

Kapur, R.P. (2000). Colonization of the murine hindgut by sacral neural crest-derived neural precursors: experimental support for an evolutionarily conserved model. *Dev Biol* 227**,** 146-155.

Kasemeier-Kulesa, J.C., Kulesa, P.M., and Lefcort, F. (2005). Imaging neural crest cell dynamics during formation of dorsal root ganglia and sympathetic ganglia. *Development* 132**,** 235-245.

Keast, J.R. (1995). Visualization and immunohistochemical characterization of sympathetic and parasympathetic neurons in the male rat major pelvic ganglion. *Neuroscience* 66**,** 655-662.

Keast, J.R. (1999). Unusual autonomic ganglia: connections, chemistry, and plasticity of pelvic ganglia. *Int Rev Cytol* 193**,** 169.

Keast, J.R., Smith-Anttila, C.J., and Osborne, P.B. (2015). Developing a functional urinary bladder: a neuronal context. *Front Cell Dev Biol* 3**,** 53. doi: 10.3389/fcell.2015.00053.

Kim, J.H., Lee, S.R., Song, Y.S., and Lee, H.J. (2013). Stem cell therapy in bladder dysfunction: where are we? And where do we have to go? *Biomed Res Int* 2013**,** 930713. doi: 10.1155/2013/930713.

Kimmel, D.L., and Mc, C.L. (1958). The development of pelvic plexuses and the distribution of the pelvic splanchnic nerves in the human embryo and fetus. *J Comp Neurol* 110**,** 271-297.

Kiss, S., Yoshiyama, M., Cao, Y.Q., Basbaum, A.I., De Groat, W.C., Lecci, A., Maggi, C.A., and Birder, L.A. (2001). Impaired response to chemical irritation of the urinary tract in mice with disruption of the preprotachykinin gene. *Neurosci Lett* 313**,** 57-60.

Lagerstrom, M.C., Rogoz, K., Abrahamsen, B., Lind, A.L., Olund, C., Smith, C., Mendez, J.A., Wallen-Mackenzie, A., Wood, J.N., and Kullander, K. (2011). A sensory subpopulation depends on vesicular glutamate transporter 2 for mechanical pain, and together with substance P, inflammatory pain. *Proc Natl Acad Sci U S A* 108**,** 5789-5794. doi: 10.1073/pnas.1013602108.

Laird, J.M., Olivar, T., Roza, C., De Felipe, C., Hunt, S.P., and Cervero, F. (2000). Deficits in visceral pain and hyperalgesia of mice with a disruption of the tachykinin NK1 receptor gene. *Neuroscience* 98**,** 345-352.

Laterza, R.M., Sievert, K.D., De Ridder, D., Vierhout, M.E., Haab, F., Cardozo, L., Van Kerrebroeck, P., Cruz, F., Kelleher, C., Chapple, C., Espuna-Pons, M., and Koelbl, H. (2015). Bladder function after radical hysterectomy for cervical cancer. *Neurourol Urodyn* 34**,** 309-315.

Le Douarin, N.M., and Smith, J. (1988). Development of the peripheral nervous system from the neural crest. *Annu Rev Cell Biol* 4**,** 375-404.

Le Lievre, C.S., Schweizer, G.G., Ziller, C.M., and Le Douarin, N.M. (1980). Restrictions of developmental capabilities in neural crest cell derivatives as tested by *in vivo* transplantation experiments. *Dev Biol* 77**,** 362-378.

Marmigere, F., and Ernfors, P. (2007). Specification and connectivity of neuronal subtypes in the sensory lineage. *Nat Rev Neurosci* 8**,** 114-127. doi: 10.1038/nrn2057.

Martik, M.L., and Bronner, M. (2017). Regulatory Logic Underlying Diversification of the Neural Crest. *Trend Genet* 33**,** 715-727.

Michel, M.C., and Igawa, Y. (2015). Therapeutic targets for overactive bladder other than smooth muscle. *Expert Opin Ther Targets* 19**,** 687-705.

Mundell, N.A., Plank, J.L., Legrone, A.W., Frist, A.Y., Zhu, L., Shin, M.K., Southard-Smith, E.M., and Labosky, P.A. (2012). Enteric nervous system specific deletion of Foxd3 disrupts glial cell differentiation and activates compensatory enteric progenitors. *Dev Biol* 363**,** 373-387. doi: 10.1016/j.ydbio.2012.01.003.

Niemczyk, J., Wagner, C., and Von Gontard, A. (2017). Incontinence in autism spectrum disorder: a systematic review. *Eur Child Adolesc Psychiatry* Epub ahead of print. doi: 10.1007/s00787-017-1062-3.

Payne, S.C., Belleville, P.J., and Keast, J.R. (2015). Regeneration of sensory but not motor axons following visceral nerve injury. *Exp Neurol* 266**,** 127-142. doi: 10.1016/j.expneurol.2015.02.026.

Rai, D., Lee, B.K., Dalman, C., Golding, J., Lewis, G., and Magnusson, C. (2013). Parental depression, maternal antidepressant use during pregnancy, and risk of autism spectrum disorders: population based case-control study. *BMJ* 346**,** f2059.

Rohrer, H. (2011). Transcriptional control of differentiation and neurogenesis in autonomic ganglia. *Eur J Neurosci* 34**,** 1563-1573. doi: 10.1111/j.1460-9568.2011.07860.x.

Russell, F.A., King, R., Smillie, S.J., Kodji, X., and Brain, S.D. (2014). Calcitonin gene-related peptide: physiology and pathophysiology. *Physiol Rev* 94**,** 1099-1142. doi: 10.1152/physrev.00034.2013.

Saban, R., Saban, M.R., Nguyen, N.B., Lu, B., Gerard, C., Gerard, N.P., and Hammond, T.G. (2000). Neurokinin-1 (NK-1) receptor is required in antigen-induced cystitis. *Am J Pathol* 156**,** 775-780. doi: 10.1016/S0002-9440(10)64944-9.

Schwen, Z., Matsuta, Y., Shen, B., Wang, J., Roppolo, J.R., De Groat, W.C., and Tai, C. (2013). Involvement of 5-HT3 receptors in pudendal inhibition of bladder overactivity in cats. *Am J Physiol Renal Physiol* 305**,** F663-671. doi: 10.1152/ajprenal.00105.2013.

Shakeel, N., Eberhard-Gran, M., Sletner, L., Slinning, K., Martinsen, E.W., Holme, I., and Jenum, A.K. (2015). A prospective cohort study of depression in pregnancy, prevalence and risk factors in a multi-ethnic population. *BMC Pregnancy Childbirth* 15. doi: 10.1186/s12884-014-0420-0.

Stewart, A.L., Anderson, R.B., Kobayashi, K., and Young, H.M. (2008). Effects of NGF, NT-3 and GDNF family members on neurite outgrowth and migration from pelvic ganglia from embryonic and newborn mice. *BMC Dev Biol* 8**,** 73. doi: 10.1186/1471-213X-8-73.

Velasquez, J.C., Goeden, N., and Bonnin, A. (2013). Placental serotonin: implications for the developmental effects of SSRIs and maternal depression. *Front Cell Neurosci* 7**,** 47. doi: 10.3389/fncel.2013.00047.

Von Gontard, A. (2013). Urinary incontinence in children with special needs. *Nat Rev Urol* 10**,** 667-674.

Wanigasekara, Y., Kepper, M.E., and Keast, J.R. (2003). Immunohistochemical characterisation of pelvic autonomic ganglia in male mice. *Cell Tissue Res* 311**,** 175-185. doi: 10.1007/s00441-002-0673-1.

Xu, L., and Gebhart, G.F. (2008). Characterization of mouse lumbar splanchnic and pelvic nerve urinary bladder mechanosensory afferents. *J Neurophysiol* 99**,** 244-253. doi: 10.1152/jn.01049.2007.

Yoshiyama, M., Mochizuki, T., Nakagomi, H., Miyamoto, T., Kira, S., Mizumachi, R., Sokabe, T., Takayama, Y., Tominaga, M., and Takeda, M. (2015). Functional roles of TRPV1 and TRPV4 in control of lower urinary tract activity: dual analysis of behavior and reflex during the micturition cycle. *Am J Physiol Renal Physiol* 308**,** F1128-1134. doi: 10.1152/ajprenal.00016.2015.

CHAPTER II

EFFECTS OF TARGETING SEROTONIN RECEPTORS IN SACRAL NEURAL CREST PROGENITORS

This chapter is a modified version of a manuscript to be submitted for publication (Ritter and Buehler et al., 2017). The journal to which this paper will be submitted, Proceedings of the National Academy of Sciences, states that authors retain their right to include their manuscripts in their dissertation.

Introduction

Urinary incontinence afflicts millions of people worldwide and dramatically impairs quality of life (Shaban et al., 2010;Coyne et al., 2014). In many cases incontinence is caused by damage to the nerves that supply the lower urinary tract. Unlike many other autonomic neurons that are in close proximity to their target organs, the autonomic neurons that innervate the bladder reside at a distance and are thus prone to damage during pelvic surgical procedures or childbirth. In addition, pelvic autonomic neurons do not appear to regenerate their processes following axotomy, which contrasts with sensory nerves that rapidly regenerate within four weeks of transection (Payne et al., 2015). As a result, there is growing interest in understanding the developmental processes that govern the formation and maturation of urinary tract innervation as a means to devise novel strategies to restore bladder function (Kim et al., 2013).

Normal bladder function relies on autonomic neural inputs to coordinate the relaxation and contraction of the bladder and urethral sphincter. In mice, autonomic innervation of the LUT is provided by the pelvic ganglia, which consist of thousands of mixed sympathetic and

parasympathetic neurons lying close to the uterine cervix in females and prostate in males. Initial efforts to discern factors that regulate pelvic ganglia neurogenesis relied on a genome-wide screen of transcription factors in high throughput whole-mount *in situ* hybridization of fetal mouse urinary tracts (Wiese et al., 2012). Key transcription factors, including those that have known roles in neural crest development and autonomic neurogenesis, such as *Phox2b*, *Gata2*, and *Hand2* were identified. However, the relationships between these factors and the expression and function of downstream signaling pathways in pelvic ganglia development have remained elusive.

In this study we sought to identify novel signaling pathways that regulate neurogenesis in fetal mouse pelvic ganglia. We undertook comparative transcriptome profiling of sacral neural crest progenitors and intact fetal pelvic ganglia at developmental time points when neuronal differentiation is ongoing. We employed the transgenic mouse line *Sox10*-H2BVenus that directly labels migrating neural crest to illuminate both progenitors populations and the forming pelvic ganglia (Corpening et al., 2011;Wiese et al., 2017). This effort identified significant up-regulation of multiple serotonin receptor genes in differentiating pelvic ganglia neurons. In particular we documented that the serotonin receptor 3A gene, *Htr3a*, is highly expressed in sacral neural crest progenitors and is maintained in cells undergoing neuronal differentiation. Treatment of isolated *Sox10*-H2BVenus+ sacral neural crest derived progenitors with a specific 5-HT3A agonist revealed a previously unknown role for this receptor in modulating differentiation potential of sacral neural crest lineages. Over-stimulating 5-HT3A in cultured fetal pelvic ganglia explants resulted in blunted neurite arbor outgrowth in a dose-dependent manner, which supports a role for this receptor in morphological maturation of neurons. Altogether this work contributes a valuable transcriptome profile data set for investigation of key

molecular factors that control sacral autonomic neuronal differentiation, and demonstrates a critical role for serotonin signaling via 5-HT3A in both neurogenesis and neuronal maturation.

Materials and Methods

Isolation of mRNA from fetal mouse lower urinary tract

All animal protocols were approved by Vanderbilt University IACUC in accordance with the NIH Guide for Care and Use of Laboratory Animals. Mice carrying the Tg(*Sox10*-HIST2H2BE/Venus)ASout and Tg(*Uchl1*-HIST2H2BE/mCherry/EGFP*)FSout transgenes (hereafter *Sox10*-H2BVenus and *Uchl1*-mCherry, respectively) and their genotyping procedures have been previously described (Corpening et al., 2011;Wiese et al., 2013). Litters from timed pregnancies were harvested at 13.5, 14.5, or 15.5 days post coitus (dpc), counting the day of plug detection as 0.5 dpc. Embryos were screen for fluorescence in whole mount, then pelvic ganglia were dissected and dissociated for flow sorting as described (Corpening et al., 2011). Pools of 4-18 intact fetal LUT or micro-dissected pelvic ganglia were combined to form single samples. At least three independent pools were collected for harvest of RNA. Total RNA was isolated as previously described (Corpening et al., 2011;Wiese et al., 2013).

Immunohistochemistry

Immunohistochemistry on fetal cryo-sections was conducted as previously described ((Ritter et al., 2017), see also Chapter III, IV, and VI). Primary and secondary antibody information is listed in Tables 2.1 and 2.2, respectively. Slides were mounted and coverslipped, then imaged on a Zeiss LSM 510 Meta confocal microscope equipped with a 20x/0.75 plan-apochromat objective.

Table 2.1 Primary antibodies used in immunohistochemistry experiments

Antigen	Host	Vendor	Dilution	RRID
PGP9.5	Rabbit, polyclonal	AbD Serotec, #7863-0504	1:4,000	AB_2210505
Peripherin (Prph)	Rabbit, polyclonal	Millipore, #AB1530	1:1,000	AB_90725
FITC-conjugated Smooth Muscle Actin (SMA)	Mouse, monoclonal	Sigma Aldrich, #F3777	1:800	AB_476977
Cy3-conjugated Glial Fibrillary Acidic Protein (GFAP)	Mouse, monoclonal	Sigma Aldrich, #C9205	1:800	AB_476889
Hu C/D	Human	Gift from Dr. Vanda Lennon, Mayo Clinic	1:10,000	N/A
DAPI	N/A	Invitrogen, D1306	1:50,000	N/A

Table 2.2 Secondary antibodies used in immunohistochemistry experiments

Antigen	Vendor	Dilution	RRID
Donkey anti-Rabbit AlexaFluor 647	Jackson ImmunoResearch, #711-605-152	1:250	AB_2492288
Donkey anti-Human AlexaFluor 647	Jackson ImmunoResearch, #709-605-149	1:2001	AB_2340578

Microarray hybridizations and data analysis

Microarray hybridizations and analysis were skillfully conducted by Dr. Sean Levy and members of the Vanderbilt Microarray Shared Resource and our collaborators, Shilin "Tiger" Zhao and Yan Guo. RNA sample concentrations were determined by RiboGreen fluorescence (ThermoFisher, #R11490) in comparison to a standard curve ranging from 1-50ng/mL. For each sample, 3ng total RNA was amplified by Nugen WT-PICO (Affymetrix, #3300), processed on the Nugen Exon Module (Affymetrix, #2000) and the FL-Ovation kit (Affymetrix, #4200), followed by hybridization to mouse Gene 1.0 ST Affymetrix arrays. Raw data were processed with Affymetrix Gene Expression Console using robust Multi-Array Average (RMA)

normalization (Irizarry et al., 2003). Differential expression analysis was performed using the LIMMA Bioconductor package (Diboun et al., 2006). A false discovery adjusted p-value of <0.05 was considered statistically significant. The top 100 up- and down-regulated genes were selected by ranking fold change relative to total embryo mRNA levels for each stage examined. These table files are available on the Southard-Smith laboratory computers, as they are too large to print as part of this dissertation.

Reverse Transcription Polymerase Chain Reaction (RT-PCR)

cDNA was synthesized from purified RNA using the High Capacity cDNA Reverse Transcription kit (ABI, Life Technologies, #4368814), with an input of 25ng RNA in accordance with the manufacturer's instructions. All cDNA was stored in small aliquots at -80°C to avoid repeated freezing and thawing. To minimize the consumption of cDNA, the TaqMan Pre-Amplification Master Mix kit (Life technologies, #4384266) was used to amplify cDNA templates for specific detection of serotonin receptor genes (*Htrs*). Primers to detect serotonin receptor gene expression were carefully designed to bridge exons and avoid regions of high homology between *Htr* gene family members and detect expression of all known splice variants. Primer sequences are listed in Table 2.3. The pooled assay mix for the amplification contained reverse and forward primers for each murine *Htr* gene, along with primers for housekeeping gene *ActB* as a control. Pre-amplified cDNA was used for traditional PCR, using the same *Htr* primers pooled in the pre-amplification mix. Thermocycling conditions were the following: 94°C 5 minutes; 34 cycles of (94°C 30 seconds, 55°C 30 seconds, 72°C 30 seconds); final extension 72°C 10 minutes. PCR products were visualized by non-denaturing polyacrylamide gel electrophoresis.

Table 2.3 Primers used to detect serotonin receptor expression in reverse-transcription PCR experiments

Gene	Forward Primer (5' to 3')	Reverse Primer (5' to 3')	Product Size (bp)
Htr1a	CTTTTCCTAGAACACGCAGCTT	TTGGGATTTCGAATAGAGAGGA	194
Htr1b	GTCTCCTGTGTACGTGAACCAA	GGCATCCTTACAGATAGGCATC	184
Htr1d	CGAGAAAGGAAAGCCACTAAGA	TGACGGGGTTAATGAGAGAGTT	181
Htr1f	GAGGAACTGTTAAACCGAATGC	TCACCAGGACAGCTACAAGAAA	190
Htr2a	GCTACAGGATGATTCGAAGGTC	TGGAAGAGCTTTTCTGATGACA	246
Htr2b	GCAGGTACATCACCTGCAATTA	GAGGAGGATGATTGATGAGGAC	209
Htr2c	ATTGGTTTGGCAGTTCGATATT	TGCAGTTTCTTCTCCATGCTTA	204
Htr3a	CTTAGGTCCTGCATCCTGTTTC	TTGACGCCCTGATAAGTAAGGT	181
Htr3b	GGGGTTACAACATGTAGGGAAA	GCTTGCTTGTCACTGCATACTC	199
Htr4	CACACAGTAGCAGCTCAAAACC	GCTTACATTTGGGTCCTCTGAC	178
Htr5a	GCTTTCAAGGTCTTCTTCTCCA	GGAAGAGTGCCCAGACATAAAC	250
Htr5b	CCAAGTCCCTGAATAATGGAAG	CCAGTAGAGTCACCACAAGCAC	193
Htr6	TGGCTGGGATACTGTAATAGCA	CCCTGAAGCTGAGTCTGAATCT	237
Htr7	AAACACAAGTTCTCAGGCTTCC	AGGTAGTGGCTGCTTTCTGTTC	172

Assessment of developmental potential in cultures of sacral neural crest

This portion of the work was conducted by Dennis Buehler. Whole LUTs were micro-dissected from 14.5 dpc *Sox10*-H2BVenus transgenic mice; Venus+ cells were isolated via fluorescence activated cell sorting (FACS). Cells were plated and grown in culture using established conditions as previously described (Bixby et al., 2002;Walters et al., 2010). The cultures were treated with either drug vehicle control, clozapine (1μM, Sigma Aldrich #C6305), or 5-HT3 receptor-specific agonist SR57227A (1μM, Sigma Aldrich #S1688). Cells were grown in self-renewal media for one week and then switched to differentiation media and cultured for

one week. Drugs were replenished every three days during the differentiation media culture period. To determine developmental potential of neural crest progenitors following exposure to these drugs, cultures were fixed and immunostained for various differentiated cell type markers (peripherin for neurons, GFAP for glia, Smooth Muscle Actin (SMA) for myofibroblasts, see Table 2.1) and counter-stained with DAPI. Colony composition was determined by counting the total number of colonies per well that labeled with peripherin, GFAP, or SMA. Colonies were classified as being purely neuronal, glial, or myofibroblase (N, G, and M, respectively), or combinations of these lineages. Percentages of colony-type were calculated by dividing the number of colonies of a particular subtype over the total number of colonies in the well. These percentages were then averaged across replicates.

Pelvic ganglia explant cultures

This portion of the work was conducted by Dennis Buehler. Pelvic ganglia cultures were established as previously described (Stewart et al., 2008). Briefly, collagen (Millipore, 08-115) was mixed with 5x DMEM (made from Gibco 12100 powdered media) to normal osmolality and adjusted to neutral pH (~6.9-7.4) using Phenol Red indicator dye. The media was then diluted to 1mg/mL final concentration in DMEM (Gibco, 31053) containing 10% fetal bovine serum (Benchmark, 100-106) and penicillin, streptomycin, and amphotericin B (Gibco, 15240-96). Pelvic ganglia from 13.5 dpc urogenital sinuses were visualized under fluorescence illumination based on expression of the *Sox10*-H2BVenus transgene (Corpening et al., 2011;Wiese et al., 2013) and micro-dissected into ice cold PBS. Individual pelvic ganglia were transferred to single wells of a 6-well tissue culture plate coated with collagen gel and gently inserted into the gel surface using micro-forceps. Agarose beads (Sigma C1461) saturated with 100ng/uL of NT-

3 (Peprotech 450-03) were positioned in the gel using a 27g needle at a position 1.0 mm from the explant center. An untreated bead was positioned at 1.0 mm on the opposite side of each explant. For 5-HT3A agonist treated collagen gels, SR57227A (Sigma, S1688) was reconstituted in sterile MilliQ water to 1000 micromolar and added to the media to achieve concentrations ranging from 10-50 micromolar. After four days of culture at 37°C in 5% CO_2, explants were fixed in neutral buffered formalin (Sigma, HT501128) with 0.1-0.5% TX-100 (Fisher Scientific, BP151) and processed for immunohistochemical detection by rinsing with wash buffer (PBS with 0.1% TX-100 with 0.5% BSA (Sigma, A2153)) and blocking in PBS with 0.1-0.5% TX-100 with 1% BSA and 5% NDS (Jackson ImmunoResearch, 017-000-121). Primary antibodies (Table 2.1) were diluted in blocking solution and applied to cultured explants overnight at 4°C. Explants were rinsed in the wash buffer described above and incubated in secondary antibody for 1-2 hours at room temperature (Table 2.2). Following staining, cultured explants were rinsed with wash buffer, post-fixed in 4% neutral buffered formalin with 0.1-0.5% TX-100 and imaged on a Leica DMI 6000B inverted fluorescent microscope.

Sholl analysis

To measure the growth of neuritic processes after drug treatment, neurite extension was measured in images of pelvic ganglia explants from each experimental condition (n=12-14) that had been stained with PGP9.5. Individual images were converted to 8 bits/channel, indexed color tiff files in Adobe Photoshop (2014 2.2 release, Adobe Systems Inc, San Jose, CA). Neurites in each image were traced semi-automatically using the NeuronJ plugin (Meijering et al., 2004) for ImageJ (version 1.50e, National Institutes of Health, USA) and saved as grayscale bitmap images. Arborization complexity was measured by Sholl analysis of neurite tracings

using the Sholl ImageJ plugin (Ferreira et al., 2014). For each image, the center of the ganglion was used as the center of analysis and the ending radius was defined by the most distal point of the neuritic arbor. A radius step size of 0.0 was used for continuous sampling of the entire arbor. The number of intersections between sampling radii and the arbor were assessed as a readout of arbor complexity.

Statistical analysis

Colony composition among drug treatment groups (vehicle control, SR57227A, clozapine) was averaged for each treatment group. Colony percentage means were statistically compared via Welch's t-test; a p-value of <0.05 was considered significant. For Sholl Analysis, the number of radii intersecting the arbor of each sample per treatment group (vehicle control, 25μM, 50μM SR57227A) were averaged. These averages were statistically compared via one-way ANOVA with Tukey's Honest Significant Difference (HSD) post-hoc test to correct for multiple comparisons. The size of the enclosing radius of the arbor of each sample per treatment groups were averaged and compared via one-way ANOVA with Tukey's HSD post-hoc test.

Results

Population of pelvic ganglia anlagen by Sox10+ *sacral neural crest progenitors*

Sox10-H2BVenus expression labels neural crest-derived stem cells and is retained in mature glia (Corpening et al., 2011). However, early differentiating neurons within the anlagen of the pelvic ganglia also briefly retain residual H2BVenus fluorescence (Wiese et al., 2012). To relate the distribution of *Sox10*+ cells to pelvic ganglia neurons during development of pelvic innervation, we examined pelvic ganglia from *Sox10*-H2BVenus+ transgenic mice at fetal stages

when autonomic neurogenesis is actively occurring. Upon staining with pan-neuronal marker Hu C/D in 13.5 dpc (days post coitus) cryo-sections, we observed Hu C/D+ neurons within the pelvic ganglia surrounded by numerous *Sox10*+ cells (Figure 2.1, Panel A). By 14.5 dpc, the pelvic ganglia have increased in size and the domain of Hu C/D expression is expanded (Figure 2.1, Panel B). Importantly, pelvic ganglia at age 15.5 dpc continue to undergo neurogenesis, as evidenced by further expansion of Hu C/D and the presence of clusters of *Sox10*-H2BVenus+ progenitor cells (Figure 2.1, Panel C). Not only did the robust and highly specific expression of the *Sox10*-H2BVenus transgene allow visualization of sacral progenitors *in situ,* it also enabled isolation of neural crest-derived progenitors from fetal lower urinary tracts via fluorescence-activated cell sorting (FACS, Figure 2.1, Panel D) for analysis of transcriptional profiles.

Identification of serotonin receptors up-regulated in differentiating pelvic ganglia

To identify the most salient genes expressed in differentiating pelvic ganglia, we micro-dissected pelvic ganglia from *Sox10*-H2BVenus+ fetal mice at ages 13.5, 14.5, and 15.5 dpc when autonomic neurogenesis is ongoing. At 13.5 dpc, H2BVenus+ cells were harvested from pelvic ganglia by FACS to obtain transcriptional profiles for early differentiating Sox10+ progenitors. RNA was isolated and purified from intact 14.5 and 15.5 dpc pelvic ganglia so that expression profiles from differentiating neurons, which are intermingled with Sox10+ progenitors, were included that otherwise would have been lost if only H2BVenus+ cells were collected at these stages. RNA from flow-sorted Sox10+ progenitors and developing pelvic ganglia were then subjected to microarray analysis. Differentially expressed genes were identified using the LIMMA Bioconductor package; the results of the LIMMA comparison can be found on the Southard-Smith laboratory computers. The top 100 most up- and down-

regulated genes were categorized as genes exhibiting the highest fold change relative to total fetus RNA levels at each stage examined. Among these top 100 genes we identified significant enrichment of expected markers of autonomic neurogenesis, including *Hand2* and *Prph*. We

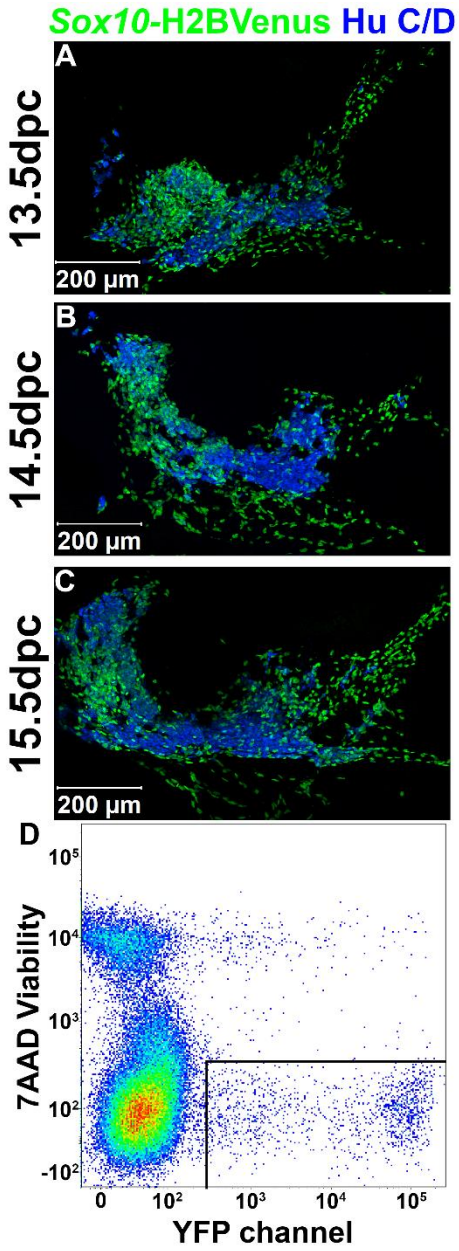

Figure 2.1 Distribution of *Sox10*-H2BVenus+ neural crest-derived progenitors and neurons in developing pelvic ganglia. *Sox10*-H2BVenus+ neural crest-derived cells can be specifically visualized by confocal microscopy and isolated via FACS. Sagittal cryo-sections of *Sox10*-H2BVenus transgenic mouse pelvic ganglia at age (**A**) 13.5 dpc, (**B**) 14.5 dpc, and (**C**) 15.5 dpc. (**D**) FACS profile of *Sox10*-H2BVenus+ cells from the urogenital sinus of 13.5 dpd transgenic mice. Viable cells that excluded 7AAD and were Venus+ were selected as shown in the boxed gated area.

also noted significant up-regulation of *Htr3a* and *Htr3b*, which encode the A and B subunits, respectively, of the type 3 serotonin receptor (5-HT3). At each fetal stage examined, *Htr3a* was significantly enriched compared to total fetal mouse RNA levels, but the highest fold change occurred at 15.5 dpc (Table 2.3). From these transcriptional profiling experiments, we conclude that serotonin receptor *Htr3a* is significantly up-regulated in fetal pelvic ganglia during stages of autonomic neurogenesis.

Multiple serotonin receptors are expressed in sacral neural crest and differentiating lower urinary tract neurons

Following the detection of serotonin receptor genes in fetal pelvic ganglia by microarray, reverse-transcription (RT) PCR was performed to validate the detection of individual 5-HTR genes (Figure 2.2). We specifically aimed to determine whether 5-HTRs are expressed in *Sox10*+ progenitors or differentiating neurons. To accomplish this, we synthesized cDNA using RNA isolated from two populations: flow-sorted sacral neural crest-derived progenitors labeled by *Sox10*-H2BVenus transgene expression, and differentiating neurons labeled by *Uchl1*-mCherry transgene expression (Wiese et al., 2013). All RNA isolates were procured from fetal mice at 15.5 dpc. We observed expression of all serotonin receptors in cDNA generated from whole fetuses as would be expected given the wide distribution of these receptors during neural development. We also detected expression of every serotonin receptor in LUT RNAs at 15.5 dpc. Serotonin receptor genes *Htr1b, Htr1d, Htr2a, Htr2b, Htr4, Htr6,* and *Htr7* are expressed in *Uchl1*+ neuronal progenitors, but not in *Sox10*+ neural crest precursors. Interestingly, *Htr3a, Htr3b,* and *Htr5b* are expressed in early neurons marked by *Uchl1*-mCherry transgene expression as well as in neural crest progenitors marked by *Sox10*-H2BVenus. Serotonin

receptor genes *Htr1a*, *Htr1f,* and *Htr2c* are not expressed in either *Sox10*+ or *Uchl1*+ pelvic ganglia populations at 15.5 dpc. From these experiments we conclude that several serotonin receptor family members are expressed in differentiated neurons within fetal pelvic ganglia, but only *Htr3* and *Htr5* receptor subunits are expressed in early progenitor cells at this stage.

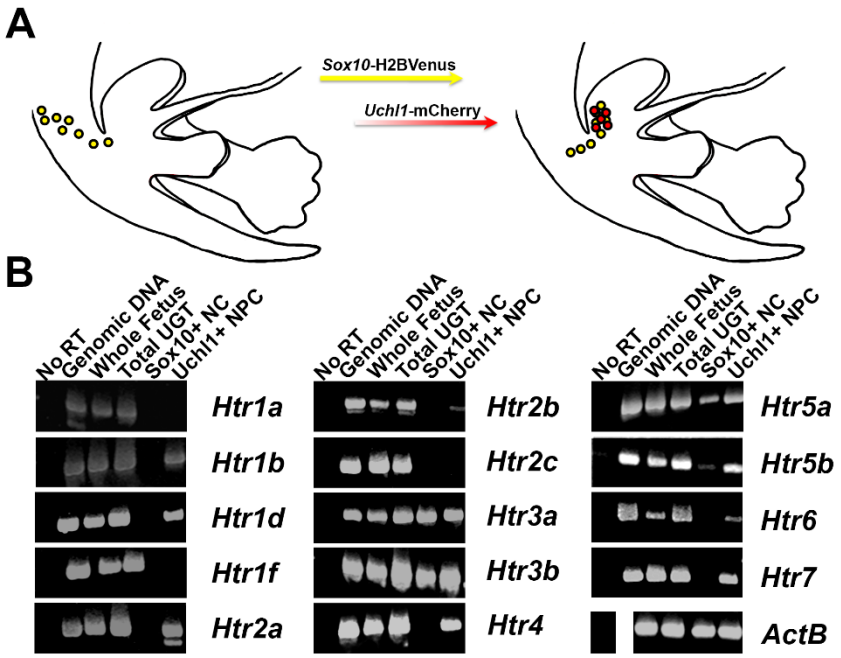

Figure 2.2 Expression of serotonin receptor genes in neural crest-derived progenitors and pelvic ganglia neuronal precursors. Reverse transcription PCR conducted on cDNA derived from distinct cell populations in the urogenital tract reveals expression of a subset of serotonin receptors in developing pelvic innervation. (**A**) Two transgenic mouse lines were used to isolate distinct cell populations within the developing urogenital tract by flow-sorting for cells labeled by the fluorescence reporter expression. Expression of *Sox10*-H2BVenus marks neural crest-derived progenitors that are undifferentiated or are differentiating towards the glial lineage. Cells expressing *Uchl1*-mCherry are undergoing neuronal differentiation. cDNA was synthesized from RNA isolated and purified from these two cell populations. (**B**) Gel electrophoresis of RT-PCR products generated by specific amplification of 5-HTR genes. cDNA was synthesized from whole mouse fetus, total lower urinary tract (bladder with attached genital tubercle), *Sox10*-H2BVenus+ cells isolated by FACS, and pelvic *Uchl1*-mCherry+ neuronal progenitor RNA. Template with no reverse transcriptase added to the cDNA synthesis reaction ("No RT") served as a negative control; genomic DNA template served as a positive control. Amplification of house-keeping gene *ActB* served as a positive control for the PCR reaction.

Perturbing serotonin receptor signaling alters differentiation outcomes of **Sox10+** *sacral neural crest progenitors* **in vitro**

Given the significant enrichment of serotonin receptors in differentiating pelvic ganglia and the sustained up-regulation of *Htr3a* across all the stages we examined, we asked what effect stimulating serotonin receptors, and 5-HT3A in particular, has on the development of sacral neural crest cells that contribute to pelvic innervation. To address this question, we micro-dissected LUT tissues, comprised of fetal bladder, PG, urethra, and genital tubercle from 14.5 dpc *Sox10*-H2BVenus+ fetuses, dissociated and flow-sorted H2BVenus+ neural crest-derived progenitors directly into low density adherent culture conditions (White et al., 2001;Bixby et al., 2002;Kruger et al., 2002;Walters et al., 2010). Under such conditions, individual progenitors form spatially distinct colonies, such that the proportions of differentiated cell types within colonies grown during exposure to serotonin-targeting drugs can thereby be assessed. Because we identified expression of multiple 5-HTRs in fetal pelvic ganglia, we opted to perturb 5-HTR signaling with a receptor antagonist, clozapine, that broadly targets several 5-HTRs. Treatment of sacral neural crest progenitor cells with clozapine, an antagonist of multiple serotonin receptors, led to a modest disruption of differentiation outcomes (Figure 2.3). Clozapine treatment increased the percentage of purely neuronal colonies compared to control cultures (45.2% ± 1.69% vehicle control, 50.9% ± 1.7% clozapine, p=0.0201, Welch's t-test). Additionally, mixed neuron/glia colonies were reduced (12.8 ± 1.38% vehicle control vs. 8.82 ± 1.28% clozapine, p=0.0367, Welch's t-test), as well as neuronal/glial/myofibroblast colonies (8.28 ± 1.21% untreated vs. 3.08 ± 0.81% clozapine, p=0.0005, Welch's t-test). Due to the significant enrichment of 5-HT3A in fetal pelvic ganglia, we also asked if over-stimulating 5-HT3A would affect sacral neural crest differentiation outcomes. Treatment of sacral neural crest

progenitors with a 5-HT3A receptor-specific agonist, SR57227A (Bachy et al., 1993), resulted in a dramatic reduction in purely neuronal colonies (45.2% ± 1.69% untreated vs. 31.3 ± 1.33% SR57227A, p=7.179e-09, Welch's t-test). Alongside the reduction in neuronal colonies, over-stimulating 5-HT3A with SR57227A also increased the percentage of mixed neuronal/myofibroblast colonies compared to the vehicle control (32.2 ± 2.04% vehicle control vs. 51.2 ± 1.78% SR57227A, p=5.236e-10, Welch's t-test). Similar to clozapine treatment, SR57227A also led to a reduction in mixed neuronal/glial colonies compared to the vehicle control (12.8 ± 1.38% vehicle control vs. 8.93 ± 1.18% SR57227A, p=0.0345, Welch's t-test). From these experiments, we conclude that perturbing serotonin receptor signaling, especially the 5-HT3A receptor, alters the differentiation outcomes of sacral neural crest progenitors *in vitro*.

Table 2.4 Effects of serotonergic drugs on sacral neural crest developmental potential

Treatment	Number of Total Colonies	Percentage of Cell Type						
		N	N+G	G	N+M	M	G+M	N+G+M
Untreated (n=45)	21.4 ± 5.4	45.2 ± 1.69	12.8 ± 1.38	1.1 ± 0.41	32.2 ± 2.04	0.3 ± 0.19	0.0 ± 0.0	8.3 ± 1.20
SR57227A (n=42)	22.1 ± 3.5	31.3 ± 1.33***	8.9 ± 1.18*	1.0 ± 0.37	51.2 ± 1.78***	1.0 ± 0.31	0.1 ± 0.11	6.4 ± 0.80
Clozapine (n=33)	24.4 ± 5.5	50.9 ± 1.72*	8.8 ± 1.28*	0.5 ± 0.24	36.6 ± 2.23	0.1 ± 0.09	0.0 ± 0.0	3.1 ± 0.81**

Percentages of colony types (N = neuronal, G = glial, M= myofibroblasts) relative to the total number of colonies per well. Values shown are average ± SEM. SR57227A and clozapine treated were compared to untreated colonies. *p<0.05, **p<0.01, ***p<0.001, assessed by Welch's t-test.

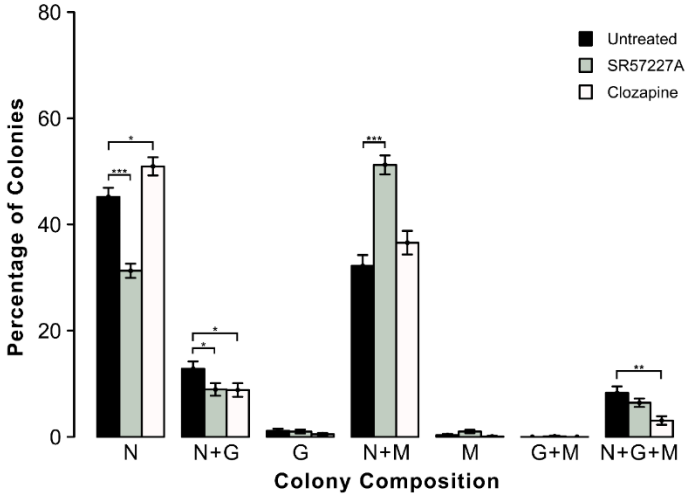

Figure 2.3 Pharmacologically perturbing serotonin signaling alters differentiation outcomes of sacral neural crest progenitors *in vitro*. *Sox10*-H2BVenus+ sacral neural crest cells were flow-sorted from 14.5dpc pelvic ganglia then grown in culture and treated with drug vehicle (negative control), SR57227A (specific 5-HT3A receptor agonist), or clozapine (mixed agonist/antagonist of several serotonin receptors). Mean ± SEM percentage of cell colonies labeled with differentiation markers of neurons (Peripherin), glia (GFAP), and smooth muscle (Smooth Muscle Actin) after exposure to either vehicle control, SR57227A, or clozapine. *p<0.05, **p<0.01, ***p<0.001, assessed by Welch's t-test. n=33-45 colonies per treatment condition.

Over-stimulating 5-HT3A in pelvic ganglia explants attenuates neurite outgrowth in vitro

Given the significant effects that over-stimulating the 5-HT3 receptor had on the developmental potential of sacral neural crest progenitors grown in culture, we sought to determine how intact pelvic ganglia explants would respond to increasing dosages of the 5-HT3 agonist SR57227A. We sub-dissected pelvic ganglia from 13.5 dpc *Sox10*-H2BVenus animals and cultured them in a collagen matrix over several days using previously described culture conditions (Stewart et al., 2008). Pelvic ganglia explants were exposed to either the drug vehicle, 25μM, or 50μM of SR57227A. Compared to vehicle-treated control pelvic ganglia explants, SR57227A-treated cultures showed diminished neurite outgrowth in a dose-dependent manner (Figure 2.4, Panels A-C'). Sholl analysis of neurite arbor complexity revealed a

substantial decrease in the average number of radii intersecting neuritic branches (Figure 2.4 Panel D, p=2.319e-08, one-way ANOVA with Tukey's HSD post-hoc test). Additionally, the average size of the arbor, as measured by the enclosing radius of the explant, was significantly reduced in SR57227A-treated cultures (Figure 2.4, Panel E, p=7.575e-07, one-way ANOVA with Tukey's HSD post-hoc test). From these experiments we conclude that normal arborization in developing pelvic ganglia is influenced by 5-HT3A receptor signaling.

Discussion

A variety of clinical disorders originate from disruption of lower urinary tract innervation. Pelvic surgeries such as prostatectomy (Cornu et al., 2014), hysterectomy (Wit and Horenblas, 2014;Laterza et al., 2015), or colo-rectal cancer surgery lead to damage to pelvic nerves and subsequent incontinence. Additionally, hyper-innervation of the bladder occurs in chronic interstitial cystitis (Dickson et al., 2006;Boudes et al., 2013). As a result, there is great need to understand the developmental processes that regulate pelvic innervation both for regenerative strategies to restore bladder innervation as well as for identification of agents to modulate aberrant innervation. To date, surprisingly little is known about the developmental signaling factors that govern pelvic ganglia neurogenesis and neuronal maturation. In the current study, we report a transcriptome profiling data set characterizing gene expression patterns in fetal mouse pelvic ganglia during stages of autonomic neurogenesis. We identified significant up-regulation of the type 3 serotonin receptor (5-HT3A, encoded by Htr3a) in early Sox10+ sacral neural crest progenitors, and determined that serotonin signaling via 5-HT3 plays a key role in neural crest differentiation outcomes and neuronal maturation.

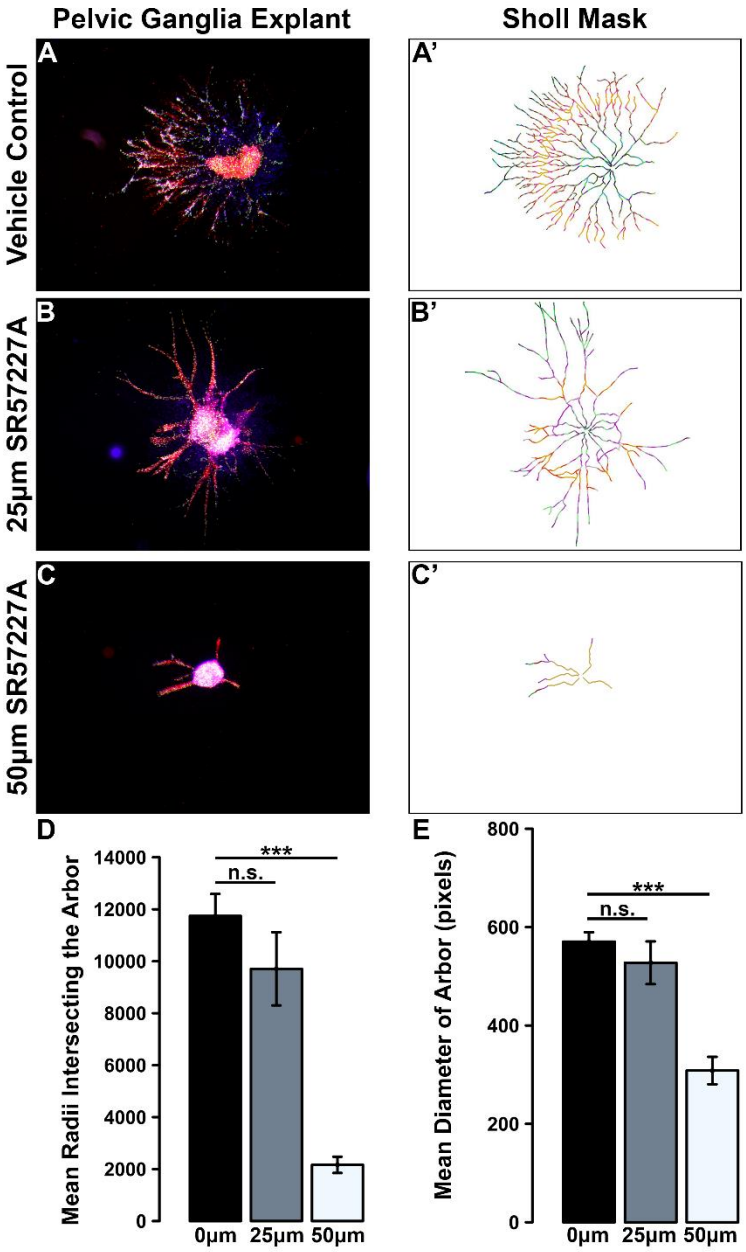

Figure 2.4 Over-stimulating 5-HT3 in cultured fetal pelvic ganglia explants diminishes neurite arbor complexity. *Sox10*-H2BVenus 13.5dpc pelvic ganglia explants treated with 5-HT3A receptor agonist SR57227A exhibit a severe reduction in the elaboration and complexity of neuronal processes compared to vehicle control. (**A-C**) Stereofluorescent microscope images of pelvic ganglia explants treated with drug vehicle (**A**), 25µm SR57227A (**B**), or 50µm SR57227A (**C**). (**A'-C'**) Sholl masks generated for pelvic ganglia explant neuronal fiber tracings that demarcate concentric radii used to quantify neurite arbor complexity and growth. (**D**) Average number of intersections of the neurite arbor with Sholl radii plotted for each treatment group. (**E**) Average diameter of the outer-most circle drawn that encompasses the entire arbor. For both plots, black brackets are SEM. n=12-14 pelvic ganglia explants per treatment group. ***= $p<0.001$, n.s. = not statistically significant, assessed via one-way ANOVA with Tukey's Honest Significant Difference test to correct for multiple comparisons.

In this study, we employed a well-characterized tool, *Sox10*-H2BVenus transgenic mice for capture and subsequent analysis of sacral neural crest cells (Corpening et al., 2011). The transcription actor *Sox10* is a critical regulator of neural crest development and a well-established marker of neural crest-derived lineages. The *Sox10*-H2BVenus transgenic line faithfully recapitulates endogenous *Sox10* gene expression (Corpening et al., 2011) and allowed us to visualize differentiating pelvic ganglia for capture of autonomic pelvic ganglia neurons in the midst of neurogenesis. The increased expression of transcription factors *Phox2b, Gata2/3,* and *Hand2* were expected in our analysis because these genes have well-established roles in orchestrating autonomic neurogenesis (Martik and Bronner, 2017). Among the most up-regulated genes expressed in differentiating neurons of pelvic ganglia, we were particularly interested in serotonin receptors for two reasons. First, serotonin receptor signaling plays critical roles in brain development (Lauder and Krebs, 1978;Mazer et al., 1997;Gaspar et al., 2003;Bonnin et al., 2007), but has not been pursued in the context of autonomic neurogenesis. Second, targeting 5-HT receptors has therapeutic potential, given the wide variety of available pharmacological agents that act of 5-HTR signaling pathways.

When we treated sacral neural crest progenitor cells with clozapine (mixed 5-HT2 receptor antagonist), we observed a modest effect on differentiation outcomes, particularly an increase in purely neuronal colonies of cells. Although clozapine is known to antagonize multiple serotonin receptors (Meltzer, 1994), the 5-HT2A receptor is the most likely mediator of increased neuronal differentiation. Within the 5-HT2 receptor family, clozapine exhibits the highest binding affinity for 5-HT2A (Schmidt et al., 1995;Yadav et al., 2011), and we readily detected 5-HT2A in our RT-PCR experiment. Interestingly, a prior study using *Htr2a* knockout animals determined that 5-HT2A is highly expressed in neural-crest derived enteric neurons, but

loss of this receptor did not alter enteric neuronal numbers, although proportions of neuronal subtypes were not determined (Fiorica-Howells et al., 2002). Our study, in conjunction with this prior work, underlines the need for further study of 5-HT2A in the development of neural crest lineages.

In contrast to treatment with clozapine, exposing sacral neural crest progenitors to the 5-HT3-specific agonist SR57227A *in vitro* led to a significant reduction in neuronal fate acquisition, with a concurrent increase in myofibroblast differentiation. To our knowledge, this is the first study to implicate the 5-HT3 receptor in specification of any cell type. This receptor is the only member of the 5-HTR family that functions as a ligand gated ion channel (Derkach et al., 1989) and is highly permeable to calcium. Given the extensive roles of calcium second messenger signaling in neuronal development (reviewed extensively in (Rosenberg and Spitzer, 2011)), it is possible that neuronal specification may be influenced by calcium flux through this receptor. Further studies employing the use of calcium imaging in sacral neural crest progenitors will be valuable in determining if this is the case.

In addition to mediating neural crest differentiation potential, we found that over-stimulating the 5-HT3 receptor with SR57227A led to a significant reduction in neurite arbor complexity. These findings are consistent with phenotypes reported in a prior study of 5-HT3 receptor mutant mice, *Htr3a*$^{vs/vs}$, in which 5-HT3 receptors are hyper-sensitive to serotonin binding and allow greater ion flux into the channel than wild type receptors (Bhattacharya et al., 2004). The bladder wall in *Htr3a*$^{vs/vs}$ mice displayed a deficit of neuronal processes, consistent with the reduced neurite arbor complexity we observed in the context of 5-HT3 receptor agonist treatment. *Htr3a*$^{vs/vs}$ animals also exhibit bladder smooth muscle hyperplasia, which is comparable to the increased myofibroblast differentiation we observed in SR57227A-treated

cultures. In contrast, further analysis conducted in our group found that the loss of the 5-HT3 receptor in *Htr3a* knockout mice results in increased innervation density in bladder smooth muscle (see Chapter IV, (Ritter et al., 2017)). These findings collectively suggest that signaling via the 5-HT3 receptor is crucial for normal development of pelvic innervation and plays an important role in neuronal morphological growth and maturation in an activity-dependent manner. Although our group and others have demonstrated roles for 5-HT3 signaling in neuronal process growth, the downstream molecular components mediating these effects remain unknown. Further studies will be needed to determine how 5-HT3 activity regulates neuronal architecture during development.

Our discovery of the importance of serotonin receptor signaling in the development of these progenitor cells represents one of myriad applications of this transcriptome profiling study. Regional differences between axial levels of neural crest populations are well established, but the sacral neural crest is significantly understudied compared to the cranial and truncal populations. Our transcriptome data set is a powerful resource for research groups interested in the identification of unique drivers of sacral neural crest development and comparing salient gene expression patterns between neural crest cell populations.

Collectively, the experimental findings presented contribute to our understanding of signaling pathways that mediate sacral neural crest development and provide a valuable source of gene expression data that will fuel future studies of autonomic neurogenesis.

Acknowledgements

We gratefully acknowledge and thank the staff of the Cell Imaging Shared Resource (CISR) core at Vanderbilt University, which is supported by NIH grants CA68485, DK20593,

P30 DK58404, DK59637, and EY08126. We also thank the staff of the Vanderbilt University Flow Cytometry Shared Resource for assistance with flow sorting and analysis. The Flow Core is supported by the Vanderbilt Ingram Cancer Center (P30 CA68485) and the Vanderbilt Digestive Disease Research Center (P30 DK058404). We thank Dr. Sean Levy and the staff of the Vanderbilt Microarray Shared Resource for experimental support in generation of the microarray data. We thank Dr. Vanda Lennon for generously providing the Hu C/D antibody. Work in EMS^2's laboratory was supported by funding from US National Institutes of Health grants R01-DK078158, RC1-DK086594, U01-DK101038, and a Pilot Award from the Vanderbilt Conte Center Grant (P50 MH096972) to EMS^2 and F31-DK097938 to KER.

References

Bachy, A., Heaulme, M., Giudice, A., Michaud, J.-C., Lefevre, I.A., Souilhac, J., Manara, L., Emerit, M.B., Gozlan, H., Hamon, M., Keane, P.E., Soubrie, P., and Le Fur, G. (1993). SR57227A: a potent and selective agonist at central and peripheral 5-HT3 receptors in vitro and in vivo. *European Journal of Pharmacology* 237**,** 299-309.

Bhattacharya, A., Dang, H., Zhu, Q.M., Schnegelsberg, B., Rozengurt, N., Cain, G., Prantil, R., Vorp, D.A., Guy, N., Julius, D., Ford, A.P., Lester, H.A., and Cockayne, D.A. (2004). Uropathic observations in mice expressing a constitutively active point mutation in the 5-HT3A receptor subunit. *J Neurosci* 24**,** 5537-5548. doi: 10.1523/JNEUROSCI.5658-03.2004.

Bixby, S., Kruger, G.M., Mosher, J.T., Joseph, N.M., and Morrison, S.J. (2002). Cell-intrinsic differences between stem cells from different regions of the peripheral nervous system regulate the generation of neural diversity. *Neuron* 35**,** 643-656.

Bonnin, A., Torii, M., Wang, L., Rakic, P., and Levitt, P. (2007). Serotonin modulates the response of embryonic thalamocortical axons to netrin-1. *Nat Neurosci* 10**,** 588-597. doi: 10.1038/nn1896.

Boudes, M., Uvin, P., Pinto, S., Freichel, M., Birnbaumer, L., Voets, T., De Ridder, D., and Vennekens, R. (2013). Crucial role of TRPC1 and TRPC4 in cystitis-induced neuronal sprouting and bladder overactivity. *PLoS One* 8**,** e69550. doi: 10.1371/journal.pone.0069550.

Cornu, J.N., Melot, C., and Haab, F. (2014). A pragmatic approach to the characterization and effective treatment of male patients with postprostatectomy incontinence. *Curr Opin Urol* 24**,** 566-570.

Corpening, J.C., Deal, K.K., Cantrell, V.A., Skelton, S.B., Buehler, D.P., and Southard-Smith, E.M. (2011). Isolation and live imaging of enteric progenitors based on Sox10-Histone2BVenus transgene expression. *genesis* 49**,** 599-618. doi: 10.1002/dvg.20748.

Coyne, K.S., Wein, A., Nicholson, S., Kvasz, M., Chen, C.I., and Milsom, I. (2014). Economic burden of urgency urinary incontinence in the United States: a systematic review. *J Manag Care Pharm* 20**,** 130-140. doi: 10.18553/jmcp.2014.20.2.130.

Derkach, V., Surprenant, A., and North, R.A. (1989). 5-HT3 receptors are membrane ion channels. *Nature* 339**,** 706-709.

Diboun, I., Wernisch, L., Orengo, C.A., and Koltzenburg, M. (2006). Microarray analysis after RNA amplification can detect pronounced differences in gene expression using limma. *BMC Genomics* 7. doi: 10.1186/1471-2164-7-252.

Dickson, A., Avelino, A., Cruz, F., and Ribeiro-Da-Silva, A. (2006). Peptidergic sensory and parasympathetic fiber sprouting in the mucosa of the rat urinary bladder in a chronic model of cyclophosphamide-induced cystitis. *Neuroscience* 141**,** 1633-1647. doi: 10.1016/j.neuroscience.2006.06.007.

Ferreira, T.A., Blackman, A.V., Oyrer, J., Jayabal, S., Chung, A.J., Watt, A.J., Sjostrom, P.J., and Van Meyel, D.J. (2014). Neuronal morphometry directly from bitmap images. *Nat Methods* 11**,** 982-984.

Fiorica-Howells, E., Hen, R., Gingrich, J., Li, Z., and Gershon, M.D. (2002). 5-HT(2A) receptors: location and functional analysis in intestines of wild-type and 5-HT(2A) knockout mice. *Am J Physiol Gastrointest Liver Physiol* 282**,** G877-893. doi: 10.1152/ajpgi.00435.2001.

Gaspar, P., Cases, O., and Maroteaux, L. (2003). The developmental role of serotonin: news from mouse molecular genetics. *Nat Rev Neurosci* 4**,** 1002-1012. doi: 10.1038/nrn1256.

Irizarry, R.A., Hobbs, B., Collin, F., Beazer-Barclay, Y.D., Antonellis, K.J., Scherf, U., and Speed, T.P. (2003). Exploration, normalization, and summaries of high density oligonucleotide array probe level data. *Biostatistics* 4**,** 249-264.

Kim, J.H., Lee, S.R., Song, Y.S., and Lee, H.J. (2013). Stem cell therapy in bladder dysfunction: where are we? And where do we have to go? *Biomed Res Int* 2013**,** 930713. doi: 10.1155/2013/930713.

Kruger, G.M., Mosher, J.T., Bixby, S., Joseph, N.M., Iwashita, T., and Morrison, S.J. (2002). Neural crest stem cells persist in the adult gut but undergo changes in self-renewal, neuronal subtype potential, and factor responsiveness. *Neuron* 35**,** 657-669.

Laterza, R.M., Sievert, K.D., De Ridder, D., Vierhout, M.E., Haab, F., Cardozo, L., Van Kerrebroeck, P., Cruz, F., Kelleher, C., Chapple, C., Espuna-Pons, M., and Koelbl, H. (2015). Bladder function after radical hysterectomy for cervical cancer. *Neurourol Urodyn* 34**,** 309-315.

Lauder, J.M., and Krebs, H. (1978). Serotonin as a differentiation signal in early neurogenesis. *Dev Neurosci* 1**,** 15-30.

Martik, M.L., and Bronner, M. (2017). Regulatory Logic Underlying Diversification of the Neural Crest. *Trend Genet* 33**,** 715-727.

Mazer, C., Muneyyirci, J., Taheny, K., Raio, N., Borella, A., and Whitaker-Azmitia, P.M. (1997). Serotonin depletion during synaptogenesis leads to decreased synaptic density and learning deficits in the adult rat: a possible model of neurodevelopmental disorders with cognitive deficits. *Brain Res* 760**,** 68-73.

Meijering, E., Jacob, M., Sarria, J.C., Steiner, P., Hirling, H., and Unser, M. (2004). Design and validation of a tool for neurite tracing and analysis in fluorescence microscopy images. *Cytometry A* 58**,** 167-176. doi: 10.1002/cyto.a.20022.

Meltzer, H.Y. (1994). An overview of the mechanism of action of clozapine. *J Clin Psychiatry* 55**,** 47-52.

Payne, S.C., Belleville, P.J., and Keast, J.R. (2015). Regeneration of sensory but not motor axons following visceral nerve injury. *Exp Neurol* 266**,** 127-142. doi: 10.1016/j.expneurol.2015.02.026.

Ritter, K.E., Wang, Z., Vezina, C.M., Bjorling, D.E., and Southard-Smith, E.M. (2017). Serotonin Receptor 5-HT3A Affects Development of Bladder Innervation and Urinary Bladder Function. *Frontiers in Neuroscience* 11. doi: 10.3389/fnins.2017.00690.

Rosenberg, S.S., and Spitzer, N.C. (2011). Calcium signaling in neuronal development. *Cold Spring Harb Perspect Biol* 3**,** a004259. doi: 10.1101/cshperspect.a004259.

Schmidt, C.J., Sorensen, S.M., Kehne, J.H., Carr, A.A., and Palfreyman, M.G. (1995). The role of 5-HT2A receptors in antipsychotic activity. *Life Sci* 56**,** 2209-2222.

Shaban, A., Drake, M.J., and Hashim, H. (2010). The medical management of urinary incontinence. *Auton Neurosci* 152**,** 4-10. doi: 10.1016/j.autneu.2009.09.022.

Stewart, A.L., Anderson, R.B., Kobayashi, K., and Young, H.M. (2008). Effects of NGF, NT-3 and GDNF family members on neurite outgrowth and migration from pelvic ganglia from embryonic and newborn mice. *BMC Dev Biol* 8**,** 73. doi: 10.1186/1471-213X-8-73.

Walters, L.C., Cantrell, V.A., Weller, K.P., Mosher, J.T., and Southard-Smith, E.M. (2010). Genetic background impacts developmental potential of enteric neural crest-derived progenitors in the Sox10Dom model of Hirschsprung disease. *Hum Mol Genet* 19**,** 4353-4372.

White, P.M., Morrison, S.J., Orimoto, K., Kubu, C.J., Verdi, J.M., and Anderson, D.J. (2001). Neural crest stem cells undergo cell-intrinsic developmental changes in sensitivity to instructive differentiation signals. *Neuron* 29**,** 57-71.

Wiese, C.B., Deal, K.K., Ireland, S.J., Cantrell, V.A., and Southard-Smith, E.M. (2017). Migration pathways of sacral neural crest during development of lower urogenital tract innervation. *Dev Biol* 429**,** 356-369.

Wiese, C.B., Fleming, N.L., Buehler, D.P., and Southard-Smith, E.M. (2013). A Uchl1-Histone2BmCherry:GFP-gpi BAC transgene for imaging neuronal progenitors. *Genesis* 51**,** 852-861.

Wiese, C.B., Ireland, S., Fleming, N.L., Yu, J., Valerius, M.T., Georgas, K., Chiu, H.S., Brennan, J., Armstrong, J., Little, M.H., Mcmahon, A.P., and Southard-Smith, E.M. (2012). A genome-wide screen to identify transcription factors expressed in pelvic Ganglia of the lower urinary tract. *Front Neurosci* 6**,** 130. doi: 10.3389/fnins.2012.00130.

Wit, E.M., and Horenblas, S. (2014). Urological complications after treatment of cervical cancer. *Nat Rev Urol* 11**,** 110-117.

Yadav, P.N., Kroeze, W.K., Farrell, M.S., and Roth, B.L. (2011). Antagonist functional selectivity: 5-HT2A serotonin receptor antagonists differentially regulate 5-HT2A receptor protein level in vivo. *J Pharmacol Exp Ther* 339**,** 99-105.

CHAPTER III

DYNAMIC EXPRESSION OF SEROTONIN RECEPTOR 5-HT3A IN DEVELOPING SENSORY INNERVATION OF THE LOWER URINARY TRACT

This chapter is a modified version of a published article (Ritter and Southard-Smith, 2017). Frontiers Publishing Group copyright policy states that authors retain the copyright of their work and are permitted to reproduce material from their own published articles, provided that the work is properly cited.

Introduction

The lower urinary tract (LUT), comprised of the bladder and urethra, relies on autonomic and sensory neural input for storage and appropriate expulsion of urine from the body. Damage to or degeneration of any neural component of this system can lead to chronic pelvic pain or bladder dysfunction, which can severely diminish patient quality of life. Additionally, sensitization of sensory components that originate within the dorsal root ganglia can occur in response to bladder inflammation or chronic interstitial cystitis. Current treatment options for these conditions tend to affect many diverse neuronal populations and thus have numerous adverse side effects. Better understanding of the molecular features of bladder-innervating sensory afferents, and how they develop, has the potential to inform more pharmacologically specific treatment options for these conditions.

Afferent fibers supplying the LUT express a wide variety of ion channels and neuropeptides with known roles in mediating mechanosensation of bladder fullness and nociceptive processing of painful stimuli (de Groat and Yoshimura, 2009). Many of these

markers, such as TRPV1 and TRPV4, have been well-studied. Surprisingly, serotonin signaling has not been as thoroughly investigated in the LUT, despite its known importance in sensory processing in other systems. Serotonin receptors are expressed in both the central and peripheral nervous systems and are involved in every level of nociception, from the peripheral site of injury or inflammation to cognitive perception of pain (Gold and Gebhart, 2010). Serotonin can exert both pronociceptive and antinociceptive effects, depending on the receptors activated in peripheral tissues and in the spinal cord. Of the 14 different serotonin receptor subtypes, 5-HT3A (encoded by the *Htr3a* gene) is known to be an especially important mediator of nociception (Zeitz et al., 2002;Kayser et al., 2007), including visceral pain. Specifically, antagonizing 5-HT3A alleviates pain associated with intestinal inflammation and irritable bowel syndrome (Chen et al., 2009;Walstab et al., 2010;Machu, 2011). Additionally, normal 5-HT3A receptor activity is required for adult LUT innervation and bladder function (Bhattacharya et al., 2004). However, it remains unclear what sensory subtypes normally express the 5-HT3A receptor and the extent to which 5-HT3A+ neurons contribute to normal bladder innervation.

Specification of the sensory neuronal lineage from neural crest progenitors occurs between 9.5 and 11 days post coitus (dpc) as neurogenesis progresses. Differentiation of DRG neurons and acquisition of sensory subtype-specific markers has been reported around 14.5 dpc (Marmigere and Ernfors, 2007;Bachy et al., 2011;Zou et al., 2012). Despite evidence that points to an effect of 5-HT3A on bladder function (Espey et al., 1998;Bhattacharya et al., 2004;Hall et al., 2015), no prior studies have assessed the expression of this receptor in DRG during the developmental stages when the LUT is being innervated. To date, *Htr3a* gene expression in DRG has only been characterized via in situ hybridization at a single developmental time point (Tecott et al., 1993;Diez-Roux et al., 2011). Using a transgenic *Htr3a*-EGFP mouse line in conjunction

with immunohistochemistry and retrograde tracing, we characterized the developmental expression patterns of 5-HT3A in DRG and the contribution of neurons expressing this receptor to adult urinary bladder sensory innervation. We find that this serotonin receptor exhibits dynamic expression patterns over the course of sensory neuron development and contributes to the majority of bladder innervation.

Materials and Methods

Animals

All experimental protocols were approved by the Vanderbilt University Institutional Animal Care and Use Committee (IACUC). Tg(*Htr3a*-EGFP)DH30Gsat/Mmnc (Stock Number 000273-UNC) transgenic mice were obtained from the Mutant Mouse Resource & Research Center at the University of North Carolina. *Htr3a*-EGFP mice were maintained as heterozygotes on an outbred Swiss Webster background (Taconic). All animals were provided food and water ad libitum and kept on a 14-h on, 10-h off light cycle. To obtain tissues at specific fetal stages, males and female mice were paired for overnight matings and the morning of observing a seminal plug was designated as 0.5 days post coitus (dpc).

Tissue Dissection

Harvested mouse fetuses were collected into ice-cold 1X Phosphate Buffered Saline (PBS). All fetuses and micro dissected tissues were fixed in 10% Neutral Buffered Formalin (NBF, Sigma Aldrich HT501128). Younger fetuses (10, 11, and 12 dpc) were fixed intact for 6 h at 4°C. Older fetuses, 14 and 18 dpc, were further sub-dissected to allow permeation of fixative to visceral tissues, then fixed overnight at 4°C. Because the DRG in P2 pups are small and

fragile, “backbone blocks” were dissected from axial levels T13 to S4 and fixed intact overnight at 4°C. P14, P28, and P90 DRG were sub-dissected and fixed for 3 h at 4°C. Following fixation, all tissues were washed in cold 1XPBS 3 times for 15 min with a final 1 h wash. Tissues for cryo-sectioning were infiltrated with 30% sucrose in 1XPBS and stored in the same solution at 4°C until the day of embedding and sectioning.

Immunohistochemistry Staining

Tissues were embedded in Tissue Freezing Medium (TFM, General Data, #TFM) and immediately sectioned in a Leica Cryostat (CM1900-UV). Sagittal sections 20 μm thick were mounted onto slides treated with 3-APES (Sigma-Aldrich, A3648). For the purpose of cell counting in adult DRGs, every fifth section was mounted to ensure a minimum gap of 100 μm between sections to avoid double-counting cells. Sections on slides were dried on a 37°C slide warmer for 30 min and protected from light. Slides were then immersed in 1XPBS-0.3% Triton-X100 for 5 min at room temperature to remove TFM and permeabilize the tissue for improved antibody penetration. Blocking solution comprised of 1XPBS-0.3%TritonX-100, 10% Bovine Serum Albumin (Sigma-Aldrich, A2153), and 5% Normal Donkey Serum (Jackson ImmunoResearch, 017-000-121, RRID AB_2337258) was applied to sections for a minimum of 30 min at room temperature. The same solution was used to dilute the primary and secondary antibodies. All antibodies used in this study have been thoroughly characterized and validated in knockout mouse lines, as summarized in Tables 3.1 and 3.2 (Cao et al., 1998;Baiou et al., 2007;Gevaert et al., 2007;Glaser et al., 2007;Cassereau et al., 2013). Blocking solution was tipped off the slides, and diluted primary antibody incubated on sections overnight at 4°C. On the following day, sections were rinsed with sterile 1XPBS and incubated in secondary antibody for

1 h at room temperature. After rinsing, 0.5 mM cupric sulfate in 50 mM ammonium acetate buffer (pH 5.0) was applied to tissue sections for 10 min to quench autofluorescence (Potter et al., 2012). Finally, a gentle rinse with sterile water was used to stop the CuSO4 quenching reaction. The slides were mounted and coverslipped with AquaPolyMount (PolySciences, Inc., 18606), and imaged using a Zeiss LSM 510Meta confocal microscope.

Table 3.1 Primary antibodies used in immunohistochemistry experiments

Antibody	**Host**	**Vendor**	**RRID**	**Dilution**	**Validation in Knockout Mouse Line**
CGRP	Rabbit	Sigma Aldrich, #C8198	AB_259091	1:1000	Glaser et al., 2007
Substance P	Rabbit	ImmunoStar, #20064	AB_572266	1:500	Cao et al., 1998
TRPV1	Rabbit	Neuromics, #RA14113	AB_2194034	1:500	Baiou et al., 2007
TRPV4	Rabbit	Alomone Labs, #ACC-034	AB_2040264	1:1000	Gevaert et al., 2007
NF200	Rabbit	Sigma Aldrich, #N4142	AB_477272	1:500	Cassereau et al., 2013
Hu	Human	Vanda Lennon, Mayo Clinic	N/A	1:10,000	N/A

All primary antibodies used, except for Hu, have been validated in knockout mouse lines.

Table 3.2 Secondary antibodies used in immunohistochemistry experiments

Antibody	Vendor	RRID	Dilution
Donkey anti-Rabbit Cy3	Jackson ImmunoResearch, #711-165-152	AB_2307443	1:1000
Donkey anti-Human Cy5	Jackson ImmunoResearch, #709-605-149	AB_2340578	1:200

Retrograde Tracing Surgery

Adult *Htr3a*-EGFP mice at 12 weeks of age were used for retrograde tracing experiments. Male mice were used exclusively to avoid confounding effects of estrous cycle on neuronal gene expression patterns (Monica Brauer and Smith, 2015). Injection of retrograde tracing dye, Fast Blue, into the bladder dome was carried out under general anesthesia as previously described (Payne et al., 2015). Briefly, mice were fully anesthetized via 4% isoflurane inhalation and kept on a heating pad for the duration of the surgery. An abdominal incision through the skin and muscle was made to reveal the bladder, which was then gently exteriorized and moistened with sterile saline solution. Fast Blue retrograde tracing dye (PolySciences, Inc., 17740-1) was injected in 9 different locations in 0.5 μL volumes: three sites near the bladder neck, three sites around the middle circumference of the bladder, and three sites near the apex of the bladder dome. A Hamilton syringe equipped with a 33G needle was used for dye injections to avoid bleeding and bladder tissue damage (Hamilton Company #7803-05). Sterile cotton swabs and surgical grade sterile saline were used to carefully remove any excess dye leaking from each injection site. To avoid any dye leakage from the injection sites, sterile cotton swabs and surgical grade sterile saline were used to carefully blot and wash away any excess dye. The bladder was then returned to the abdominal cavity, and the muscle and skin were subsequently sutured. Mice were treated with pre-operative and post-operative analgesic for pain management (buprenex, 0.1 mg/kg, Patterson Veterinary Supply 12496075705). To permit transport of dye back to the neuron somata in the DRG, mice were euthanized on the 7th day following dye tracer injection. Dorsal root ganglia were sub-dissected and processed as described above.

Cell Counting

Images were captured via confocal microscopy using an Olympus FV-1000 inverted confocal microscope. Images were then exported from the FluoView viewing software as.tiff files and assembled in Adobe Photoshop (2014 2.2 release, Adobe Systems Inc.). Due to heterogeneity in expression intensity of the *Htr3a*-EGFP transgene, images were minimally adjusted for optimal brightness and contrast. Numbers of neurons (Hu+ cells), *Htr3a*-EGFP+ cells, Fast Blue+ cells, and cells labeled with markers of sensory neurons were manually quantified by visual inspection of assembled confocal stacks. Proportions of neuronal subtypes were calculated as the number of immuno-positive cells for each marker over the total number of Hu+ neurons for each section. Cells were counted from three to six sections of three DRG from each axial level group from four *Htr3a*-EGFP animals.

Data Analysis

One-way ANOVA was conducted to examine differences in average *Htr3a*-EGFP and Fast Blue proportions between all axial levels examined (L1,L2; L3-L5; L6,S1). Differences in *Htr3a*-EGFP and Fast Blue proportions between specific axial level groups were analyzed by Welch's t-test. P-values were corrected for multiple comparisons; p-values less than 0.05 were considered to be statistically significant. Proportions of neuronal subtype markers between lumbar and sacral axial levels were analyzed by Welch's t-test; p-values less than 0.05 were considered to be statistically significant.

Results

Htr3a-EGFP is expressed early in sensory nervous system development

We first sought to define the time point at which *Htr3a* expression initiates during early phases of DRG neurogenesis. To visualize *Htr3a* gene expression, we employed the Tg (*Htr3a*-EGFP) DH30Gsat BAC transgenic reporter mouse line, hereafter referred to as *Htr3a*-EGFP. Validation of this reporter line as an accurate readout of endogenous gene expression has been performed by other groups (Gong et al., 2003;Vucurovic et al., 2010). Using *Htr3a*-EGFP transgenic tissues, the earliest stage at which we observed transgene expression by whole mount imaging was 10 dpc, where strong EGFP fluorescence was evident in the neural crest derived cranial ganglia and within the neural tube (Figure 3.1, Panel A). Hu C/D, a pan-neuronal marker, was strongly expressed in DRG of 11 dpc fetuses along their entire length; however, *Htr3a*-EGFP expression in the DRG was restricted to cervical and upper thoracic axial levels at this stage (data not shown). We first observed *Htr3a*-EGFP transgene expression in lumbosacral DRG that are known to provide bladder innervation at 12 pdc (Figure 3.1, Panels B and C). At this stage *Htr3a*-EGFP expression was observed in a rostral to caudal gradient among maturing DRG (Figure 3.1, Panels B and C) within a subset of Hu+ differentiated neurons (Figure 3.1, Panels D–D"). The rostral vs. caudal difference in *Htr3a*-EGFP expression intensity was prominent, with many neurons exhibiting *Htr3a*-EGFP in one lumbosacral DRG while few cells express the transgene in an immediately adjacent lumbosacral DRG. Additionally, at 12 dpc neuronal processes extending from lumbosacral DRG toward the urogenital sinus and pelvic region are visibly labeled by EGFP (Figure 3.1, Panel C). These experiments show that the 5-HT3A receptor is expressed early in neural crest-derived (Hu+) neurons and is first expressed in lumbosacral DRG by 12 dpc.

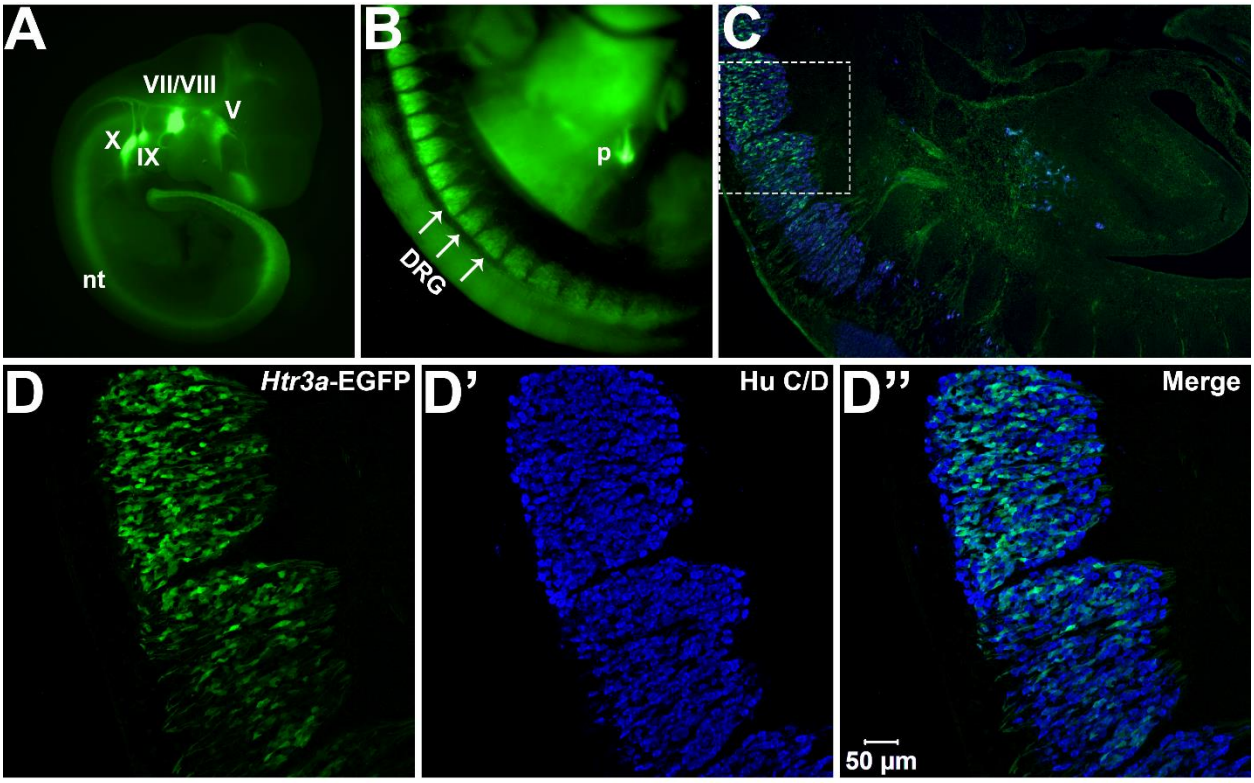

Figure 3.1 *Htr3a* is expressed early in fetal development of sensory neurons. (**A**) Lateral whole-mount image of an *Htr3a*-EGFP transgenic fetus age 10dpc. EGFP fluorescence is visible in the cranial ganglia (V, VII/VIII, IX, X) and neural tube (nt). (**B**) Lateral whole-mount view of an *Htr3a*-EGFP 12 dpc mouse fetus at the trunk axial level between the forelimbs and hindlimbs. *Htr3a*-EGFP transgene expression is evident in the dorsal root ganglia (DRG) and pancreas (p). (**C**) Sagittal cryo-section of *Htr3a*-EGFP 12 dpc fetus, stained with Hu to label all neurons (blue). EGFP expression is observed in the lumbosacral DRG. (**D-D"**) 200x magnification of two sacral DRG seen in (C). Counter-staining with Hu allows comparison of EGFP fluorescence to the total neuronal population.

Htr3a-EGFP co-localizes with neuropeptides CGRP and Substance P in a subset of DRG neurons

Calcitonin Gene Related Peptide (CGRP) and Substance P (SP) have well-established roles in modulating adult LUT function and pain processing (Laird et al., 2000;Saban et al., 2000;Kiss et al., 2001;Lagerstrom et al., 2011;Russell et al., 2014) and are normally produced by unmyelinated C-fiber nociceptive neurons (Arms and Vizzard, 2011). However, the expression patterns of these neuropeptides in developing mouse lumbosacral DRG projecting to the bladder are unknown. Using immunohistochemistry on *Htr3a*-EGFP+ transgenic tissues, we sought to define co-expression patterns of nociceptive neuropeptides and *Htr3a* in developing lumbosacral DRG. At stage 14 dpc, *Htr3a*-EGFP was strongly expressed in the majority of lumbosacral DRG neurons; however, CGRP expression was negligible at this stage (Figure 3.2. Panels A–A"). By 18 dpc, CGRP was clearly present with a continuous gradient of expression intensity that ranged from moderate to strong between individual cells. Immunostaining for CGRP was observed to co-localize with *Htr3a*-EGFP fluorescence in a subset of large-diameter neurons (Figure 3.2, Panels B–B"). We observed that *Htr3a*-EGFP transgene expression gradually becomes restricted to a subset of cells during the course of postnatal development. This restriction became notable as early as postnatal day (P)2 and was also prevalent at P14 and P28. Specifically, as DRG development progressed, the number of neurons expressing *Htr3a*-EGFP diminished. Among the neurons that remained *Htr3a*-EGFP+, there was considerable heterogeneity in expression intensity, with some cells exhibiting bright EGFP fluorescence while others are substantially dimmer. Despite the gradual restriction of *Htr3a*-EGFP expression and the heterogeneity in expression intensity between individual neurons, partial co-localization with CGRP was maintained through postnatal development and into adulthood (Figure 3.2, Panels C–E").

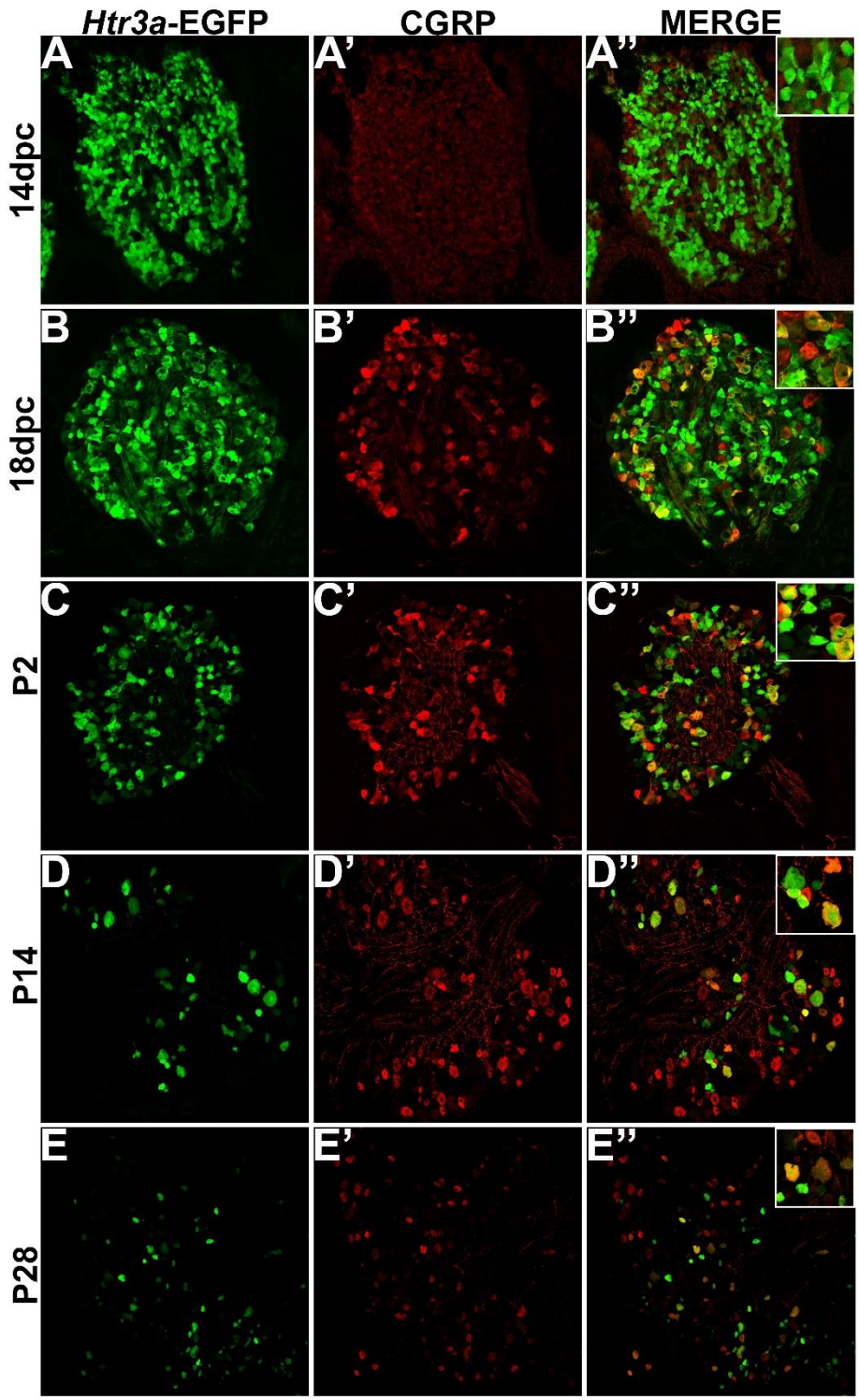

Figure 3.2 *Htr3a*-EGFP and Calcitonin Gene Related Peptide (CGRP) are co-expressed in a subset of neurons through development and adulthood. Confocal images of cryosections from *Htr3a*-EGFP transgenic animals stained with anti-CGRP are shown. All DRG presented are from lumbosacral axial levels. (**A-A"**) Sagittal section of 14 dpc fetal DRG. (**B-B"**) Sagittal section of 18 dpc fetal DRG. (**C-C"**) Coronal section of P2 DRG. (**D-D"**) Cryosection of P14 male DRG. (**E-E"**) Cryosection of P28 male DRG. All zoom insets are 400x.

While CGRP and SP are often co-expressed in afferent neurons, other evidence suggests that these neuropeptides do not always overlap and have functionally distinct roles in nociception (Su et al., 1986;Kestell et al., 2015). Given this information we examined co-expression patterns of SP and *Htr3a*-EGFP. Upon staining for SP, we noted faint and diffuse expression throughout the ganglion and partial overlap with *Htr3a*-EGFP transgene fluorescence at 14 dpc (Figure 3.3, Panels A–A"). Co-localization by immunohistochemical staining of 18 dpc DRG for SP revealed that the majority of SP+ neurons also expressed *Htr3a*-EGFP (Figure 3.3, Panels B–B"). However, shortly after birth at P2, co-localization of *Htr3a*-EGFP and SP lessened as *Htr3a*-EGFP developed a heterogeneous pattern of expression intensity among individual neurons within the ganglion (Figure 3.3, Panels C–C"). Substance P staining in postnatal DRG was more uniform; all SP+ neurons exhibited a similar level of expression intensity. At 2 and 4 weeks after birth, only a subset of DRG neurons co-expressed *Htr3a*-EGFP and SP (Figure 3.3, Panels D–E"). From these experiments we conclude that fetal lumbosacral DRG neurons widely co-express 5-HT3A and the neuropeptides CGRP and Substance P, and as postnatal maturation of the DRG occurs, expression of these markers becomes refined to a subpopulation of neurons.

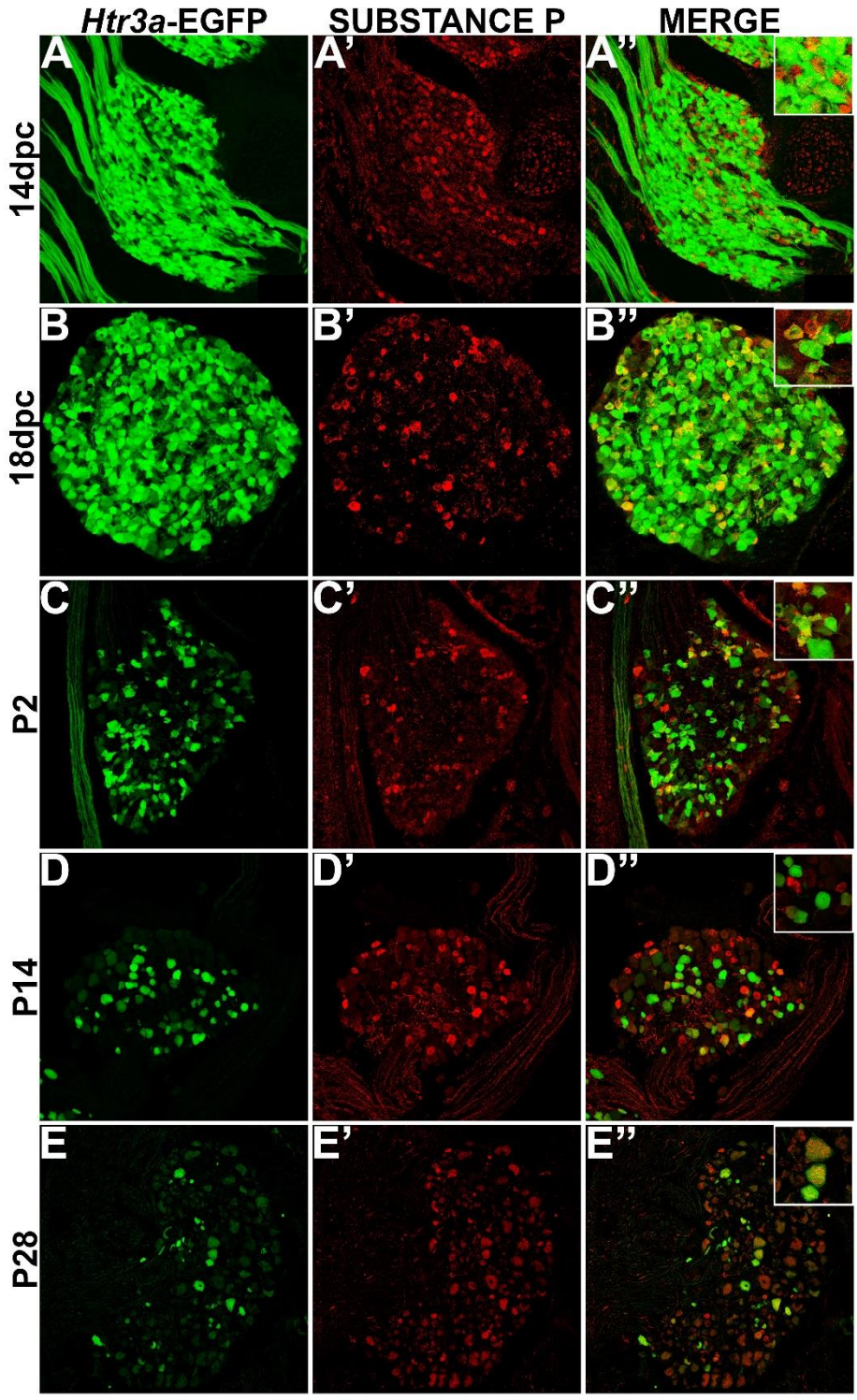

Figure 3.3 Some, but not all, *Htr3a*-EGFP neurons express Substance P neuropeptide. Confocal images of cryo-sections from *Htr3a*-EGFP transgenic animals stained with anti-Substance P are shown. All DRG presented are from lumbosacral axial levels. (**A-A"**) Sagittal section of 14 dpc fetal DRG. (**B-B"**) Sagittal section of 18 dpc fetal DRG. (**C-C"**) Coronal section of P2 DRG. (**D-D"**) Cryosection of P14 male DRG. (**E-E"**) Cryosection of P28 male DRG. All zoom insets are 400x.

The majority of TRPV1+ neurons co-express Htr3a-EGFP

Transient Receptor Potential (TRP) channels are necessary for normal adult bladder function (Birder et al., 2002;Arms and Vizzard, 2011;Yoshiyama et al., 2015). Despite the known physiological interaction of 5-HT3A and TRPV1 receptors in other sensory ganglia (Loyd et al., 2011;Kim et al., 2014), the co-localization of TRPV1 with *Htr3a* has not previously been examined during development. To address this gap in knowledge we conducted immunostaining on *Htr3a*-EGFP lumbosacral DRG for TRPV1. At 14 dpc we found diffuse, very low expression of the TRPV1 receptor (Figure 3.4, Panels A–A"). By 18 dpc, TRPV1 expression was weak and diffuse throughout the ganglion, with only a few cells exhibiting strong expression. Of the TRPV1+ cells at 18 dpc, nearly all of them co-express *Htr3a*-EGFP (Figure 3.4, Panels B–B"). TRPV1 expression increased in a subset of neurons by P2 at the same time that *Htr3a*-EGFP became less widespread and began to show heterogeneous levels of EGFP fluorescence among individual neurons (Figure 3.4, Panels C–C"). Heterogeneous expression of the *Htr3a*-EGFP transgene and partial co-localization with TRPV1 was consistently observed at P14 and P28 (Figure 3.4, Panels D–E"). From these experiments we conclude that as DRG neuronal populations mature, there is substantial overlap of *Htr3a* and TRPV1 expression, but lumbosacral DRG also exhibit many *Htr3a*+;TRPV1- neurons.

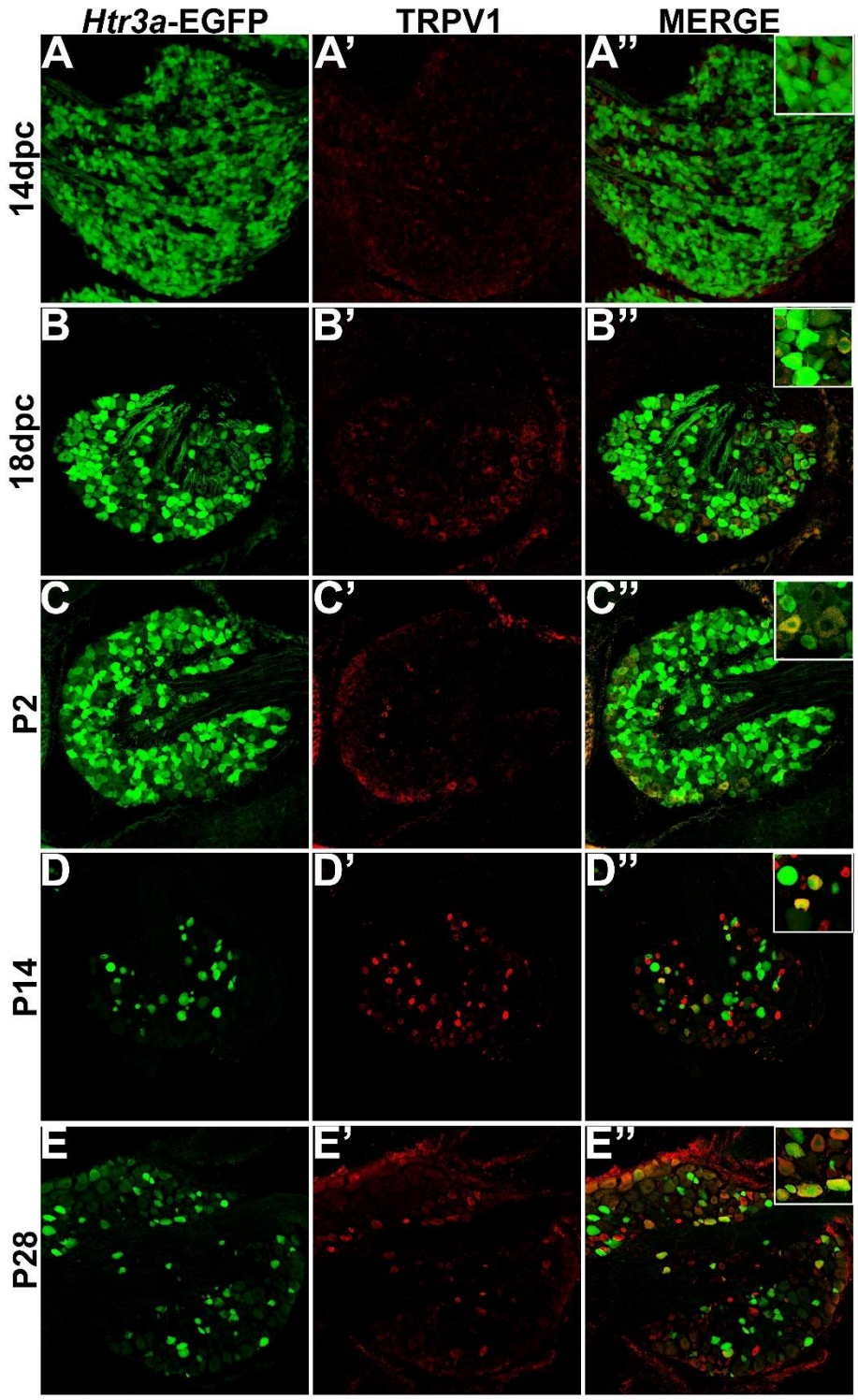

Figure 3.4 The majority of adult TRPV1+ neurons also express *Htr3a*-EGFP. Confocal images of cryo-sections from Htr3a-EGFP transgenic animals stained with anti-TRPV1 are shown. All DRG presented are from lumbosacral axial levels. (**A-A"**) Sagittal section of 14 dpc fetal DRG. (**B-B"**) Sagittal section of 18 dpc fetal DRG. (**C-C"**) Coronal section of P2 DRG. (**D-D"**) Cryosection of P14 male DRG. (**E-E"**) Cryosection of P28 male DRG. All zoom insets are 400x.

Htr3a-EGFP does not co-localize with TRPV4

Despite the known importance of TRPV4 in visceral nociception and adult bladder function (Cenac et al., 2008;Christianson et al., 2009;Everaerts et al., 2010;Franken et al., 2014;Yoshiyama et al., 2015), developmental expression patterns of this nociceptive marker in DRG have not previously been examined. To determine co-localization patterns of *Htr3a*-EGFP and TRPV4, we stained transgenic tissues for TRPV4. While we did observe positive staining in other known TRPV4+ tissues (kidney, bone, brain; data not shown), we did not detect TRPV4 in fetal or neonatal lumbosacral DRG (Figure 3.5, Panels A–C"). TRPV4 expression was detected in a subset of P14 and P28 DRG neurons; however, we did not observe overlap of TRPV4 immuno-staining with *Htr3a*-EGFP transgene expression at any of the stages examined (Figure 3.5, Panels D–E").

Htr3a-EGFP is expressed in a subset of myelinated sensory neurons

Following our characterization of *Htr3a*-EGFP in nociceptive C-fiber neurons, we next wanted to define patterns of overlap with mechanosensitive Aδ nociceptors. To this end we conducted immunohistochemical staining for Neurofilament 200 (NF200), a known marker of myelinated Aδ sensory neurons (Lawson et al., 1993). While expression of *Htr3a*-EGFP was prominent in the majority of cells in 14 dpc DRGs, NF200 was dim in a subset of cells and rarely overlapped with *Htr3a*-EGFP (Figure 3.6, Panels A–A"). By 18 dpc, however, many neurons expressed NF200 and some of these NF200+ cells also co-expressed *Htr3a*-EGFP (Figure 3.6, Panels B–B"). At P2, widespread co-expression of *Htr3a*-EGFP and NF200 occurred and was maintained at P14 and P28 (Figure 3.6, Panels C–E").

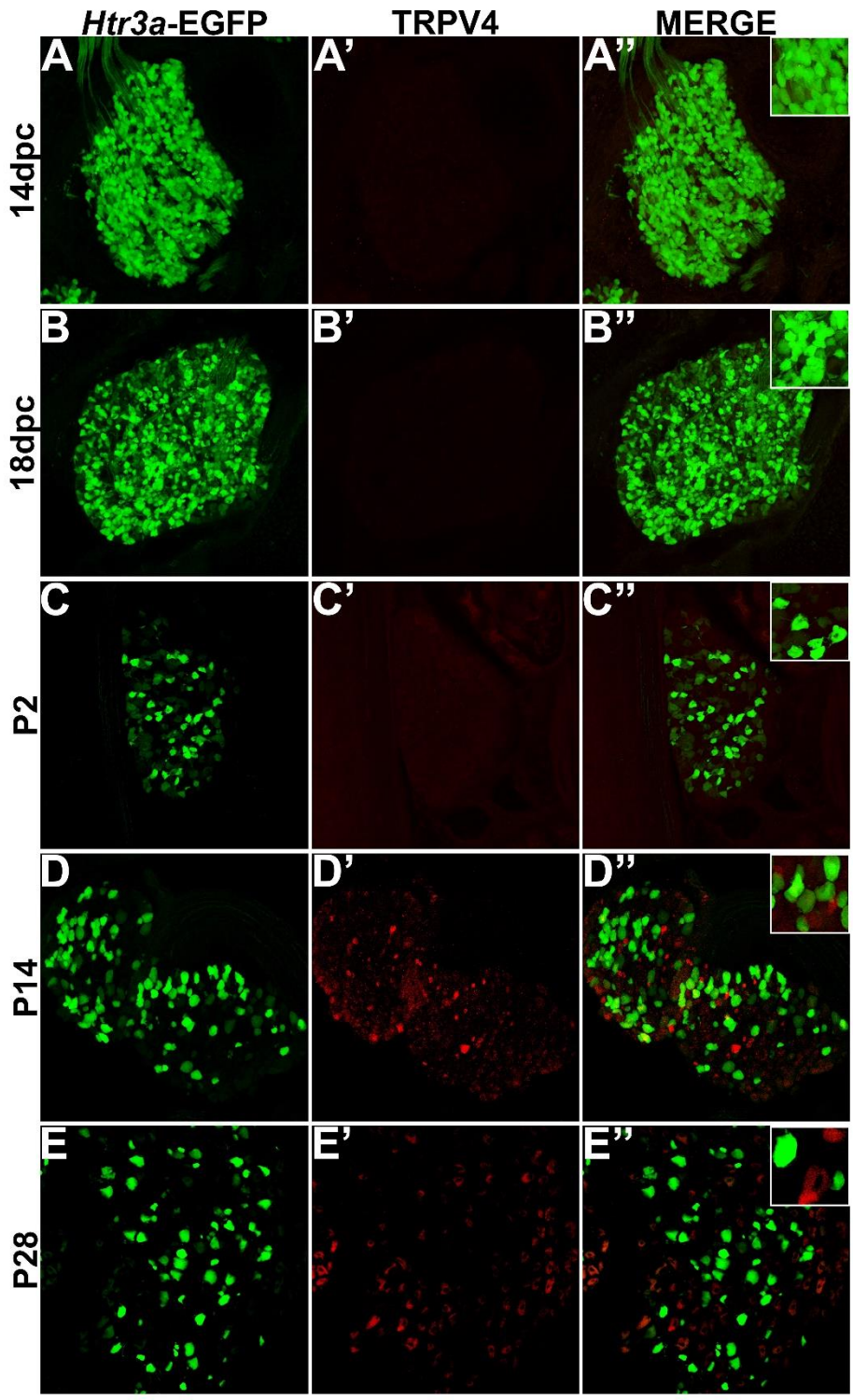

Figure 3.5 *Htr3a*-EGFP does not co-localize with TRPV4 in lumbosacral DRG. Confocal images of cryo-sections from Htr3a-EGFP transgenic animals stained with anti-TRPV4 are shown. All DRG presented are from lumbosacral axial levels. (**A-A"**) Sagittal section of 14 dpc fetal DRG. (**B-B"**) Sagittal section of 18 dpc fetal DRG. (**C-C"**) Coronal section of P2 DRG. (**D-D"**) Cryosection of P14 male DRG. (**E-E"**) Cryosection of P28 male DRG. All zoom insets are 400x.

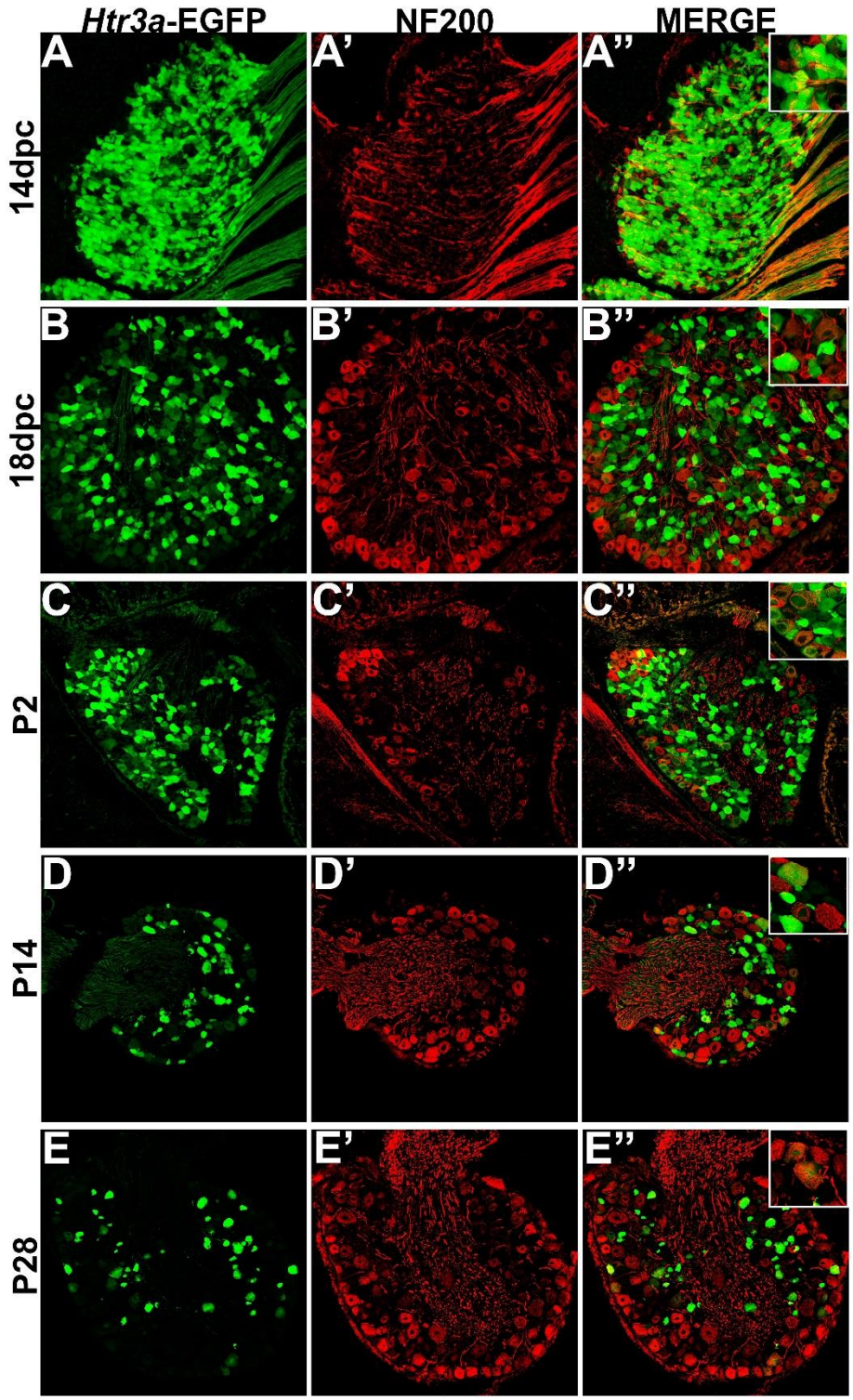

Figure 3.6 A subset of *Htr3a*-EGFP neurons express Neurofilament 200. Confocal images of cryo-sections from Htr3a-EGFP transgenic animals stained with anti-NF200 are shown. All DRG presented are from lumbosacral axial levels. (**A-A**") Sagittal section of 14 dpc fetal DRG. (**B-B"**) Sagittal section of 18 dpc fetal DRG. (**C-C"**) Coronal section of P2 DRG. (**D-D"**) Cryosection of P14 male DRG. (**E-E"**) Cryosection of P28 male DRG. All zoom insets are 400x.

Htr3a-EGFP is expressed in the majority of bladder-innervating afferent neurons

Given the known significance of 5-HT3A signaling in visceral nociception and neural control of bladder function (Zeitz et al., 2002;Bhattacharya et al., 2004;Faerber et al., 2007;Hall et al., 2015), we next sought to determine the proportion of 5-HT3A+ DRG neurons that contribute to bladder sensory innervation in adult mice. To do this, we conducted retrograde tracing of bladder innervation in adult male transgenic mice by injecting Fast Blue (FB) dye into the detrusor and quantified proportions of *Htr3a*-EGFP+ neurons whose soma were labeled with FB (Table 3.3 and Figure 3.7, Panel D). Among all three of the axial level groups, we noted significant differences in proportions of *Htr3a*-EGFP+ and FB+ neurons ($p = 1.5564e-6$ and $p = 8.8e-16$, respectively). At lumbar axial levels (L1, L2), nearly 25% of all Hu+ neurons express *Htr3a*-EGFP (Figure 3.7, Panels A–A"). Sacral axial level DRG neurons (L6, S1) are known to supply the majority of bladder sensory innervation, and we observed a similar proportion of *Htr3a*-EGFP expression in this population (23.9% of total L6, S1 Hu+ neurons expressed *Htr3a*-EGFP; Figure 3.7, Panels C–C"). Significantly fewer numbers of neurons within L3-L5 axial level DRGs, which do not contribute to bladder sensory innervation, showed *Htr3a*-EGFP+ expression (20.7% of Hu+ neurons were *Htr3a*-EGFP+, $p = 7.168e-9$ compared to L1, L2 and $p = 0.002092$ compared to L6, S1; Figure 3.7, Panels B–B"). When we quantified total numbers of neurons labeled by Fast Blue (FB+) retrograde tracing, we observed that nearly 3% of L1, L2 total neurons (Hu+) innervate the detrusor. In contrast, nearly 12% of L6, S1 neurons, a four-fold increase relative to lumbar levels, were labeled by Fast Blue in our experiments ($p = 8.8e-16$). We only very rarely observed any FB+ neurons in L3-L5 DRGs (0.067% of all Hu+ L3-L5 neurons; 26 out of 57,073 cells). The proportions of retrograde traced neurons in each of these axial levels are consistent with prior percentages reported for adult mice by other research groups (Keast and De Groat, 1992;Brumovsky et al., 2012).

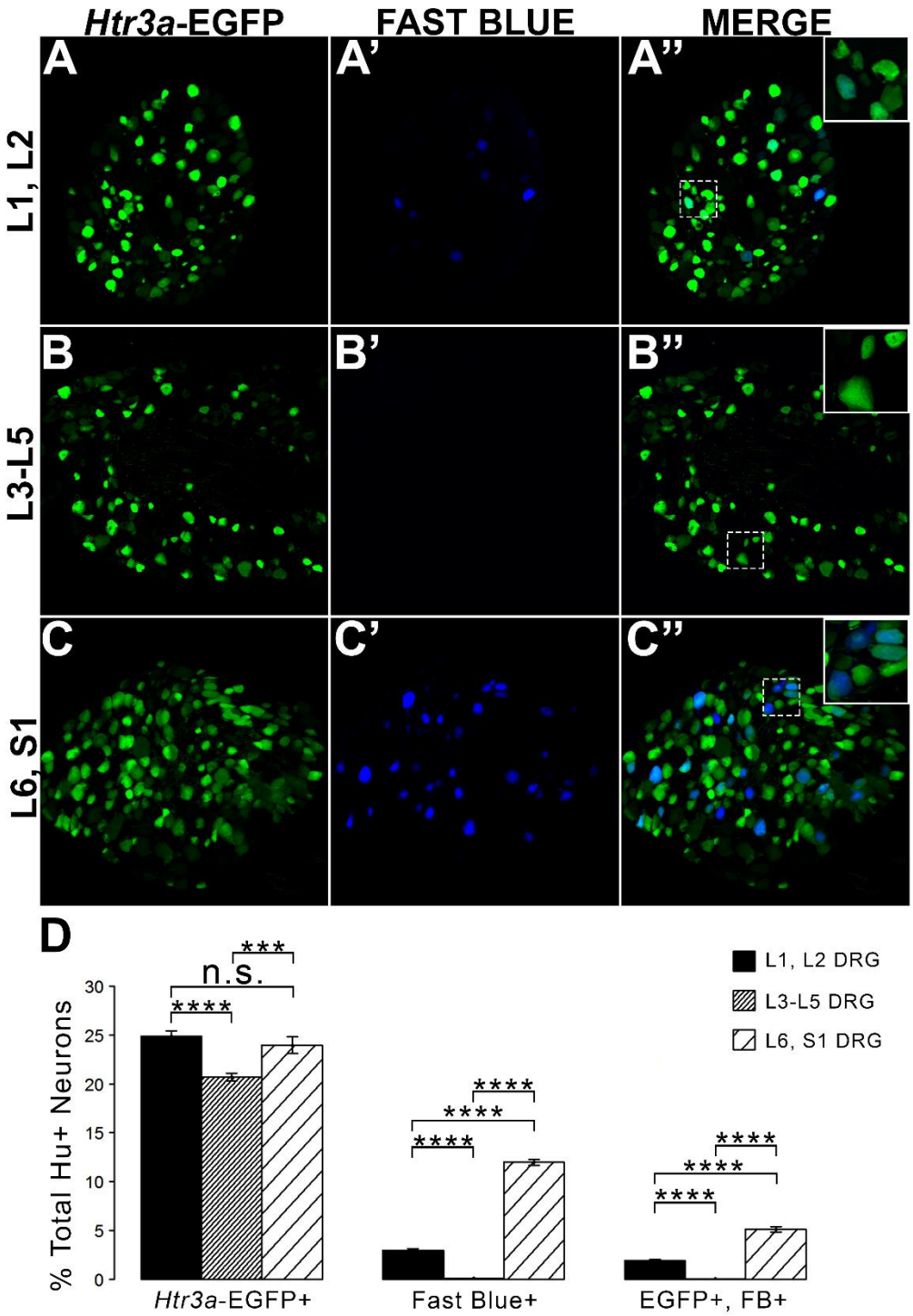

Figure 3.7 L1, L2 and L6, S1 axial levels harbor bladder-projecting neurons. Images of lumbosacral DRG harvested from *Htr3a*-EGFP transgenic male mice after retrograde tracing of bladder-projecting neurons are shown. (**A-A"**) L1, L2 axial level DRG sections. (**B-B"**) L3-L5 axial level DRG sections. (**C-C"**) L6, S1 axial level DRG sections. (**D**) Average percentages of Hu+ DRG neurons expressing *Htr3a*-EGFP transgene, labeling with Fast Blue, and co-labeling with *Htr3a*-EGFP and Fast Blue at axial level groups L1, L2; L3-L5; and L6, S1. Error bars are standard error of the mean, n=4 animals, 3-5 sections from 3 DRG quantified from each animal. ***p<0.005, ****p<0.001. Differences that are not significant (n.s.) are also indicated.

Table 3.3 Proportions of total neurons (Hu+) expressing *Htr3a*-EGFP and projecting to the bladder (Fast Blue+)

Neuronal Population	**L1, L2**	**L3-L5**	**L6, S1**
Htr3a-EGFP+/Hu+	24.89 ± 0.56%	20.68 ± 0.38%	23.97 ± 0.85%
Fast Blue+/Hu+	2.97 ± 0.14%	0.063 ± 0.025%	11.99 ± 0.30%
EGFP+, FB+/Hu+	1.92 ± 0.10%	0.027 ± 0.0099%	5.10 ± 0.28%
Total Hu+ Neurons Counted	47,208	57,073	40,415

Values are average proportions plus or minus standard error of the mean.

Table 3.4 Proportions of bladder-projecting (Fast Blue+) neuronal subtypes in lumbar (L1, L2) and sacral (L6, S1) axial levels

	Average Proportion in L1, L2	**Marker+ out of Total FB+ Neurons Counted**	**Average Proportion in L6, S1**	**Marker+ out of Total FB+ Neurons Counted**
Htr3a-EGFP+/FB+	62.75 ± 0.02%	938 out of 1431	40.29 ± 0.015%	1967 out of 4691
CGRP+/FB+	52.03 ± 4.46%	284 out of 463	36.96 ± 1.95%	494 out of 1340
EGFP+,CGRP+/FB+	36.73 ± 3.97%	198 out of 463	19.62 ± 1.51%	267 out of 1340
SubsP+/FB+	42.82 ± 3.96%	166 out of 387	37.66 ± 2.05%	464 out of 1240
EGFP+,SubsP+/FB+	32.34 ± 3.56%	124 out of 387	17.29 ± 1.75%	236 out of 1340
TRPV1+/FB+	19.74 ± 3.90%	56 out of 333	20.71 ± 2.45%	215 out of 1046
EGFP+,TRPV1+/FB+	13.99 ± 3.34%	40 out of 333	7.38 ± 1.42%	90 out of 1046
NF200+/FB+	32.42 ± 4.23%	90 out of 248	66.62 ± 3.19%	682 out of 1065
EGFP+,NF200+/FB+	16.49 ± 2.55%	51 out of 248	36.32 ± 2.54%	367 out of 1065

Proportions of each marker or combination of markers were calculated for each DRG section and were then averaged. Averages are listed as percentages of total Fast Blue+ neurons plus or minus the standard error of the mean. Total numbers of neurons counted for each marker or combination of markers, out of all Fast Blue+ neurons counted, for all sections, is listed for L1, L2 and L6, S1 axial levels.

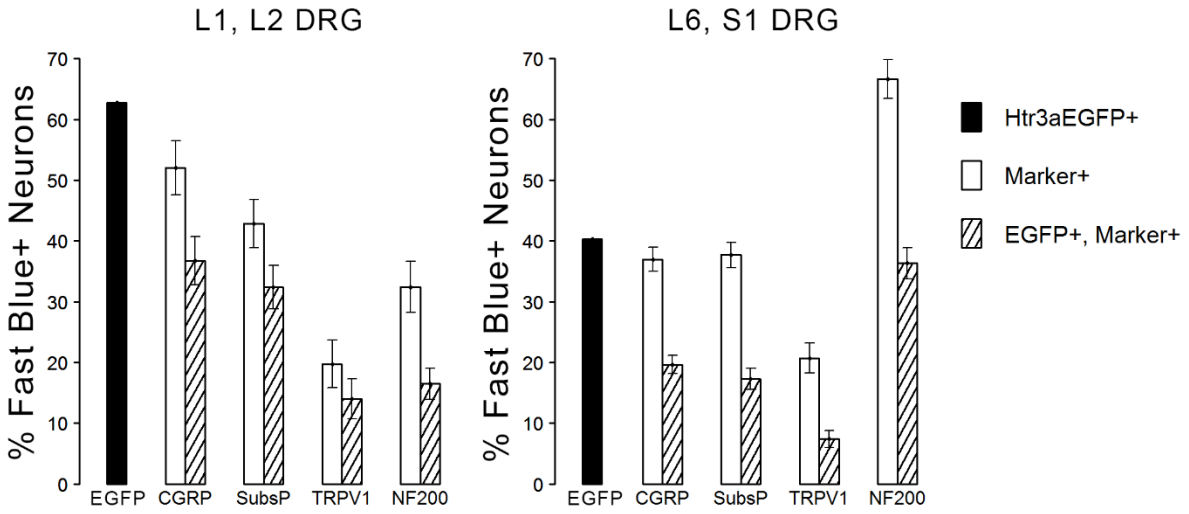

Figure 3.8 Distinct patterns of 5-HT3A receptor in subclasses of bladder-projecting afferents. Average percentages of bladder-projecting (Fast Blue+) neurons expressing the *Htr3a*-EGFP transgene and markers of sensory neurons subtypes in L1, L2 and L6, S1 DRG. Gray coloring represents L1, L2 proportions and black coloring represents L6, S1 proportions. *Htr3a*-EGFP average proportions in L1, L2 and L6, S1 DRG are the leftmost bars solid bars. Markers of sensory neuron subtypes CGRP, Substance P, TRPV1, NF200 (solid bars) and co-expression of *Htr3a*-EGFP and subtype markers (striped bars) are grouped by the marker used. Error bars are standard error of the mean, n=4 animals, 3-5 sections from 3 DRG quantified from each animal. ***p<0.005, ****p<0.001. Differences that are not significant (n.s.) are also indicated.

Given that we had observed co-localization of *Htr3a* expression with markers of multiple types of nociceptive sensory neurons during development of lumbosacral DRG, we next sought to determine whether these subclasses of bladder-innervating neurons in adult mice maintain expression of the 5-HT3A receptor. To do this, we stained DRG sections from adult *Htr3a*-EGFP mice that had been processed for Fast Blue retrograde labeling of bladder projections for CGRP, Substance P, TRPV1, and NF200 (Figure 3.8 and Table 3.4). Of all bladder-innervating neurons at the L1, L2 axial levels (that is, all Fast Blue+ neurons), the majority of them express *Htr3a*-EGFP (62.8%). In more caudal DRG (L6, S1), where the majority of bladder sensory innervation originates, 40.3% of Fast Blue+ DRG neurons express *Htr3a*-EGFP. The difference in proportions of *Htr3a*-EGFP+, FB+ neurons in the lumbar and sacral axial levels was statistically

significant (p = 4.349e-15). CGRP staining was observed in approximately half of all FB+ L1, L2 neurons (52.0%), while 36.9% of FB+ L6, S1 neurons were CGRP+ (p = 0.00292). In L1, L2 DRGs, 36.7% of FB+ neurons co-expressed *Htr3a*-EGFP and CGRP, but this proportion was reduced by half in L6, S1 neurons (19.6%) (p = 0.000162). When we stained for Substance P, we found similar expression levels in FB+ neurons in L1, L2 and L6, S1 DRG (42.8 vs. 37.7%, p = 0.251). However, we did observe a significant difference in proportions of FB+ neurons co-expressing *Htr3a*-EGFP and Substance P (32.4% of L1, L2 and 17.3% of L6, S1 FB+ neurons, p = 0.000310). Unlike the markers for peptidergic neurons, TRPV1 staining was nearly equivalent in FB+ neurons for both axial level groups; 19.7% of L1, L2 neurons were FB+ and 20.7% of L6, S1 neurons were labeled by Fast Blue (p = 0.8332). Despite the fact that proportions of TRPV1+ neurons were comparable in both lumbar and sacral bladder innervating DRG, there was a 2-fold difference in the numbers of *Htr3a*-EGFP+, TRPV1+ neurons in these locations. While 13.9% of TRPV1+ L1, L2 neurons exhibited co-expression of *Htr3a*-EGFP, only 7.4% of neurons were *Htr3a*-EGFP+, TRPV1+ among L6, S1 neurons. However, this difference did not reach statistical significance (p = 0.0741). Proportions of FB+ neurons that stained for NF200 were strikingly different from the other markers we examined. We found that 32.4% of FB+ L1, L2 neurons are NF200+, but this population was doubled in L6, S1 axial levels (66.6%) (p = 1.94e-8). NF200 and *Htr3a*-EGFP co-localize in 16.5% of FB+ L1, L2 neurons and in 36.3% of FB+ L6, S1 neurons (p = 7.544e-7). From these experiments we conclude that there are significant differences in the proportions of sensory neuron types that express the 5-HT3A receptor among the DRG groups that contribute to bladder innervation. The emerging expression patterns and intensity of expression for each of the markers we examined relative to *Htr3a* are graphically summarized in Figure 3.9.

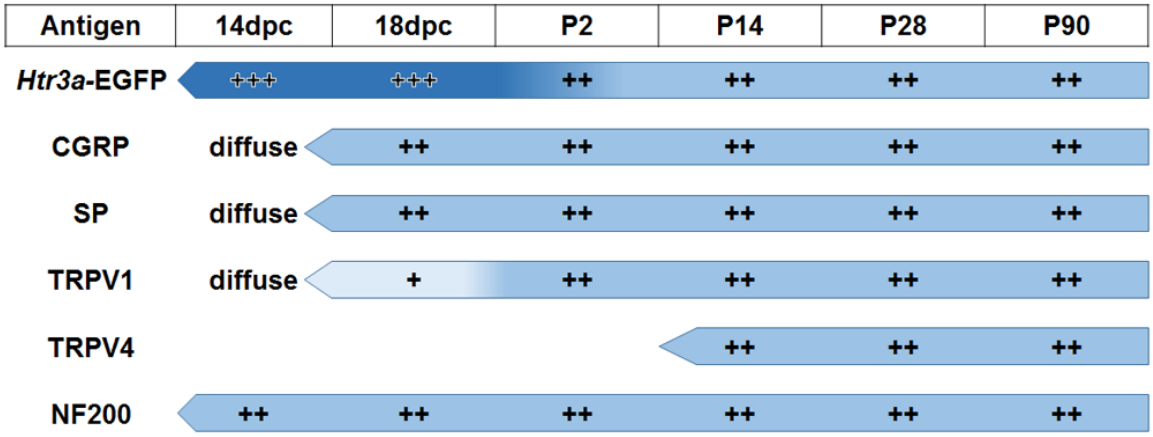

Figure 3.9 Summary of developmental expression patterns in lumbosacral *Htr3a*-EGFP+ dorsal root ganglia neurons. At 14 and 18 dpc, *Htr3a*-EGFP fluorescence is uniformly intense in the majority of lumbosacral DRG neurons. Fluorescence intensity diversifies at postnatal day 2, with some cells still strongly expressing the transgene while others are moderate or dim. This pattern is maintained through postnatal development and adulthood. Neuropeptides CGRP and Substance P are both extremely weak and diffuse at 14 dpc but their expression level increases by 18 dpc. The expression patterns observed for these makers at 18 dpc is maintained through adulthood. TRPV1 expression is negligible at fetal stages but escalates after birth at P2 and maintains expression levels. TRPV4 is not detected until P2 but is maintained from that time point to adulthood. NF200, unlike the other markers, is expressed strongly in the majority of neurons at 14 dpc and its expression levels are stable through all time points examined.

Discussion

Serotonin (5-hydroxytryptamine, 5-HT) is a known mediator of nociception, but contradictory effects are observed due to the wide variety of serotonin receptor subtypes expressed by nociceptors and their target tissues. One such receptor, 5-HT3A (encoded by *Htr3a* in mice), is a ligand-gated ion channel with previously established roles in potentiating pain (Zeitz et al., 2002;Hall et al., 2015). Despite its known expression in fetal neural crest derivatives (Tecott et al., 1993;Tecott et al., 1995), comprehensive temporal profiling of 5-HT3A in developing sensory neuron populations has not been pursued. In this study we used the *Htr3a*-EGFP transgenic reporter line as a surrogate in combination with immunohistochemical labeling to identify neuron populations expressing 5-HT3A relative to a variety of nociceptive markers in normal fetal and postnatal DRG development.

We first noted expression of the *Htr3a*-EGFP transgene at 10 dpc in the neural tube and cranial ganglia, followed by up-regulation in lumbosacral DRG by 12 dpc. The early and sustained expression in sensory lineages suggests a functional role for 5-HT3A in differentiation of sensory neurons; however, the specific effects of this receptor in sensory neurogenesis and maturation remains to be determined.

Given that 5-HT3A is known to be involved in nociceptive processing (Zeitz et al., 2002), especially in visceral pain and inflammation (Randich et al., 2008;Kato, 2013), we sought to define the complement of nociceptive neuron subtypes that express the 5-HT3A receptor in development. Neuropeptides CGRP and Substance P are known effectors of inflammation and nociceptive processing (Laird et al., 2000;Saban et al., 2000;Kiss et al., 2001;Lagerstrom et al., 2011;Russell et al., 2014), but surprisingly their temporospatial expression patterns in development have not previously been reported. We found at 14 dpc both of these neuropeptides are detectable at low levels by immunohistochemistry in lumbosacral DRGs, while *Htr3a*-EGFP expression is much more widespread among neurons and is robustly transcribed. By 18 dpc, CGRP and Substance P expression is stronger and largely co-localizes with *Htr3a*-EGFP. In postnatal stages we noted the acquisition of a heterogeneous pattern of *Htr3a*-EGFP transgene expression, in which some neurons very strongly express *Htr3a*-EGFP while others show moderate or dim levels. Despite these changes in transgene expression, CGRP and Substance P expression patterns remained consistent from 18 dpc through P2, P14, and P28. Previous studies reported 5-HT3A receptor expression in “nonpeptidergic” sensory neurons based on relatively infrequent (4%) co-localization of 5-HT3A+ neurons identified by in situ hybridization with SP+ neurons that were detected by immunohistochemistry (Zeitz et al., 2002). In contrast, we found that the majority of SP+ neurons in developing and adult DRG expressed the *Htr3a*-EGFP

transgene, indicating that at least some 5-HT3A+ populations are in fact peptidergic. The difference between our findings and prior reports maybe due to stages examined, DRG axial levels evaluated, greater ease of detecting EGFP fluorescence transgene vs. in situ hybridization signal, or differences between the mouse strains assayed.

TRP channels, namely TRPV1 and TRPV4, are key mediators of multimodal nociceptive processing in the lower urinary tract (Birder et al., 2002;Arms and Vizzard, 2011;Yoshiyama et al., 2015). Prior developmental studies of TRPV1 expression utilizing RT-PCR identified dynamic expression levels of this receptor over time, with low levels at 14 dpc (Hjerling-Leffler et al., 2007). While this finding could have been attributable to high expression in a few neurons with increasing numbers of neurons expressing the receptor over time, our immunohistochemical data shows that, in fact, TRPV1 is widely expressed at low levels through the DRG at 14 dpc. As lumbosacral DRG develop and mature, TRPV1 is expressed at higher levels in a relatively small proportion of total DRG neurons compared to *Htr3a*. The intensity of TRPV1 protein staining continues to increase and stabilizes by P2, with partial co-localization with *Htr3a*-EGFP in some DRG neurons. In marked contrast, TRPV4 protein is not detected until P14 and very rarely overlaps with *Htr3a*-EGFP transgene expression. This finding is especially interesting given that TRPV1 and TRPV4 have been implicated together in bladder afferent signaling (Janssen et al., 2016). The significant proportion of neurons co-expressing *Htr3a*-EGFP and NF200 indicates that 5-HT3A is not unique to a single nociceptive population, but is present in neurons of diverse sensory modalities and functions.

The second aim of our study was to determine the neurochemical diversity of 5-HT3A+ neurons that contribute to bladder sensory innervation. To this end we conducted retrograde tracing with Fast Blue dye in adult *Htr3a*-EGFP male mice and quantified proportions of 5-

HT3A+ sensory neuronal subtypes projecting to the bladder. Co-staining DRG sections with nociceptive markers CGRP, SP, TRPV1, and NF200 revealed differences in proportions of *Htr3a*+ subtypes in lumbar (L1, L2) and sacral (L6, S1) groups of bladder-innervating DRG. The majority of Fast Blue+ lumbar neurons expressed *Htr3a*-EGFP, while less than half of the FB+ sacral neurons were EGFP+. This difference in expression may have a functional consequence; the majority of bladder muscle innervation is derived from the sacral DRG group (L6, S1) and these afferents are primarily stretch-sensitive mechanoreceptors expressing NF200 (Xu and Gebhart, 2008). This finding is especially interesting in the context of research conducted by other groups. In guinea pig *ex vivo* bladder preparations, direct application of serotonin resulted in significant excitation of stretch-sensitive bladder muscle afferents (Zagorodnyuk et al., 2009). Given the high proportion of sacral bladder afferents co-expressing *Htr3a* and NF200, these excitatory effects may be due to activation of this serotonin receptor. Future studies could determine if L6, S1 bladder afferents co-expressing *Htr3a* and NF200 also function to detect stretch of the bladder detrusor.

Given the large proportion of bladder-innervating neurons expressing *Htr3a* in male mice, 5-HT3A likely plays an important role in bladder afferent neural activity. In our retrograde tracing studies we focused only on male mice to avoid estrous cycles as a confounding factor in gene expression (Monica Brauer and Smith, 2015). Since neurogenic bladder and bladder pain syndromes occur more frequently and with greater severity in women than men, sex-specific variation in gene expression may be a contributing factor to these differences (Irwin et al., 2006;Chrysanthopoulou and Doumouchtsis, 2014;Monica Brauer and Smith, 2015). It will be of interest in subsequent studies to investigate sex differences in *Htr3a* gene expression patterns throughout development or into adulthood.

The substantial proportions of bladder-innervating afferents expressing 5-HT3A we identified were not unexpected, given prior reports examining the role of this receptor in micturition. Pharmacological activation of 5-HT3A at spinal and supraspinal terminals resulted in inhibited sensory processing and a decreased micturition threshold volume (Espey et al., 1998). Complementary experiments showed that intrathecal administration of a 5-HT3A antagonist led to bladder nociceptive hypersensitivity (Hall et al., 2015), further supporting a critical role for 5-HT3A in sensory mediation of bladder filling and voiding. Future studies will need to focus on elucidating the specific functional impact of this receptor on bladder contractility and the consequences of its absence during nervous system development.

Overall our work is the first to delineate the expression patterns of a well-studied serotonin receptor in the understudied system of bladder innervation in the context of sensory neuron development. The work presented here serves as a foundation for future studies focusing on the contribution of the 5-HT3A receptor to common disorders such as chronic pelvic pain and urinary incontinence.

Acknowledgements

We gratefully acknowledge and thank Dr. Sam Wells and the support staff of the Cell Imaging Shared Resource (CISR) Core at Vanderbilt for advice and assistance in confocal imaging. The CISR Core is supported by NIH grants CA68485, DK20593, P50-DK58404, HD15052, DK59637, and EY08126. Work done in the CISR was supported in part by a Vanderbilt Kennedy Center Core Scholarship funded by P30-HD15052. The mouse strain used for this research project, Tg(*Htr3a*-EGFP)DH30Gsat/Mmnc (Stock Number 000273-UNC), was

obtained from the Mutant Mouse Regional Resource Center, a NCRR-NIH funded strain repository, and was donated to the MMRRC by the NINDS funded GENSAT BAC transgenic project. Hu antibody was generously donated by Dr. Vanda Lennon (Mayo Clinic). We are also grateful for the excellent training in retrograde tracing surgery techniques from Dr. Janet Keast at the University of Melbourne. This work was supported by US National Institutes of Health grants U01 DK101038 and R01 DK078158 to EMS2 and NIH F31 DK097938 to KER.

References

Arms, L., and Vizzard, M.A. (2011). Neuropeptides in lower urinary tract function. *Handb Exp Pharmacol***,** 395-423. doi: 10.1007/978-3-642-16499-6_19.

Bachy, I., Franck, M.C., Li, L., Abdo, H., Pattyn, A., and Ernfors, P. (2011). The transcription factor Cux2 marks development of an A-delta sublineage of TrkA sensory neurons. *Dev Biol* 360**,** 77-86. doi: 10.1016/j.ydbio.2011.09.007.

Baiou, D., Santha, P., Avelino, A., Charrua, A., Bacskai, T., Matesz, K., Cruz, F., and Nagy, I. (2007). Neurochemical characterization of insulin receptor-expressing primary sensory neurons in wild-type and vanilloid type 1 transient receptor potential receptor knockout mice. *J Comp Neurol* 503**,** 334-347. doi: 10.1002/cne.21389.

Bhattacharya, A., Dang, H., Zhu, Q.M., Schnegelsberg, B., Rozengurt, N., Cain, G., Prantil, R., Vorp, D.A., Guy, N., Julius, D., Ford, A.P., Lester, H.A., and Cockayne, D.A. (2004). Uropathic observations in mice expressing a constitutively active point mutation in the 5-HT3A receptor subunit. *J Neurosci* 24**,** 5537-5548. doi: 10.1523/JNEUROSCI.5658-03.2004.

Birder, L.A., Nakamura, Y., Kiss, S., Nealen, M.L., Barrick, S., Kanai, A.J., Wang, E., Ruiz, G., De Groat, W.C., Apodaca, G., Watkins, S., and Caterina, M.J. (2002). Altered urinary bladder function in mice lacking the vanilloid receptor TRPV1. *Nat Neurosci* 5**,** 856-860. doi: 10.1038/nn902.

Brumovsky, P.R., La, J.H., Mccarthy, C.J., Hokfelt, T., and Gebhart, G.F. (2012). Dorsal root ganglion neurons innervating pelvic organs in the mouse express tyrosine hydroxylase. *Neuroscience* 223**,** 77-91. doi: 10.1016/j.neuroscience.2012.07.043.

Cao, Y.Q., Mantyh, P.W., Carlson, E.J., Gillespie, A.M., Epstein, C.J., and Basbaum, A.I. (1998). Primary afferent tachykinins are required to experience moderate to intense pain. *Nature* 392**,** 390-394. doi: 10.1038/32897.

Cassereau, J., Nicolas, G., Lonchampt, P., Pinier, M., Barthelaix, A., Eyer, J., and Letournel, F. (2013). Axonal regeneration is compromised in NFH-LacZ transgenic mice but not in NFH-GFP mice. *Neuroscience* 228**,** 101-108. doi: 10.1016/j.neuroscience.2012.10.011.

Cenac, N., Altier, C., Chapman, K., Liedtke, W., Zamponi, G., and Vergnolle, N. (2008). Transient receptor potential vanilloid-4 has a major role in visceral hypersensitivity

symptoms. *Gastroenterology* 135**,** 937-946, 946 e931-932. doi: 10.1053/j.gastro.2008.05.024.

Chen, S., Li, J., Zhang, L., Dong, X., Gao, W., Mo, J., Chen, H., Xiao, S., and Li, Y. (2009). 5-HT 3 receptors mediate the time-dependent vagal afferent modulation of nociception during chronic food allergen-sensitized visceral hyperalgesia in rats. *Neurogastroenterol Motil* 21**,** 1222-e1113. doi: 10.1111/j.1365-2982.2009.01335.x.

Christianson, J.A., Bielefeldt, K., Altier, C., Cenac, N., Davis, B.M., Gebhart, G.F., High, K.W., Kollarik, M., Randich, A., Undem, B., and Vergnolle, N. (2009). Development, plasticity and modulation of visceral afferents. *Brain Res Rev* 60**,** 171-186. doi: 10.1016/j.brainresrev.2008.12.004.

Chrysanthopoulou, E.L., and Doumouchtsis, S.K. (2014). Challenges and current evidence on the management of bladder pain syndrome. *Neurourol Urodyn* 33**,** 1193-1201. doi: 10.1002/nau.22475.

De Groat, W.C., and Yoshimura, N. (2009). Afferent nerve regulation of bladder function in health and disease. *Handb Exp Pharmacol***,** 91-138. doi: 10.1007/978-3-540-79090-7_4.

Diez-Roux, G., Banfi, S., Sultan, M., Geffers, L., Anand, S., Rozado, D., Magen, A., Canidio, E., Pagani, M., Peluso, I., Lin-Marq, N., Koch, M., Bilio, M., Cantiello, I., Verde, R., De Masi, C., Bianchi, S.A., Cicchini, J., Perroud, E., Mehmeti, S., Dagand, E., Schrinner, S., Nurnberger, A., Schmidt, K., Metz, K., Zwingmann, C., Brieske, N., Springer, C., Hernandez, A.M., Herzog, S., Grabbe, F., Sieverding, C., Fischer, B., Schrader, K., Brockmeyer, M., Dettmer, S., Helbig, C., Alunni, V., Battaini, M.A., Mura, C., Henrichsen, C.N., Garcia-Lopez, R., Echevarria, D., Puelles, E., Garcia-Calero, E., Kruse, S., Uhr, M., Kauck, C., Feng, G., Milyaev, N., Ong, C.K., Kumar, L., Lam, M., Semple, C.A., Gyenesei, A., Mundlos, S., Radelof, U., Lehrach, H., Sarmientos, P., Reymond, A., Davidson, D.R., Dolle, P., Antonarakis, S.E., Yaspo, M.L., Martinez, S., Baldock, R.A., Eichele, G., and Ballabio, A. (2011). A high-resolution anatomical atlas of the transcriptome in the mouse embryo. *PLoS Biol* 9**,** e1000582. doi: 10.1371/journal.pbio.1000582.

Espey, M.J., Du, H.J., and Downie, J.W. (1998). Serotonergic modulation of spinal ascending activity and sacral reflex activity evoked by pelvic nerve stimulation in cats. *Brain Res* 798**,** 101-108.

Everaerts, W., Zhen, X., Ghosh, D., Vriens, J., Gevaert, T., Gilbert, J.P., Hayward, N.J., Mcnamara, C.R., Xue, F., Moran, M.M., Strassmaier, T., Uykal, E., Owsianik, G., Vennekens, R., De Ridder, D., Nilius, B., Fanger, C.M., and Voets, T. (2010). Inhibition of the cation channel TRPV4 improves bladder function in mice and rats with cyclophosphamide-induced cystitis. *Proc Natl Acad Sci U S A* 107**,** 19084–19089. doi: www.pnas.org/cgi/doi/10.1073/pnas.1005333107.

Faerber, L., Drechsler, S., Ladenburger, S., Gschaidmeier, H., and Fischer, W. (2007). The neuronal 5-HT3 receptor network after 20 years of research--evolving concepts in management of pain and inflammation. *Eur J Pharmacol* 560**,** 1-8. doi: 10.1016/j.ejphar.2007.01.028.

Franken, J., Uvin, P., De Ridder, D., and Voets, T. (2014). TRP channels in lower urinary tract dysfunction. *British Journal of Pharmacology* 171**,** 2537-2551. doi: 10.1111/bph.2014.171.issue-10.

Gevaert, T., Vriens, J., Segal, A., Everaerts, W., Roskams, T., Talavera, K., Owsianik, G., Liedtke, W., Daelemans, D., Dewachter, I., Van Leuven, F., Voets, T., De Ridder, D.,

and Nilius, B. (2007). Deletion of the transient receptor potential cation channel TRPV4 impairs murine bladder voiding. *J Clin Invest* 117**,** 3453-3462. doi: 10.1172/JCI31766.

Glaser, S.S., Ueno, Y., Demorrow, S., Chiasson, V.L., Katki, K.A., Venter, J., Francis, H.L., Dickerson, I.M., Dipette, D.J., Supowit, S.C., and Alpini, G.D. (2007). Knockout of alpha-calcitonin gene-related peptide reduces cholangiocyte proliferation in bile duct ligated mice. *Lab Invest* 87**,** 914-926. doi: 10.1038/labinvest.3700602.

Gold, M.S., and Gebhart, G.F. (2010). Nociceptor sensitization in pain pathogenesis. *Nat Med* 16**,** 1248-1257. doi: 10.1038/nm.2235.

Gong, S., Zheng, C., Doughty, M.L., Losos, K., Didkovsky, N., Schambra, U.B., Nowak, N.J., Joyner, A., Leblanc, G., Hatten, M.E., and Heintz, N. (2003). A gene expression atlas of the cental nervous system based on bacterial artificial chromosomes. *Nature* 425**,** 917-925.

Hall, J.D., Dewitte, C., Ness, T.J., and Robbins, M.T. (2015). Serotonin enhances urinary bladder nociceptive processing via a 5-HT receptor mechanism. *Neurosci Lett* 604**,** 97-102. doi: 10.1016/j.neulet.2015.07.048.

Hjerling-Leffler, J., Alqatari, M., Ernfors, P., and Koltzenburg, M. (2007). Emergence of functional sensory subtypes as defined by transient receptor potential channel expression. *J Neurosci* 27**,** 2435-2443. doi: 10.1523/JNEUROSCI.5614-06.2007.

Irwin, D.E., Milsom, I., Hunskaar, S., Reilly, K., Kopp, Z., Herschorn, S., Coyne, K., Kelleher, C., Hampel, C., Artibani, W., and Abrams, P. (2006). Population-based survey of urinary incontinence, overactive bladder, and other lower urinary tract symptoms in five countries: results of the EPIC study. *Eur Urol* 50**,** 1306-1314; discussion 1314-1305. doi: 10.1016/j.eururo.2006.09.019.

Janssen, D.A., Hoenderop, J.G., Heesakkers, J.P., and Schalken, J.A. (2016). TRPV4 mediates afferent pathways in the urinary bladder. A spinal c-fos study showing TRPV1 related adaptations in the TRPV4 knockout mouse. *Pflugers Arch* 468**,** 1741-1749. doi: 10.1007/s00424-016-1859-9.

Kato, S. (2013). Role of serotonin 5-HT(3) receptors in intestinal inflammation. *Biol Pharm Bull* 36**,** 1406-1409.

Kayser, V., Elfassi, I.E., Aubel, B., Melfort, M., Julius, D., Gingrich, J.A., Hamon, M., and Bourgoin, S. (2007). Mechanical, thermal and formalin-induced nociception is differentially altered in 5-HT1A-/-, 5-HT1B-/-, 5-HT2A-/-, 5-HT3A-/- and 5-HTT-/- knock-out male mice. *Pain* 130**,** 235-248. doi: 10.1016/j.pain.2006.11.015.

Keast, J.R., and De Groat, W.C. (1992). Segmental distribution and peptide content of primary afferent neurons innervating the urogenital organs and colon of male rats. *J Comp Neurol* 319**,** 615-623. doi: 10.1002/cne.903190411.

Kestell, G.R., Anderson, R.L., Clarke, J.N., Haberberger, R.V., and Gibbins, I.L. (2015). Primary afferent neurons containing calcitonin gene-related peptide but not substance P in forepaw skin, dorsal root ganglia, and spinal cord of mice. *J Comp Neurol* 523**,** 2555-2569. doi: 10.1002/cne.23804.

Kim, Y.S., Chu, Y., Han, L., Li, M., Li, Z., Lavinka, P.C., Sun, S., Tang, Z., Park, K., Caterina, M.J., Ren, K., Dubner, R., Wei, F., and Dong, X. (2014). Central terminal sensitization of TRPV1 by descending serotonergic facilitation modulates chronic pain. *Neuron* 81**,** 873-887. doi: 10.1016/j.neuron.2013.12.011.

Kiss, S., Yoshiyama, M., Cao, Y.Q., Basbaum, A.I., De Groat, W.C., Lecci, A., Maggi, C.A., and Birder, L.A. (2001). Impaired response to chemical irritation of the urinary tract in mice with disruption of the preprotachykinin gene. *Neurosci Lett* 313**,** 57-60.

Lagerstrom, M.C., Rogoz, K., Abrahamsen, B., Lind, A.L., Olund, C., Smith, C., Mendez, J.A., Wallen-Mackenzie, A., Wood, J.N., and Kullander, K. (2011). A sensory subpopulation depends on vesicular glutamate transporter 2 for mechanical pain, and together with substance P, inflammatory pain. *Proc Natl Acad Sci U S A* 108**,** 5789-5794. doi: 10.1073/pnas.1013602108.

Laird, J.M., Olivar, T., Roza, C., De Felipe, C., Hunt, S.P., and Cervero, F. (2000). Deficits in visceral pain and hyperalgesia of mice with a disruption of the tachykinin NK1 receptor gene. *Neuroscience* 98**,** 345-352.

Lawson, S.N., Perry, M.J., Prabhakar, E., and Mccarthy, P.W. (1993). Primary sensory neurones: neurofilament, neuropeptides, and conduction velocity. *Brain Res Bull* 30**,** 239-243.

Loyd, D.R., Weiss, G., Henry, M.A., and Hargreaves, K.M. (2011). Serotonin increases the functional activity of capsaicin-sensitive rat trigeminal nociceptors via peripheral serotonin receptors. *Pain* 152**,** 2267-2276. doi: 10.1016/j.pain.2011.06.002.

Machu, T.K. (2011). Therapeutics of 5-HT3 receptor antagonists: current uses and future directions. *Pharmacol Ther* 130**,** 338-347. doi: 10.1016/j.pharmthera.2011.02.003.

Marmigere, F., and Ernfors, P. (2007). Specification and connectivity of neuronal subtypes in the sensory lineage. *Nat Rev Neurosci* 8**,** 114-127. doi: 10.1038/nrn2057.

Monica Brauer, M., and Smith, P.G. (2015). Estrogen and female reproductive tract innervation: cellular and molecular mechanisms of autonomic neuroplasticity. *Auton Neurosci* 187**,** 1-17. doi: 10.1016/j.autneu.2014.11.009.

Payne, S.C., Belleville, P.J., and Keast, J.R. (2015). Regeneration of sensory but not motor axons following visceral nerve injury. *Exp Neurol* 266**,** 127-142. doi: 10.1016/j.expneurol.2015.02.026.

Potter, K.A., Simon, J.S., Velagapudi, B., and Capadona, J.R. (2012). Reduction of autofluorescence at the microelectrode-cortical tissue interface improves antibody detection. *J Neurosci Methods* 203**,** 96-105. doi: 10.1016/j.jneumeth.2011.09.024.

Randich, A., Shaffer, A.D., Ball, C.L., and Mebane, H. (2008). Serotonergic and noradrenergic facilitation of the visceromotor reflex evoked by urinary bladder distension in rats with inflamed bladders. *Neurosci Lett* 442**,** 253-256. doi: 10.1016/j.neulet.2008.07.031.

Ritter, K.E., and Southard-Smith, E.M. (2017). Dynamic Expression of Serotonin Receptor 5-HT3A in Developing Sensory Innervation of the Lower Urinary Tract. *Front Neurosci* 10**,** 592. doi: 10.3389/fnins.2016.00592.

Russell, F.A., King, R., Smillie, S.J., Kodji, X., and Brain, S.D. (2014). Calcitonin gene-related peptide: physiology and pathophysiology. *Physiol Rev* 94**,** 1099-1142. doi: 10.1152/physrev.00034.2013.

Saban, R., Saban, M.R., Nguyen, N.B., Lu, B., Gerard, C., Gerard, N.P., and Hammond, T.G. (2000). Neurokinin-1 (NK-1) receptor is required in antigen-induced cystitis. *Am J Pathol* 156**,** 775-780. doi: 10.1016/S0002-9440(10)64944-9.

Su, H.C., Wharton, J., Polak, J.M., Mulderry, P.K., Ghatei, M.A., Gibson, S.J., Terenghi, G., Morrison, J.F., Ballesta, J., and Bloom, S.R. (1986). Calcitonin gene-related peptide immunoreactivity in afferent neurons supplying the urinary tract: combined retrograde tracing and immunohistochemistry. *Neuroscience* 18**,** 727-747.

Tecott, L., Shtrom, S., and Julius, D. (1995). Expression of a serotonin-gated ion channel in embryonic neural and nonneural tissues. *Mol Cell Neurosci* 6**,** 43-55. doi: 10.1006/mcne.1995.1005.

Tecott, L.H., Maricq, A.V., and Julius, D. (1993). Nervous system distribution of the serotonin 5-HT3 receptor mRNA. *Proc Natl Acad Sci U S A* 90**,** 1430-1434.

Vucurovic, K., Gallopin, T., Ferezou, I., Rancillac, A., Chameau, P., Van Hooft, J.A., Geoffroy, H., Monyer, H., Rossier, J., and Vitalis, T. (2010). Serotonin 3A receptor subtype as an early and protracted marker of cortical interneuron subpopulations. *Cereb Cortex* 20**,** 2333-2347. doi: 10.1093/cercor/bhp310.

Walstab, J., Rappold, G., and Niesler, B. (2010). 5-HT(3) receptors: role in disease and target of drugs. *Pharmacol Ther* 128**,** 146-169. doi: 10.1016/j.pharmthera.2010.07.001.

Xu, L., and Gebhart, G.F. (2008). Characterization of mouse lumbar splanchnic and pelvic nerve urinary bladder mechanosensory afferents. *J Neurophysiol* 99**,** 244-253. doi: 10.1152/jn.01049.2007.

Yoshiyama, M., Mochizuki, T., Nakagomi, H., Miyamoto, T., Kira, S., Mizumachi, R., Sokabe, T., Takayama, Y., Tominaga, M., and Takeda, M. (2015). Functional roles of TRPV1 and TRPV4 in control of lower urinary tract activity: dual analysis of behavior and reflex during the micturition cycle. *Am J Physiol Renal Physiol* 308**,** F1128-1134. doi: 10.1152/ajprenal.00016.2015.

Zagorodnyuk, V.P., Brookes, S.J., Spencer, N.J., and Gregory, S. (2009). Mechanotransduction and chemosensitivity of two major classes of bladder afferents with endings in the vicinity to the urothelium. *J Physiol* 587**,** 3523-3538. doi: 10.1113/jphysiol.2009.172577.

Zeitz, K.P., Guy, N., Malmberg, A.B., Dirajlal, S., Martin, W.J., Sun, L., Bonhaus, D.W., Stucky, C.L., Julius, D., and Basbaum, A.I. (2002). The 5-HT3 Subtype of Serotonin Receptor Contributes to Nociceptive Processing via a Novel Subset of Myelinated and Unmyelinated Nociceptors. *Journal of Neuroscience* 22**,** 1010-1019.

Zou, M., Li, S., Klein, W.H., and Xiang, M. (2012). Brn3a/Pou4f1 regulates dorsal root ganglion sensory neuron specification and axonal projection into the spinal cord. *Dev Biol* 364**,** 114-127. doi: 10.1016/j.ydbio.2012.01.021.

CHAPTER IV

SEROTONIN RECEPTOR 5-HT3A AFFECTS DEVELOPMENT OF BLADDER INNERVATION AND URINARY BLADDER FUNCTION

This chapter is a modified version of a published article (Ritter et al., 2017). Frontiers Publishing Group copyright policy states that authors retain the copyright of their work and are permitted to reproduce material from their own published articles, provided that the work is properly cited.

Introduction

The lower urinary tract (LUT, bladder and urethra) is responsible for the storage and timely elimination of urine and is controlled by autonomic, sensory, and central motor innervation. The autonomic components are comprised of the pelvic ganglia (PG), which harbor both sympathetic and parasympathetic neurons (Wanigasekara et al., 2003). The coordination of these neural components allows the bladder smooth muscle to relax as it fills with urine while the internal urethral sphincter contracts to prevent urine leakage, and vice versa when the micturition reflex is initiated (de Groat et al., 2015). When any of these neural components do not function properly, urinary incontinence or retention can occur and severely diminish quality of life. The nerves supplying bladder innervation are prone to damage in instances of spinal cord injury and during surgical procedures in the lower abdomen (Zullo et al., 2003;Wyndaele, 2016). Additionally, LUT dysfunction can arise during the course of natural aging (Wagg et al., 2007). Despite the widespread prevalence of these conditions, treatment options remain limited. Regenerative strategies aimed at restoring LUT innervation are promising (Kim et al., 2013), and

such efforts require a deeper understanding of the molecular processes governing the development of LUT innervation (Keast et al., 2015).

In an effort to characterize patterns of gene expression in the development of LUT sensory innervation, we previously examined expression of the serotonin receptor 5-HT3A (encoded by the *Htr3a* gene) in developing dorsal root ganglia (Ritter and Southard-Smith, 2017). In these analyses we also observed pronounced expression of *Htr3a* in fetal mouse pelvic ganglia that supply autonomic innervation to the bladder. This finding is of particular interest in the context of a previous study reporting severe voiding dysfunction in *Htr3a*$^{vs/vs}$ mice that express a constitutively active form of 5-HT3A (Bhattacharya et al., 2004). However, the role of 5-HT3A signaling in the development of LUT autonomic innervation has not been previously examined in detail.

Given the evidence of 5-HT3A receptor activity in adult LUT function and expression of this receptor early in fetal LUT development, we tested the hypothesis that 5-HT3A is required for the development and function of bladder innervation. Using the *Htr3a*-/- knockout line, we demonstrate here that 5-HT3A is required for normal micturition in male mice. Conducting the spontaneous void spot assay in pre-pubescent *Htr3a* mutant mice revealed aberrant urinary voiding in male, but not female, knockout animals. Anesthetized bladder cystometry revealed that in males, the loss of 5-HT3A receptor activity diminishes bladder voiding efficiency. At the cellular level we found that 5-HT3A is required for the maturation of autonomic and sensory neuronal fibers innervating bladder smooth muscle. Collectively our results demonstrate a novel role for 5-HT3A in peripheral nervous system development and further highlight this receptor as a critical signaling component in the regulation of micturition.

Materials and Methods

Animals

All experimental protocols were approved by the Institutional Animal Care and Use Committee (IACUC) at Vanderbilt University and University of Wisconsin-Madison. Tg(*Htr3a*-EGFP)DH30Gsat/Mmnc (RRID: MMRRC_000273-UNC) transgenic mice were obtained from the Mutant Mouse Resource & Research Center and maintained as heterozygotes on an outbred Swiss Webster background. Tg(*ChAT*-EGFP)GH293Gsat/Mmucd (hereafter *ChAT*-EGFP) transgenic reporter mice were obtained from the Mutant Mouse Resource and Research Center and maintained as homozygotes on a C57BL6/J background. B6.129X1-*Htr3a*^{tm1Jul}/J (RRID: IMSR_JAX:005251, hereafter referred to as *Htr3a*-/-) mice were acquired from The Jackson Laboratory and maintained on a C57BL6/J background. To generate *ChAT*-EGFP; *Htr3a*-KO animals for pelvic ganglia gene expression studies, *ChAT*-EGFP/EGFP homozygotes were bred to *Htr3a*-/- mice to generate *ChAT*-EGFP/+;*Htr3a*+/- animals. These progeny were then mated to produce *ChAT*-EGFP/+;*Htr3a*+/+, *Htr3a*+/-, and *Htr3a*-/- animals. This breeding strategy was adopted to avoid comparing expression patterns of heterozygous versus homozygous expression of the *ChAT*-EGFP transgene. All mice were housed in a modified barrier facility at approximately 25°C and 25-40% humidity. Mice were maintained on a 14-hour on, 10-hour off light cycle and housed in rectangular polypropylene micro-isolator cages (Lab Products Inc., #10025, 29.2cm x 19.0cm x 12.7cm) and provided standard diet (Purina PicoLab Laboratory Rodent Diet #5L0D) and water *ad libitum*. Males and females were paired for timed matings to obtain fetal tissues at specific developmental stages; the morning of observation of a seminal plug was designated as 0.5 days post coitus (dpc).

Tissue collection

Male and female mouse fetuses were dissected in ice-cold 1X Phosphate Buffered Saline (PBS) and fixed in 10% Neutral Buffered Formalin (NBF, Sigma Aldrich HT501128) overnight at 4°C. Following fixation, tissues were washed three times in 1XPBS for 15 minutes each and then finally washed for 1 hour. Tissues were then infiltrated with 30% sucrose in 1XPBS and stored in the same solution at 4°C until the day of embedding and cryo-sectioning. To obtain pelvic ganglia and bladders at adult stages, mice were anesthetized by isoflurane inhalation and euthanized by cervical dislocation. A lower abdominal incision was made to reveal the lower urinary tract and the pelvic ganglia were carefully teased away from the neck of the bladder and pinned out flat on petri dishes lined with Sylgard (Ellsworth Adhesives, #4019862). The pelvic ganglia were fixed in 10% NBF overnight at room temperature while gently shaking. Bladders were removed by cutting the proximal urethra and the ureters. To remove urine and allow bladder relaxation so that smooth muscle was not stretched thin, bladders were flushed with 1XPBS and subsequently emptied using a needle and syringe before fixation in 10% NBF overnight at 4°C. Bladders and pelvic ganglia were washed three times in 1XPBS for 15 minutes each, followed by 1 hour of washing in 1XPBS and infiltrated with 30% sucrose at 4°C.

Immunohistochemistry

Cryo-sections: Fixed tissues for cryo-sectioning were embedded in Tissue Freezing Medium (TFM, General Data, #TFM) and immediately sectioned with a Leica Cryostat (CM1900-UV). Sagittal sections of 20µm thickness were cut and mounted onto 3-APES treated slides (Sigma Aldrich, A3648) and dried for 30 minutes at 37°C on a slide warmer. Slides were then submerged in 1XPBS-0.3% Triton X-100 to dissolve residual TFM for five minutes.

Blocking solution (1XPBS-0.3% Triton X-100, 10% Bovine Serum Albumin (Sigma Aldrich, A2153), 5% Normal Donkey Serum (Jackson ImmunoResearch, 017-000-121), 0.45μm sterile filtered) was applied to sections for at least 30 minutes at room temperature. Sections were then incubated in primary antibodies diluted in blocking solution overnight at 4°C. Primary antibody information can be found in Table 4.1. On the following day, sections were rinsed with sterile 1XPBS and incubated in secondary antibodies diluted in blocking solution for one hour at room temperature. Secondary antibody information can be found in Table 4.2. After rinsing with sterile 1XPBS, sections were incubated in 0.5mM cupric sulfate in 50mM ammonium acetate buffer, pH5.0, for 10 minutes at room temperature to quench autofluorescence (Potter et al., 2012). Sterile water was used to quench the cupric sulfate reaction. Slides were finally mounted with AquaPolyMount (PolySciences, Inc., 18606) and coverslipped.

Whole-mount Pelvic Ganglia: Following fixation and rinsing, pelvic ganglia were blocked at least 24 hours at 4°C in the same blocking solution used for cryo-sections. Tissues were then incubated in primary antibody dilutions for 48 hours at 4°C in a 24-well tissue culture plate and rinsed three times, 20 minutes each, in sterile 1XPBS. Pelvic ganglia were then incubated in secondary antibody dilutions for one hour at room temperature while rocking. Tissues were rinsed three times, 20 minutes each, in sterile 1XPBS and then incubated in 0.5mM cupric sulfate in 50mM ammonium acetate buffer, pH5.0, for ten minutes at room temperature to quench autofluorescence. The cupric sulfate quenching reaction was quenched by transferring the tissues to sterile water. Tissues were mounted onto slides with AquaPolyMount and coverslipped and allowed to dry before imaging. Confocal microscopy of immunohistochemical experiments was conducted using a Zeiss LSM 510-Meta confocal microscope, equipped with a 20x/0.75 plan-apochromat objective.

Table 4.1 Primary antibodies used in immunohistochemistry experiments

Antibody	Host	Vendor	RRID	Dilution
Tyrosine Hydroxylase (TH)	Sheep	Millipore, #AB1542	AB_11213126	1:1,000
Vesicular Acetylcholine Transporter (vAChT)	Rabbit	Synaptic Systems, #139-103	AB_887694	1:1,000
Calcitonin Gene Related Peptide (CGRP)	Rabbit	Sigma Aldrich, #C8198	AB_259091	1:1,000
Neurofilament 200 (NF200)	Rabbit	Sigma Aldrich, #N4142	AB_477272	1:500
β-III Tubulin (Tuj1)	Rabbit	Covance, #PRB-435P	AB_291637	1:10,000
Hu C/D	Human	Gift of Vanda Lennon	N/A	1:10,000

All primary antibodies were diluted in blocking solution as described in Materials & Methods.

Table 4.2 Secondary antibodies used in immunohistochemistry experiments

Antibody	Vendor	RRID	Dilution
Donkey anti-Rabbit Cy3	Jackson ImmunoResearch, #711-165-152	AB_2307443	1:1,000
Donkey anti-Rabbit AlexaFluor 647	Jackson ImmunoResearch, #711-605-152	AB_2492288	1:250
Donkey anti-Rabbit AlexaFluor 488	Jackson ImmunoResearch, #711-545-152	AB_2313584	1:400
Donkey anti-Sheep Cy3	Jackson ImmunoResearch, #713-165-147	AB_2340728	1:1,000
Donkey anti-Human AlexaFluor 647	Jackson ImmunoResearch, #709-605-149	AB_2340578	1:200

All secondary antibodies were diluted in blocking solution as described in Materials & Methods.

Spontaneous void spot assay

Spontaneous void spots assays (VSA) were conducted as published (Keil et al., 2016), but with modifications as described here. Additional details of the VSA are also described in Chapter VII, in the section titled "Spontaneous Void Spot Assay." Mice of the same sex were housed in groups of five animals or fewer per cage. Whatman filter paper (3mm, chromatography grade, GM Healthcare #3030-347) was cut into sheets to precisely fit the bottom of a standard mouse cage (see section Animals in Materials & Methods) and autoclaved in foil-wrapped packets. The assay was conducted at the same time each day (12:00pm-1:00pm) to avoid circadian variability in micturition behavior. To conduct the assay, each mouse was placed

in its own void assay cage (a cage identical to the animals' home cage, with no food, water, or bedding) with a piece of autoclaved Whatman filter paper on the floor of the cage. The void assay cages were then returned to the cage rack and left undisturbed for the duration of the assay (one hour). Voiding was assessed for one hour to minimize stress and anxiety from prolonged food and water deprivation. At the end of the hour, the mice were carefully lifted out of the trial cages and returned to their home cages. Prior to the VSA trial days, five days of assay acclimation that entailed placing the animals in individual cages with Whatman paper were conducted to minimize the effects of novel environment (i.e., the assay cage and Whatman paper) on micturition behavior. Following acclimation and two days of rest, three consecutive trials were carried out. For each acclimation and trial, the same void assay cage was used for each animal. Acclimation and testing took place while the animals were 4-5 weeks old to minimize the effects of sex hormones and estrous cycling on micturition behavior.

The soiled sheets of Whatman paper were stained with Ninhydrin (2% w/v dilution in 190-proof ethanol, Sigma Aldrich, 151173) and allowed to air-dry overnight. Dried Ninhydrin-stained sheets were scanned to a computer as TIF files. Urine void spots were identified by their purple coloration due to Ninhydrin staining and round shape; non-urine marks were identified as either fecal material (brown spots/smudges) or paw prints (purple paw-print shapes). These non-urine artifacts were erased in Adobe Photoshop prior to analysis. The particle analysis tool in ImageJ (http://imagej.nih.gov/ij/) was used to measure the total number of void spots greater than $0.02cm^2$ and the surface area of each individual void spot. Staining with Ninhydrin allows clear visualization of the borders of overlapping voids, which were manually counted by drawing a line on the border between overlapping spots and using the freehand selection tool to count them separately. These measurements were then incorporated into the analysis. The total

number of individual voids and the combined area of total voids were averaged over the three days of trial.

Anesthetized bladder cystometry

Cystometric recordings were made in mice under urethane anesthesia using established methods (Uvin et al., 2012;Boudes et al., 2013;Bjorling et al., 2015;Roman et al., 2016). Briefly, mice were weighed and anesthetized with urethane (1.43g/kg, subcutaneous injection). Thirty minutes later, the bladder was carefully exposed through a lower midline abdominal incision. A PE 50 cannula with the end flared was inserted into the dome of the bladder and secured with a 6.0 silk purse string suture. Muscle and skin layers were then closed separately with a 5.0 silk suture. One hour after cannula implantation, the distal part of the cannula was connected to a physiological pressure transducer (Memscap AS, Norway) and an infusion pump (Harvard Apparatus, Holliston, MA) via a 3-way stopcock. Room temperature saline was infused at a rate of 0.8mL/hour for 60-90 minutes to stabilize voiding patterns and elicit repetitive micturition cycles. Intravesical pressure was recorded continuously using a PowerLab data collection system (ADInstruments, Colorado Springs, CO) connected to a PC computer. The voided volume of saline was quantified by collecting voided saline on small filter papers weighed before and after voiding. Additionally, void volume was simultaneously measured using a force transducer (Model FT03, Grass Instruments) placed underneath the distal tip of the urethra to collect voided infusate. The force transducer was calibrated using known volumes of infusate to generate a pressure-volume curve. At least six reproducible micturition cycles were recorded and used to quantify multiple parameters. Specifically, intercontractile interval (ICI, time between micturition events), maximal voiding pressure (VP), bladder capacity (BC, defined as

the saline infusion rate multiplied by the intercontractile interval), void volume (VV), and non-voiding bladder contraction (NVC, intravesical pressure increases >5 mmHg during the filling phase, without the release of fluid from the urethra) and voiding efficiency (VE, voided volume/bladder capacity x 100) were determined (Vera and Nadelhaft, 2001;Fullhase et al., 2013;Lai et al., 2016;Wu et al., 2016). Estrous cycle phase in female mice was not recorded prior to conducting cystometry.

Analysis of bladder innervation density

Sagittal cryo-sections were obtained of *Htr3a*+/+, *Htr3a*+/-, and *Htr3a*-/- 18.5dpc and adult male bladders and were stained for markers of various neuronal subtypes: Tuj1 (all neurons), vesicular acetylcholine transporter (vAChT, cholinergic), CGRP (peptidergic nociceptive sensory), and NF200 (myelinated Aδ sensory). Three to five cryo-sections per animal, for each genotype class, were imaged. For each cryo-section, five images (665μm x 508μm) were captured: superior and inferior bladder neck (referred to as "Bladder Neck"), and superior, inferior, and apex bladder dome (referred to as "Bladder Dome"). All five images collectively are referred to as "Total Bladder". Imaging was conducted on a Leica DMI6000B fluorescent microscope equipped with a 20x objective and software zoom set to 1.0x. Using ImageJ software (http://imagej.nih.gov/ij/) the grayscale images were processed using the threshold function to set the minimum gray value of the image that would be counted as true fluorescence and not background or auto-fluorescence. The same minimum gray value threshold was used for all images captured within one replicate of immunohistochemistry. To quantify innervation density in bladder smooth muscle, three non-contiguous 75 μm-diameter regions equivalent to 150 pixels were selected in each image and the ImageJ measure function was used

to calculate the percentage of pixels in the selected area that were greater than or equal to the minimum gray value threshold. The percentages of pixels above the minimum gray value obtained from each randomly selected region were averaged for each image. Then, these values were averaged for each designated bladder domain (bladder dome, bladder neck, or total bladder).

Statistical analysis

Average voiding frequency assessed by spontaneous void spot assay was averaged across three days of experiments and across animals segregated by sex and *Htr3a* genotype. The means were then statistically compared by one-way ANOVA followed by Tukey's Honest Significant Difference (HSD) post-hoc test to correct for multiple comparisons of pairs of means. A p-value of less than 0.05 was considered statistically significant. Anesthetized bladder cystometry data was averaged across animals segregated by sex and *Htr3a* genotype and then statistically compared by one-way ANOVA followed by Tukey's HSD post-hoc test. A p-value of less than 0.05 was considered statistically significant. Bladder smooth muscle innervation density was measured by calculating the percentage of pixels within a selected area that correspond to neuronal fiber staining. These measurements were averaged across male animals of each genotype (*Htr3a*+/+, *Htr3a*+/-, and *Htr3a*-/-), and means were statistically compared by one-way ANOVA followed by Tukey's HSD post-hoc test. A p-value of less than 0.05 was considered statistically significant. All numerical data are presented as the mean ± standard error of the mean (SEM). All study authors had access to study data, and all authors reviewed and approved the manuscript.

Results

Serotonin receptor 5-HT3A is expressed in mouse fetal and adult major pelvic ganglia

In our previous study examining expression of *Htr3a* in developing dorsal root ganglia (Ritter and Southard-Smith, 2017), we also observed transgene fluorescence in the autonomic pelvic ganglia during fetal stages. To further characterize the expression of this serotonin receptor in developing autonomic LUT innervation, we evaluated the distribution and cell type specificity of *Htr3a* in *Htr3a*-EGFP transgenic tissues (Tg(*Htr3a*-EGFP)DH30Gsat/Mmnc, hereafter referred to as *Htr3a*-EGFP) by immunohistochemistry and confocal microscopy. We detected widespread *Htr3a*-EGFP co-expression with pan-neuronal marker Hu C/D in fetal pelvic ganglia at 14.5dpc (Figure 4.1, Panels A-A"). Expression of *Htr3a* is maintained through later fetal development at 18.5dpc pelvic ganglia neurons (Figure 4.1, Panels B-B") and into adulthood (Figure 4.1, Panels C-C"). From these experiments we conclude that serotonin receptor 5-HT3A is expressed early in developing autonomic LUT innervation, and its expression is maintained in many pelvic ganglia neurons through sexual maturity in adult mice.

Htr3a-/- males, but not females, exhibit increased urinary voiding frequency

Given previous reports indicating a role for 5-HT3A receptor signaling in micturition (Bhattacharya et al., 2004;Schwen et al., 2013), and the widespread expression of *Htr3a* in pelvic ganglia neurons, we sought to determine if 5-HT3A is required for normal urinary voiding. To do this we employed the B6.129X1-*Htr3a*^{tm1Jul}/J (hereafter *Htr3a*-/-) mouse line, which is a global knockout of *Htr3a* gene expression that has been bred to congenicity on the C57BL/6J inbred strain (Zeitz et al., 2002). Bladder function was initially assessed in *Htr3a* mutants and wild type littermates by spontaneous void spot assays (VSA) that have been shown in prior

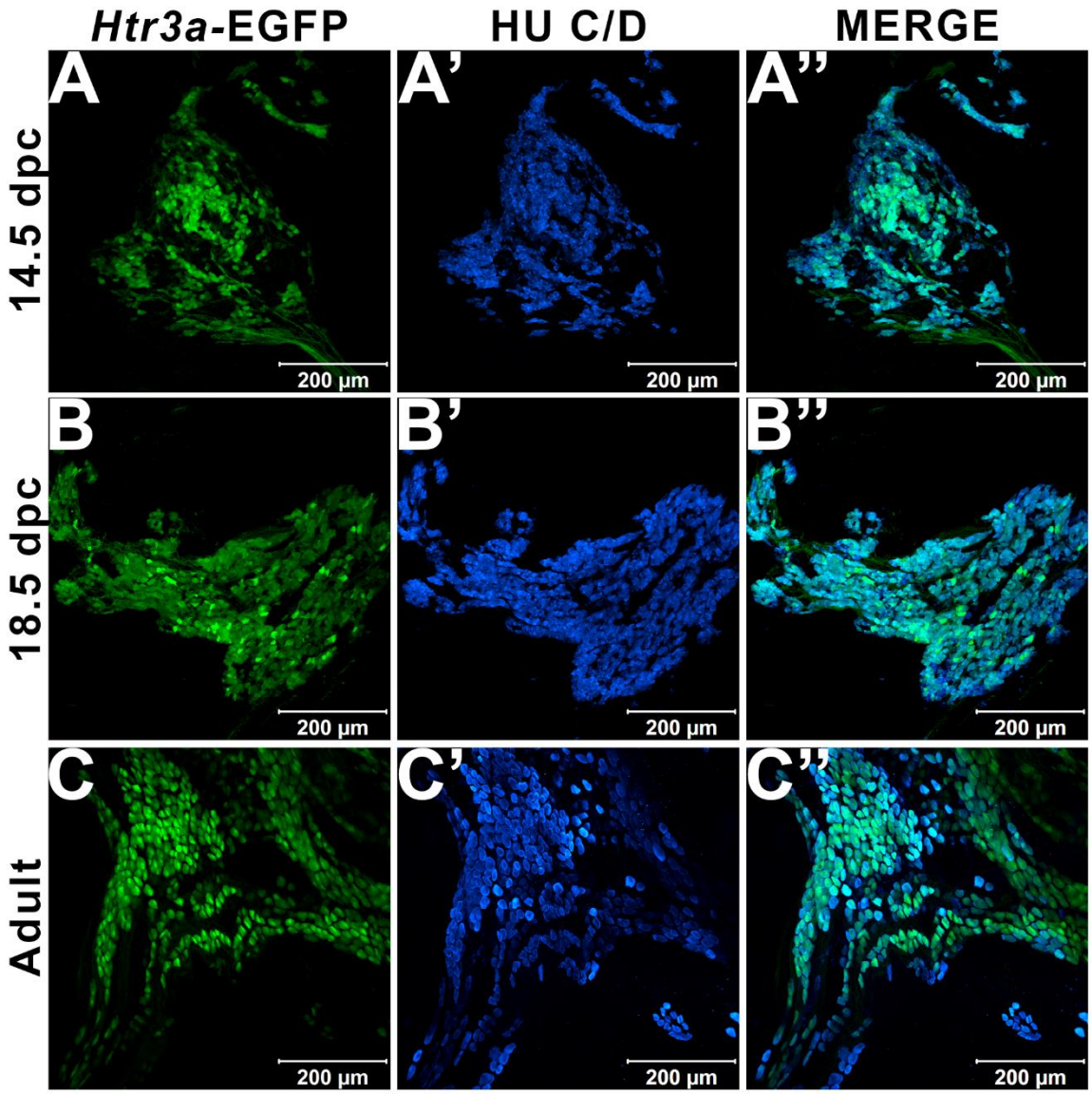

Figure 4.1 Serotonin receptor *Htr3a* is expressed in many neurons within fetal and adult major pelvic ganglia. Confocal images of *Htr3a*-EGFP pelvic ganglia stained with pan-neuronal marker Hu C/D. (**A-A"**) 14.5dpc sagittal section of pelvic ganglia. (**B-B"**) 18.5dpc sagittal section of pelvic ganglia. (**C-C"**) Adult (12 weeks old) male whole mount pelvic ganglia. Scale bar = 200µm in all images.

studies to be a reliable assessment of micturition in mice (Yu et al., 2014;Bjorling et al., 2015;Keil et al., 2016). In one hour assessments conducted across three consecutive days, we observed male wild type and heterozygous animals had very similar voiding frequencies (9.63 ± 0.98 voids and 10.69 ± 1.64 voids, respectively, p=0.8894, one-way ANOVA with Tukey's HSD post-hoc test), while homozygous mutant males exhibited an increased number of voids that averaged 18.21 ± 2.19 (Figure 4.2). The difference in male voiding frequencies was significantly increased compared to both wild type and *Htr3a*+/- littermates (p=0.0046 and p=0.0074, respectively, one-way ANOVA with Tukey's HSD post-hoc test, n=15-25 animals per genotype). However, wild type, heterozygous, and *Htr3a* female homozygous mutants did not differ significantly in their average voiding frequencies despite a trending increase in void frequency in female *Htr3a*-/- mice that trends in the same direction as that seen for *Htr3a*-/- males (6.97 ± 1.29, 6.42 ± 0.99, and 9.98 ± 1.27 voids, respectively, p=0.09108, one-way ANOVA, n=13-19 animals per genotype). Total void surface area averaged over three trial days was not significantly different among *Htr3a* genotypes in males or females (data not shown). From these experiments we conclude that male *Htr3a*-/- mutant mice have more frequent urinary voids.

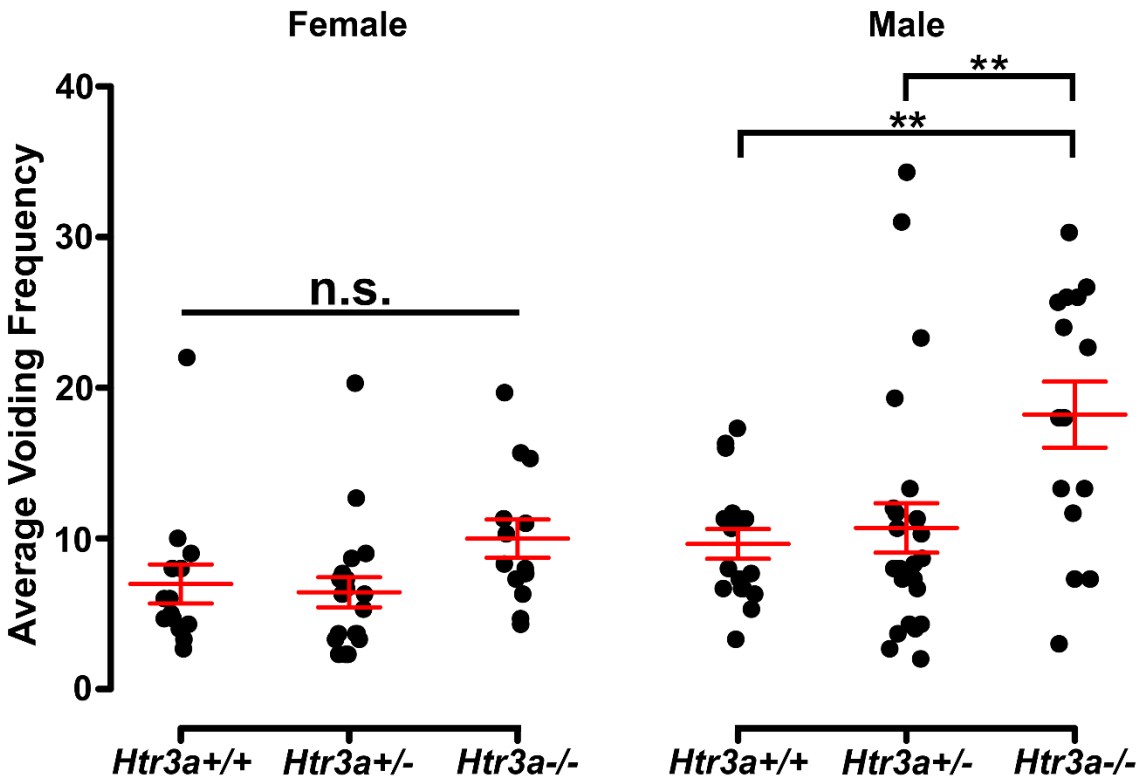

Figure 4.2 Male *Htr3a-/-* mice, but not females, exhibit increased urinary voiding frequency in a spontaneous void spot assay. Plot of average voiding frequency (number of individual voids over the testing period) assessed by void spot assays in female and male *Htr3a*+/+, *Htr3a*+/-, and *Htr3a*-/- 5-week old mice. Individual black dots represent different animals within each genotype class. The red lines indicate mean ± SEM. Female homozygous mutants trend towards increased voiding frequency but the difference in means is not statistically significant (p=0.0911, one-way ANOVA). Male homozygous mutants, however, exhibit increased voiding frequency relative to wild type (p=0.0046, one-way ANOVA with Tukey's HSD post-hoc test) and heterozygous (p=0.0074, one-way ANOVA with Tukey's HSD post-hoc test) littermates. n=13-25 animals per group.

Male Htr3a-/- urinary voiding efficiency is impaired

The 5-HT3A receptor is expressed not only in the autonomic pelvic ganglia and sensory dorsal root ganglia supplying bladder innervation, but also in other aspects of the micturition circuitry. Recent work has shown that 5-HT3A is expressed in Barrington's nucleus, the locus coeruleus, periaqueductal gray, and entorhinal cortex (Koyama et al., 2017), all of which have been previously implicated in relaying autonomic output and cortical regulation of voiding behavior (Fowler et al., 2008). Because the *Htr3a*-/- mutant line used in our studies is a global knockout, micturition centers in the brain expressing 5-HT3A may also be affected. To determine if the effects of 5-HT3A loss observed in the spontaneous void spot assay are due to autonomic dysfunction or cognitive control of voiding behavior, we conducted anesthetized bladder cystometry in vivo in female and male *Htr3a*+/+, *Htr3a*+/-, and *Htr3a*-/- adult mice. Anesthesia of the animals during cystometry allows isolation of involuntary urinary voiding and eliminates the behavioral component of micturition. Parameters measured during anesthetized cystometry included bladder volume-to-body weight ratio, intercontractile interval, maximal voiding pressure, void volume, bladder capacity, and non-voiding bladder contractions. There were no significant differences between any of the *Htr3a* genotype classes for these measures among either male or female mice (Table 4.3). Representative cystometric traces that illustrate comparable values are shown in Figure 4.3, Panels A-B. In addition, we measured voiding efficiency, which is defined as the percentage of bladder capacity expelled in one voiding event (Figure 4.3, Panel C). Normally, an efficient bladder will expel its entire bladder capacity in one voiding event, which would be reflected in a voiding efficiency value of nearly 100%. Wild type male mice exhibited an average voiding efficiency of 97.24 ± 3.01% while heterozygous mice had a voiding efficiency of 94.39 ± 1.98% and homozygous mutant voiding efficiency was 87.30

± 3.12% (n=7-14 animals per genotype). This level of voiding efficiency was significantly different for male *Htr3a*-/- mice compared to wild type littermates (p=0.0357, one-way ANOVA with Tukey's HSD post-hoc test). Despite the significant difference in voiding efficiency for homozygous mice, voiding efficiency of heterozygous mice was not significantly different from wild type or homozygous littermates (p=0.7068 and p=0.0826 respectively, one-way ANOVA with Tukey's HSD post-hoc test). Average voiding efficiencies of *Htr3a*+/+, *Htr3a*+/-, and *Htr3a*-/- females were similar, with values of 90.19 ± 6.60%, 90.35 ± 3.01%, and 86.43 ± 4.49% respectively (p=0.7701, one-way ANOVA, n=6-10 animals per genotype). Given the detrimental effect of *Htr3a* gene loss on the ability of homozygous males to efficiently empty bladder content, we conclude that 5-HT3A is required for maintaining normal lower urinary tract function in male mice.

Table 4.3 Summary of anesthetized bladder cystometry measurements

Cystometric Parameter	**Female *Htr3a*+/+**	**Female *Htr3a*+/-**	**Female *Htr3a*-/-**	**One-way ANOVA p-value**	**Male *Htr3a*+/+**	**Male *Htr3a*+/-**	**Male *Htr3a*-/-**	**One-way ANOVA p-value**
Voiding Efficiency	90.19% ± 6.60%	90.35 ± 3.01%	86.43 ± 4.49%	0.7701	97.24% ± 3.01%	94.39 ± 1.98%	87.30% ± 3.12%	**0.0287***
Bladder Volume/Body Weight Ratio (mm^3/g)	33.96 ± 6.92	32.25 ± 5.71	34.88 ± 7.99	0.9618	78.48 ± 22.23	64.51 ± 10.89	38.97 ± 7.90	0.2000
Bladder Capacity (μL)	54.43 ± 8.01	63.69 ± 6.55	80.97 ± 17.33	0.3427	77.55 ± 11.55	69.81 ± 11.18	75.51 ± 16.66	0.9153
Intercontractile Interval (sec)	244.92 ± 36.06	286.59 ± 29.49	364.44 ± 77.99	0.3423	348.41 ± 51.98	314.17 ± 50.31	339.80 ± 74.96	0.9154
Void Volume (μL)	50.38 ± 8.99	58.32 ± 6.75	67.17 ± 12.94	0.5490	77.84 ± 11.61	66.58 ± 10.21	64.60 ± 13.61	0.7609
Maximum Void Pressure (mmHg)	26.62 ± 3.75	28.56 ± 1.09	32.09 ± 1.26	0.1556	20.53 ± 1.38	21.40 ± 1.36	23.38 ± 2.20	0.5388
Non-Voiding Contractions	0.083 ± 0.083	0.280 ± 0.207	0.478 ± 0.329	0.5979	1.39 ± 0.41	1.40 ±0.38	1.01 ± 0.33	0.7178

Anesthetized bladder cystometry was conducted to determine the effects of 5-HT3A receptor loss on unconscious voiding activity. Mean values ± SEM are given for female and male wild type, heterozygous, and homozygous *Htr3a*KO adult mice. One-way ANOVA was conducted to determine if differences in means were significant among female and male mice. The statistically significant p-value (<0.05) is presented in bold with an asterisk. Voiding efficiency is defined as the percent bladder capacity expelled in a voiding event. Bladder volume-to-body weight ratio was calculated by dividing the bladder volume (mm^3) by the animal's total body weight. Bladder capacity is defined as the intervoid interval multiplied by the infusion rate of saline during the assay. Intercontractile interval is defined as the time (in seconds) between voiding events. Void volume is defined as the volume of infusate voided during a micturition event. Maximum void pressure is defined as the peak intravesical bladder pressure immediately prior to micturition. Non-voiding contractions are defined as rhythmic increases in intravesical pressure that occur between micturition events.

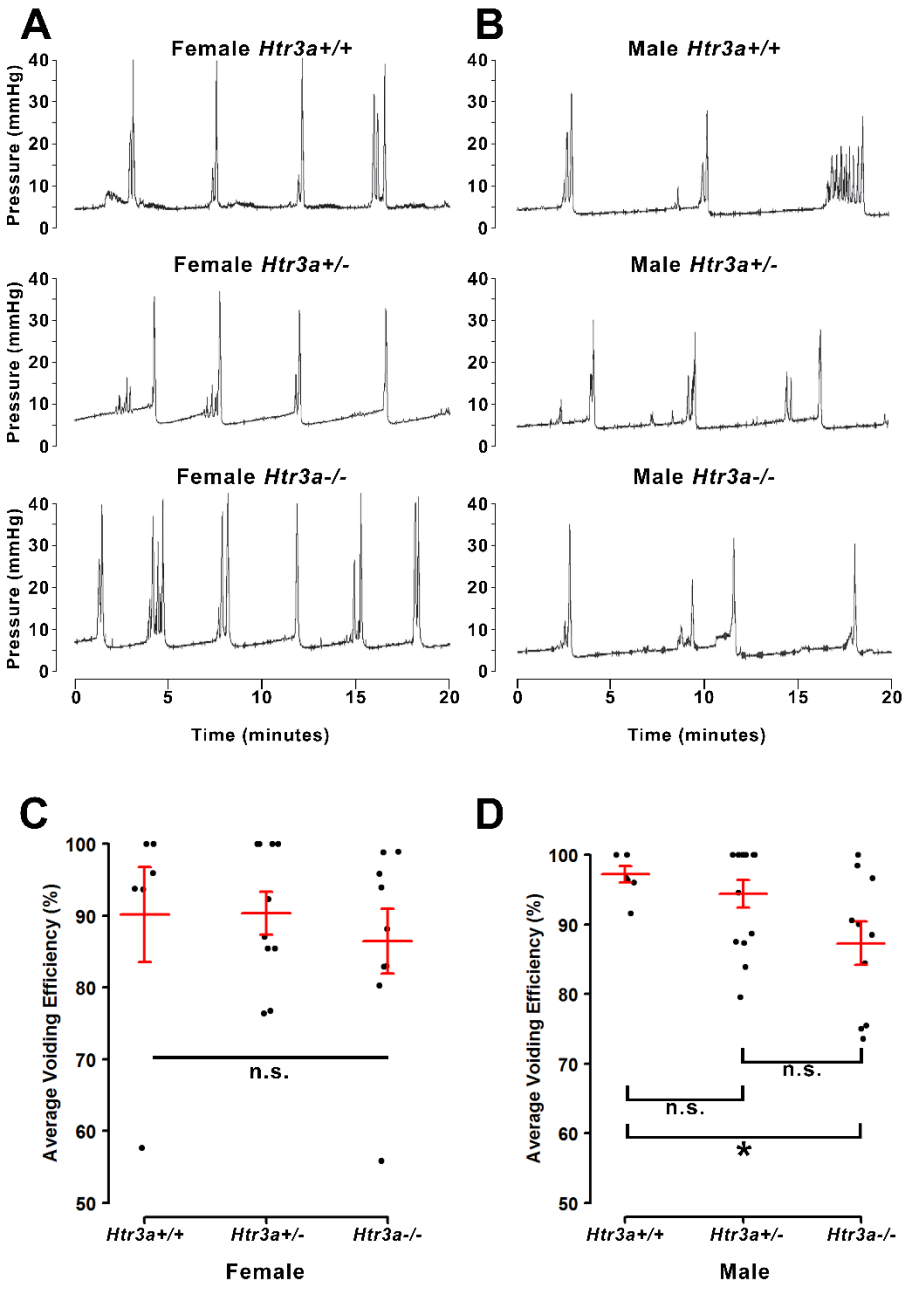

Figure 4.3 Male, but not female, *Htr3a-/-* mice demonstrate decreased bladder voiding efficiency compared to wild type mice. Voiding efficiency, calculated as the percentage bladder capacity expelled per void, was measured in adult *Htr3a*KO animals *in vivo* via anesthetized bladder cystometry. Intraluminal bladder pressure (mmHg) was measured over time (minutes) *in vivo* in (**A**) female adult mice, and (**B**) male adult mice. (**C**) Jitter plot of voiding efficiency in female *Htr3a*+/+, *Htr3a*+/-, and *Htr3a-/-* adult mice. Red lines indicate mean ± SEM. The difference in voiding efficiency in female mice was not significant (p=0.7701, one-way ANOVA). (**D**) Jitter plot of voiding efficiency in male *Htr3a*+/+, *Htr3a*+/-, and *Htr3a*-/- adult mice. *Htr3a*-/- males demonstrate a significant decrease in voiding efficiency compared to wild type littermates (p=0.0357, one-way ANOVA with Tukey's HSD post-hoc test). The difference between *Htr3a*+/- and wild type littermates was not significant (p=0.7068, one-way ANOVA with Tukey's HSD post-hoc test), nor was the difference between *Htr3a*+/- and homozygotes (p=0.0826, one-way ANOVA with Tukey's HSD post-hoc test). n=6-14 animals per group.

Loss of 5-HT3A disrupts autonomic neuronal marker expression patterns in fetal pelvic ganglia

Given the consequences of *Htr3a* gene loss on adult bladder function and our observation of *Htr3a* expression in fetal mouse pelvic ganglia, we examined the effects of *Htr3a* loss on the development of pelvic ganglia neurons. To assess the composition of pelvic ganglia during development, we monitored the appearance of cholinergic neurons that comprise the majority of pelvic ganglia neuronal subtypes (Wanigasekara et al., 2003) as well as noradrenergic neurons labeled by tyrosine hydroxylase (TH) expression. *Htr3a* mutants were crossed with the Tg(*ChAT*-EGFP)GH293Gsat/Mmucd (hereafter *ChAT*-EGFP) transgenic reporter mouse line (Gong et al., 2003) to facilitate imaging of cholinergic neurons, as direct visualization by GFP labeled discrete cholinergic neurons more readily than several commercially available ChAT antisera (data not shown). Progeny from intercrosses of *ChAT*-EGFP; *Htr3a*+/- mice were sectioned sagittally and stained for TH and the pan-neuronal marker Hu C/D. At 14.5dpc, we observed a visible reduction in *ChAT*-EGFP expression in *Htr3a*+/- and *Htr3a*-/- pelvic ganglia compared to *Htr3a*+/+ littermates, along with a concurrent increase in TH expression (n=4 animals per genotype, Figure 4.4). However, when we examined expression of these markers in adult (6-8 weeks old) male and female pelvic ganglia, the differences between *Htr3a* genotypes seen at 14.5dpc were no longer apparent among multiple replicates examined (n=6 animals per genotype, Figure 4.5). Expression of TH in adult pelvic ganglia across all three genotype classes was comparable to prior reports of noradrenergic neurons in adult mice (Yan and Keast, 2008). From these experiments we conclude that loss of 5-HT3A receptor produces a transient disruption of expression of autonomic neuronal subtype markers in fetal pelvic ganglia.

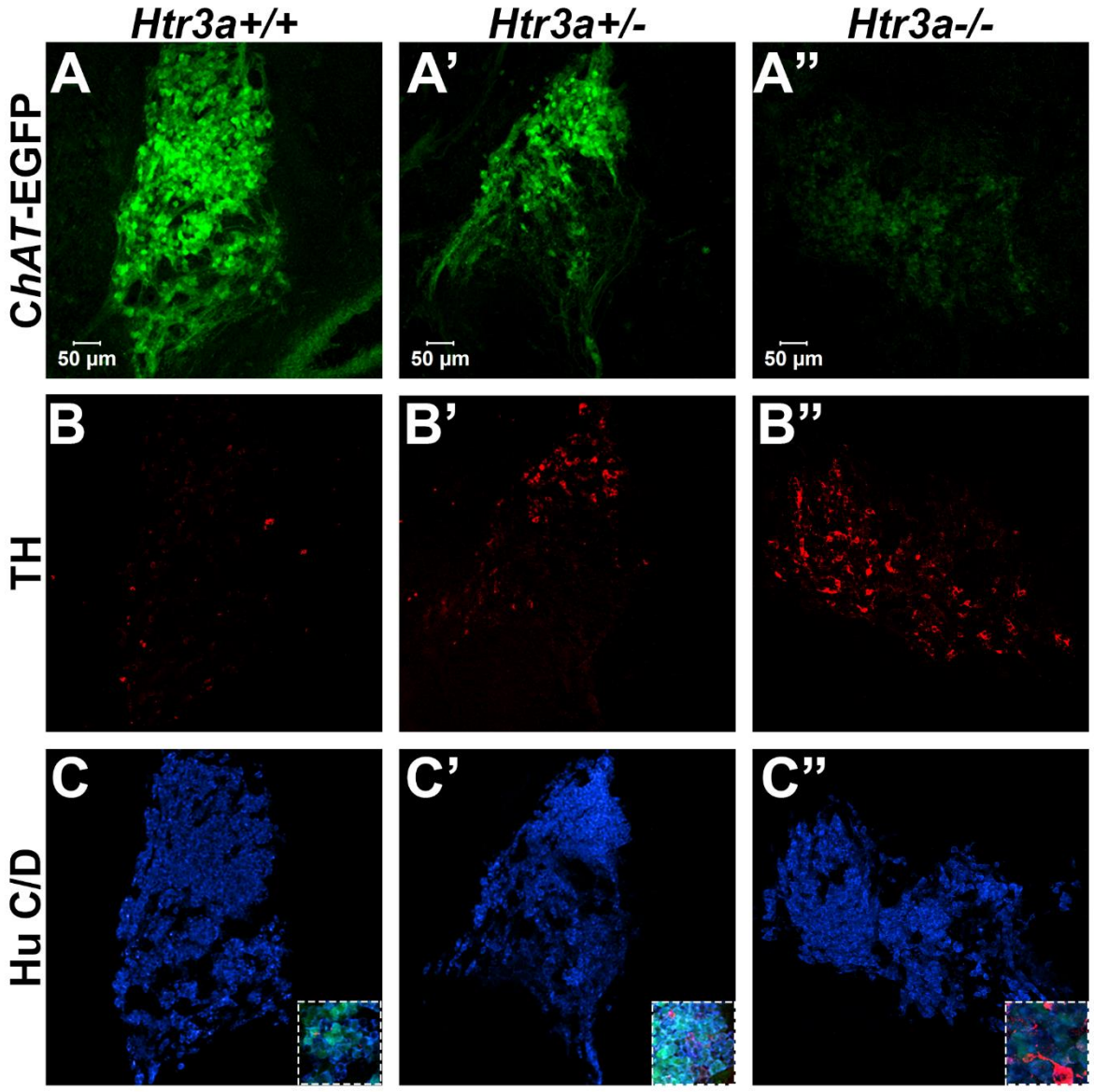

Figure 4.4 Loss of serotonin receptor *Htr3a* increases expression of tyrosine hydroxylase in fetal pelvic ganglia. Confocal images of sagittal cryo-sections of male 14.5dpc *ChAT*-EGFP; *Htr3a*KO pelvic ganglia stained with adrenergic neuronal marker tyrosine hydroxylase (TH) and pan-neuronal marker Hu C/D. (**A-A"**) *ChAT*-EGFP, labeling cholinergic neurons, is markedly reduced in *Htr3a* mutant fetal pelvic ganglia compared to wild type. (**B-B"**) TH, labeling adrenergic neurons, is increased in *Htr3a* mutant fetal pelvic ganglia compared wild type (**C-C"**) Expression of pan-neuronal marker Hu C/D is similar among all three genotypes examined at 14.5dpc. Insets show 5X zoom of merged images of all three markers. n=4 animals per genotype.

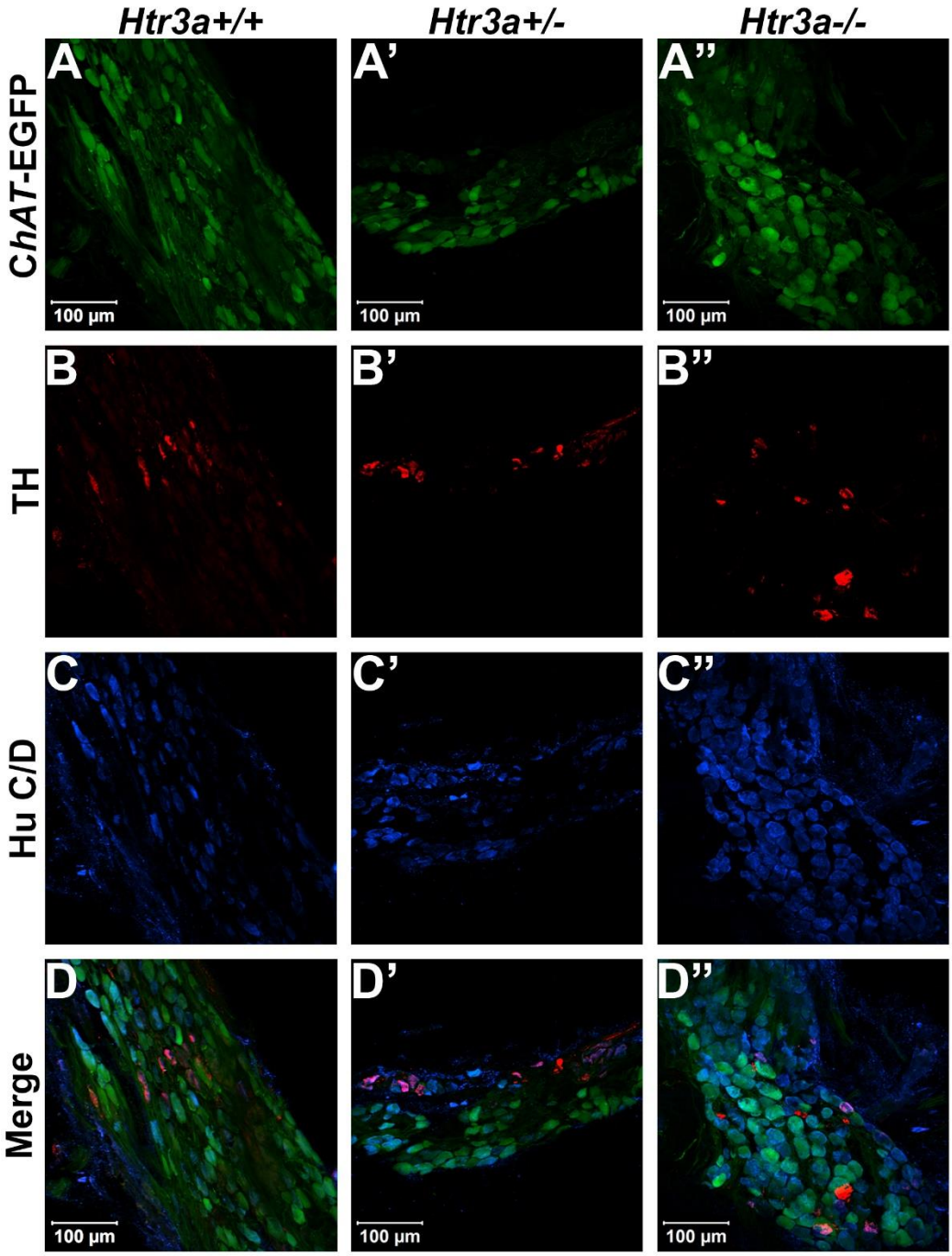

Figure 4.5 Autonomic marker expression patterns are normal in adult *Htr3a* mutant pelvic ganglia. Confocal images of cryo-sections of adult (6 weeks old) male *ChAT*-EGFP; *Htr3a*KO pelvic ganglia stained with adrenergic neuronal marker TH and pan-neuronal marker Hu C/D. Expression patterns of (**A-A"**) *ChAT*-EGFP; (**B-B"**) TH; and (**C-C"**) Hu C/D are similar among *Htr3a*+/+, *Htr3a*+/-, and *Htr3a*-/- pelvic ganglia. (**D-D"**) merged images of panels A-C, A'-C', and A"-C". n=6 animals per genotype.

Htr3a mutant bladder detrusor is more densely innervated compared to wild type

The 5-HT3A receptor has been previously implicated in mediating neuronal morphological complexity in the developing mouse brain (Chameau et al., 2009;Oostland et al., 2013). Specifically, *Htr3a*-/- mice exhibit hyper-elaboration of pyramidal neuronal dendritic fibers in the developing cortex; however, its role in peripheral neuronal development in vivo has not been reported. To determine if loss of 5-HT3A alters aspects of peripheral neuronal development or neuronal morphology, we conducted immunohistochemistry and measured innervation density of bladder smooth muscle on sagittal section from 18.5dpc *Htr3a*+/+, *Htr3a*+/-, and *Htr3a*-/- mice (n=5 animals per genotype). After staining for a variety of neuronal markers, we measured the percentage of pixels of a minimum intensity level within a fixed area of bladder smooth muscle for three domains (total bladder, bladder neck, and bladder dome) as a proxy for average area innervated by labeled neuronal fibers. These measurements, along with statistical p-values, are listed in Table 4.4.

We first asked if overall innervation patterns differed between wild type, heterozygous, and *Htr3a*-/- fetal tissues by staining for the pan-neuronal marker Tuj1 (β-III tubulin) that strongly labels neuronal fibers. Interestingly, Tuj1+ staining was significantly increased in all areas of bladder smooth muscle examined in *Htr3a*+/- and *Htr3a*-/- samples compared to wild type littermates ($p=0.0232$ and $p=0.0057$ respectively, one-way ANOVA with Tukey's HSD post-hoc test). The average innervation density in wild type bladders was 9.87 ± 1.15%, while *Htr3a*+/- and *Htr3a*-/- Tuj1+ innervation densities were nearly doubled (16.22 ± 1.57% and 17.82 ± 1.58%, respectively) (Figure 4.6, Panels A-A"). The difference between *Htr3a*+/- and *Htr3a*-/- Tuj1+ innervation density measurements was not statistically significant ($p=0.7193$, one-way ANOVA with Tukey's HSD post-hoc test).

Table 4.4 Measurements of 18.5 dpc bladder smooth muscle innervation density

		Percentage Innervation Density in 18.5dpc Bladder Smooth Muscle (average ± SEM)			One-way ANOVA	One-way ANOVA with Tukey's post-hoc HSD p-values		
Neuron Marker		*Htr3a+/+*	*Htr3a+/-*	*Htr3a-/-*	Overall	+/+ vs. +/-	+/- vs. -/-	+/+ vs. -/-
Tuj1	Total	9.87 ± 1.15	16.22 ± 1.57	17.82 ± 1.58	**0.0052**	**0.0232**	0.7193	**0.0057**
	Neck	10.67 ± 1.76	18.27 ± 1.52	18.99 ± 2.17	**0.0135**	**0.0315**	0.9595	0.1928
	Dome	9.34 ± 0.82	14.76 ± 1.80	17.04 ± 1.38	**0.0061**	**0.0432**	0.4997	**0.0055**
vAChT	Total	7.23 ± 1.71	15.06 ± 4.19	18.47 ± 2.33	**0.0316**	0.1601	0.6706	**0.0283**
	Neck	7.80 ± 1.94	13.95 ± 3.07	19.28 ± 3.14	**0.0335**	0.3081	0.4029	**0.0269**
	Dome	6.85 ± 1.63	14.67 ± 4.10	17.92 ± 1.99	**0.0248**	0.1327	0.6637	**0.0223**
CGRP	Total	1.29 ± 0.24	1.43 ± 0.34	2.38 ± 0.78	0.2986	N/A	N/A	N/A
	Neck	1.62 ± 0.35	1.94 ± 0.46	3.18 ± 1.05	0.2777	N/A	N/A	N/A
	Dome	1.08 ± 0.18	1.08 ±0.28	1.84 ± 0.63	0.3612	N/A	N/A	N/A
NF200	Total	8.05 ± 1.69	10.07 ± 1.92	11.42 ± 2.32	0.5118	N/A	N/A	N/A
	Neck	9.13 ± 1.85	10.29 ± 1.77	12.92 ± 2.35	0.4284	N/A	N/A	N/A
	Dome	7.33 ± 1.78	9.92 ± 2.08	10.42 ± 2.31	0.5488	N/A	N/A	N/A

Innervation density was measured by calculating the percentage of pixels in a selected region of 18.5dpc bladder smooth muscle that exceeded the threshold intensity level for neuronal fiber staining. Average percentages were calculated from values obtained from images of superior and inferior bladder neck ("Bladder Neck"), and superior, inferior, and apex of bladder dome ("Bladder Dome"). "Total Bladder" innervated density was calculated by averaging the percentage values from both bladder neck and bladder dome. Overall differences in means were statistically compared with one-way ANOVA; Tukey's Honest Significant Difference (HSD) post-hoc test was conducted to compare pairs of means. Statistically significant p-values ($p<0.05$) are presented in bold.

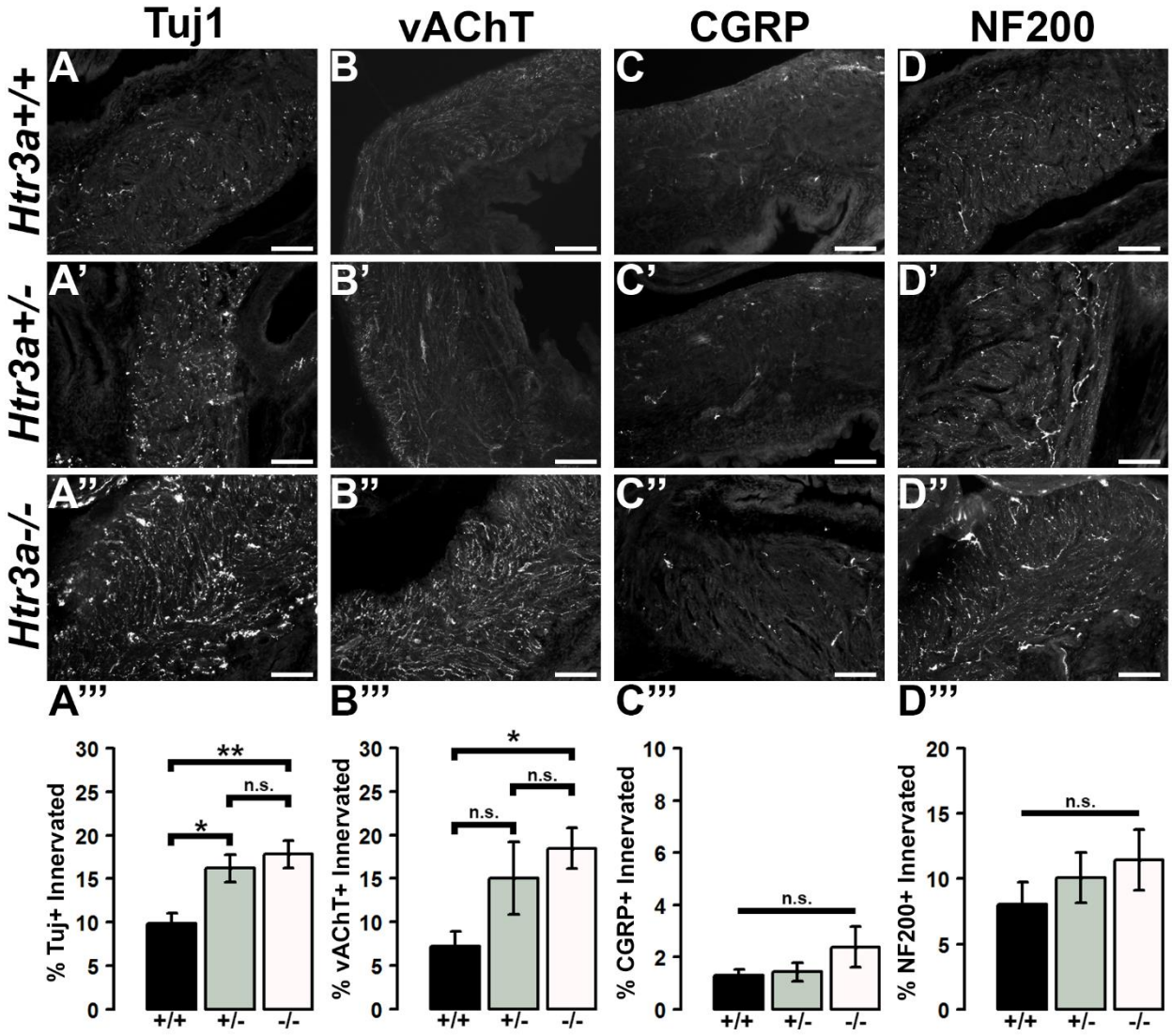

Figure 4.6 Loss of serotonin receptor *Htr3a* leads to increased density of autonomic innervation in late fetal bladder smooth muscle. Sagittal cryo-sections of *Htr3a*+/+, *Htr3a*+/-, and *Htr3a*-/- 18.5dpc bladders stained with neuronal markers. (**A-A"**) Tuj1, pan-neuronal marker; (**B-B"**) vesicular acetylcholine transporter (vAChT), marker of cholinergic autonomic neurons; (**C-C"**) Calcitonin Gene Related Peptide (CGRP), marker of peptidergic sensory neurons; (**D-D"**) Neurofilament 200 (NF200), marker of Aδ mechanosensory neurons. Innervation density was quantified by measuring the percentage of pixels within fixed areas of bladder smooth muscle images that met the gray value threshold indicative of neuronal fiber staining. Bar plots of innervation density illustrate quantification of combined superior and inferior bladder neck and superior, inferior, and apex of bladder dome innervated ± SEM by Tuj1+ (**A"'**), vAChT+ (**B"'**), CGRP+ (**C"'**), and NF200+ (**D"'**) fibers. Overall differences in means were assessed by one-way ANOVA; statistical significance of differences between pairs of means are listed in Table 4.4. $p<0.05$ was considered significant. n=5 animals per genotype. Scale bar = 100μm.

Given the large proportion of cholinergic neurons found in the autonomic pelvic ganglia and their critical role in mediating bladder contractility (de Groat and Yoshimura, 2015), we next asked if 18.5dpc *Htr3a* mutants would exhibit perturbed cholinergic innervation patterns in the bladder smooth muscle. Upon staining with vesicular acetylcholine transporter (vAChT), we observed that 7.23 ± 1.71% of the wildtype bladder smooth muscle received vAChT+ innervation, while average innervation density in *Htr3a*+/- and *Htr3a*-/- animals was 15.06 ± 4.19% and 18.47 ± 2.33% respectively. The increase in *Htr3a*-/- vAChT+ bladder innervation density was significant compared to wild type bladder ($p=0.0283$, one-way ANOVA with Tukey's HSD post-hoc test), but *Htr3a*+/- innervation density was not significantly different compared to either wild type or homozygous bladder ($p=0.1601$ and $p=0.6706$ respectively, one-way ANOVA with Tukey's HSD post-hoc test) (Figure 4.6, Panels B-B").

The sensation of bladder filling and muscle stretch is primarily detected by sensory afferent neurons in the dorsal root ganglia (de Groat and Yoshimura, 2015). During our prior analysis of *Htr3a* expression in the developing dorsal root ganglia, we documented that many bladder-innervating sensory neurons expressing *Htr3a* also express neuropeptide Calcitonin Gene Related Peptide (CGRP) and mechanosensory marker Neurofilament 200 (NF200) (Ritter and Southard-Smith, 2017). We were interested to see if these populations would be affected by loss of *Htr3a*. Upon staining for CGRP, we did not observe any significant differences in CGRP+ innervation density of bladder at 18.5dpc ($p=0.2986$, one-way ANOVA) (Figure 4.6, Panels C-C"). CGRP+ innervation density in *Htr3a*+/+, *Htr3a*+/-, and *Htr3a*-/- averaged 1.29 ± 0.24%, 1.43 ± 0.34%, and 2.38 ± 0.78%, respectively. Similarly, fetal bladders across these three genotypes did not differ significantly in NF200+ innervation density (Figure 4.6, Panels D-D"). Innervation density of NF200+ fibers were 8.05 ± 1.69%, 10.01 ± 1.92%, and 11.42 ±

2.32% for *Htr3a*+/+, *Htr3a*+/-, and *Htr3a*-/- respectively (p=0.5118, one-way ANOVA). From these experiments we conclude that in late fetal development, loss of *Htr3a* gene expression results in an overall increase in the presence of neuronal fibers in fetal bladder smooth muscle, with cholinergic fibers being particularly enriched while sensory fibers are not at this stage of development.

Due to the refining of neural architecture that may occur over the postnatal developmental period (Purves and Lichtman, 1980;Tapia et al., 2012), we sought to determine if differences in innervation patterns would also be present in adult *Htr3a* mutants. We conducted the same staining and analysis procedures on adult male *Htr3a*+/+, *Htr3a*+/-, and *Htr3a*-/- bladder sagittal sections (n=5 animals per genotype, Table 4.5). Quantification of Tuj1+ staining in adult bladder tissues similarly revealed a significant increase in innervation density in *Htr3a*-/- mutant bladder compared to wild type (p=0.0033, one-way ANOVA with Tukey's HSD post-hoc test) (Figure 4.7, Panels A-A"). The average adult wild type Tuj1+ innervation density was 6.32 ± 0.72%, while *Htr3a*+/- bladders were 9.01 ± 0.81% innervated and *Htr3a*-/- bladders exhibited a two-fold increase in innervation density, with average percent innervated values of 12.54 ± 1.49%. The difference between *Htr3a*+/- and wild type Tuj1 innervation density was not significant (p=0.2082, one-way ANOVA with Tukey's HSD post-hoc test), nor was the difference between *Htr3a*+/- and *Htr3a*-/- Tuj1 innervation density (p=0.0828, one-way ANOVA with Tukey's HSD post-hoc test).

When we stained for vAChT to visualize cholinergic fibers in adult bladder tissues we noted that *Htr3a* mutants maintained higher than normal levels of cholinergic fiber density into adulthood, and the difference among genotypes was more pronounced than in fetal samples. Adult *Htr3a*+/+ bladder smooth muscle tissues had an average vAChT+ innervation density of

Table 4.5 Measurements of adult bladder smooth muscle innervation density

		Percentage Innervation Density in Adult Bladder Smooth Muscle (average ± SEM)			One-way ANOVA	One-way ANOVA with Tukey's post-hoc HSD p-values		
Neuron Marker		*Htr3a+/+*	*Htr3a+/-*	*Htr3a-/-*	Overall	+/+ vs. +/-	+/- vs. -/-	+/+ vs. -/-
Tuj1	Total	6.32 ± 0.72	9.01 ± 0.81	12.54 ± 1.49	**0.0044**	0.2082	0.0828	**0.0033**
	Neck	6.89 ± 0.57	9.89 ± 1.09	12.38 ± 0.94	**0.0034**	0.0832	0.1631	**0.0026**
	Dome	5.94 ± 0.87	8.51 ± 1.01	12.64 ± 2.42	**0.0351**	0.5106	0.2016	**0.0294**
vAChT	Total	3.74 ± 0.54	6.94 ± 1.36	11.98 ± 1.57	**0.0018**	0.2041	**0.0344**	**0.0014**
	Neck	4.19 ± 0.95	7.56 ± 1.84	12.04 ± 1.74	**0.0131**	0.3130	0.1477	**0.0102**
	Dome	3.43 ± 0.39	6.59 ± 1.15	11.95 ± 1.62	**0.0008**	0.1789	**0.0183**	**0.0006**
CGRP	Total	2.32 ± 0.43	4.49 ± 0.89	7.43 ± 1.17	**0.0052**	0.2323	0.0867	**0.0039**
	Neck	2.53 ± 0.43	5.07 ± 0.85	8.71 ± 1.97	**0.0153**	0.3605	0.1459	**0.0122**
	Dome	2.18 ± 0.49	4.10 ± 1.03	6.59 ± 0.77	**0.0069**	0.2426	0.1082	**0.0053**
NF200	Total	3.01 ± 0.29	6.06 ± 0.83	7.92 ± 0.79	**0.0009**	**0.0219**	0.1759	**0.0007**
	Neck	4.26 ± 0.68	5.45 ± 0.80	9.59 ± 1.33	**0.0057**	0.6754	**0.0279**	**0.0061**
	Dome	2.18 ± 0.12	6.42 ± 1.08	6.81 ± 0.79	**0.0019**	**0.0059**	0.9316	**0.0031**

Innervation density was measured by calculating the percentage of pixels in a selected region of adult bladder smooth muscle that exceeded the threshold intensity level for neuronal fiber staining. Average percentages were calculated from values obtained from images of superior and inferior bladder neck ("Bladder Neck"), and superior, inferior, and apex of bladder dome ("Bladder Dome"). "Total Bladder" innervated density was calculated by averaging the percentage values from both bladder neck and bladder dome. Overall differences in means were statistically compared with one-way ANOVA; Tukey's Honest Significant Difference (HSD) post-hoc test was conducted to compare pairs of means. Statistically significant p-values ($p<0.05$) are presented in bold.

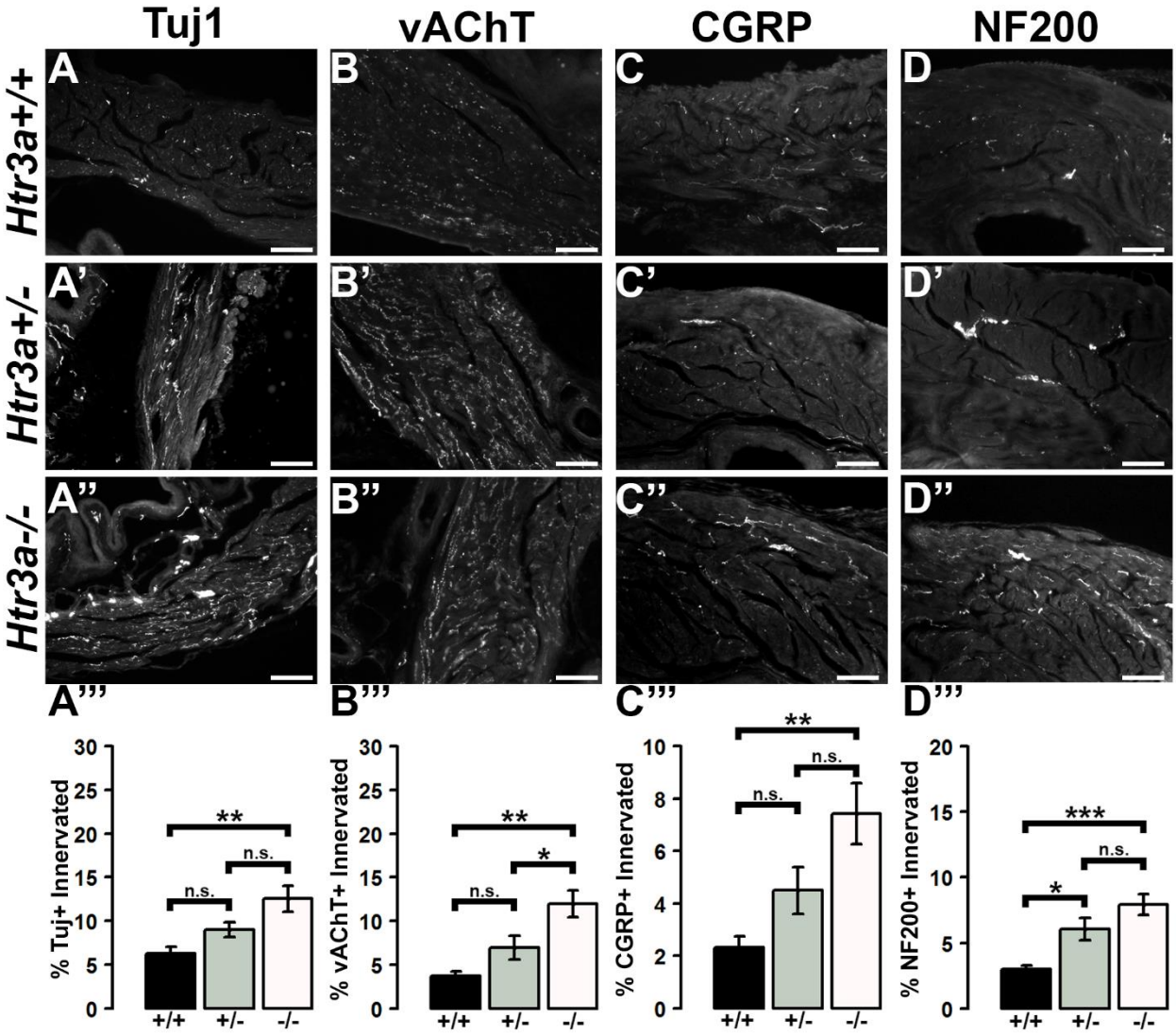

Figure 4.7 Loss of serotonin receptor *Htr3a* leads to increased density of both autonomic and sensory innervation in adult bladder smooth muscle. Sagittal cryo-sections of *Htr3a*+/+, *Htr3a*+/-, and *Htr3a*-/- adult male bladders stained with neuronal markers. (**A-A"**) Tuj1, pan-neuronal marker; (**B-B"**) vesicular acetylcholine transporter (vACHT), marker of autonomic cholinergic neurons; (**C-C"**) Calcitonin Gene Related Peptide (CGRP), marker of peptidergic sensory neurons; (**D-D"**) Neurofilament 200 (NF200), marker of Aδ mechanosensory neurons. Innervation density was quantified by measuring the percentage of pixels within fixed areas of bladder smooth muscle images that met the gray value threshold indicative of neuronal fiber staining. Bar plots of innervation density illustrate quantification of combined superior and inferior bladder neck and superior, inferior, and apex of bladder dome innervated ± SEM by Tuj1+ (**A"'**), vAChT+ (**B"'**), CGRP+ (**C"'**), and NF200+ (**D"'**) fibers. Overall differences in means were assessed by one-way ANOVA; statistical significance of differences between pairs of means are listed in Table 4.5. $p<0.05$ was considered significant. n=5 animals per genotype. Scale bar = 100μm.

3.74 ± 0.54% (Figure 4.7, Panels B-B"). In contrast, *Htr3a*+/- and *Htr3a*-/- bladder tissues had an average innervation density of 6.94 ± 1.36% and 11.98 ± 1.57%, respectively. *Htr3a*-/- vAChT+ innervation density was significantly increased compared to both wild type and heterozygous littermates (p=0.0014 and p=0.0344 respectively, one-way ANOVA with Tukey's HSD post-hoc test), but *Htr3a*+/- vAChT+ innervation was not significantly different from wild type (p=0.2041, one-way ANOVA with Tukey's HSD post-hoc test).

Quantification of sensory innervation density by immunohistochemical localization of CGRP+ fibers revealed that, in contrast to density of sensory innervation in fetal tissues, bladder smooth muscle of adult *Htr3a*-/- mutants is more densely innervated by sensory fibers than that of wild type (p=0.0039, one-way ANOVA with Tukey's HSD post-hoc test) (Figure 4.7, Panels C-C"). Wild type bladder had an average CGRP+ innervation density of 2.32 ± 0.43%, while *Htr3a*+/- innervation density levels were 4.49 ± 0.89% and *Htr3a*-/- CGRP+ innervation was increased approximately three-fold, values of 7.43 ± 1.17%. *Htr3a*+/- CGRP+ innervation density was not significantly different from either wild type or *Htr3a*-/- tissues (p=0.2323 and p=0.0867 respectively, one-way ANOVA with Tukey's HSD post-hoc test).

Staining adult bladder tissues with NF200 also revealed a highly significant increase in mechanosensory neuronal innervation of both adult *Htr3a*+/- and *Htr3a*-/- mutant bladder smooth muscle compared to wild type (p=0.0219 and p=0.0007 respectively, one-way ANOVA with Tukey's HSD post-hoc test) (Figure 4.7, Panels D-D"). *Htr3a*+/+ average NF200+ innervation density was 3.01 ± 0.29%, while *Htr3a*+/- and *Htr3a*-/- innervation densities were 6.06 ± 0.83% and 7.92 ± 0.79% respectively. The difference between *Htr3a*+/- and *Htr3a*-/- NF200+ innervation density measurements was not statistically significant (p=0.1759, one-way ANOVA with Tukey's HSD post-hoc test). From our experiments on adult *Htr3a* mutant

tissues, we conclude that loss of *Htr3a* gene expression has sustained effects on innervation densities beyond fetal and postnatal development, in which mutant bladder smooth muscle has an overabundance of neuronal fibers, including cholinergic, neuropeptidergic, and mechanosensory.

Discussion

While the effects of serotonin signaling in neural development have been studied for decades, the 5-HT3A serotonin receptor has only recently been recognized as a key player in developmental mechanisms (Engel et al., 2013). These recent studies of 5-HT3A signaling in neural development have been focused on the CNS. The goal of this study was to define the expression and role of 5-HT3A in the development of urinary bladder innervation and determine whether this serotonin receptor is required for normal voiding in adult mice. Using a knockout mouse model of 5-HT3A deficiency, we demonstrate a novel role for this serotonin receptor in the development of the peripheral nervous system architecture and show that perturbing 5-HT3A signaling has lasting effects on visceral organ function in adult animals. The analysis presented has important ramifications for the potential impact of pharmacological agents taken during pregnancy that may have long-lasting effects on bladder innervation and function in later life.

Expression of 5-HT3A was first demonstrated in 14.5dpc autonomic pelvic ganglia via in situ hybridization over two decades ago (Tecott et al., 1993;Tecott et al., 1995); surprisingly, these findings have not been further investigated. Our expression analysis using the *Htr3a*-EGFP transgenic reporter allele confirms expression of 5-HT3A in fetal pelvic ganglia at stages when neurogenesis is actively occurring (Wiese et al., 2017). Moreover, our results show for the first time that the 5-HT3A receptor is maintained in adult pelvic ganglia and is expressed in the majority of adult pelvic ganglia neurons (Figure 4.1).

VSAs have been established as a means to quantify urinary voiding in an environment as similar to the animals' home cage environment as possible and thus eliminate many confounding factors inherent to other methods of urinary voiding assessment (Yu et al., 2014;Keil et al., 2016). Our VSA study of *Htr3a* mutant mice revealed an increase in voiding frequency in male Htr3a mutants compared to wild type littermates (Figure 4.2). This is the first report of any urinary tract dysfunction in *Htr3a* homozygous loss of function mutants. Because detection of any urinary dysfunction requires unique experimental assays and careful analysis of large animal cohorts, this aspect of the *Htr3a* knockout phenotype was most likely overlooked by prior studies of these mutants that observed the animals in their home cage environment.

Differences in voiding frequency measured in a 4-hour VSA have not been previously reported for wild type post-pubescent male and female mice on a C57BL6/J background (Bjorling et al., 2015). We had anticipated that there would be no sex specific effects in our analysis of *Htr3a* mutants. Remarkably, we found that loss of the 5-HT3A receptor in *Htr3a* knockout mice differentially affects voiding patterns of males and females by VSA before the onset of reproductive maturity. The increased voiding frequency we observed in male *Htr3a* mutants suggests that 5-HT3A receptor activity normally functions in male mice to inhibit urinary voiding. It should be noted that female *Htr3a*-/- animals in our VSA study exhibited a slight trending increase in urinary voiding frequency compared to wild type animals, but the increase in frequency was not statistically significant. Our observation suggests that the 5-HT3A receptor may be involved in inhibiting micturition in both males and females, but does so to a greater extent in male mice. In contrast, a pharmacological study conducted in cats demonstrated that 5-HT3A receptor signaling inhibits the micturition drive in both male and female cats (Schwen et al., 2013). A separate study examining the effects of 17alpha-estradiol and 17beta-

estradiol in vitro found that these hormones can act as allosteric antagonists of 5-HT3A in an exogenous expression system (Wetzel et al., 1998;Oz et al., 2002), but the mechanisms by which sex hormones may alter 5-HT3A activity in regulating urinary voiding in vivo are unknown. Interestingly, estrogen receptors are expressed in parasympathetic pelvic ganglia neurons (Purves-Tyson et al., 2007) and sex hormones have been shown to influence pelvic ganglia neuron function (Keast, 2006), providing an avenue by which 5-HT3A may mediate urinary tract function in a sex-specific manner. Further studies focused on determining if sex hormones regulate 5-HT3A signaling in vivo and how this signaling contributes to sex differences in micturition circuitry would be valuable.

Because *Htr3a* is expressed in many brain regions involved in cognitive control of micturition and our study relied upon a global *Htr3a* knockout mouse line, there is the possibility that the increase in urinary frequency observed in male *Htr3a* mutants could be due to abnormal cognitive control of when and where to void. However, the anesthetized bladder cystometry assay we applied addresses this issue by specifically measuring involuntary, autonomic urinary bladder voiding (Figure 4.3). The finding that male *Htr3a* mutants exhibit decreased voiding efficiency is consistent with the results obtained in our VSA testing. The results of both of these experiments together suggest that 5-HT3A receptor signaling is required in males for maintaining normal urinary tract function. There are multiple aspects of lower urinary tract function that could affected by the loss of 5-HT3A activity, including bladder detrusor contractility and its coordination with urethral sphincter relaxation (detrusor-sphincter dyssynergia). Future studies combining the use of cystometry with electromyography recordings of the external urethral sphincter would be valuable for elucidating these mechanisms in *Htr3a* mutants.

A prior study utilizing the *Htr3a*$^{vs/vs}$ mouse model, which expresses a constitutively active hypersensitive form of the 5-HT3A receptor, also reported poor urinary bladder function in adult males (Bhattacharya et al., 2004) that were accompanied by bladder wall hyperplasia. However, in contrast to the deficits reported in the *Htr3a*$^{vs/vs}$ hypersensitive mutants, we did not find any evidence of bladder outlet obstruction or other overt LUT malformations in *Htr3a*KO mice. Our findings in concert with those of Bhattacharya et al. indicate that the control of micturition in mice is acutely sensitive to levels of 5-HT3A receptor activity and highlight the importance of interrogating gene function from multiple angles. Both the *Htr3a*-/- and the *Htr3a*$^{vs/vs}$ mutants are constitutive alleles, with the effect of the receptor variants exerted through the entire window of endogenous gene expression. Given that *Htr3a* is expressed during LUT development and into adulthood, our studies raise the intriguing question of whether 5-HT3A receptor activity is required at a specific time during the development of bladder innervation. Use of an inducible *Htr3a* mutant allele in conjunction with assays of urinary tract function will be needed to determine the developmental time point when 5-HT3A receptor activity is most critical for establishing normal voiding patterns in adults.

The pelvic ganglia in mice are unique among autonomic structures in that they are comprised of both sympathetic and parasympathetic neurons (Keast, 1995;Wanigasekara et al., 2003). Given the widespread and sustained expression of 5-HT3A in these structures, we sought to determine if *Htr3a* knockout would affect expression of autonomic neuronal subtype markers. Interestingly, we observed expression of TH is visibly up-regulated in *Htr3a* homozygous mutant fetal pelvic ganglia compared to wild type and heterozygous littermates, with a concurrent down-regulation of cholinergic marker ChAT. However, by adulthood the discernable differences in TH+ and ChAT+ cells seen at 14.5dpc were no longer apparent

(Figures 4.4 and 4.5). Prior work has established that TH and ChAT levels in pelvic ganglia neurons can be profoundly affected by circulating sex hormones (Melvin and Hamill, 1987;Keast, 2006); thus, it is possible that 5-HT3A receptor signaling is not required for post-pubescent TH and ChAT gene expression. Stage-specific effects of 5-HT3A knockout to discern the effects of this receptor on neurochemical profiles in the pelvic ganglia could be explored in the future with an inducible *Htr3a* mutant allele.

The 5-HT3A receptor has been previously shown to be critical for the morphological maturation of neurons in the CNS (Chameau et al., 2009;Smit-Rigter et al., 2011;Oostland et al., 2013), but whether *Htr3a* expression is required for normal peripheral neuronal morphology has not been previously investigated. In the present study, we found that loss of *Htr3a* gene expression leads to an excess of neuronal fibers innervating the smooth muscle of the bladder, indicating the requirement of this receptor for the normal maturation of neural architecture in peripheral tissue. Regardless of *Htr3a* genotype, bladder smooth muscle intensity was reduced in adult tissues compared to 18.5dpc (with exception being CGRP+ fibers, Figures 4.6 and 4.7). This is likely due to the pruning of neuronal branches that normally occurs in postnatal development (Purves and Lichtman, 1980;Riccomagno and Kolodkin, 2015). The exception of CGRP+ fibers suggests that there are neuronal subtype-specific differences in the time course of neuronal process outgrowth and maturation. It is also possible that expression of CGRP in neuronal fibers within the bladder changes over postnatal development. Our prior study examining gene expression profiles in developing dorsal root ganglia indicates that CGRP expression is somewhat dynamic through development (Ritter and Southard-Smith, 2017), but further work is needed to explore these possibilities further.

The observation that loss of one or both copies of the *Htr3a* gene leads to an increase in bladder smooth muscle innervation density of all four neuronal markers examined suggests that 5-HT3A may act to either inhibit neuronal fiber outgrowth, or may possibly be involved in the process of fiber pruning in postnatal development. Other research groups have reported similar effects of 5-HT3A loss; the apical dendrites of layer II/III cortical pyramidal neurons in the brain exhibit significantly more complex branching morphology in *Htr3a*-/- mice compared to wild type littermates (Chameau et al., 2009;Smit-Rigter et al., 2011). However, other groups have reported contradictory results from in vitro studies of this receptor – in PC12 cells, 5-HT3A receptor activation promotes neurite outgrowth via increased calcium flux (Homma et al., 2006). Interestingly, the study by Bhattacharya et al. using the hyperactive *Htr3a*$^{vs/vs}$ variant described reduced nerve fiber density in bladder smooth muscle whereas our analysis looking at loss of *Htr3a* function identified increased innervation. Together, these findings suggest that the density of bladder innervation is dependent on the levels of 5-HT3A receptor activity. In light of these results, future studies are needed to identify the molecular factors downstream of 5-HT3A activation that govern neuronal architecture in peripheral neurons as a pathway to defining mechanisms that control bladder innervation.

Our results collectively have important implications for human neural development. The changes in adult male voiding function that derive from loss of 5-HT3A in mice may occur as a result of deficient 5-HT signaling in the fetus, the adult, or both. While mouse studies cannot be directly translated to humans, the results of altered 5-HT3A receptor signaling that we describe suggest more thorough investigation focused on the outcomes of pharmacological intervention at this receptor during gestation is warranted. Ondansetron, a potent 5-HT3A receptor antagonist, is commonly prescribed to pregnant women to treat severe nausea (McParlin et al., 2016;Taylor

et al., 2017). Additionally, the selective serotonin reuptake inhibitor (SSRI) fluoxetine, which is also prescribed frequently to pregnant women for the treatment of depression, has been shown by other groups to interact with 5-HT3A (Eisensamer et al., 2003;Smit-Rigter et al., 2012). Overall, the current study highlights the importance of 5-HT3A receptor signaling in adult urinary bladder function and demonstrates a novel role for this receptor in autonomic and sensory nervous system development.

Acknowledgements

This work was supported by grants (NIH U01 DK101038 and Pilot Award Support from the Vanderbilt Conte Center for Neuroscience Research P50 MH096972) to EMS^2, grant NIH U54 DK103410 to DEB, ZW, and CMV (co-authors of this manuscript), and NIH F31-DK097938 to KER. Imaging performed in Vanderbilt University's Cell Imaging Shared Resource (CISR) is supported by NIH grants CA68485, DK20593, P50-DK58404, HD15052, DK59637, and EY08126. Two of the mouse strains used in this work, Tg(*Htr3a*-EGFP)DHGsat/Mmnc (stock number 000273-UNC) and Tg(*ChAT*-EGFP)CH293Gsat/Mmucd were acquired from the Mutant Mouse Research Resource Center (MMRRC), a NCRR-NIH funded mouse line repository, and were donated to the MMRRC by the NINDS-funded GENSAT BAC transgenic project. We are grateful for the Hu C/D antibody generously donated by Dr. Vanda Lennon at the Mayo Clinic.

References

Bhattacharya, A., Dang, H., Zhu, Q.M., Schnegelsberg, B., Rozengurt, N., Cain, G., Prantil, R., Vorp, D.A., Guy, N., Julius, D., Ford, A.P., Lester, H.A., and Cockayne, D.A. (2004). Uropathic observations in mice expressing a constitutively active point mutation in the 5-HT3A receptor subunit. *J Neurosci* 24**,** 5537-5548. doi: 10.1523/JNEUROSCI.5658-03.2004.

Bjorling, D.E., Wang, Z., Vezina, C.M., Ricke, W.A., Keil, K.P., Yu, W., Guo, L., Zeidel, M.L., and Hill, W.G. (2015). Evaluation of voiding assays in mice: impact of genetic strains and sex. *Am J Physiol Renal Physiol* 308**,** F1369-1378. doi: 10.1152/ajprenal.00072.2015.

Boudes, M., Uvin, P., Pinto, S., Freichel, M., Birnbaumer, L., Voets, T., De Ridder, D., and Vennekens, R. (2013). Crucial role of TRPC1 and TRPC4 in cystitis-induced neuronal sprouting and bladder overactivity. *PLoS One* 8**,** e69550. doi: 10.1371/journal.pone.0069550.

Chameau, P., Inta, D., Vitalis, T., Monyer, H., Wadman, W.J., and Van Hooft, J.A. (2009). The N-terminal region of reelin regulates postnatal dendritic maturation of cortical pyramidal neurons. *Proc Natl Acad Sci U S A* 106**,** 7227-7232. doi: 10.1073/pnas.0810764106.

De Groat, W., and Yoshimura, N. (2015). "Anatomy and physiology of the lower urinary tract," in *Handbook of Clinical Neurology,* eds. D.B. Vodusek & F. Boller. Elsevier), 61-108.

De Groat, W.C., Griffiths, D., and Yoshimura, N. (2015). Neural control of the lower urinary tract. *Compr Physiol* 5**,** 327-396. doi: 10.1002/cphy.c130056.

Eisensamer, B., Rammes, G., Gimpl, G., Shapa, M., Ferrari, U., Hapfelmeier, G., Bondy, B., Parsons, C., Gilling, K., Zieglgansberger, W., Holsboer, F., and Rupprecht, R. (2003). Antidepressants are functional antagonists at the serotonin type 3 (5-HT3) receptor. *Mol Psychiatry* 8**,** 994-1007. doi: 10.1038/sj.mp.4001314.

Engel, M., Smidt, M.P., and Van Hooft, J.A. (2013). The serotonin 5-HT3 receptor: a novel neurodevelopmental target. *Front Cell Neurosci* 7**,** 76. doi: 10.3389/fncel.2013.00076.

Fowler, C.J., Griffiths, D., and De Groat, W.C. (2008). The neural control of micturition. *Nat Rev Neurosci* 9**,** 453-466. doi: 10.1038/nrn2401.

Fullhase, C., Campeau, L., Sibaev, A., Storr, M., Hennenberg, M., Gratzke, C., Stief, C., Hedlund, P., and Andersson, K.E. (2013). Bladder function in a cannabinoid receptor type 1 knockout mouse. *BJU Int* 113**,** 144-151.

Gong, S., Zheng, C., Doughty, M.L., Losos, K., Didkovsky, N., Schambra, U.B., Nowak, N.J., Joyner, A., Leblanc, G., Hatten, M.E., and Heintz, N. (2003). A gene expression atlas of the cental nervous system based on bacterial artificial chromosomes. *Nature* 425**,** 917-925.

Homma, K., Kitamura, Y., Ogawa, H., and Oka, K. (2006). Serotonin induces the increase in intracellular Ca2+ that enhances neurite outgrowth in PC12 cells via activation of 5-HT3 receptors and voltage-gated calcium channels. *J Neurosci Res* 84**,** 316-325. doi: 10.1002/jnr.20894.

Keast, J.R. (1995). Visualization and immunohistochemical characterization of sympathetic and parasympathetic neurons in the male rat major pelvic ganglion. *Neuroscience* 66**,** 655-662.

Keast, J.R. (2006). Plasticity of Pelvic Autonomic Ganglia and Urogenital Innervation. *Int Rev Cytol* 248**,** 141-208. doi: 10.1016/s0074-7696(06)48003-7.

Keast, J.R., Smith-Anttila, C.J., and Osborne, P.B. (2015). Developing a functional urinary bladder: a neuronal context. *Front Cell Dev Biol* 3**,** 53. doi: 10.3389/fcell.2015.00053.

Keil, K.P., Abler, L.L., Altmann, H.M., Bushman, W., Marker, P.C., Li, L., Ricke, W.A., Bjorling, D.E., and Vezina, C.M. (2016). Influence of animal husbandry practices on void spot assay outcomes in C57BL/6J male mice. *Neurourol Urodyn* 35**,** 192-198. doi: 10.1002/nau.22692.

Kim, J.H., Lee, S.R., Song, Y.S., and Lee, H.J. (2013). Stem cell therapy in bladder dysfunction: where are we? And where do we have to go? *Biomed Res Int* 2013**,** 930713. doi: 10.1155/2013/930713.

Koyama, Y., Kondo, M., and Shimada, S. (2017). Building a 5-HT3A Receptor Expression Map in the Mouse Brain. *Sci Rep* 7**,** 42884. doi: 10.1038/srep42884.

Lai, H., Yan, Q.T., Cao, H., Chen, P., Xu, Y., Jiang, W., Wu, Q., Huang, P., and Tan, B. (2016). Effect of SQW on the bladder function of mice lacking TRPV1. *BMC Complement Altern Med* 16**,** 465.

Mcparlin, C., O'donnell, A., Robson, S.C., Beyer, F., Moloney, E., Bryant, A., Bradley, J., Muirhead, C.R., Nelson-Piercy, C., Newbury-Birch, D., Norman, J., Shaw, C., Simpson, E., Swallow, B., Yates, L., and Vale, L. (2016). Treatments for Hyperemesis Gravidarum and Nausea and Vomiting in Pregnancy: A Systematic Review. *JAMA* 316**,** 1392-1401. doi: 10.1001/jama.2016.14337.

Melvin, J.E., and Hamill, R.W. (1987). The Major Pelvic Ganglion: Androgen Control of Postnatal Development. *J Neurosci* 7**,** 1607-1612.

Oostland, M., Buijink, M.R., and Van Hooft, J.A. (2013). Serotonergic control of Purkinje cell maturation and climbing fibre elimination by 5-HT3 receptors in the juvenile mouse cerebellum. *J Physiol* 591**,** 1793-1807. doi: 10.1113/jphysiol.2012.246413.

Oz, M., Zhang, L., and Spivak, C.E. (2002). Direct noncompetitive inhibition of 5-HT(3) receptor-mediated responses by forskolin and steroids. *Arch Biochem Biophys* 404**,** 293-301.

Potter, K.A., Simon, J.S., Velagapudi, B., and Capadona, J.R. (2012). Reduction of autofluorescence at the microelectrode-cortical tissue interface improves antibody detection. *J Neurosci Methods* 203**,** 96-105. doi: 10.1016/j.jneumeth.2011.09.024.

Purves-Tyson, T.D., Arshi, M.S., Handelsman, D.J., Cheng, Y., and Keast, J.R. (2007). Androgen and estrogen receptor-mediated mechanisms of testosterone action in male rat pelvic autonomic ganglia. *Neuroscience* 148**,** 94-104.

Purves, D., and Lichtman, J.W. (1980). Eliminaton of Synapses in the Developing Nervous System. *Science* 210**,** 153-157.

Riccomagno, M.M., and Kolodkin, A.L. (2015). Sculpting Neural Circuits by Axon and Dendrite Pruning. *Annu Rev Cell Dev Biol* 13**,** 779-805.

Ritter, K.E., and Southard-Smith, E.M. (2017). Dynamic Expression of Serotonin Receptor 5-HT3A in Developing Sensory Innervation of the Lower Urinary Tract. *Front Neurosci* 10**,** 592. doi: 10.3389/fnins.2016.00592.

Ritter, K.E., Wang, Z., Vezina, C.M., Bjorling, D.E., and Southard-Smith, E.M. (2017). Serotonin Receptor 5-HT3A Affects Development of Bladder Innervation and Urinary Bladder Function. *Frontiers in Neuroscience* 11. doi: 10.3389/fnins.2017.00690.

Roman, K., Murphy, S.F., Done, J.D., Mckenna, K.E., Schaeffer, A.J., and Thumbikat, P. (2016). Role of PAR2 in the Development of Lower Urinary Tract Dysfunction. *Journal of Urology* 196**,** 588-598.

Schwen, Z., Matsuta, Y., Shen, B., Wang, J., Roppolo, J.R., De Groat, W.C., and Tai, C. (2013). Involvement of 5-HT3 receptors in pudendal inhibition of bladder overactivity in cats. *Am J Physiol Renal Physiol* 305**,** F663-671. doi: 10.1152/ajprenal.00105.2013.

Smit-Rigter, L.A., Noorlander, C.W., Von Oerthel, L., Chameau, P., Smidt, M.P., and Van Hooft, J.A. (2012). Prenatal fluoxetine exposure induces life-long serotonin 5-HT(3) receptor-dependent cortical abnormalities and anxiety-like behaviour. *Neuropharmacology* 62**,** 865-870. doi: 10.1016/j.neuropharm.2011.09.015.

Smit-Rigter, L.A., Wadman, W.J., and Van Hooft, J.A. (2011). Alterations in Apical Dendrite Bundling in the Somatosensory Cortex of 5-HT(3A) Receptor Knockout Mice. *Front Neuroanat* 5**,** 64. doi: 10.3389/fnana.2011.00064.

Tapia, J.C., Wylie, J.D., Kasthuri, N., Hayworth, K.J., Schalek, R., Berger, D.R., Guatimosim, C., Seung, H.S., and Lichtman, J.W. (2012). Pervasive synaptic branch removal in the mammalian neuromuscular system at birth. *Neuron* 74**,** 816-829. doi: 10.1016/j.neuron.2012.04.017.

Taylor, L.G., Bird, S.T., Sahin, L., Tassinari, M.S., Greene, P., Reichman, M.E., Andrade, S.E., Haffenreffer, K., and Toh, S. (2017). Antiemetic use among pregnant women in the United States: the escalating use of ondansetron. *Pharmacoepidemiol Drug Saf* 26**,** 592-596. doi: 10.1002/pds.4185.

Tecott, L., Shtrom, S., and Julius, D. (1995). Expression of a serotonin-gated ion channel in embryonic neural and nonneural tissues. *Mol Cell Neurosci* 6**,** 43-55. doi: 10.1006/mcne.1995.1005.

Tecott, L.H., Maricq, A.V., and Julius, D. (1993). Nervous system distribution of the serotonin 5-HT3 receptor mRNA. *Proc Natl Acad Sci U S A* 90**,** 1430-1434.

Uvin, P., Everaerts, W., Pinto, S., Alpizar, Y.A., Boudes, M., Gevaert, T., Voets, T., Nilius, B., Talavera, K., and De Ridder, D. (2012). The Use of Cystometry in Small Rodents: A Study of Bladder Chemosensation. *Journal of Visualized Experiments* 66.

Vera, P.L., and Nadelhaft, I. (2001). Clozapine inhibits micturition parameters and the external urethral sphincter during cystometry in anesthetized rats. *Brain Res* 901**,** 219-229.

Wagg, A.S., Cardozo, L., Chapple, C., De Ridder, D., Kelleher, C., Kirby, M., Milsom, I., and Vierhout, M. (2007). Overactive bladder syndrome in older people. *BJU Int* 99**,** 502-509. doi: 10.1111/j.1464-410X.2006.06677.x.

Wanigasekara, Y., Kepper, M.E., and Keast, J.R. (2003). Immunohistochemical characterisation of pelvic autonomic ganglia in male mice. *Cell Tissue Res* 311**,** 175-185. doi: 10.1007/s00441-002-0673-1.

Wetzel, C.H., Hermann, B., Behl, C., Pestel, E., Rammes, G., Zieglgansberger, W., Holsboer, F., and Rupprecht, R. (1998). Functional antagonism of gonadal steroids at the 5-hydroxytryptamine type 3 receptor. *Mol Endocrinol* 12**,** 1441-1451.

Wiese, C.B., Deal, K.K., Ireland, S.J., Cantrell, V.A., and Southard-Smith, E.M. (2017). Migration pathways of sacral neural crest during development of lower urogenital tract innervation. *Dev Biol* 429**,** 356-369.

Wu, L., Zhang, X., Xiao, N., Huang, Y., Kavran, M., Elrashidy, R.A., Wang, M., Daneshgari, F., and Liu, G. (2016). Functional and Morphological Alterations of the Urinary Bladder in Type 2 Diabetic FVBdb/db Mice. *J Diabetes Complications* 30**,** 778-785.

Wyndaele, J.J. (2016). The management of neurogenic lower urinary tract dysfunction after spinal cord injury. *Nat Rev Urol* 13**,** 705-714. doi: 10.1038/nrurol.2016.206.

Yan, H., and Keast, J.R. (2008). Neurturin regulates postnatal differentiation of parasympathetic pelvic ganglion neurons, initial axonal projections, and maintenance of terminal fields in male urogenital organs. *J Comp Neurol* 507**,** 1169-1183. doi: 10.1002/cne.21593.

Yu, W., Ackert-Bicknell, C., Larigakis, J.D., Maciver, B., Steers, W.D., Churchill, G.A., Hill, W.G., and Zeidel, M.L. (2014). Spontaneous voiding by mice reveals strain-specific lower urinary tract function to be a quantitative genetic trait. *Am J Physiol Renal Physiol* 306**,** F1296-1307. doi: 10.1152/ajprenal.00074.2014.

Zeitz, K.P., Guy, N., Malmberg, A.B., Dirajlal, S., Martin, W.J., Sun, L., Bonhaus, D.W., Stucky, C.L., Julius, D., and Basbaum, A.I. (2002). The 5-HT3 Subtype of Serotonin Receptor Contributes to Nociceptive Processing via a Novel Subset of Myelinated and Unmyelinated Nociceptors. *Journal of Neuroscience* 22**,** 1010-1019.

Zullo, M.A., Manci, N., Angioli, R., Muzii, L., and Panici, P.B. (2003). Vesical dysfunctions after radical hysterectomy for cervical cancer: a critical review. *Critical Reviews in Oncology/Hematology* 48**,** 287-293.

CHAPTER V

SUMMARY AND FUTURE DIRECTIONS

Lower urinary tract dysfunction significantly impacts quality of life and remains difficult to treat. The identification of novel signaling components involved in the development and maturation of bladder innervation would provide novel therapeutic targets for treatment of neurogenic bladder. In this dissertation I identified serotonin receptor 3A (5-HT3A, *Htr3a*) as a key regulator of autonomic and sensory innervation development and discovered its requirement for normal adult urinary tract function. In this chapter I provide a brief summary of my major experimental findings with a particular focus on their broader impact and discuss potential avenues for future research.

Roles for serotonin receptors in developing pelvic ganglia and bladder function

Despite decades of extensive study of adult LUT innervation and physiology, very little is known about the molecular components underlying the neural development of this system. In an effort to identify such factors, a microarray transcriptome profiling study was conducted in 13.5, 14.5, and 15.5 dpc pelvic ganglia from *Sox10*-H2BVenus transgenic mice (Chapter II). At these developmental time points when autonomic neurogenesis is progressing, *Htr3a* was found to be significantly enriched relative to total fetus mRNA levels. While *Htr3a* ultimately became the focus of this dissertation, other transcripts were identified in this study that would be of great interest in future work.

The B subunit of the 5-HT3 receptor (encoded by *Htr3b*) was also found to be significantly up-regulated in differentiating pelvic ganglia. This subunit is not required for assembly or function of the 5-HT3 receptor (Davies et al., 1999) and cannot form homopentamers. Interestingly, prior work has shown that 5-HT3A/B heteropentamers are less permeable to calcium and exhibit increased single channel conductance compared to 5-HT3A homopentamers (Davies et al., 1999;Noam et al., 2008). To the best of my knowledge, no developmental studies of 5-HT3B receptor subunit function have been published – defining developmental expression patterns of *Htr3b* can be conducted readily, as a *Htr3b*-EGFP transgenic reporter is available (Tg(*Htr3b*-EGFP)DP271GSat) and a viable *Htr3b*-KO mutant mouse line has recently been generated (Dickinson et al., 2016). These mutant animals could be used to determine how large of a role the 5-HT3B subunit plays in the function of 5-HT3 receptors in the lower urinary tract.

Another serotonin receptor gene, encoding the type 2A receptor (*Htr2a*) was found to be enriched in differentiating pelvic ganglia both by microarray profiling and reverse transcription PCR (Chapter II). The 5-HT2A receptor has been previously shown to be required for the development and/or maintenance of enteric neuroeffectors and components of the intestinal smooth muscle itself (Fiorica-Howells et al., 2002). Future studies examining roles for 5-HT2A signaling in other neural crest derived populations, such as the dorsal root ganglia and autonomic pelvic ganglia, would be valuable - especially in the light of a recent report that 5-HT2A activity stimulates contraction of bladder urothelial strips *ex vivo* (Moro et al., 2016). Additionally, rodent models of partial bladder outlet obstruction (BOO) exhibit significant up-regulation of *Htr2a* mRNA compared to non-BOO control animals (Sakai et al., 2013), indicating that there are clinical implications for further interrogation of 5-HT2A function in the lower urinary tract.

One could employ *Htr2a* knockout animals to determine if 5-HT2A activity is required for normal bladder function *in vivo.* Additionally, *Htr2a* knockout and wild type control mice could be compared in their responses to the induction of bladder outlet obstruction.

Downstream effectors of 5-HT3A mediating neural development

The studies reported in this dissertation examined the consequences of over-stimulating or depleting 5-HT3A receptor activity (Chapters II and IV) and support a critical role for 5-HT3A in peripheral nervous system development. The molecular factors downstream of 5-HT3A activation that mediate these effects need to be determined. Based on prior work on 5-HT3A conducted by other groups, there are several signaling pathways that are likely candidates.

Homopentameric 5-HT3A receptors are permeable to calcium upon binding of serotonin (Derkach et al., 1989). Calcium signaling plays extensive roles in neural development (Figure 5.1, from (Rosenberg and Spitzer, 2011)), and a recent study demonstrated the requirement of calcium flux via 5-HT3A receptors in the appropriate migration speed and direction of postnatal neuroblasts from the subventricular zone (Garcia-Gonzalez et al., 2017). Given these observations, 5-HT3A-mediated calcium flux may regulate neural development in the context of autonomic neurogenesis. To test this hypothesis, one could employ the *Sox10*-MSUM transgenic reporter mouse line generated in the Southard-Smith laboratory to isolate neural crest progenitors from the developing lower urinary tract. The *Sox10*-MSUM transgene allows live detection of calcium flux in cultured cells (unpublished data, Southard-Smith laboratory). This transgenic line provides an elegant way to determine how pharmacologically perturbing 5-HT3 receptor signaling would affect calcium flux in isolated *Sox10*-MSUM+ sacral neural crest progenitors, and how any potential changes in calcium signaling would ultimately affect the survival and

differentiation of these cells *in vitro*. Because *Sox10* is down-regulated in progenitors committed to a neuronal lineage (Corpening et al., 2011), this proposed experiment would be limited to early-stage progenitor cells. However, calcium indicator dye, such as Fura-2, could be used to visualize real-time calcium flux in isolated *Htr3a*-EGFP+ neurons isolated from the lower urinary tract. Additionally, the *Htr3a*-Cre mouse line could be crossed with another genetically encoded calcium indicator reporter line, Rosa26-GCaMP6, to study calcium flux in cells expressing the 5-HT3 receptor.

In a prior study focused on roles for 5-HT3 signaling in cortical development, the secreted glycoprotein reelin (encoded by *reln*) was found to be an important downstream mediator of 5-HT3 activation (Chameau et al., 2009). These authors found that Cajal-Retzius cells, which lie in layer I of the developing neocortex and have known roles in orchestrating laminar organization by secretion of reelin (Frotscher, 1997), express functional 5-HT3 receptor in perinatal development. Upon activation of 5-HT3 receptors, Cajal-Retzius cells secrete reelin near the apical dendrites of layer II/III pyramidal neurons. In the canonical reelin signaling pathway, reelin binds to the VLDL receptor and ApoER2 receptor to subsequently activate intracellular signaling mediators, such as Dab1 and Lis1 (Ranaivoson et al., 2016). However, Chameau et al. 2009 discovered that the effects of reelin on dendritic arbor elaboration are in fact mediated by a non-canonical signaling pathway involving the binding of the N-terminal fragment of reelin to β1/β3 integrin receptors. By knocking out *Htr3a*, or using an antibody to bind and block the N-terminus of reelin, or pharmacological inhibition of β1/β3 integrin receptors, the authors observed an increase in the complexity of the dendritic arbor of layer II/III pyramidal neurons. These experimental findings are in line with the increased density of innervation I

observed in bladder smooth muscle of *Htr3a-/-* mice (Chapter IV), and set the stage for further pursuit of the role of 5-HT3 receptor signaling in neural crest biology.

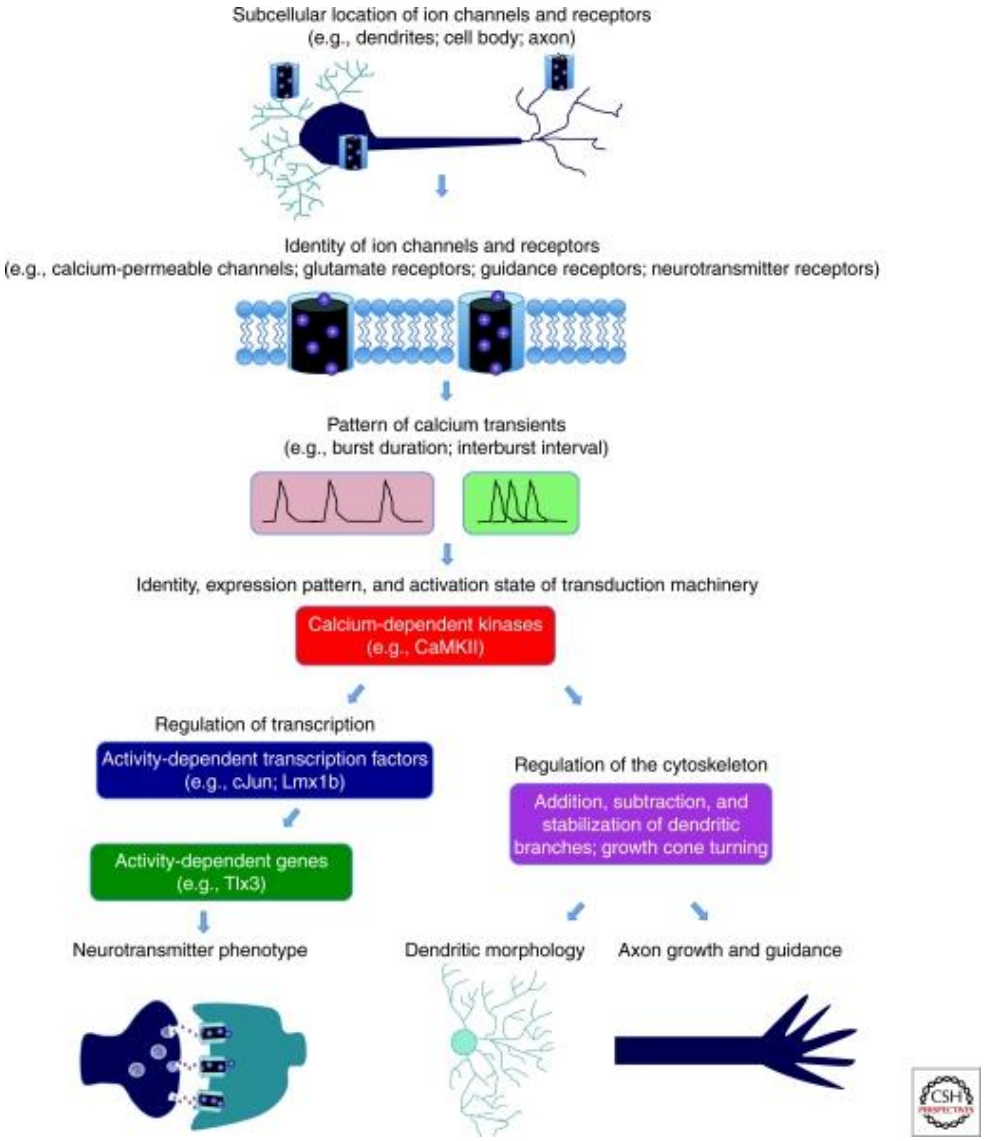

Figure 5.1 Mechanisms of calcium signaling in neuronal development. Flux of calcium via ion channels, such as the 5-HT3A receptor, leads to downstream activation of molecular components that drive changes in gene expression and cellular morphology that underlie neuronal differentiation. From Rosenberg and Spitzer, 2011.

Integrins are heterodimeric transmembrane proteins that have well-established roles throughout neural crest developmental processes, particularly in cell migration and neuronal fiber outgrowth (Previtali et al., 2001). The ends of neuronal processes, termed growth cones, rely on integrin receptors to interpret the extracellular environment (guidance and repulsion cues) and ultimately form substrate contacts and functional synapses. Ligand binding of integrin receptors leads to neuritic outgrowth or growth cone contraction by stimulating the activity of intracellular regulators of the actin cytoskeleton, as well as by direct interaction with cytoskeletal components (Schmidt et al., 1995;Myers et al., 2011). The known importance of integrin receptor signaling in cytoskeletal dynamics presents a likely mechanism for how 5-HT3 receptor activity influences the development of neuronal morphological maturation. Whether the 5-HT3/reelin/integrin receptor signaling mechanism is active in developing neural crest cells is an open question – in fact, reelin signaling outside the brain has only been studied in the context of sympathetic preganglionic neurons in the spinal cord, which are not neural crest-derived (Yip et al., 2003;Yip et al., 2007). Interestingly, *reln* gene expression has been detected by *in situ* hybridization in 14.5 dpc pelvic ganglia in the Eurexpress database (Diez-Roux et al., 2011) and is significantly enriched in 15.5 dpc pelvic ganglia (2.55 fold change, p=4.16e-9) in the transcriptome profiling experiment described in Chapter II. Given that urinary dysfunction is typically only observed in experiments specifically designed to assess voiding activity, mice expressing a mutant form of *reln* ("reeler" mice) have not been reported to exhibit any time of urinary voiding phenotype. To determine if reelin signaling is involved in lower urinary tract dysfunction, voiding patterns could be assessed in reeler mice using the spontaneous void spot assay and anesthetized bladder cystometry methods described in Chapter IV. Because β1 integrin receptors are also required for early neural crest cell migration (Turlo et al., 2012), β1

integrin receptor knockout is embryonic lethal. To interrogate β1 integrin receptor function in the context of pelvic ganglia neuronal development, one could sub-dissect and culture *Sox10*-H2BVenus+ pelvic ganglia explants as described in Chapter II and determine if β1 integrin receptors are expressed in these cells via immunohistochemistry. If β1 integrin receptors are expressed, their function in neuronal process outgrowth could be determined by treating these cultures with echistatin, which is a potent inhibitor of β1/β3 integrin receptors, and measuring the complexity and size of the neuritic arbor via Sholl analysis. Additionally, the N-terminal fragment of reelin could be applied to these explant cultures and subsequent effects on neurite morphology could be determined. If conducted, these studies would be the first report of reelin signaling in any neural crest cell type and would provide further alternative mechanisms by which neuronal fiber regeneration could be regulated in a therapeutic context (e.g., pharmacological inhibition of β1/β3 integrin receptors to stimulate neurite growth).

Htr3a **lineage analysis**

In the characterization of *Htr3a* gene expression in fetal development, I noted strong fluorescence of *Htr3a*-EGFP in neural crest derivatives as early as 10.5 dpc (Chapter III). Given the early timing of its expression, and the abundant supply of serotonin to the embryo via the placenta (Bonnin and Levitt, 2011), 5-HT3A receptor signaling may be involved in the development of multiple neural crest lineages in early embryonic development. Additionally, in the experiments focused on developmental potential of sacral neural crest progenitors in response to serotonergic drugs (Chapter II), agonizing 5-HT3 receptors was found to increase the percentage of mixed neuronal/myofibroblast colonies and decrease the percentage of purely neuronal colonies compared to control samples. This finding is the first report of 5-HT3 activity

in lineage determination of any cell type, and raises interesting questions about how this receptor mediates neural crest stem cell fate choice. To approach this question in an *in vivo* setting (and demonstrate that the observed results are not an artifact of culture conditions), I envision several experiments that can be conducted using transgenic mouse lines readily available in the Southard-Smith laboratory.

First, fate mapping analyses can be performed using the Tg(*Htr3a*-Cre)NO152GSat (hereafter *Htr3a*-Cre) transgenic mouse line to trace lineages derived from *Htr3a*-expressing cells. I have used these animals to examine the contribution of *Htr3a*-derived cells in postnatal pelvic and dorsal root ganglia (see Chapter VI), but have not thoroughly explored other tissues in these animals. While I did not observe *Htr3a*-Cre+ smooth muscle cells in sagittal cryo-sections of adult bladder, this does not rule out that smooth muscle cells do not derive from *Htr3a*+ lineages. These cells may at developmental time points earlier than what I examined, and I did not apply any markers of smooth muscle cells in my immunohistochemistry experiments in these animals. *Htr3a*-derived lineages in the bladder should be determined in animals younger than P28, and more careful histological examination of smooth muscle should be conducted. The outcome of these experiments will be particularly interesting because of the phenotype observed in *Htr3a*$^{vs/vs}$ mutant animals that express a hypersensitive form of the 5-HT3A receptor – these mice exhibit both hyperplasia and hypertrophy of bladder smooth muscle (Bhattacharya et al., 2004). Male *Htr3a*$^{vs/vs}$ mutants also have partial bladder outlet obstruction, which is known to cause bladder hyperplasia and hypertrophy (Khan et al., 2000). However, these mutants may also present with bladder hyperplasia due to increased differentiation of bladder smooth muscle cells from over-stimulation of the mutant 5-HT3A receptor. Determining the involvement of

Htr3a in the lineage origins of bladder smooth muscle will be critical for reconciling the findings of this dissertation (particularly Chapter II) and those of Bhattacharya et al. 2004.

The second experimental approach for defining roles of *Htr3a* in developmental lineage segregation involves the use of a newly generated "floxed" allele of *Htr3a* (hereafter *Htr3a*-flox). This mouse line expresses *Htr3a* normally until cells expressing *Htr3a* are exposed to Cre recombinase. Because the *Htr3a*-KO mouse line employed in this dissertation is a global knockout in every cell that expresses *Htr3a*, determining exactly when and where 5-HT3 receptor activity mediates developmental processes in this mouse line is challenging. The *Htr3a*-flox allele, in conjunction with either an inducible Cre line or a cell type-specific Cre, would permit a more targeted and controlled means to determine the requirement of 5-HT3A at specific developmental time points and in defined cell populations. For example, the *Sox10*-CrehGH transgenic mouse line (Musser et al., 2015), which is specific to neural crest-derived lineages, could be used to drive *Htr3a* excision only in neural crest cells. Characterization of the progeny of these crosses would reveal the requirement of *Htr3a* in neural crest development while excluding any confounding effects of 5-HT3 loss in CNS neurons. Given the dynamic nature of *Htr3a* gene expression (Chapter III), its temporal effects in the maturation of nerve fibers in bladder smooth muscle (Chapter IV), and its established roles in adult lower urinary tract physiology (Schwen et al., 2013), a time course study of loss of gene expression in *Sox10*-CreERT2;*Htr3a*-flox mice would be extremely valuable for improving our understanding of the temporal requirement of 5-HT3 receptor activity in neural crest development. The *Sox10*-CreERT2 mouse line harbors a tamoxifen-inducible Cre driven by *Sox10* expression and would allow fine-tuned deletion of *Htr3a* at any developmental time point. One confound to these proposed experiments is that *Sox10* is expressed in oligodendrocytes within the CNS (Hornig et

al., 2013), so both of these *Sox10* transgenes would be active in oligodendrocyte lineages as well. However, to the best of my knowledge, *Htr3a* is not expressed in oligodendrocytes, so *Sox10* activity in this lineage would not affect these proposed experiments. Alternatively, Cre rcombinase driven by *Prph* expression could be used, as peripherin expression is specific to peripheral neurons (however, *Prph* does not label all autonomic neurons). The *Advillin*-Cre transgenic mouse line is another available tool for targeting peripheral neurons. Even though the immunohistochemistry I conducted in Chapter IV determined that *Htr3a* loss does not have lasting effects on TH and ChAT expression, roles for 5-HT3 activity in differentiation of neuronal subtypes cannot be completely ruled out. The absence of differences in TH and ChAT proportions in 6-week old pelvic ganglia does not necessarily mean that the expression of other autonomic neuronal markers, such as NET (norepinephrine transporter), NOS (nitric oxide synthase), or VIP (vasoactive intestinal peptide) are not perturbed. The aforementioned proposed studies could include examination of other neuronal subtype markers to determine if 5-HT3 affects neuronal subtype differentiation outcomes within the pelvic ganglia.

Clinical implications of perturbing 5-HT3A in development

The studies in Chapters II and IV indicate that perturbing normal 5-HT3A receptor signaling in development can profoundly alter bladder innervation and disrupt normal urinary tract function in adulthood. These findings have substantial implications for human health and the potential consequences of perturbing 5-HT3A signaling *in utero*.

Ondansetron (marketed as Zofran) is a 5-HT3A receptor specific antagonist that is prescribed primarily as a treatment for post-operative and chemotherapy-induced vomiting and nausea. Ondansetron is also the first-choice option for pregnant women with severe hyperemesis

gravidarum. In studies of ondansetron risk for fetal development, the primary readouts for risk have been gross birth defects, gestational age (preterm birth), and birth weight (Pasternak et al., 2013;Carstairs, 2016;Fejzo et al., 2016). Most prior studies conclude that ondansetron does not increase risk for these traits, although one group reported increased risk of cleft palate in ondansetron-exposed children[1] (Anderka et al., 2012). However, no longitudinal studies of long-term effects of ondansetron exposure *in utero* have been conducted. It remains unclear if antagonizing 5-HT3A in fetal development affects neural development in ways that are only detectable in later postnatal maturation. Given that ondansetron is capable of crossing the placental barrier (Siu et al., 2006) and 5-HT3A is expressed very early in both the CNS and neural crest lineages (Chapter III), determining the consequences of prolonged fetal 5-HT3A antagonism is of critical importance. To address this research question, one could orally administer ondansetron to healthy, wild type pregnant mice and conduct phenotyping studies of the offspring. Onset of mature voiding behavior (i.e., onset of vesicovesical reflex for urinary voiding and no longer relying on perigenital stimulation for voiding) could be assessed in ondansetron-exposed pups using methods similar to those employed in the laboratory of Margaret Vizzard (Girard et al., 2016). Adult urinary voiding function could be assessed in these animals using the void spot assay and anesthetized bladder cystometry methods described in Chapter III.

[1] Increased incidence of cleft palate in children exposed to ondansetron *in utero* is particularly interesting, given the neural crest origins of this craniofacial structure and prior reports of disturbance of gene expression in cultured mouse embryonic neural crest-derived mandibular mesenchyme following exposure to ondansetron. Moiseiwitsch, J.R., and Lauder, J.M. (1997). Regulation of gene expression in cultured embryonic mouse mandibular mesenchyme by serotonin antagonists. *Anat Embryol (Berl)* 195**,** 71-78.

Many women also experience major depressive disorder during pregnancy and rely on the use of selective serotonin reuptake inhibitors (SSRIs) for treatment. Fluoxetine (marketed as Prozac) is commonly prescribed (Kiryanova et al 2013) but adverse fetal risk outcomes studies have been inconclusive. A prior report has demonstrated that fluoxetine acts as an allosteric antagonist of the 5-HT3A receptor (Eisensamer et al., 2003), but the effects of *in utero* exposure to this drug on 5-HT3A activity in fetal development are unknown. Given the extensive use of fluoxetine by pregnant women, this research question should also be pursued using the methods suggested above. On a broader scale, a longitudinal study of lower urinary tract symptoms (LUTS) in children of women treated with 5-HT3-interacting drugs could be conducted to determine if these children are at a higher risk for LUTS than non-exposed children.

Roles for *Htr3a* in bladder inflammation and interstitial cystitis

The majority of this dissertation has been focused on developmental roles for serotonin receptor signaling in the neural control of the lower urinary tract. While not directly related to neurodevelopment, exploring the potential function of 5-HT3 receptor activity in the context of bladder inflammation could be clinically impactful. The rationale for this proposed future direction comes from numerous studies of 5-HT3 receptors in intestinal inflammation. Antagonists of 5-HT3, including ondansetron and tropisetron, relieve inflammatory symptoms in patients suffering from inflammatory bowel disease and colitis (Mousavizadeh et al., 2009;Kato, 2013;Utsumi et al., 2016). However, no studies on potential roles for 5-HT3 receptors in bladder inflammation or interstitial cystitis have been conducted. Mast cells that express Tph1 and secrete serotonin are present within the urothelium of the bladder and become active in interstitial cystitis (Theoharides et al., 1982;Theoharides et al., 1995). Additionally, *Htr3a* is

expressed in neuropeptidergic sensory neurons with known roles in mediating bladder neuroinflammation (Chapter III). It is plausible that 5-HT3 receptors could be involved in inflammatory signaling pathways in interstitial cystitis via mast cell serotonin signaling. Because antagonists of 5-HT3 relieve inflammation as mentioned above, I hypothesize that *Htr3a*-KO animals lacking 5-HT3 receptor expression would exhibit a less severe inflammatory response to bladder irritation. To test this, one could induce chronic interstitial cystitis by administration of cyclophosphamide (CYP) to wild type and *Htr3a-/-* adult mice. CYP is a commonly used pharmacological agent in rodent models of interstitial cystitis and the disease condition in rodents closely mimics symptoms observed in humans (Everaerts et al., 2010;Aronsson et al., 2012;Ito et al., 2017). Following induction of bladder inflammation, routine hematoxylin & eosin staining of bladder sections (described in Chapter VI) could be used to score inflammatory responses in wild type versus *Htr3a-/-* mice. To demonstrate that any potential differences in *Htr3a-/-* inflammatory responses are due to mast cell-secreted serotonin, one could conduct similar experiments in *Tph1-/-*; *Htr3a-/-* mice that lack expression of the non-neuronal isoform of tryptophan hydroxylase. Because neuromodulatory cells of the urethra also secrete serotonin (Iwanaga et al., 1994), a *Tph1* knockout could be driven by a mast cell-specific Cre line, such as c-Kit (*Kit*$^{tm1(cre/ERT2)Dsa}$) and a floxed *Tph1* mouse line (*Tph1*$^{tm1a(KOMP)Wtsi}$). Similarly, these experiments could be done in *Tph2-/-; Htr3a-/-* animals to determine the role of neuronal serotonin in 5-HT3-mediated bladder inflammation.

Conclusions

This dissertation contributes to the field of serotonin biology by demonstrating the requirement of 5-HTR signaling, particularly 5-HT3A, in neural crest differentiation, peripheral

neuronal maturation, and urinary bladder function. The experimental findings reported here lay the foundation for future studies that ultimately have the potential to improve the quality of life for patients with urinary dysfunction, and caution for adverse fetal risk of perturbing 5-HT3 signaling in development.

References

Anderka, M., Mitchell, A.A., Louik, C., Werler, M.M., Hernandez-Diaz, S., Rasmussen, S.A., and Study, N.B.D.P. (2012). Medications used to treat nausea and vomiting of pregnancy and the risk of selected birth defects. *Birth Defects A Clin Mol Teratol* 94**,** 22-30.

Aronsson, P., Johnsson, M., Vesela, R., Winder, M., and Tobin, G. (2012). Adenosine receptor antagonism suppresses functional and histological inflammatory changes in the rat urinary bladder. *Auton Neurosci* 171**,** 49-57. doi: 10.1016/j.autneu.2012.10.006.

Bhattacharya, A., Dang, H., Zhu, Q.M., Schnegelsberg, B., Rozengurt, N., Cain, G., Prantil, R., Vorp, D.A., Guy, N., Julius, D., Ford, A.P., Lester, H.A., and Cockayne, D.A. (2004). Uropathic observations in mice expressing a constitutively active point mutation in the 5-HT3A receptor subunit. *J Neurosci* 24**,** 5537-5548. doi: 10.1523/JNEUROSCI.5658-03.2004.

Bonnin, A., and Levitt, P. (2011). Fetal, maternal, and placental sources of serotonin and new implications for developmental programming of the brain. *Neuroscience* 197**,** 1-7. doi: 10.1016/j.neuroscience.2011.10.005.

Carstairs, S.D. (2016). Ondansetron use in pregnancy and birth defects: a systematic review. *Obstet Gynecol* 127**,** 878-883.

Chameau, P., Inta, D., Vitalis, T., Monyer, H., Wadman, W.J., and Van Hooft, J.A. (2009). The N-terminal region of reelin regulates postnatal dendritic maturation of cortical pyramidal neurons. *Proc Natl Acad Sci U S A* 106**,** 7227-7232. doi: 10.1073/pnas.0810764106.

Corpening, J.C., Deal, K.K., Cantrell, V.A., Skelton, S.B., Buehler, D.P., and Southard-Smith, E.M. (2011). Isolation and live imaging of enteric progenitors based on Sox10-Histone2BVenus transgene expression. *genesis* 49**,** 599-618. doi: 10.1002/dvg.20748.

Davies, P.A., Pistis, M., Hanna, M.C., Peters, J.A., Lambert, J.J., Hales, T.G., and Kirkness, E.F. (1999). The 5-HT3B subnit is a major determinant of serotonin-receptor function. *Nature* 397**,** 359-363.

Derkach, V., Surprenant, A., and North, R.A. (1989). 5-HT3 receptors are membrane ion channels. *Nature* 339**,** 706-709.

Dickinson, M.E., Flenniken, A.M., Ji, X., Teboul, L., Wong, M.D., White, J.K., Meehan, T.F., Weninger, W.J., Westerberg, H., Adissu, H., Baker, C.N., Bower, L., Brown, J.M., Caddle, L.B., Chiani, F., Clary, D., Cleak, J., Daly, M.J., Denegre, J.M., Doe, B., Dolan, M.E., Edie, S.M., Fuchs, H., Gailus-Durner, V., Galli, A., Gambadoro, A., Gallegos, J., Guo, S., Horner, N.R., Hsu, C.W., Johnson, S.J., Kalaga, S., Keith, L.C., Lanoue, L., Lawson, T.N., Lek, M., Mark, M., Marschall, S., Mason, J., Mcelwee, M.L., Newbigging, S., Nutter, L.M., Peterson, K.A., Ramirez-Solis, R., Rowland, D.J., Ryder,

E., Samocha, K.E., Seavitt, J.R., Selloum, M., Szoke-Kovacs, Z., Tamura, M., Trainor, A.G., Tudose, I., Wakana, S., Warren, J., Wendling, O., West, D.B., Wong, L., Yoshiki, A., International Mouse Phenotyping, C., Jackson, L., Infrastructure Nationale Phenomin, I.C.D.L.S., Charles River, L., Harwell, M.R.C., Toronto Centre For, P., Wellcome Trust Sanger, I., Center, R.B., Macarthur, D.G., Tocchini-Valentini, G.P., Gao, X., Flicek, P., Bradley, A., Skarnes, W.C., Justice, M.J., Parkinson, H.E., Moore, M., Wells, S., Braun, R.E., Svenson, K.L., De Angelis, M.H., Herault, Y., Mohun, T., Mallon, A.M., Henkelman, R.M., Brown, S.D., Adams, D.J., Lloyd, K.C., Mckerlie, C., Beaudet, A.L., Bucan, M., and Murray, S.A. (2016). High-throughput discovery of novel developmental phenotypes. *Nature* 537**,** 508-514. doi: 10.1038/nature19356.

Diez-Roux, G., Banfi, S., Sultan, M., Geffers, L., Anand, S., Rozado, D., Magen, A., Canidio, E., Pagani, M., Peluso, I., Lin-Marq, N., Koch, M., Bilio, M., Cantiello, I., Verde, R., De Masi, C., Bianchi, S.A., Cicchini, J., Perroud, E., Mehmeti, S., Dagand, E., Schrinner, S., Nurnberger, A., Schmidt, K., Metz, K., Zwingmann, C., Brieske, N., Springer, C., Hernandez, A.M., Herzog, S., Grabbe, F., Sieverding, C., Fischer, B., Schrader, K., Brockmeyer, M., Dettmer, S., Helbig, C., Alunni, V., Battaini, M.A., Mura, C., Henrichsen, C.N., Garcia-Lopez, R., Echevarria, D., Puelles, E., Garcia-Calero, E., Kruse, S., Uhr, M., Kauck, C., Feng, G., Milyaev, N., Ong, C.K., Kumar, L., Lam, M., Semple, C.A., Gyenesei, A., Mundlos, S., Radelof, U., Lehrach, H., Sarmientos, P., Reymond, A., Davidson, D.R., Dolle, P., Antonarakis, S.E., Yaspo, M.L., Martinez, S., Baldock, R.A., Eichele, G., and Ballabio, A. (2011). A high-resolution anatomical atlas of the transcriptome in the mouse embryo. *PLoS Biol* 9**,** e1000582. doi: 10.1371/journal.pbio.1000582.

Eisensamer, B., Rammes, G., Gimpl, G., Shapa, M., Ferrari, U., Hapfelmeier, G., Bondy, B., Parsons, C., Gilling, K., Zieglgansberger, W., Holsboer, F., and Rupprecht, R. (2003). Antidepressants are functional antagonists at the serotonin type 3 (5-HT3) receptor. *Mol Psychiatry* 8**,** 994-1007. doi: 10.1038/sj.mp.4001314.

Everaerts, W., Zhen, X., Ghosh, D., Vriens, J., Gevaert, T., Gilbert, J.P., Hayward, N.J., Mcnamara, C.R., Xue, F., Moran, M.M., Strassmaier, T., Uykal, E., Owsianik, G., Vennekens, R., De Ridder, D., Nilius, B., Fanger, C.M., and Voets, T. (2010). Inhibition of the cation channel TRPV4 improves bladder function in mice and rats with cyclophosphamide-induced cystitis. *Proc Natl Acad Sci U S A* 107**,** 19084–19089. doi: www.pnas.org/cgi/doi/10.1073/pnas.1005333107.

Fejzo, M.S., Macgibbon, K.W., and Mullin, P.M. (2016). Ondansetron in pregnancy and risk of adverse fetal outcomes in the United States. *Reprod Toxicol* 62**,** 87-91.

Fiorica-Howells, E., Hen, R., Gingrich, J., Li, Z., and Gershon, M.D. (2002). 5-HT(2A) receptors: location and functional analysis in intestines of wild-type and 5-HT(2A) knockout mice. *Am J Physiol Gastrointest Liver Physiol* 282**,** G877-893. doi: 10.1152/ajpgi.00435.2001.

Frotscher, M. (1997). Dual role of Cajal-Retzius cells and reelin in cortical development. *Cell Tissue Res* 290**,** 315-322.

Garcia-Gonzalez, D., Khodosevich, K., Watanabe, Y., Rollenhagen, A., Lubke, J.H.R., and Monyer, H. (2017). Serotonergic Projections Govern Postnatal Neuroblast Migration. *Neuron* 94**,** 534-549 e539. doi: 10.1016/j.neuron.2017.04.013.

Girard, B.M., Peterson, A., Malley, S., and Vizzard, M.A. (2016). Accelerated onset of the vesicovesical reflex in postnatal NGF-OE mice and the role of neuropeptides. *Exp Neurol* 285**,** 110-125.

Hornig, J., Frob, F., Vogl, M.R., Hermans-Borgmeyer, I., Tamm, E.R., and Wegner, M. (2013). The transcription factors Sox10 and Myrf define an essential regulatory network module in differentiating oligodendrocytes. *PloS Genet* 9**,** e1003907.

Ito, H., Pickering, A.E., Igawa, Y., Kanai, A.J., Fry, C.H., and Drake, M.J. (2017). Muro-Neuro-Urodynamics; a Review of the Functional Assessment of Mouse Lower Urinary Tract Function. *Front Physiol* 8**,** 49. doi: 10.3389/fphys.2017.00049.

Iwanaga, T., Han, H., Hoshi, O., Kanazawa, H., Adachi, I., and Fujita, T. (1994). Topographical relation between serotonin-containing paraneurons and peptidergic neurons in the intestine and urethra. *Biol Signals* 3**,** 259-270.

Kato, S. (2013). Role of serotonin 5-HT(3) receptors in intestinal inflammation. *Biol Pharm Bull* 36**,** 1406-1409.

Khan, M.A., Shukla, N., Thompson, C.S., Mumtaz, F.H., Mikhailidis, D.P., and Morgan, R.J. (2000). Endothelin-1 and urinary bladder hyperplasia following partial bladder outlet obstruction. *J Cardiovac Pharmacol* 36**,** S262-263.

Moiseiwitsch, J.R., and Lauder, J.M. (1997). Regulation of gene expression in cultured embryonic mouse mandibular mesenchyme by serotonin antagonists. *Anat Embryol (Berl)* 195**,** 71-78.

Moro, C., Edwards, L., and Chess-Williams, R. (2016). 5-HT2A receptor enhancement of contractile activity of the porcine urothelium and lamina propria. *Int J Urol* 23**,** 946-951.

Mousavizadeh, K., Rahimian, R., Fakhfouri, G., Aslani, F.S., and Ghafourifar, P. (2009). Anti-inflammatory effects of 5-HT receptor antagonist, tropisetron on experimental colitis in rats. *Eur J Clin Invest* 39**,** 375-383.

Musser, M.A., Correa, H., and Southard-Smith, E.M. (2015). Enteric neuron imbalance and proximal dysmotility in ganglionated intestine of the Sox10Dom/+ Hirschsprung mouse model. *Cell Mol Gastroenterol Hepatol* 1**,** 87-101.

Myers, J.P., Santiago-Medina, M., and Gomez, T.M. (2011). Regulation of axonal outgrowth and pathfinding by integrin-ECM interactions. *Dev Neurobiol* 71**,** 901-923.

Noam, Y., Wadman, W.J., and Van Hooft, J.A. (2008). On the voltage-dependent Ca2+ block of serotonin 5-HT3 receptors: a critical role of intracellular phosphates. *J Physiol* 586**,** 3629-3638. doi: 10.1113/jphysiol.2008.153486.

Pasternak, B., Svanstrom, H., and Hviid, A. (2013). Ondansetron in pregnancy and risk of adverse fetal outcomes. *N Engl J Med* 368**,** 814-823.

Previtali, S.C., Feltri, M.L., Archelos, J.J., Quattrini, A., Wrabetz, L., and Hartung, H. (2001). Role of integrins in the peripheral nervous system. *Prog Neurobiol* 64**,** 35-49.

Ranaivoson, E.M., Von Daake, S., and Comoletti, D. (2016). Structural Insights into Reelin Function: Present and Future. *Front Cell Neurosci* 10. doi: 10.3389/fncel.2016.00137.

Rosenberg, S.S., and Spitzer, N.C. (2011). Calcium signaling in neuronal development. *Cold Spring Harb Perspect Biol* 3**,** a004259. doi: 10.1101/cshperspect.a004259.

Sakai, T., Kasahara, K., Tomita, K., Ikegaki, I., and Kuriyama, H. (2013). 5-Hydroxytryptamine-induced bladder hyperactivity via the 5-HT2A receptor in partial bladder outlet obstruction in rats. *Am J Physiol Renal Physiol* 304**,** F1020-1027. doi: 10.1152/ajprenal.00365.2012.

Schmidt, C.E., Dai, J., Lauffenburger, D.A., Sheetz, M.P., and Horwitz, A.F. (1995). Integrin-cytoskeletal interactions in neuronal growth cones. *J Neurosci* 15**,** 3400-3407.

Schwen, Z., Matsuta, Y., Shen, B., Wang, J., Roppolo, J.R., De Groat, W.C., and Tai, C. (2013). Involvement of 5-HT3 receptors in pudendal inhibition of bladder overactivity in cats. *Am J Physiol Renal Physiol* 305**,** F663-671. doi: 10.1152/ajprenal.00105.2013.

Siu, S.S., Chan, M.T., and Lau, T.K. (2006). Placental transfer of ondansetron during early human pregnancy. *Clin Pharmacokinet* 45**,** 419-423.

Theoharides, T.C., Bondy, P.K., Tsakalos, N.D., and Askenase, P.W. (1982). Differential release of serotonin and histamine from mast cells. *Nature* 297**,** 229-231.

Theoharides, T.C., Sant, G.R., El-Mansoury, M., Letourneau, R., Ucci Jr, A.A., and Meares Jr, E.M. (1995). Activation of bladder mast cells in interstitial cystitis: a light and electron microscopic study. *J Urol* 153**,** 629-636.

Turlo, K.A., Noel, O.D., Vora, R., Larussa, M., Fassler, R., Hall-Glenn, F., and Iruela-Arispe, M.L. (2012). An essential requirement for B1 integrin in the assembly of extracellular matrix proteins within the vascular wall. *Dev Biol* 365**,** 23-35.

Utsumi, D., Matsumoto, K., Amagase, K., Horie, S., and Kato, S. (2016). 5-HT3 receptors promote colonic inflammation via activation of substance P/neurokinin-1 receptors in dextran sulphate sodium-induced murine colitis. *Br J Pharmacol* 173**,** 1835-1849. doi: 10.1111/bph.13482.

Yip, Y.P., Capriotti, C., and Yip, J.W. (2003). Migratory pathway of sympathetic preganglionic neurons in normal and reeler mutant mice. *J Comp Neurol* 460**,** 94-105.

Yip, Y.P., Kronstadt-O'brien, P., Capriotti, C., Cooper, J.A., and Yip, J.W. (2007). Migration of sympathetic preganglionic neurons in the spinal cord is regulated by Reelin-dependent Dab1 tyrosine phosphorylation and CrkL. *J Comp Neurol* 502**,** 635-643.

CHAPTER VI

EXTENDED METHODS AND SHORT STUDIES

Animals

Genotyping

Tissues for genotyping were collected from postnatal and adult animals as ear punches, or occasionally tail snips, and tail snips or limb buds from fetal samples. Tissues were incubated in tail digest buffer (comprised of 10mM Tris pH 8.0, 10mM EDTA, 0.5% SDS, and 100mM NaCl) and 0.125mg/mL Proteinase K (Gojira, Cat # PK 1001, stock concentration 10mg/mL) at 55°C overnight. DNA was isolated via traditional phenol-chloroform extraction and ethanol precipitation. Isolated DNA was resuspended in 200uL TE buffer, pH 7.5; especially large DNA pellets from fetal samples were resuspended in 400uL buffer. PCR cycling conditions and primers used are listed in Table 6.1. PCR products were analyzed via gel electrophoresis on non-denaturing 10% acrylamide gels with 1X TBE buffer.

ChAT-EGFP and Htr3a-EGFP. Thermocycler conditions for genotyping EGFP reporter lines are as follows: 94°C 5 min, [94°C 30 sec with 0.5°C/sec ramp, 72°C 30 sec, 72°C 30 sec with 0.5°C/sec ramp to 72°C] repeated for 30 cycles, 72°C 10 min, hold at 10°C indefinitely. The EGFP PCR reaction is prone to false-positive bands if too much DNA template is added to the reaction and if there are more than 30 cycles; my genotyping was highly successful with the use of only 1 μL undiluted DNA from one ear punch.

Table 6.1 Primers and PCR buffers used for mouse genotyping

Mouse Line/Trait	Product Amplified	MS2 Lab Primer Names	Forward Primer (5' – 3')	Reverse Primer (5' – 3')	Buffer
ChAT-, *Htr3a*-EGFP	EGFP sequence 300bp	EGFP F, EGFP R	CCTACGGCGTGCAGTGCTTCAGC	CGGCGAGCTGCACGCTGCGTCCTC	PCRB2.5
Htr3a KO	regions flanking *Htr3a* exons 7-8 +/+: 400bp +/-: 400bp, 210bp -/-: 210bp	Htr3a KO F1, F2, R1	F1: AACAGCTATGCAGAAATGAAGTT F2: GGCTGACTGCGTAGAATAAAGG	TGGATGTGGAATGTGTGCGAG	PCRB2.0
Htr3a-Cre	Cre sequence, 490 bp	WNT-Cre F, R	ATTCTCCCACCGTCAGTACG	CGTTTTCTGAGCATACCTGGA	PCRB2.5
Sex (M/F)	exon 9 of *Kdm5c* (chrX) and exon 10 of *Kdm5d* (chrY) M: 350bp, 301bp F: 301bp	Smc1, Smc2	TGAAGCTTTTGGCTTTGAG	CCGCTGCCAAATTCTTTGG	TNK50

MS2 lab primer names are provided to assist fellow Southard-Smith lab members in locating these primers for future studies. Buffer names refer to buffers made in the Southard-Smith lab.

Htr3a KO. Thermocycler conditions for genotyping the *Htr3a* knockout mouse line are as follows: 94°C 3 min, [94°C 30 sec with 0.5°C/sec ramp, 63°C 1 min, 72°C 1 min with 0.5°C/sec ramp to 72°C] repeated for 35 cycles, 72°C 2 min, hold at 10°C indefinitely. Interestingly, some *Htr3a-/-* pups could be identified at the time of weaning by a solid gray belly that would later develop into salt-and-pepper ticking all over the body in adulthood. These animals were always genotyped as *Htr3a-/-* without exception; however, not all *Ht3a-/-* pups had this unusual coat phenotype. This PCR also works best with only 1 μL DNA template from undiluted ear punch preps.

Htr3a-Cre. Thermocycler conditions for genotyping the Cre transgene are as follows: 94°C 5 min, [94°C 15 sec with 0.5°C/sec ramp, 58°C 30 sec, 72°C 40 sec with 0.5°C/sec ramp to 72°C] repeated for 35 cycles, 72°C 5 min, hold at 10°C indefinitely. This genotyping protocol can be used for any Cre transgene line used in the Southard-Smith lab; previous attempts with Jackson Laboratory's recommended *Htr3a*-Cre-specific protocol yielded accurate but low-yield results with many non-specific bands.

Sex (male/female). Thermocycler conditions for genotyping fetal tissues for sex are as follows: 94°C 5 min, [94°C 30 sec with 0.5°C/sec ramp, 55°C 30 sec, 72°C 30 sec with 0.5°C/sec ramp to 72°C] repeated for 30 cycles, 72°C 10 min, hold at 10°C indefinitely. This PCR amplifies exons 9 and 10 of two extremely homologous genes on the X and Y mouse chromosomes, *Kdm5c* and *Kdm5d*, respectively. *Kmd5d* has an intron between exons 9 and 10 that is unique to the Y chromosome, which results in the amplification of two bands in male DNA samples but only one band in females.

Embryo collection and processing

Females used for embryo collection were paired with breeder males typically in late afternoon; vaginal seminal plugs identified the following morning were designated as 0.5 dpc (E0.5). On the day of dissection, pregnant females were brought up to the lab and fully anesthetized via isoflurane inhalation and euthanized by cervical dislocation. A lower abdominal incision was made to expose the uterine horns, which were then sub-dissected and placed in a 100mm petri dish with ice-cold 1X PBS. Embryos were removed from the uterus and their amniotic sacs with small dissecting scissors and #5 FST forceps. If screening for fluorescence, embryos were quickly examined using either a Zeiss Stero Lumar.V12 fluorescent stereomicroscope or a Leica M205 FA fluorescent stereomicroscope. Either tail snips or limb buds were removed for genotyping (see previous section, Genotyping). For embryos age E13.5dpc and older, slits were made in both sides of the rib cage for each embryo to allow greater permeation of fixative into interior tissues. Embryos age E16.5dpc and older were bisected at the level of the forearm and hind limbs were removed to allow better fixative permeation. Embryos aged E10.5 were fixed in 10% NBF for 6 hours while rotating on a nutator

at 4°C and protected from light. Embryos aged E11.5 through 18.5 were fixed overnight in 10% NBF while rotating on a nutator at 4°C and protected from light. Tissues were typically fixed in 12-well or 6-well tissue culture dishes to keep genotyped embryos separated, but embryos that did not require genotyping were usually fixed in 50mL conical tubes filled with fixative. Following fixation, embryos were washed 3 times 15-20 minutes each wash in 1X PBS (0.22μm sterile filtered) and then washed in 1X PBS for one hour. Embryos were then infiltrated with 30% sucrose in 1XPBS overnight (or until they sank to the bottom of the dish or tube) to protect against crystallization during freezing for cryo-sectioning.

The only exception to this protocol was for processing embryos for immunohistochemical staining with the goat anti-serotonin (5-HT) antibody (Immunostar, Cat # 20079). Fixing tissues (fetal or adult) in 4% PFA with 3% sucrose added resulted in much better 5-HT staining, compared to fixing in 10% NBF (Gershon and Ross, 1966). The addition of sucrose to the fixative creates a hypertonic solution that prevents 5-HT leakage from cells upon fixation, and thus allows much more effective antibody binding. In my experience, 5-HT staining worked well with either freshly prepared sucrose fixative or once-thawed frozen sucrose fixative.

Dorsal root ganglia collection, processing, and analysis

P2 dorsal root ganglia collection and processing

Because early postnatal dorsal root ganglia (DRG) are very small, fragile, and sticky, I opted to use "backbone blocks" to section and stain P2 DRG. P2 pups were brought back to the lab and fully anesthetized via isoflurane inhalation and decapitated. The skin on the torso was completely removed and a frontal midline incision was made to open the rib cage. Thoracic

organs were completely removed, along with the fore limbs. Small spring scissors were used to cut off the ribs approximately 2 mm from the spinal column, and then the spinal column was cut at the level of the last two ribs and at the level of the pelvis. Altogether, the backbone block encompassed axial levels T11 to S2. Backbone blocks were fixed overnight in 10% NBF at 4°C on a nutator protected from light in a 12-well tissue culture dish. They were subsequently washed three times in sterile filtered 1X PBS for 15-20 minutes each, with a final wash for one hour in sterile 1X PBS. Samples were infiltrated with 30% sucrose in 1X PBS until they sank to the bottom of the dish (at least overnight). For cryo-sectioning, backbone blocks were placed in the bottom of the cryo-mold for frontal sections through the block, such that many DRG are cut within one cryo-section. This method of embedding and sectioning reduces the number of slides and the amount of antibody needed for a given experiment.

Adult dorsal root ganglia collection and processing

Dorsal root ganglia acquired from animals P14 and older were dissected in a similar manner as reported by other research groups (Malin et al., 2007). Animals were fully anesthetized by isoflurane inhalation and euthanized via cervical dislocation. After wetting the fur with ethanol, the skin and the head were removed. A midline incision was made on the front of the animal to expose the thoracic and abdominal viscera, which were then removed. All the dorsal musculature was removed to expose the dorsal aspect of the spinal column. Using small curved spring scissors (Fine Science Tools, Cat # 91501-09), parallel cuts were made on the left and right sides of the spinal column starting at upper thoracic axial levels (Figure 6.1). Because the first several cuts are difficult to get started, beginning the spinal column dissection at an axial level away from the desired region is highly recommended. When the cuts are made properly,

the dorsal side of the vertebrae will start to curl up as a strip and the spinal cord will be fully exposed. Dorsal root ganglia were then plucked using #5 fine forceps with tips bent at a 45° angle (Fine Science Tools, Cat # 11251-35) and fixed in 10% NBF for 4 hours at 4°C on a nutator while protected from light. Following fixation DRG were then washed four times 20 minutes each in sterile filtered 1XPBS, followed by a last wash for one hour in sterile 1XPBS and infiltration with 30% sucrose. The large quantity of glia encasing the DRG led to slower sucrose infiltration; DRG typically did not sink until after about 48 hours in 30% sucrose.

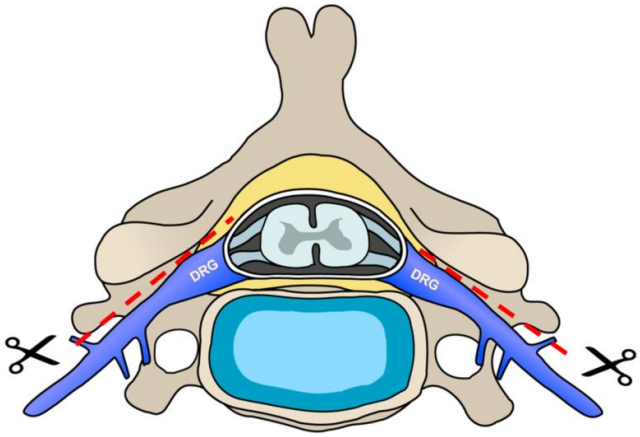

Figure 6.1 Dissection strategy for removal of DRG from animals age P14 and older. Red dashed lines indicate the cutting plane. Great care must be taken to avoid cutting the DRG, but when executed properly this dissection method expedites the DRG removal process as the DRG are visible and accessible. Once the dorsal aspect of the vertebrae have been removed, the dorsal nerve root can be pinched with forceps and used to extract the ganglion. This figure has been modified from a WikiMedia Commons file contributed by user debivort, licensed under the Creative Commons Attribution-Share Alike 3.0 Unported license.

Processing of dissected DRG was greatly improved by the use of 1.7mL centrifuge tubes that had been repurposed as wash buckets. These were created by heating a disposable razor blade over a Bunsen burner and slicing a 1.7mL centrifuge tube at the 1000µL gradation line and stamping on a piece of fine white tulle ribbon (recommended by Lydia Kos, Florida International University) to the bottom of the capped half of the tube while the plastic was still partially

molten (Figure 6.2). These wash buckets can be used in 24-well tissue culture plates and transferred from well to well for each wash.

Figure 6.2 Wash buckets used for DRG processing. The tulle ribbon used as "mesh" can be procured easily and affordably from any craft store.

Immunohistochemistry on dorsal root ganglia cryo-sections

DRG were embedded for cryo-sectioning by placing several DRG directly onto the bottom of the cryo-mold. Embedding and sectioning multiple DRG at once conserves 3-APES slides and reduces the volume of antibody dilution required. If DRG needed to be distinguished on the slide (e.g., DRG from same axial level but from different animals), they were arranged in the cryo-mold in an asymmetric pattern which was recorded and noted at the time of imaging (Figure 6.3, Panel A). Excess 1XPBS was wicked away with the corner of a Kimwipe; this step helps keep the DRG on the bottom of the cryo-mold when tissue freezing medium is poured on top. DRG were cut on the cryostat as 20μm sections and thaw-mounted onto 3-APES treated slides. Cryo-sections were mounted onto alternating slides to ensure a sizeable gap between sections on one slide to avoid double-counting cell type proportions (Figure 6.3, Panel B).

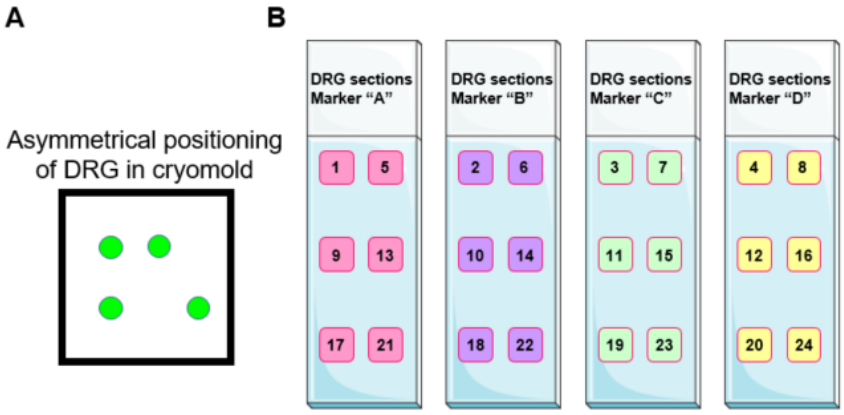

Figure 6.3 Strategy for embedding DRG and alternating DRG cryo-sections on slides to avoid double-counting cells and maximize the number of sections that can be quantified within a given experiment. (**A**) Dorsal root ganglia from the same axial level but different animals were arranged in an asymmetric pattern in the bottom of the cryomold. The asymmetric pattern allowed identification of each sample at the time of imaging the sections on the slide. (**B**) The colored squares represent cryo-sections, the numbers within the squares represent the order in which the sections were cut. This alternating section strategy allowed even distribution of serial sections across all slides. Microscope slide cartoons are modified from Servier Medical Art (smart.servier.com).

The slides were then dried for 30 minutes at 37°C on a slide warmer. Excess tissue freezing medium was removed by incubating the slides in 1XPBS-0.3% TX-100 at room temperature for 5 minutes. Sections were then blocked for at least 30 minutes in blocking solution (1XPBS-0.3% TX-100, 10% BSA, 5% NDS, 0.45µm sterile filtered) at room temperature; blocking time occasionally was extended to overnight at 4°C. The slides were tipped to let blocking solution drip off and primary antibody dilutions were applied directly to the tissue sections (approximately 500µL per slide). Table 6.2 lists the optimized staining conditions for all primary antibodies used on DRG sections.

Table 6.2 Primary antibodies used in analysis of dorsal root ganglia neuronal subtypes

Antigen	Host	Vendor, Cat #	Dilution in Block	Incubation Time	Notes
Hu C/D	Human	Gift of Vanda Lennon	1:10,000	>5 hrs RT or O/N 4°C	Can be reused ~15-20 times
CGRP	Rabbit	Sigma Aldrich, C8198	1:1,000	>5 hrs RT or O/N 4°C	Can be reused ~15-20 times
Substance P	Rabbit	Immunostar, 20064	1:500	O/N 4°C	Can be reused ~15-20 times
TRPV1	Rabbit	Neuromics, RA14113	1:250	O/N 4°C	Can be reused 4-5 times
TRPV4	Rabbit	Alomone Labs, ACC-034	1:500	O/N 4°C	Can be reused 5-6 times
NF200	Rabbit	Sigma Aldrich, N4142	1:500	O/N 4°C	Can be reused ~15-20 times, labels processes very well
TH	Sheep	Millipore, AB1542	1:1,000	O/N 4°C	Can be reused ~15-20 times
PGP9.5	Rabbit	AbD Serotec, 7863-0504	1:4,000	>5 hrs RT or O/N 4°C	Can be reused ~15-20 times
Tuj1	Rabbit	Covance, PRB-435P	1:10,000	O/N 4°C	Can be reused ~15-20 times, but better for labeling processes (not neuronal soma)

Primary antibody dilutions can be reused multiple times if great care is taken to ensure that the dilutions remain sterile. A new dilution should be made when detection intensity begins to diminish or when the sterility of the dilution has been compromised.

Following incubation, primary antibody dilutions were conserved by tipping the slides and allowing the solution to drip into the appropriate antibody dilution storage tube. DRG sections were then washed by either gently pouring 1XPBS over the slides (approximately 20 seconds), or by pipetting 1XPBS directly onto the tissue sections three times 5-10 minutes each. The former method is much faster but the risk of losing DRG sections is much higher; the latter method takes more time but guarantees that no sections are lost. After washing, sections were incubated in secondary antibody dilutions (Table 6.3).

Table 6.3 Secondary antibodies used to detect primary antibodies in DRG immunohistochemistry

Antigen	Host	Vendor, Cat #	Dilution in Block	Incubation Time
anti-Human AlexaFluor 647	Donkey	Jackson ImmunoResearch, 709-605-149	1:200	1 hr, RT
anti-Rabbit Cy3	Donkey	Jackson ImmunoResearch, 711-165-152	1:1,000	1 hr, RT
anti-Rabbit AlexaFluor 647	Donkey	Jackson ImmunoResearch, 711-605-152	1:250	1 hr, RT
anti-Sheep Cy3	Donkey	Jackson ImmunoResearch, 713-165-147	1:1,000	1 hr, RT

Secondary antibody dilutions are never reused. Care should be taken to avoid excessive light exposure.

Slides were tipped to allow the secondary antibody to drip off the slide. Secondary antibody dilutions were never reused. Washes were conducted as described for the primary antibodies. After the last wash, 0.5mM $CuSO_4$ made in 50mM Ammonium Acetate buffer pH5.0 was applied directly to DRG sections to quench auto-fluorescence for 10 minutes (Potter et al., 2012). After exactly 10 minutes of incubation, the slides were dunked in MilliQ water to quench the $CuSO_4$ reaction. Slides were then coverslipped with AquaPolyMount (PolySciences Inc, Cat # 18606), sealed with clear nail polish (Maybelline Express Finish, 4155451378), and allowed to fully dry before confocal imaging.

Confocal imaging

DRG sections were imaged on either a Zeiss LSM 510 Meta confocal microscope or an Olympus FV-1000 confocal microscope. Images were captured with a 20x objective and software zoom set to 0.7x regardless of which microscope was used. Pinhole, laser power, gain, and amplifier offset were all optimized for each marker used; pinhole was always set to a minimum of 1.0 Airey units. These values were subject to change from one experiment to the next, depending on the intensity of secondary antibody staining and the amount of background evident. Optimization of imaging settings at each imaging session, rather than simply reusing settings established in a different experiment, is strongly recommended. However, these settings

may be found in the original LSM and FV files. Images for the purpose of cell counting were captured at 512x512 pixel resolution with faster scanning speed to expedite the process of data collection. All other images were captured at 1024x1024 with slower scan speed to generate high resolution ("publication quality") images. For all images, the laser scanning method was set to "Line", with the line scan averaging method set to "Mean" and number of scans set to 4. These laser scanning settings result in a slightly longer imaging time, because each line of the image is being scanned four times and each pixel within the line is the result of the average of each of the four scans. This laser scanning averaging method slightly lengthens total image acquisition time but remarkably improves image quality.

Cell counting

Counting of proportions of DRG neuronal subtypes was conducted manually using Adobe Photoshop software (2014 2.2 release, Adobe Systems Inc.). For each DRG image, each channel was exported from the Olympus FluoView software as a .tiff file and merged in Photoshop by selecting the "Linear Dodge" layer setting for each channel. For each marker or combination of markers to be counted, an additional layer in the image was created for adding marks to the image without altering the original. As cells were counted, dots were made over each counted cell using the paint tool while manually clicking with a counting device simultaneously. Different colors of paint were used for each marker so they could be easily distinguished when counting combinations of markers. Numerical values were written by hand and tabulated in an Excel spreadsheet. Proportions of DRG neuronal subtypes were either calculated as the percentage of Hu+ neurons expressing a given neuronal subtype marker, or in the instance of retrograde traced neurons the percentage of Fast Blue+ neurons expressing a

given neuronal subtype marker. For each marker examined, a minimum of three DRG sections from three separate DRG from a given axial level (L1, L2; L3-L5; L6, S1) from four separate animals were counted.

Pelvic ganglia collection, processing, and analysis

Immunohistochemistry on fetal cryo-sections

To assess neuronal subtype composition of fetal pelvic ganglia, immunohistochemistry (IHC) was conducted on sagittal cryo-sections of fetal animals aged E12.5, E14.5, and E18.5. Once fetal samples were completely infiltrated with sucrose (see section Embryo Collection and Processing), they were positioned in the bottom of a cryo-mold laying on their side. The best sections of pelvic ganglia are obtained when the sample is embedded at a slight angle, rather than perfectly parallel with the bottom of the cryo-mold (Figure 6.4). This is best achieved when tissue freezing medium is poured into the cryo-mold first, rather than pouring medium over the sample.

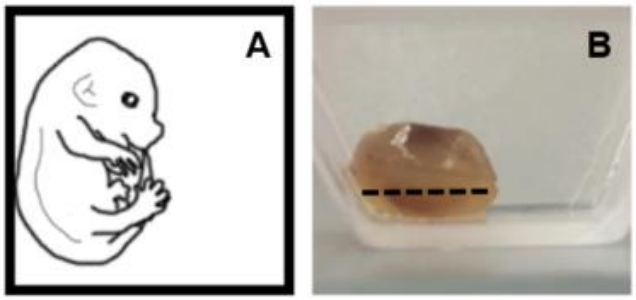

Figure 6.4 Embedding fetal sample in cryo-mold for optimal PG sectioning. Positioning the sample at a slight angle allows capturing of sections that contain DRG, PG, and the nerve tracts coming from DRG and spinal cord to the LUT. (A) Top view of fetus in the cryo-mold. Using the interior wall of the cryo-mold helps in positioning the sample at a slight angle. (B) Side-view of the fetus in the cryo-mold; the rump of the fetus is in view. Dotted line represents the cutting plane that would capture lumbosacral DRG and the left pelvic ganglion in one section.

Samples embedded in cryo-molds were then frozen by placing the molds directly onto flat, level slabs of dry ice. This method has the advantage of slow freezing; fast freezing in a dry ice/ethanol bath increases the likelihood that the sample will shift as the tissue freezing medium freezes rapidly. Fetal cryo-sections were cut on a cryostat at 20μm thickness and thaw-mounted onto 3-APES treated slides. The presence of PG in sections was confirmed by screening with an Olympus BX41 fluorescent microscope before proceeding with the IHC protocol.

Slides were dried at 37°C for 30 minutes on a slide warmer. Excess tissue freezing medium was removed with a 5 minute incubation in 1XPBS-0.3% TX-100 (0.22μm sterile filtered) at room temperature. Blocking solution (1XPBS-0.3% TX-100, 10% BSA, 5% NDS, 0.45μm sterile filtered) was applied directly to cryo-sections. Incubation in block was at least 30 minutes at room temperature; blocking was occasionally extended to overnight at 4°C. Block was removed by tipping the slides and allowing the solution to pour off. Dilutions of primary antibodies were applied directly to fetal cryo-sections. Optimized IHC conditions for primary antibodies used to label PG neuronal subtypes are listed in Table 6.4.

Following incubation, primary antibody dilutions were conserved by tipping slides over the respective primary antibody dilution storage tubes and allowing the solution to drip off the slide. Slides were then washed by gently pouring sterile filtered 1XPBS over the slides (approximately 20 seconds for each slide). Dilutions of secondary antibodies were then directly applied to each cryo-section; optimized conditions for secondary antibodies used are listed in Table 6.5.

Table 6.4 Primary antibodies used in the analysis of fetal pelvic ganglia neuronal subtypes

Antigen	Host	Vendor, Cat#	Dilution in Block	Incubation Time	Notes
Hu C/D	Human	Gift of Vanna Lennon	1:10,000	>5 hrs RT or O/N 4°C	Can be reused ~15-20 times
CGRP	Rabbit	Sigma Aldrich, C8198	1:1,000	>5 hrs RT or O/N 4°C	Can be reused ~15-20 times
Substance P	Rabbit	Immunostar, 20064	1:500	O/N 4°C	Can be reused ~10 times
TRPV1	Rabbit	Neuromics, RA14113	1:250	O/N 4°C	Can be reused 4-5 times
NF200	Rabbit	Sigma Aldrich, N4142	1:500	O/N 4°C	Can be reused ~10 times, labels processes very well
TH	Sheep	Millipore, AB1542	1:1,000	O/N 4°C	Can be reused ~10-12 times
vAChT	Rabbit	Synaptic Systems, 139-103	1:1,000	O/N 4°C	Can be reused ~10-12 times, labels processes very well
PGP9.5	Rabbit	AbD Serotec, 7863-0504	1:4,000	>5 hrs RT or O/N 4°C	Can be reused ~15-20 times

Table 6.5 Secondary antibodies used in fetal pelvic ganglia immunohistochemistry

Antigen	Host	Vendor, Cat #	Dilution in Block	Incubation Time
anti-Human AlexaFluor 647	Donkey	Jackson ImmunoResearch, 709-605-149	1:200	1 hr, RT
anti-Rabbit Cy3	Donkey	Jackson ImmunoResearch, 711-165-152	1:1,000	1 hr, RT
anti-Rabbit AlexaFluor 488	Donkey	Jackson ImmunoResearch, 711-545-152	1:400	1 hr, RT
anti-Rabbit AlexaFluor 647	Donkey	Jackson ImmunoResearch, 711-605-152	1:250	1 hr, RT
anti-Sheep Cy3	Donkey	Jackson ImmunoResearch, 713-165-147	1:1,000	1 hr, RT

Slides were tipped to allow secondary antibody dilutions to drip off. Secondary antibody dilutions were never reused. Slides were then washed by gently pouring sterile filtered 1XPBS over slides (approximately 20 seconds per slide). Auto-fluorescence is especially obstructive in fetal cryo-sections due to residual erythrocytes found in blood vessels in bladder smooth muscle

near the pelvic ganglia; to address this issue, 0.5mM $CuSO_4$ in 50mM Ammonium Acetate buffer pH5.0 was applied directly to cryo-sections. Slides were incubated in $CuSO_4$ for exactly 10 minutes at room temperature. Slides were dunked in MilliQ water to quench the $CuSO_4$ reaction. Slides were coverslipped with AquaPolyMount and premium coverslips (Fisher Scientific, 12-548-5P) and allowed to fully dry overnight before confocal imaging.

Adult pelvic ganglia collection and processing

Pelvic ganglia from postnatal and adult animals aged P10 and older were sub-dissected from animals expressing a transgenic fluorescent reporter that allowed visualization of PG neurons (*Htr3a*-EGFP, *ChAT*-EGFP, *Htr3a*-Cre;Rosa-tdTomato). Animals were fully anesthetized via isoflurane inhalation and euthanized by cervical dislocation. Ventral abdominal fur was soaked with 100% ethanol and a midline incision was made through the skin and muscle of the abdomen, starting approximately 0.5cm above the urethra and extending to the mid-abdomen. Under the guidance of a fluorescent stereomicroscope (Leica M205 FA) equipped with the appropriate filter, the bladder was carefully exposed and manipulated using #5 forceps (Fine Science Tools, 11252-30). Small spring scissors (Fine Science Tools, 91500-09) were used to cut the ureters, the urethra (approximately 0.25cm distal to the bladder neck), and snip away extraneous fat. Great care was taken to avoid damaging the pelvic ganglia. Once the bladder and proximal urethra were extracted, they were transferred to a clean petri dish for further sub-dissection. The PG were carefully peeled off the neck of the bladder using sharp #5 forceps, starting at the dorsal aspect of the bladder neck and moving towards the bladder dome.

Once removed, pelvic ganglia were pinned out flat in a Sylgard-lined 60mm petri dish (Ellsworth Adhesives, 4019862) with minutien pins (Fine Science Tools, 26002-20). Only 3-4

pins were used to avoid afflicting unnecessary damage to the PG. The pins were placed in connective tissue/fatty portions of the ganglia to avoid puncturing neurons. Pinned PG were fixed in 10% NBF overnight at room temperature while rocking two-dimensionally on a rocker and protected from light. The following day, pins were removed and washed in 1XPBS for future reuse; PG were transferred to 24-well tissue culture dishes for further processing.

Fixed PG were washed four times in sterile 1XPBS 20 minutes each, with a final wash for one hour in 1XPBS. Pelvic ganglia that were eventually cryo-sectioned were incubated overnight in 30% sucrose; PG used for whole-mount IHC were stored in blocking solution (1XPBS-0.3% TX-100, 10% BSA, 5% NDS) for at least 24 hours. If kept sterile, PG can be stored in block protected from light at 4°C indefinitely.

Immunohistochemistry on adult pelvic ganglia cryo-sections

The methods described here for obtaining cryo-sections of adult pelvic ganglia were optimized by following the recommendations of Janet Keast, to whom I am grateful for sharing her expertise with me. Upon full infiltration with sucrose, PG were embedded by positioning a single ganglion directly onto the bottom of a cryo-mold (PolySciences Inc, #18986). Fine forceps were used to carefully nudge the nerves of the ganglion to ensure the tissue was as flat as possible. The corner of a Kimwipe was used to wick away excess sucrose/PBS from the tissue. Once the ganglion was positioned precisely, tissue freezing medium was quickly poured on top. Quickly dispensing the medium onto the tissue, rather than slowly "drizzling" it over the sample, minimizes the movement of the tissue on the bottom of the cryo-mold. The sample in the mold was then placed directly onto a flat, level slab of dry ice (folded paper towels or bunched Kimwipes were helpful in making the slab level). Slow freezing of the sample, without the

application of dry ice, aids in minimizing movement of tissue that may occur if the tissue freezing medium freezes too rapidly.

Cryo-sections of PG were cut on a cryo-stat at 14μm thickness and thaw-mounted onto 3-APES treated slides. Slides were dried on a slide warmer for 30 minutes at 37°C; excess tissue freezing medium was removed by incubating slides in 1XPBS-0.3% TX100 for 5 minutes at room temperature. Sections were then blocked with blocking solution (1XPBS-0.3% TX-100, 10% BSA, 5% NDS, 0.45μm sterile filtered) for at least 30 minutes at room temperature. Primary antibody dilutions were applied directly to PG sections on slides (approximately 500μL per slide). The same primary antibody staining conditions listed in Table 6.4 were also used for adult PG cryo-sections. Following incubation, primary antibody dilutions were conserved by tipping the slides over the primary antibody dilution storage tubes and allowing the solution to drip off the corner of the slide into the tube. Slides were then washed three times 10 minutes each at room temperature in sterile filtered 1XPBS applied directly to tissue sections (approximately 750μL per slide). In experiments where several primary antibodies were used on the same tissue sections (e.g., staining for both Hu C/D and TH), incubations in primary antibodies were conducted serially to avoid mixing dilutions of different antibodies. Because the Hu C/D antibody is scarce, it was always used first (followed by other antibodies) to avoid risk of contamination with other antibody dilutions. The same washing conditions were conducted after each primary antibody used. Secondary antibodies were diluted in blocking solution and applied directly to tissue sections. The same secondary antibody staining conditions listed in Table 6.5 were used for adult PG cryo-sections. If multiple secondary antibodies were used (e.g., Donkey anti-Human and Donkey anti-Sheep), they were diluted together in blocking solution and applied to tissue sections (rather than conducting serial incubations in separate

secondary antibody dilutions as with the primary antibodies). Following incubation, secondary antibody dilutions were allowed to drip off the slides. Slides were washed three times 10 minutes each in sterile filtered 1XPBS at room temperature. To quench autofluorescence, sections were incubated in 0.5mM $CuSO_4$ pH5.0 in 50mM Ammonium Acetate buffer for exactly 10 minutes at room temperature. The $CuSO_4$ reaction was quenched by dunking slides in MilliQ water. Slides were coverslipped with AquaPolyMount (PolySciences Inc, #18606) and premium coverslips (Fisher Scientific, 12-548-5P) and allowed to dry overnight before confocal imaging.

Immunohistochemistry on whole mount postnatal and adult pelvic ganglia

Initial attempts at immunohistochemistry on postnatal and adult pelvic ganglia were conducted in whole mount. This method was working well until issues arose with the Donkey anti-Human AlexaFluor 647 (Jackson ImmunoResearch, 711-605-152) secondary antibody. A "speckled" background fluorescence would frequently occur, but not always. Despite this drawback, whole mount IHC has the advantage of allowing the staining and imaging of an entire ganglion at once, rather than running the risk of obtaining cryo-sections of PG at an angle and only capturing partial sections of the ganglion.

Each step in the whole mount IHC procedure was conducted in individual wells of 24-well tissue culture dishes, wrapped in foil, and rocking on a nutator. Pelvic ganglia were blocked in blocking solution (1XPBS-0.5% TX-100, 0.1% Tween, 10% BSA, 5% NDS, 0.45μm sterile filtered) at least 24 hours at 4°C. For this step and all others following, approximately 1.0mL was used to allow sufficient circulation of the tissue samples in solution. PG were transferred from blocking solution to primary antibody dilution for 48 hours, regardless of the antibody

used. PG were then washed in 1XPBS-0.5% TX-100, 0.1% Tween four times 20 minutes each at 4°C. If multiple primary antibodies were used, staining was conducted in a serial fashion to avoid combining primary antibody dilutions. Following the last primary antibody incubation and wash steps, PG were incubated in secondary antibody dilutions. The same secondary antibody conditions listed in Table 6.5 were used for whole mount PG IHC. PG were then washed four times 20 minutes each in 1XPBS-0.5% TX-100, 0.1% Tween. Incubation in 0.5mM $CuSO_4$ in 50mM Ammonium Acetate buffer pH5.0 for 10 minutes was conducted to quench autofluorescence. The $CuSO_4$ reaction was quenched by transferring the PG to MilliQ water. Using #5 forceps, PG were mounted onto regular microscope slides (Fisher Superfrost Plus, #12-550-15) with AquaPolyMount (PolySciences Inc, 18606) and round coverslips (Fisher Scientific, #12-545-85). Mounting PG was improved by adding a droplet of MilliQ water to the PG and using the forceps to arrange the ganglion and its nerves on the slide, and then using a Kimwipe to wick away excess liquid before adding the mounting media. Slides were sealed with clear nail polish (Maybelline Express Finish, 4155451378) and allowed to dry overnight before confocal imaging. Previous lab members have found success in the use of cut notebook paper enforcers and using them as "spacers" to create an embedding pocket on the slide for mounting thick samples. In my own work I found that the combination of copious amounts of mounting media and gentle, evenly-applied pressure to the round coverslips was sufficient for mounting adult pelvic ganglia without air bubbles.

Retrograde tracing surgery

The dorsal root ganglia harbor neurons that target a variety of tissues other than the bladder smooth muscle. In order to determine which DRG neurons directly innervate the

bladder, and how many of them express serotonin receptor 5-HT3A, retrograde tracing of neuronal processes was conducted in *Htr3a*-EGFP adult male mice. In this procedure, a retrograde tracer dye (such as Fast Blue or FluoroGold) is injected into the target tissue of interest (bladder smooth muscle), which is then transported in a retrograde manner from the neuromuscular synapse to the neuron cell body. Because the retrograde transport process takes several days, this procedure must be carried out as a survival surgery. The following methods were developed from training received in Janet Keast's laboratory at the University of Melbourne, Australia, in February 2014. Additional training in the use of the rodent anesthesia machine was received from Daphne Molnar (Vanderbilt Division of Animal Care). For future lab members who may conduct retrograde tracing, or any other type of survival surgery, videos of the entire surgical procedure were recorded and may be found on the lab computers (file name "Retrograde Trace Surgery_Entire Procedure", under the folder titled "Retrograde Tracing Surgery" – other short videos of each step can be found in this same folder).

Preparing tools and equipment for surgery

Conducting survival surgery requires careful planning and preparation of surgical materials prior to the day of operation. Details of the equipment and disposable surgery supplies needed for conducting retrograde tracing surgery are listed in Tables 6.6 and 6.7 respectively. Because surgery preparation is somewhat time-intensive, surgeries were conducted on multiple animals (maximum four) in one day.

Two days before surgery, three Deltaphase isothermal heating pads were warmed in a 55°C oven. While these pads can be microwaved, this drastically diminishes their longevity

(they will crack open suddenly and leak molten wax everywhere and completely ruin all surgery plans). Slow heating in a dry oven or water bath is strongly recommended.

Table 6.6 Tools and equipment required for retrograde tracing surgery

Tool or Piece of Equipment	**Vendor, Cat #**	**Notes**
Magnification Glasses with LED Head Lamps	201030635091.9 (Purchased from Amazon.com)	Not required but helpful during surgery for enhanced visibility
Pet Stylique Trimmer, 3/8" blade	Wahl, 5540 (Purchased from Amazon.com)	Uses 1 AA battery, includes cleaning brush
Tungsten carbide needle drivers	Fine Science Tools, 12500-12	
Size AA blunt-tip forceps	Electron Microscopy Sciences, 0103-AA-PO	
Spring scissors	Fine Science Tools, 91500-09	Ensure blades are sharpened before use
Hardened fine scissors, sharp tips	Fine Science Tools, 14090-09	Ensure blades are sharpened before use
Microliter syringe 600 series, 5.0µL volume, removable needle	Hamilton Company, 7633-01	Must be cleaned with sterile saline after use
Microliter syringe needles – 33GA, removable, 6-pack, 2" length, 12° berated tip	Hamilton Company, 7803-05	Needles get clogged extremely easily; must be cleaned after each use with tungsten wire
Tungsten wire	Hamilton Company, 18300	Wires should be cleaned with sterile saline and ethanol after each use
Deltaphase isothermal heating pad	BrainTree Scientific Inc, 39DP	Pads are in solid form at RT, must be warmed in 55°C oven at least 36 hours before use
Small reptile tank electric heating pad	ZooMed Laboratories Inc, RH-7 (Purchased from PetSmart)	
Germinator 500 dry sterilizer with glass beads	SouthPointe Surgical Supply, GRM5-1450	Tools are *very hot* when removed from sterilizer; let cool on surgical drape for 2 min before touching animal tissue
VetQuip RC2 Rodent Circuit Controller Anesthesia System	VetQuip Inc, 922100 (Provided by Vanderbilt DAC)	Requires two oxygen tanks and isoflurane
Activated charcoal adsorption filter	VetQuip Inc, 931401 (Provided by Vanderbilt DAC)	Two canisters needed: one for anesthesia induction chamber, one for nose piece

Table 6.7 Disposable items required for retrograde tracing surgery

Disposable Item	Vendor, Cat #	Notes
Chlorhexidine skin disinfectant	Bimeda, 1CHL001	Aliquot into 1.7mL Eppendorf tubes from large jug
70% rubbing alcohol wipes	Fisher Scientific, 22-031-350	Need one wipe per animal
Sterile saline topical solution	Mountainside Medical Equipment, WL64938-009-01	Need ~1.0mL per animal for moistening tissue throughout surgery
Systane eye protectant gel	Alcon, NDC 0065047401 (Purchased from Target)	2-3 mm diameter dollop on each eye
Sterile cotton gauze pads, 3.0" square	Fisher Scientific, 22-415-468	Need one pad per animal to collect shaved fur and dander
Sterile cotton buds	Fisher Scientific, 23-400-114	Need 2-3 buds per animal for applying disinfectant and soaking up any excess Fast Blue
Sterile surgical drape, 18" x 26"	Fisher Scientific, NC9047621	Need one drape per animal to cover isothermal pad
Sterilization pouches, 3.5" x 9"	Fisher Scientific, 0-812-51	Three pouches are needed for each procedure day: one for scissors and forceps, one for needle drivers, one for Hamilton syringe
Nitrile sterile surgical gloves, 12" length	Fisher Scientific, 19-898-431	Proper size is important; measure palm width around the knuckles to ensure proper fit
Monocryl sterile, synthetic, undyed monofilament absorbable suture, 5-0, 18", 19mm PS-2 precision point reverse cutting 3/8c needle	Ethicon Y495G (Purchased from Moore Medical, Item # 54190)	Suture type was selected following the recommendations of Vanderbilt IACUC
Polypropylene monofilament synthetic non-absorbable suture, 5-0, 18", 19mm P-3 precision point reverse cutting 3/8c needle	ProAdvantage P428698 (Purchased from Mountainside Medical)	Suture type was selected following the recommendations of Vanderbilt IACUC
Fast Blue retrograde tracing dye	PolySciences Inc, 17740-1	Must be re-suspended in sterile saline prior to use, preferably one week in advance
DietGel 76A gelatinized food pack	Clear H_2O, 72-07-5022 (Provided by Vanderbilt DAC)	Need one pack per animal per day of recovery
HydroGel gelatinized water pack	Clear H_2O, 70-01-2022 (Provided by Vanderbilt DAC)	Need one pack per animal per day of recovery
Isoflurane, liquid for inhalation	Piramal HealthCare, NDC# 66794-017-25	This is the same type of isoflurane used regularly in the Southard-Smith lab for mouse euthanasia
Buprenex (buprenorphine, 0.1mg/mL working concentration)	Patterson Veterinary Supply, 12496075705	Must be procured by DEA licensed PI
BD Falcon 1mL syringe, tuberculin slip tip	Fisher Scientific, 14-823-434	Can load one dose for each animal in one syringe
BD Precision Glide 30G needle	Fisher Scientific, 14-821-13A	

The isothermal pads were monitored throughout the two days in the oven to ensure complete softening of the wax inside the pads. On the morning of surgery the softened isothermal pads were transported to the animal facility in a Styrofoam insulated container.

On the day before surgery, all surgical tools were autoclaved in sterilization pouches on a dry autoclave cycle. The small spring scissors, small sharp-tip scissors, AA forceps, and Hamilton syringe were autoclaved in one pouch while the tungsten carbide needle drivers were autoclaved in a separate pouch. The small animal hair trimmer was cleaned with the cleaning brush included with the trimmer to remove mouse fur from previous use. Additionally, the trimmer was tested to ensure proper functioning and the batteries were replaced as needed. Fast Blue was reconstituted in sterile saline at a concentration of 2.5% w/v in injection-grade sterile saline (the same saline used during surgery) and thoroughly mixed by vortexing. Because the Fast Blue is "gritty" in consistency, thorough mixing is critical to ensure that the Hamilton injection needles do not become clogged during the surgery. The reconstituted Fast Blue was stored at room temperature wrapped in foil; great care was taken to avoid light exposure as much as possible. Finally, the animals undergoing the surgery were examined to ensure their health and ability to withstand survival surgery.

The surgical procedures were carried out early in the morning to avoid administering postoperative analgesia in the evening during the "lights off" cycle in the animal facility. The Deltaphase isothermal pads were brought to the surgical procedure room (831 Preston Research Building) in a Styrofoam insulating container, along with the following materials: autoclaved tools, one suture of each type for each animal, the requisite volume of pre-operative analgesic preloaded in a syringe, vial of Fast Blue, Hamilton 33GA needles, and animal welfare

monitoring sheets (one for each animal). All the other supplies listed in Table 6.6 were stored in the surgical procedure room.

MB10 was sprayed on all working surfaces of the pre-operative preparation area, the surgical hood, the anesthesia equipment, and the post-operative recovery area and allowed to soak for 10 minutes. During this time, the surgical record sheets for each animal were completed and post-operative recovery care cards were filled out. After wiping off all the MB10 solution, all the surgical equipment, tools, and supplies were set up in their appropriate areas of use (Figure 6.5).

During the preparatory steps, regular nitrile gloves (MicroFlex XCEED, #XC-310-S) were worn and hands were disinfected with liberal use of MB10. The Germinator 500 glass bead sterilizer, sharps waste container, and scale for weighing animals were placed in the pre-operative preparation area. The Germinator 500 was turned on immediately to save time; the machine takes approximately 20 minutes to reach sterilization temperature. The anesthesia equipment, housed on a rolling cart, was then positioned to the right side of the surgical procedure hood. The anesthesia induction chamber was placed inside the hood and plastic tubing was installed to connect the chamber to an activated charcoal filtration canister and the anesthesia machine. The vial of Fast Blue and the sterilization pouches containing the surgical tools were placed inside the procedure hood. A packet of sterile gauze and sterile cotton buds were also placed inside the procedure hood. In the post-operative recovery area, a clean cage was positioned partially on top of the electric heating mat. It is critical that only half of the cage is positioned over the heating mat, as this allows the animal to choose the warmer or cooler side of the cage while recovering from anesthesia. The heating mat was plugged in at this time to allow enough time for the cage bedding material to become warm.

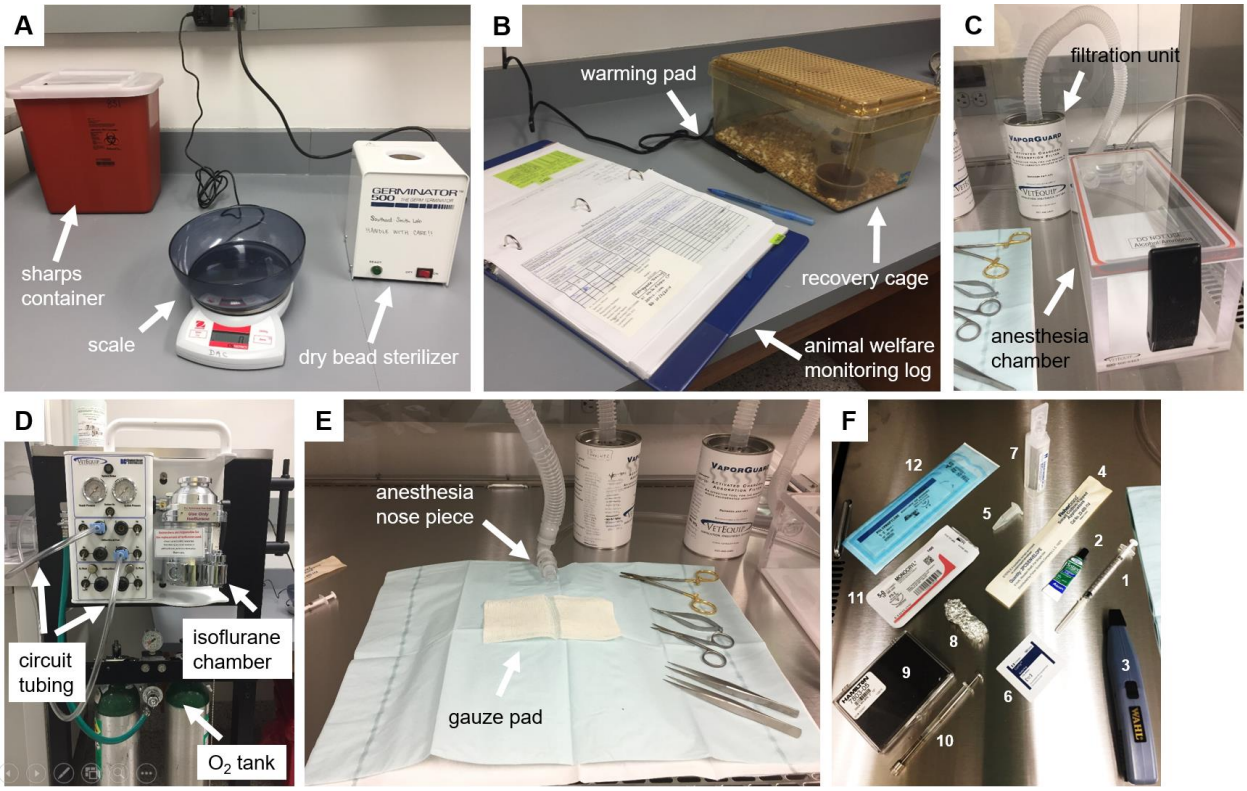

Figure 6.5 Tools and equipment for retrograde tracing surgery. (**A**) Pre-operative preparation area, including the Germinator 500 dry bead sterilizer, scale for measuring animal weight, and a sharps container for disposal of needle and syringe used to administer pre-operative analgesia. (**B**) Post-operative recovery area, including the animal welfare monitoring log and the animal's recovery cage partially positioned over an electric warming pad. (**C**) Chamber for inducing anesthesia and the tubing connecting the chamber to an activated charcoal adsorption filter and the anesthesia machine. (**D**) The anesthesia machine includes an isoflurane chamber, two oxygen tanks, and two circuits connected to the anesthesia induction chamber and the nose piece. (**E**) The surgical field, including an isothermal heating pad covered with a sterile surgical drape, a gauze pad for capturing animal fur and dander, sterilized surgical tools, and the nose piece of the anesthesia machine. (**F**) Surgical tools and supplies required for surgery, numbered in their order of use: 1) Buprenex in a 1mL syringe equipped with a 30G needle for delivery of pre-operative analgesia, 2) Systane eye protectant gel, 3) Battery powered fur trimmer, 4) Sterile cotton buds, 5) Chlorhexidine skin disinfectant, 6) Rubbing alcohol wipe, 7) Sterile saline solution, 8) Fast Blue, wrapped in foil, 9) Hamilton 33GA needles, 10) Hamilton syringe, 11) Monocryl internal suture, 12) Polypropylene external suture.

Packages of HydroGel and DietGel were placed inside the front edge of the recovery cage, along with regular chow and a clean water bottle in the feeding rack of the cage. The post-operative animal welfare monitoring sheet and post-operative care cage card, along with a disinfected writing utensil, were placed in the post-operative recovery area as well. Next, the

home cage(s) of the animals undergoing surgery were brought into the procedure room and placed in the pre-operative preparation area. Finally, one isothermal pad was removed from the Styrofoam insulating container and placed in the middle of the work surface inside the procedure hood. This step was last to keep the pad as warm as possible up to the start of the procedure.

From this point, regular nitrile gloves were removed and discarded. Hands were washed thoroughly with surgical grade scrub and sterile nitrile gloves were put on. A sterile surgical drape was folded and placed over the isothermal heating pad. The sterile surgical tools were removed from their sterilization pouches and positioned along the edge of the surgical drape. The Hamilton 33GA needle was attached to the Hamilton syringe (Figure 6.6) and 5.0µL of Fast Blue was loaded into the syringe, which was carefully placed to the side of the surgical procedure area. If the needle became clogged with Fast Blue granules, a new needle was inserted into the Hamilton syringe and loading of Fast Blue was attempted again. As previously mentioned, having all six Hamilton needles on hand in the surgical suite is helpful in instances of clogging.

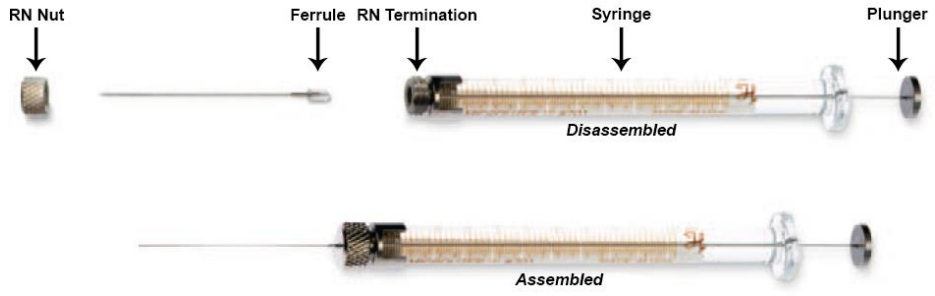

Figure 6.6 Assembly of the Hamilton syringe and 33GA removable needle. The needle is extremely fine and should be handled with care. The needle has a ferrule on the end, which fits snugly into the needle termination hub on the end of the syringe. The removable needle nut then slides over the needle and screws onto the syringe. The syringe and needles are stored in the Surgical Supplies box in the Southard-Smith laboratory. This diagram is modified from the Hamilton Syringe and Needle Assembly Guide.

Preoperative preparation of animals for surgery

Once all the surgical equipment was set up and prepared, the first animal undergoing surgery was taken from its home cage and weighed on the metric scale. The animal's weight was recorded on the animal welfare monitoring sheet and the appropriate dosage of Buprenex was calculated. The animal was then transferred from the scale to the anesthesia chamber. The anesthesia machine was turned on and isoflurane was channeled to the anesthesia chamber at a concentration of 4%. Once the animal's breathing had slowed and was no longer responsive to gently turning the chamber, the animal was removed and immediately placed on the isothermal pad. The animal, lying on its back, was then fitted with the nose piece of the anesthesia machine and the isoflurane flow was switched to the nose piece channel and the concentration of isoflurane was turned down to 2.5%. The paw pinch test was conducted to ensure the animal was completely anesthetized. A pre-operative dose of buprenorphine was administered via subcutaneous injection.

Next, Systane eye protectant gel was dabbed onto each eye, with great care taken to not poke the eyeball or smear gel onto the animal's whiskers. It should be noted that the warmth of the isothermal heating pad will cause the eye protectant gel to melt slightly during the surgery, and gel should be reapplied to the eyes as needed. Then, a pad of gauze was placed underneath the lower half of the animal and the small animal hair trimmer was used to shave the belly fur of the lower abdomen. Great care was taken to obtain a clean, close shave without nicking the animal's skin. Fur and dander were collected on the gauze pad, which was then folded and disposed of after shaving. The disinfection of skin occurred in two steps: first, a sterile cotton bud soaked in chlorhexidine was used to wipe the skin in an outward spiral pattern, then an alcohol disinfecting wipe was used to clean the second from the center out to edges (Figure 6.7).

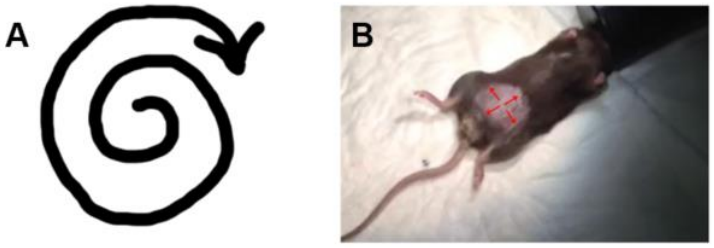

Figure 6.7 Disinfection of lower abdominal skin prior to surgery. (A) The sterile cotton bud soaked in chlorhexidine is swirled in outward spiral, starting from the center of the shaved area and moving outward to the edge of the shaved skin. (B) An alcohol disinfecting wipe is used to disinfect the skin, again moving inside out, with a new edge of the wipe being used for each direction (depicted by the red arrows).

Following disinfection of skin, a final paw-pinch test was conducted to ensure full anesthesia of the animal before proceeding with surgery.

Performing surgery: abdominal incisions and exposing the bladder

The skin was gently grasped on the midline with blunt tip AA forceps at the level of the hips, while small sharp-tip scissors were used to make a clean, vertical cut approximately 1.0 cm long. Great care was taken to avoid creating ragged edges of skin. Next, the abdominal muscle was gently grasped with blunt tip AA forceps and the small sharp-tip scissors were used to make a clean, vertical cut through the muscle along the *linea alba* ("white line") (Figure 6.8, Panel A). The *linea alba* contains relatively few nerves and blood vessels compared to other surrounding areas of abdominal muscle, making it an ideal incision point. As with the skin, care was taken to avoid creating ragged edges and nicking any glands or organs underneath the muscle. Once the muscle incision was made, the bladder was clearly visible. Blunt tip AA forceps were used to gently grasp the adventitia of the apex of the bladder dome and lift it up and out of the abdominal

cavity (Figure 6.8, Panel B). Droplets of sterile saline solution were administered to the exposed bladder to keep the tissue moist.

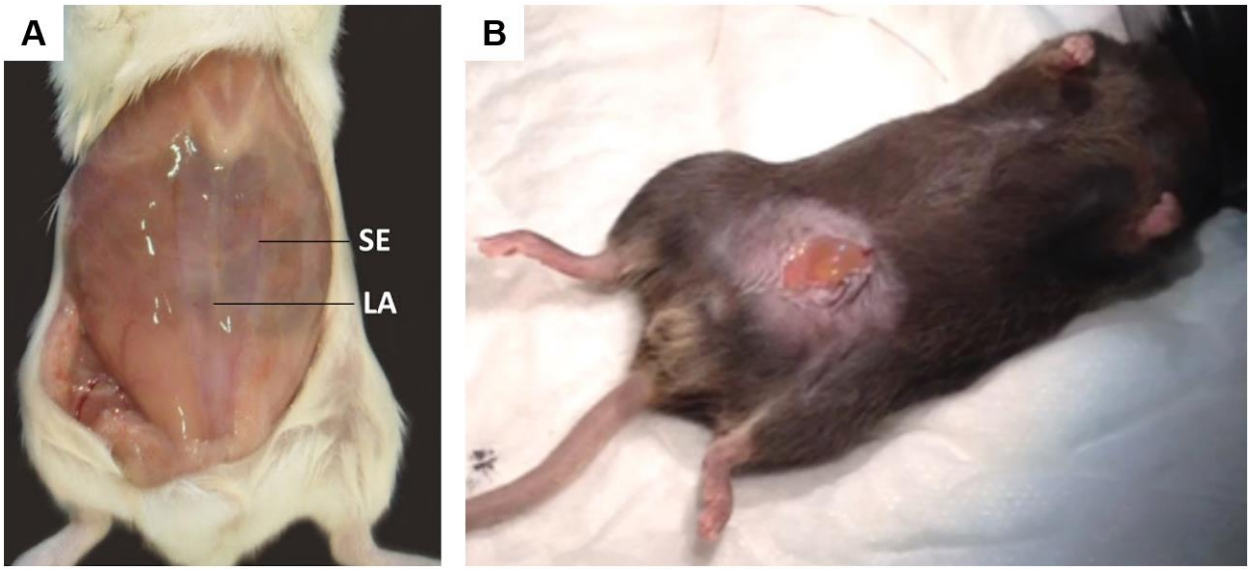

Figure 6.8 Lower abdominal incisions in retrograde tracing surgery. (**A**) The *linea alba* ("white line") is an ideal location to make a vertical incision through the abdominal musculature to expose the bladder. This photograph is strictly for *linea alba* illustration purposes; the skin incision is substantially larger than what should be made for surgery. (**B**) Once the musculature has been cut, the bladder can be exposed by using blunt tip forceps to gently grip the adventitia of the bladder dome and lift it up and out of the abdominal cavity.

Performing surgery: injecting Fast Blue retrograde tracing dye

While gently grasping the adventitia on the apex of the bladder dome with blunt AA forceps, injections of Fast Blue retrograde tracing dye were made in nine locations (~0.5µL each injection) in the bladder detrusor (illustrated in Figure 6.9). Great care was taken to ensure the tip of the needle penetrated through the serosa of the bladder and into the detrusor, without fully puncturing the bladder. Achieving the correct needle depth is absolutely critical for labeling the neuronal population of interest. An injection that is too shallow primarily labels fibers innervating the serosa of the bladder, which previous groups have shown is primarily innervated by L1, L2 DRG neurons (de Groat serosa paper). However, if the needle is injected too deeply,

the bladder will be completely punctured, allowing urine to leak from the bladder lumen into the abdominal cavity. In the event this occurs, the animal must be euthanized immediately.

Slow removal of the needle from the bladder detrusor helped reduce the risk of dye leakage onto surrounding tissue. When dye leakage did occur, a sterile cotton bud was used to quickly dab the injection site and remove excess dye.

Once the injections were complete, the bladder was carefully tucked back into place in the abdominal cavity of the animal.

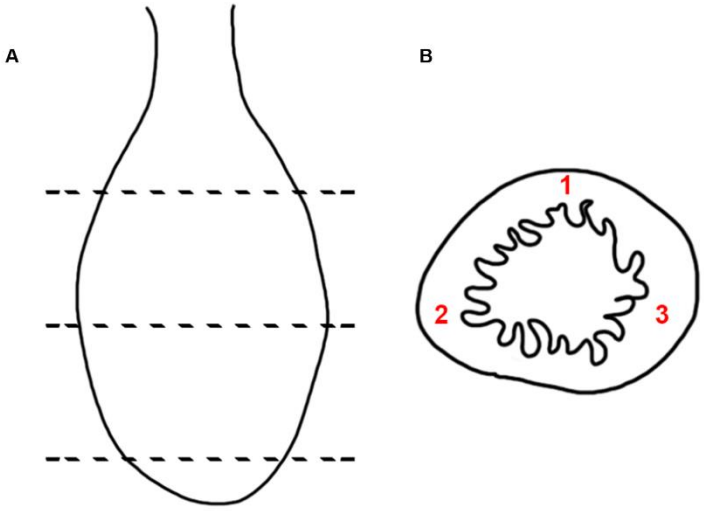

Figure 6.9 Injection of retrograde tracer into the bladder. (**A**) Superior view of the bladder dome. Dashed lines indicate the three planes in which retrograde tracer injections were made. Injections were made at three points near the bladder neck (top dashed line), at the middle or widest part of the bladder dome (middle dashed line), and near the apex of the bladder dome (bottom dashed line). (**B**) Transverse section of the bladder dome. Sites of injection are numbered. A total of nine injections were made, three within each of the planes demarcated by the dashed lines.

Suturing muscle and skin

The abdominal musculature and skin were sutured separately. The musculature was sutured using the Monocryl monofilament absorbable suture. Needle drivers and blunt AA forceps were used to make interrupted square knot sutures approximately 3mm apart.

Musculature sutures were made with externalized knots to prevent the ends of the suture material irritating visceral organs (Figure 6.10). Small spring scissors were used to snip the ends of the suture material. Interrupted square knot sutures with internalized knots approximately 3mm apart were then made to close the skin incision. Internalized knots prevent the animal from picking the stitches apart. The ends of the suture material of the last skin stitch were carefully tucked underneath the skin to prevent the animal from untying the stitch. Table 6.8 describes how externalized knots for the musculature and internalized knots for the skin were tied, and there are videos on the Southard-Smith laboratory computers that demonstrate proper suturing technique (located in the folder titled "Retrograde Tracing Surgery").

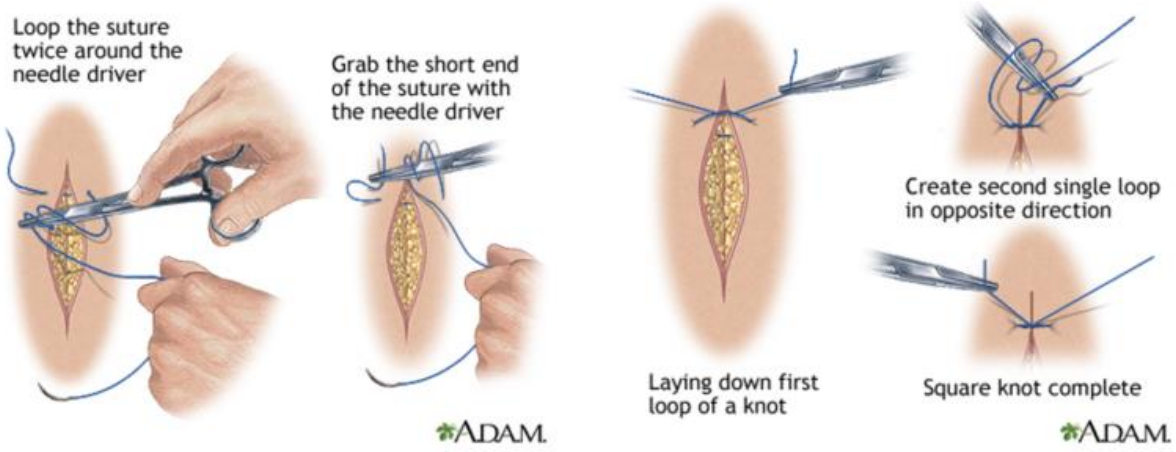

Figure 6.10 Suturing musculature and skin in retrograde tracing surgery. This schematic depicts the method for tying musculature sutures with externalized knots. The same technique applies for suturing skin with internalized knots, except that the suture is threaded with the ends of the suture material facing the interior of the animal. This figure is from ADAM Medical images (http://www.adamimages.com/Home).

Table 6.8 Strategy for tying musculature and skin sutures

Tissue	Suture Material	First Knot Tied	Second Knot Tied	Third Knot Tied
Abdominal Musculature	Monocryl monofilament absorbable suture	2 wraps with needle drivers OVER the suture thread	1 wrap with needle drivers UNDER the suture thread	1 wrap with needle drivers OVER the suture thread
Skin	Polypropylene monofilament non-absorbable suture	2 wraps with needle drivers UNDER the suture thread	1 wrap with needle drivers OVER the suture thread	1 wrap with needle drivers UNDER the suture thread

Once the suture passed through both sides of the incision, the suture thread was wrapped around the closed tips of the needle drivers as described. Then, the short end of the suture was clasped with the needle drivers and the knot was tightened. Second and third knots on the suture were made as described before moving on to the next suture. All musculature sutures were completed before tying the skin sutures.

Recovery from anesthesia and post-operative monitoring

Once the suturing was complete, the animal was carefully transferred from the isothermal heating pad to the post-operative recovery cage. The animal was positioned, lying on its back, in the area of the cage over the electric heating pad. The animal was carefully monitored for ten minutes to confirm full recovery from anesthesia (completely mobile and able to walk around cage, smelling food and water packs, grooming face, and overall alert disposition). The recovery cage was then placed on the rack in the animal housing room.

During the first 48 hours after surgery, the animal was checked and given buprenorphine via subcutaneous injection every 12 hours. After the first 48 hours, the animal was checked every 12 hours. Burprenorphine was provided as needed for pain management. In the event that stitches had been removed, the animal was euthanized. The standard operating procedure for assessment of pain and proper wound healing (established by the Vanderbilt IACUC, in accordance with animal welfare guidelines established by the National Institutes of Health) was followed.

One week after retrograde tracing surgery, the animal was euthanized via isoflurane inhalation followed by cervical dislocation. The lower urinary tract and dorsal root ganglia were

sub-dissected and processed as previously described (see sections Dorsal root ganglia collection, processing, and analysis; Pelvic ganglia collection, processing, and analysis).

Hematoxylin & Eosin staining of fetal tissue and adult bladder

Paraffin embedding and microtome sectioning

Wildtype mouse fetuses aged 15.5 dpc were sub-dissected from pregnant dams and fixed overnight at 4°C in 10% NBF. On the following day the fetuses were washed twice, 20 minutes each, in sterile 1XPBS at room temperature. They were then placed in 70% ethanol and stored at 4°C until the time of paraffin embedding, but not stored in ethanol longer than 48 hours as prolonged dehydration leads to brittle tissue and poor sectioning quality. Meanwhile, pellets of McCormick Scientific Paraplast X-tra (VWR, 15159-486) were melted in a cork-insulated glass beaker in an oven designated for paraffin use at 58°C. The samples were then washed in increasing concentrations of ethanol: 50%, 70%, 95%, then 100%, with three 20-minute washes in each grade of ethanol. The samples were then washed in histological grade xylenes (Fisher Scientific, X3P-1GAL) three times, 10 minutes each. During these washes, xylenes were warmed in a glass beaker on a hot plate in a fume hood before adding to molten paraffin. *Xylenes vapors are extremely toxic and this step should only be performed in a fume hood.* The samples were washed in 1:1 xylene and paraffin in Wheaton 12mL glass scintillation vials (Fisher Scientific, 03-335-20F) for 1 hour at 58°C inside a vacuum oven. The samples were then transferred to scintillation vials filled with 100% molten paraffin and were incubated in the 58°C oven, under vacuum, overnight.

The following day, a heating block (VWR Scientific Standard Heating Block, 549060-00) was covered with foil and the temperature was set to 42°C. The base of a plastic histology

embedding cassette (Fisher Scientific, 15182702C) and a medium-size (15 x 15 x 5mm) tissue embedding base mold (Fisher Scientific, 22-038217) were placed on the heating block and allowed to warm up before embedding. Curved-tip forceps (Fine Science Tools, 11080-02) were also pre-warmed on the heating block for several minutes. The glass scintillation vial containing the tissue sample and molten paraffin was then carefully poured into the tissue embedding base mold and the warm curved-tip forceps were used to arrange the tissue sample and push any bubbles to the corners of the base mold. The base of the histology cassette was then carefully placed on top of the base mold, which was then moved to the bench top and allowed to solidify. The base mold was then removed and discarded.

Adult *Htr3a+/+*, *Htr3a+/-*, and *Htr3a-/-* bladders were sub-dissected and fixed in 10% NBF overnight at 4°C. Bladders were then washed three times 20 minutes each in sterile 1XPBS and bisected along the sagittal plane. One half of each bladder were then sent to the Translational Pathology Shared Resource (TPSR) at Vanderbilt University for paraffin embedding.

The following microtome sectioning protocol was carried out on a Thermo Shandon Finesse ME+ motorized microtome (ThermoFisher Scientific, 77500102 Issue 7) and applies to both 15.5dpc whole fetus samples and bisected adult bladder samples. A water bath and slide warmer were turned on to 37°C and allowed to warm up for approximately 10 minutes. During this time, excess paraffin was sliced off the edges of the histology cassette with a disposable razor blade to ensure proper positioning of the cassette on the microtome cassette holder. Superfrost Plus histology slides (not 3-APES treated, Fisher Scientific, 12-550-15) were labeled as needed with pencil. The histological cassette containing the tissue sample was then locked into place in the microtome's cassette holder. The microtome was turned on and the wheel and

blade protector were unlocked. A new Shandon MB35 Premier microtome blade (35°/80mm, ThermoFisher Scientific, 3050835) was installed if any nicks on the cutting edge were visible. Sections of 10μm thickness were cut as one continuous "ribbon" of about 4-5 sections in length, which was then carefully lifted off the microtome stage with a paintbrush to the warm water bath. The bristles of the paintbrush were used to carefully remove air bubbles from underneath the sections. A labeled slide was then dipped into the water bath and the ribbon of sections were mounted onto the slide from underneath in a smooth scooping motion. The slide was then immediately placed on the warm slide warmer. After completion of sectioning, slides dried on the slide warmer for one hour and were then processed for H&E staining.

In the event of crumbling or tearing of sections, a frozen ice pack was directly applied to the freshly cut surface of the sample and held in place for approximately 20 seconds. If poor sectioning continued, the microtome blade was replaced or repositioned in the microtome.

Hematoxylin & eosin staining

The following H&E staining protocol is the result of much optimization alongside a previous graduate student in the lab, Melissa Musser. All steps were carried out at room temperature using the Sakura Tissue Tek slide staining system (VWR, 25608-902). Approximately 250mL of liquid was sufficient for each step and allowed full submersion of each slide. The tissue sections were deparaffinized with two 2-minute incubations in histological grade xylenes (Fisher Scientific, XP31-1GAL). Xylenes were re-used until they were no longer effective in removing paraffin. The tissue sections were then re-hydrated in serial ethanol dilutions (100%, 90%, 70%, and 50%), with two minutes spent in each dilution. The slides were then incubated in fresh deionized water for two minutes.

The slides were then stained with 0.22μm sterile filtered Harris Hematoxylin (VWR, 84000090) by slowly dipping three times. The slides were then washed in tap water for 5 minutes. Following the first tap water wash, the slides were then transferred to an emptied 1000μL Matrix pipet tip box, which was then placed directly under running tap water. The tap water was supplied at high enough pressure to ensure flow of water underneath the slides, but care was taken to avoid direct contact of the water stream with the slides as this may dislodge the tissue sections. After five minutes of washing with running tap water, the slides were then slowly dipped three times in 1% acid (1mL 12N HCl in 99mL 70% ethanol) and then incubated for one minute in 0.1% sodium bicarbonate. The slides were then rinsed under running tap water, in the same manner as described above, for ten minutes. Following the tap water rinse, the slides were then washed in 80% ethanol for two minutes and then stained with Eosin Y (1% alcoholic, Harleco, 15204-132) for five minutes. The tissue sections were then dehydrated through 2-minute washes in 90%, 95%, and 100% ethanol, with two additional 2-minute washes in xylenes. After the second wash in xylenes, the slides were allowed to air dry in the fume hood for 30 minutes before mounting with Permount mounting medium (Fisher Scientific, SP15-100) and traditional glass coverslips (Fisher Scientific, 12-545-F).

Slides were allowed to completely dry before imaging on an Olympus BX-41 microscope equipped with an Olympus DP70 camera. In instances where the tissue sections stained too heavily, slides were allowed to "fade" for one week before imaging. Figure 6.10 demonstrates successful H&E staining on wildtype 15.5dpc bladder and adult female wildtype bladder.

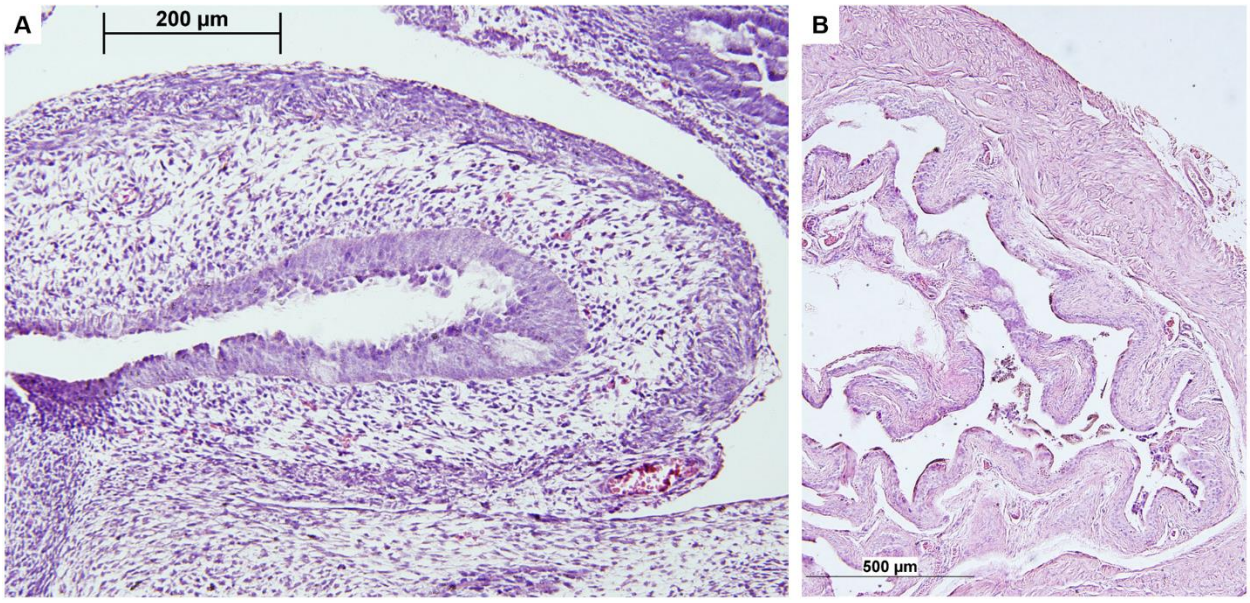

Figure 6.11 Hematoxylin & Eosin staining of wild type bladder. (**A**) 15.5dpc sagittal section. (**B**) Adult female sagittal section.

Immunohistochemistry on adult bladder via DAB colorimetric staining

The protocol described here was optimized from a protocol and personal communication from Dr. Janet Keast at the University of Melbourne, Victoria, Australia.

Transcardial perfusion

Transcardial perfusion was carried out in accordance with a protocol approved by the Vanderbilt IACUC. Male wildtype Swiss Webster mice (age P28) were anesthetized with sodium pentobarbital, administered via intraperitoneal injection at a dosage of 60mg/kg body weight from a working stock concentration of 50mg/mL. The variable flow mini-pump perfusion apparatus (Fisher Scientific, 13-876-1) was assembled in the fume hood along with the following items: 30mL sterile filtered 1XPBS, 30mL freshly prepared 4% paraformaldehyde, small sharp-tip dissection scissors (Fine Science Tools, 14090-09), curved tip forceps (Fine Science Tools, 11080-02), a Surflo winged infusion 25G butterfly needle set (Fisher Scientific,

22-258092), and four 27G disposable needles (Fisher Scientific, 14-821-13B). Three to five minutes later, the paw pinch test was conducted to ensure full anesthesia. Another dose of sodium pentobarbital was given if the animal was still responsive to paw pinching. The animal was pinned by all four paws to a piece of Styrofoam, lying on its back. The abdominal fur was wetted with 100% ethanol and small scissors were used to incise the skin and muscle over the rib cage. Curved tip forceps were used to grip the xiphoid process and the ventral portion of the rib cage was cut away with small scissors to reveal the heart. The right atrial chamber was snipped with small scissors and the butterfly needle was immediately inserted into the apex of the left ventricle of the heart. The mini pump was set to low speed and approximately 30mL of sterile filtered 1XPBS was pumped through the animal's vascular system to clear the vessels of blood. The animal was then perfused with 4% paraformaldehyde. Following perfusion, the animal was then immediately dissected. Perfusion of subsequent animals did not commence until bladder dissection was complete.

Flat-mount fixation of whole adult bladder

Immediately after perfusion, the bladder was quickly sub-dissected by gently gripping the adventitia of the apex of the bladder dome with fine forceps and cutting the proximal urethra approximately 0.50 cm away from the bladder neck with small spring scissors. Once sub-dissected, small spring scissors were used to bisect the bladder longitudinally on the ventral/inferior side, up to the apex of the bladder dome. This resulted in a completely flattened bladder (Figure 6.12) that was then pinned down with minutien pins (Fine Science Tools, 26002-20) to a Sylgard-lined 60mm petri dish (Ellsworth Adhesives, 4019862). The pins were placed only along the perimeter of the bisected bladder. The orientation of the bladder in the dish

during fixation (urothelium facing up or down) is arbitrary. Each bladder dissected was pinned down in its own Sylgard-lined dish with the animal's ear tag number written on the lid of the dish.

The flat-mount bladders were fixed in freshly prepared 4% paraformaldehyde for approximately 18 hours at room temperature while gently shaking on an orbital shaker (VWR, DS-500E). The Sylgard-lined dishes were kept inside a pipet tip box to prevent any potential spillage of formaldehyde. Following fixation, the bladders were removed from the dishes by carefully plucking out each minutien pin with fine forceps (Fine Science Tools, 11252-30), taking care to not tear the bladder tissue. They were transferred to individual wells of a 12-well tissue culture dish (Fisher Scientific, 08-772-29) and washed 3 times, 30 minutes each, in sterile filtered 1XPBS at room temperature.

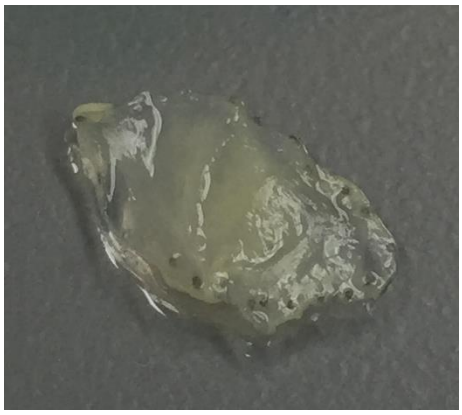

Figure 6.12 Flat-mount fixation of whole adult urinary bladder. The bladder was bisected along the ventral/inferior length of the bladder dome, starting with the bladder neck and ending at the apex of the bladder dome. The bladder was then pinned out flat in a Sylgard-lined dish using minutien pins along the edge of the bladder (pin holes are visible on the right edge in this image).

Immunohistochemistry via DAB staining

From this point forward, all staining and washing steps were carried out on rotating nutators at room temperature (unless otherwise noted) in 12-well tissue culture dishes and the bladders were transferred to new wells for each step. Bladders were washed in 50% ethanol for 30 minutes, followed by a 30 minute wash in 50% ethanol, 3% hydrogen peroxide. The hydrogen peroxide was diluted from a previously unopened bottle of 30% stock (Fisher Scientific, H325-100). While hydrogen peroxide does not expire until one month after opening the bottle, fresh stock is recommended due to the time intensive nature of this protocol. The bladders were then washed for 30 minutes in 0.1M Phosphate Buffer (PB), pH7.4, with 10% Normal Donkey Serum (Jackson ImmunoResearch, 017-000-121). The recipe for PB can be found in Table 6.9. During this wash step, the primary antibody dilution was prepared in a blocking solution comprised of 0.1M PB with 0.05% thimerosal (antimicrobial agent, Fisher Scientific, BP2542-10), 10% Normal Donkey Serum, and 0.2% Triton X-100. The bladders were stained for Calcitonin Gene Related Peptide (CGRP) using a Rabbit anti-CGRP antibody (Sigma Aldrich, C8198, RRID: AB_259091) at a dilution of 1:1000, and Tyrosine Hydroxylase (TH) with a Sheep anti-TH antibody (Millipore, AB1542, RRID: AB_90755). The bladders were incubated in primary antibody for 48 hours, although this may be extended to 5 days if necessary.

Table 6.9 Recipes for phosphate buffer solutions used in colorimetric DAB staining

	Monobasic Solution	**Dibasic Solution**
Amount in 1L H_2O	27.6g sodium phosphate monobasic monohydrate (Fisher Scientific, S369-500)	53.6g sodium phosphate dibasic heptahydrate (Fisher Scientific, S373-500)
Volume of Solution to make 0.1M PB	95mL	405mL

Recipes for monobasic and dibasic sodium phosphate solutions that comprise 0.1M phosphate buffer (PB). Once the monobasic and dibasic solutions are made, the dibasic solution is slowly added to the monobasic solution while stirring on a stir plate. Once combined, 500mL H_2O is added to the mixture to obtain 1L of 0.1M PB. These concentrations should yield pH7.4, but pH was checked with a pH meter.

The primary antibody dilutions were recovered from the tissue culture wells and stored in conical tubes at 4°C. The bladders were washed 3 times, 30 minutes each, in 0.1M PB, pH7.4. During these wash steps the secondary antibody dilutions were prepared as follows: 0.1M PB with 0.05% thimerosal, 10% Normal Donkey Serum, 0.02% Triton X-100, and a Donkey anti-Rabbit Biotin-SP conjugated secondary antibody (1:1000, Jackson ImmunoResearch, 711-065-152), or a Donkey anti-Sheep Biotin-SP conjugated secondary antibody (1:1000, Jackson ImmunoResearch, 713-065-147). The bladders were incubated in the secondary antibody dilution for 48 hours, although this step may be extended to 5 days if necessary.

The bladders were then washed 3 times, 30 minutes each, in 0.1M PB, pH7.4. While the bladders were washing, the VectaStain Elite Avidin Biotin Complex (ABC) kit was prepared (Vector Laboratories, PK-6100). The ABC solution was diluted in the same blocking solution used for the primary and secondary antibodies, and the two ABC solutions ("Solution A" and "Solution B") were added at a concentration of 6μL/mL. The ABC solution must be allowed to incubate at room temperature for 30 minutes before applying to tissue samples. The bladders were incubated in the ABC solution for 48 hours.

The bladders were then washed twice, 30 minutes each, in 0.1M PB, pH7.4. They were then washed in 0.1M sodium acetate buffer, pH6.0 for 30 minutes. While the samples washed in sodium acetate, the 3,3'-diaminobenzidine (DAB) solution was prepared. *This chemical is extremely toxic and should be handled with upmost care exclusively in the fume hood*. One 10mg tablet of DAB (Sigma Aldrich, D5905) was dissolved in 0.1M sodium acetate buffer, pH 6.0, 2mg/mL D-glucose (Sigma Aldrich, G7021-100G), and 0.4mg/mL ammonium chloride (Fisher Scientific, A661-500). The bladders were pre-incubated in DAB solution for 20 minutes on a nutator in the fume hood. In an Eppendorf tube, glucose oxidase (Sigma Aldrich, G0543-

10KU) was added to sodium acetate buffer at a dilution of 1:10 and mixed by inversion. This glucose oxidase dilution was then added to fresh DAB solution at a concentration of 0.2µL/mL and was mixed thoroughly. The pre-incubation DAB solution was removed and the DAB/glucose oxidase solution was added to the bladder samples. The progression of DAB staining was monitored periodically in the fume hood and briefly under a Leica MZ125 light microscope. The DAB staining reaction was complete after 5 hours and 40 minutes; however, this time varies considerably and the DAB staining reaction is not reversible. The experimenter must monitor staining on an hourly basis to ensure the tissue samples are not over stained.

Following the DAB staining reaction, the bladders were washed for 30 minutes in 0.1M sodium acetate buffer, pH 6.0, then twice in 0.1M PB pH7.4. They were then mounted onto 3-APES slides, with one bladder per slide, and allowed to dry for 8 hours or overnight in the fume hood. While Dr. Keast's original protocol for this procedure calls for gelatinized slides, I found that 3-APES treated slides (which are normally used for cryo-sections) worked well for this procedure, as long as the slides are handled with care.

After the bladders were mounted and dried on 3-APES slides, the bladders went through a dehydration process. The slides were placed in a histological glass slide washing rack and washed twice, 15 minutes each, in the following solutions: MilliQ water, increasing ethanol dilutions (30%, 50%, 70%, 90%, 95%, 100%), and then finally CitriSolv (Fisher Scientific, 22-143975). Finally, Permount mounting medium (Fisher Scientific, SP15-100) was applied in large dollops directly onto the bladders and 22mm round coverslips (Fisher Scientific, 12-545-85) were applied. The slides were allowed to completely dry in the fume hood (at least overnight). The edges of the coverslips were sealed with clear non-fluorescent nail polish (Maybelline Express Finish, 4155451378) before imaging on an Olympus BX41 microscope.

Figure 6.13 illustrates the results of staining for TH (Figure 6.13, Panel A) and CGRP (Figure 6.13, Panel B) via DAB colorimetric immunohistochemistry. This method provides an excellent view of overall innervation patterning of bladder smooth muscle; however, it also has drawbacks. First, this procedure requires a minimum of nine days to complete, which is much longer than traditional fluorescent IHC on cryo-sections of bladder. Second, the DAB staining reaction is much more variable and difficult to reproduce across samples, which may become a confounding factor if this method is used to compare staining patterns over multiple replicates of IHC. Third, obtaining a large enough field of depth via bright-field microscopy is difficult, whereas this issue is resolved in fluorescent confocal microscopy by compiling serial images in a z-stack.

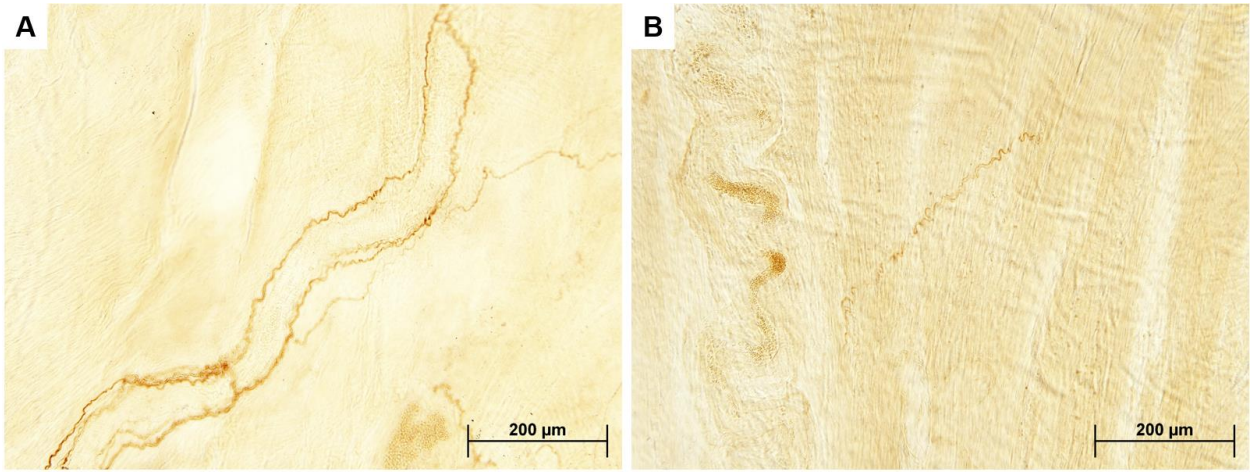

Figure 6.13 Immunohistochemistry via DAB colorimetric staining in adult bladder. (**A**) Staining for tyrosine hydroxylase (adrenergic fibers) reveals thick nerve bundles supplying the bladder smooth muscle. (**B**) Sparse staining for Calcitonin Gene Related Peptide (CGRP, nociceptive sensory fibers) in bladder smooth muscle.

Spontaneous void spot assay

The spontaneous void spot assay (VSA) is a relatively straight-forward and cost-effective method to semi-quantitatively define urinary voiding patterns in postnatal mice. The protocol described here elaborates on the procedure reported in Chapter III, section Materials & Methods.

As with any assay of animal behavior, variability in environmental factors that may affect assay outcome must be avoided as much as possible. Great care was taken to conduct void spot assays in the most reproducible and uniform manner.

Experimental design

Other research groups have previously conducted VSAs on mice (Yu et al., 2014;Bjorling et al., 2015;Keil et al., 2016). The methodology I have established improves the VSA procedure in several ways. First, prior VSA studies were conducted on a single day. I opted to include a five day acclimation period to reduce the effects of novel environment on micturition behavior, and chose to conduct the trial portion of the assay over three consecutive days. Averaging the voiding frequency across three trial days ameliorates the effects of day-to-day variability in voiding behavior.

Second, prior VSA studies assayed voiding patterns in animals over a four-hour time period. Because no food or water is available to the mice during the VSA, I chose to conduct the assays for one hour rather than four hours to reduce the effects of the stress of fasting and dehydration on urinary voiding.

Third, in prior VSA studies the urine was visualized via UV illumination in a large electrophoresis gel imaging unit. I chose to visualize urine in my VSAs with Ninhydrin staining for several reasons: 1) UV illumination does not allow distinction of overlapping voids, which

leads to multiple voids counting as one large void, while Ninhydrin clearly stains the borders of void spots; 2) UV illumination requires a large gel imaging unit, while Ninhydrin-stained assays can be scanned directly to a computer with a normal bed scanner; and 3) Ninhydrin strongly and permanently binds nitrogen-rich compounds (such as urine), which is beneficial for archiving VSAs and the ability to re-assess them later if needed. A previous member of the Southard-Smith laboratory, Jean-Marc DeKeyser, originally conceived the idea of trying Ninhydrin staining in VSAs. I am immensely grateful for his input.

The VSA was conducted with five days of acclimation, followed by a two day break, and three days of trial. The acclimation to the assay was initiated when the animals were approximately age P28 (± 3 days). This age was chosen for two reasons: 1) the animals are well beyond the age of requiring perineal stimulation to initiate voiding (approximately P12, (Girard et al., 2016)), and 2) conducting the assay before the onset of sexual maturity (P42) prevents any influence estrous cycling and high testosterone levels on voiding behavior (Mucignat-Caretta et al., 2004;Game` et al., 2008;Bjorling et al., 2015). The two day break between acclimation and trial was planned to avoid conducting the assay during biweekly cage changes in the animal facility, as this process creates noise and commotion that may affect voiding behavior.

To avoid the effects of circadian variability in micturition behavior, VSAs were conducted at the same time for each acclimation and trial day (12:00pm-1:00pm). This time was chosen because previous VSA studies by other groups were conducted in the 10:00am-2:00pm time range, and I found that I was able to commit to this time frame consistently over many months.

Preparing the animals

Male and female 4-week old mice were used for void spot assays. Mice were collected from multiple breeding units and genotyped from ear punches. Ear punch location, as well as unique tail stripe patterns, were used to identify animals within their home cages to avoid scruffing mice to read ear tags during the assay. Although social dominance is known to influence conscious micturition behavior (Desjardins et al., 1973;Hou et al., 2016), animals were group housed by sex (maximum five animals per cage) to reduce costs. Laminated "Do Not Disturb" cards were placed on the home cages of the animals used in the assay to avoid any effect cage change may have on voiding behavior.

Preparing filter paper

Whatman filter paper (3mm, chromatography grade, 35 x 43 cm sheets, GE Healthcare #3030-347) was used to collect urinary voids in the assay. The filter paper was handled exclusively with clean gloves to avoid contamination with fingerprints or other materials that may be stained by Ninhydrin. A guillotine-style 18" paper cutter (Staples, 1388223) was used to cut pieces of filter paper to the dimensions of the bottom of the animal cages used in the assay (Figure 6.14). From a 35 x 43 cm sheet of filter paper, two sheets can be cut that precisely fit the bottom of the cage; these sheets should be reserved for the three trial days of the VSA. The third piece cut is slightly too narrow to fit the cage; however, these thinner pieces can be used for the five days of acclimation. Combining all five acclimation days and three days of trial, each animal included in the VSA needs eight sheets of cut filter paper. The filter papers used in the three trial days were labeled on one side with the animal ID number and the date of the assay

before autoclaving to save time in the animal facility. Acclimation sheets were not labeled since they were not included in quantification.

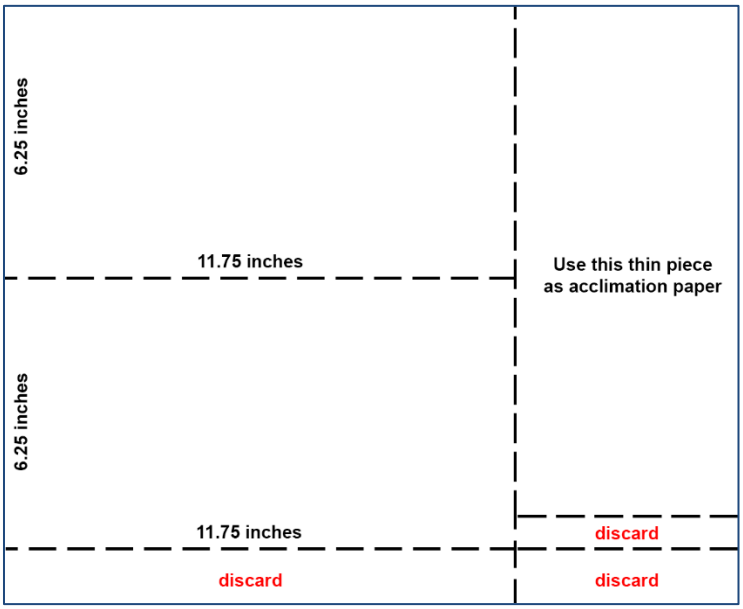

Figure 6.14 Template for cutting sheets of filter paper for void spot assays. Sheets of Whatman filter paper, size 35 x 43 cm, were cut using a large guillotine-style paper cutter to produce two sheets precisely sized for the bottom of the assay cages. The pieces cut that were slightly too narrow were used for assay acclimation to conserve resources.

Cut and labeled sheets of filter paper were wrapped in four foil packets: one large packet containing enough sheets for five days of assay acclimation and three separate foil packets for each assay trial day. Several extra pieces of assay paper were also autoclaved in case one was dropped on the floor during the assay. Autoclaved packets of assay paper were stored in the animal facility and labeled appropriately.

Preparing assay cages

The void spot assays were conducted in the same type of cage used for animal housing and kept on the same rack as the animals' home cages. Empty cages free of any bedding material were requested at least one week in advance from the Division of Animal Care

technician. In the event that VSAs were planned to begin on short notice, clean cages were emptied of bedding material and wiped down with an MB10-soaked paper towel to eliminate all bedding material dust. Because the metal cage card holders that snap onto cage lids can unexpectedly fall off and induce startle-response voiding, cage card holders were not used on assay cages. Instead, index cards with the animal's identification number were taped to the front of each assay cage (Figure 6.15, Panel A).

Each assay cage was placed in the same position on the cage rack for every day of the acclimation and testing period. The water dispensing nozzle (referred to by the DAC as a "lixit") for each of the assay cages was disabled by placing a metal snap-on covering over the nozzle to prevent water consumption during the assay. The metal nozzle coverings were thoroughly disinfected with MB10 prior to installation.

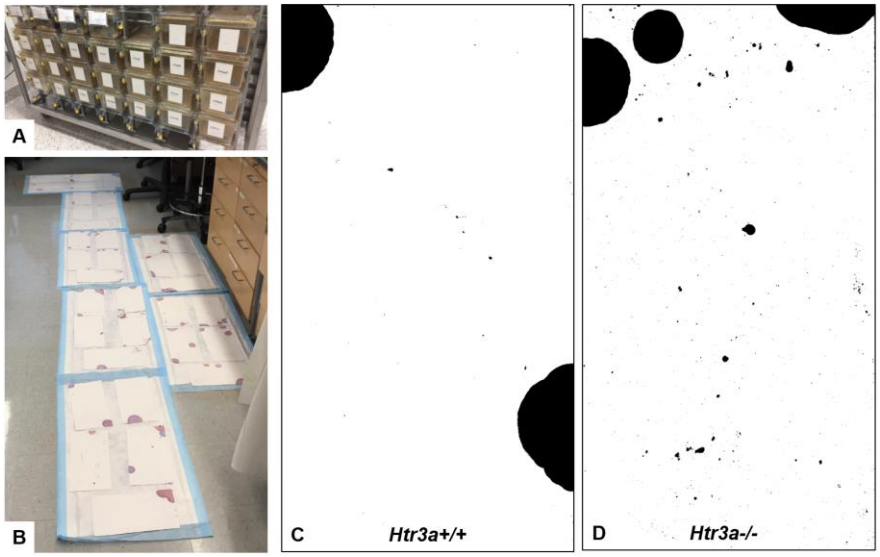

Figure 6.15 Preparation and analysis of void spot assays. (**A**) Void spot assay cage were placed on the same cage rack as the animals' home cages. VSA cages are completely empty and identifying cards are taped onto the front of each cage to avoid the usage of metal cage card holders that may fall off and evoke startle-response voiding. (**B**) VSA papers stained with Ninhydrin. Care was taken to contain all Ninhydrin mist on the disposable absorbent pads. (**C**) Representative processed VSA of a male *Htr3a+/+* animal. (**D**) Representative processed VSA of a male *Htr3a-/-* animal.

Conducting the assay

Void spot assays were conducted consistently between 12:00pm-1:00pm. Fellow members of the lab were advised to avoid working in the mouse room during the assay to avoid unnecessary noises or movement that may evoke startle-response voiding. I arrived in the mouse room approximately 10-15 minutes before the start of the assay to remove all the assay cages and place a single piece of autoclaved Whatman filter paper in the bottom of each cage. For smaller cohorts, all the assay cages can be stacked in one hood; for the larger cohorts, both hoods were used. Animals were placed in their respective assay cages in the same order each day, which not only streamlines the process of moving the animals each day, but also allows for optimized stacking of the assay cages within the hood. The first animals to be placed in void spot assay cages were the first to be removed from assay cages and returned to their home cages. Animals were carefully lifted out of their home cages by the base of their tail, being careful to not make any sudden movements that might startle the animals. Animals in their assay cages were promptly returned to their designated spaces on the cage rack. I left the mouse room during the assay and returned after the first animals had been in their assay cages for one hour. As before, animals were carefully lifted out of the assay cages and returned to their home cages and great care was taken to avoid startling the mice. On acclimation days, the Whatman filter paper sheets were discarded. On trial/testing days, the filter papers were placed back into their original foil packet and a new piece of foil was placed between each sheet to avoid contaminating adjacent filter papers with wet urine. Fecal pellets were shaken off the assay papers and removed from the assay cages.

I noted that some animals were prone to chewing the corners of the filter paper during the void spot assay. I found no correlation between *Htr3a* genotype and this chewing behavior;

however, the animals exclusively chewed the corners where they had previously urinated. This was determined in the Ninhydrin staining process, because the borders of the chewed areas stain with Ninhydrin without exception.

After the third and final assay day, the assay cages were removed from the cage rack and placed in the dirty cage area of the mouse room. Mice used in the assay were subsequently used for conduction of anesthetized bladder cystometry or dissection of LUT tissues.

Visualizing urine by Ninhydrin staining

Staining the soiled VSA filter papers was conducted exclusively over weekends to avoid disturbance of normal workflow in the laboratory and to limit the inhalation of potential allergens found in mouse urine. An N95 respirator mask (3M, 9211) was worn through the entire urine staining procedure. *Mouse urine is particularly rich compounds known to elicit allergic reactions. A properly fitted respirator mask is strongly recommended to limit personal exposure to urine vapors, especially because the Ninhydrin crystals are dissolved in 95% ethanol which quickly evaporates.* Disposable absorbent pads (VWR Scientific, 56616-030) were placed on the floor of the laboratory to prevent Ninhydrin staining of the floor tiles. Soiled VSA papers from all three days of trial were arranged on the disposable absorbent pads, allowing a border of approximately 3 inches between the edges of the filter paper and the edge of the pad. Filter papers were aligned very close to each other but not touching (Figure 6.15, Panel B).

Ninhydrin (Sigma Aldrich, 151173) was dissolved in 95% ethanol at a concentration of 2% weight/volume (1.5 g/750 mL in a Rubbermaid Heavy Duty spray bottle (32 ounce capacity, Rubbermaid, 9C03-06). A stir bar was placed in the bottom of the spray bottle and Ninhydrin was dissolved in approximately 5 minutes at room temperature with stirring at medium-high

speed. When fully dissolved, the Ninhydrin solution should be transparent and pale yellow in hue. Ninhydrin solution was freshly prepared for each round of staining.

The assay papers were thoroughly misted with Ninhydrin solution. Care was taken to ensure that each filter paper was completely covered with no dry areas. Chewed corners of the assay papers were pressed flat once sprayed with Ninhydrin; this step expedites the scanning process later. The sprayed filter papers were allowed to air-dry over the weekend and were collected first thing in the morning. The dry, stained filter papers were kept in foil packets until they were scanned; following scanning they were stored in sealed biohazard bags.

Quantification of voiding frequency

Void spot assay papers from the three testing days were scanned into an Apple computer using a Brother MFC-7460DN printer/scanner/copier. The assay papers were scanned in color at a resolution of 300dpi; scan images were saved as .tiff files. The bed of the scanner was thoroughly sanitized with household disinfectant to avoid spreading of mouse urine to other lab members.

The image files were then processed in Adobe Photoshop (2014 2.2 release, Adobe Systems Inc.). Because urine spots are stained purple and are round with smooth edges, non-urine Ninhydrin staining was easily discerned. Fecal material and smears were identified by their color and shape and removed from the image using the Eraser tool. Paw prints (created when a mouse urinates, immediately walks across the urine, and tracks it onto non-soiled parts of the paper) were easily identified by their shape and were also erased using the Eraser tool. "Haziness" of Ninhydrin staining may occur if a mouse has been sitting in one place on the filter paper for a long time, as the animal's belly fur may leave a residue (especially if the animal

walked over fresh urine before resting). Hazy staining can also be eliminated using the Eraser tool. The Hue/Saturation tool was used to desaturate the image. Corners of the paper that had been chewed during the assay were filled in using the Paint tool, with the Paint color set to pure black (Figure 6.15, Panels C and D).

Voiding frequency and void surface area were quantified in ImageJ (http://imagej.nih.gov/ij/). The image files pre-processed in Photoshop were opened in ImageJ (File > Open). The Threshold tool (Image > Threshold) was used to threshold each image. The thresholding method was set to "Default" and the color was set to "B&W" with the "Dark Background" box left un-checked. The threshold values slider was toggled to highlight the void spots. The Analyze Particles tool was used to measure the number and size of the void spots (Measure > Analyze Particles). The minimum size particle was set to 0.02 cm^2 to prevent counting of background flecks or debris. This minimum particle size has been previously used by other groups conducting spontaneous void spot assays (Yu et al., 2014;Keil et al., 2016). The "Display Results" box was checked to generate tabulated data of quantified void spots, which were then exported from ImageJ as an Excel file. Voiding frequency (the number of void spots on the assay paper) and void surface area (a readout of void volume) were averaged for each animal across the three days of trial. Detailed results of the void spot assay studies conducted in *Htr3a* mutant mice are described in Chapter III.

Analysis of urine specific gravity in *Htr3a* mutant mice

While assessing urinary void spot patterns in *Htr3a* mutants, a trending decrease in average void surface area was noted in female *Htr3a+/-* and *Htr3a-/-* mice. To determine if

Htr3a mutants had more concentrated urine, urine specific gravity was measured in male and female *Htr3a+/+*, *Htr3a+/-*, and *Htr3a-/-* adult mice.

Urine was collected following the completion of the spontaneous void spot assay (see Section "Spontaneous void spot assay" in this chapter). Mice were placed in the same empty cages used for conducting the VSA, except no Whatman filter paper was placed in the cage. Mice were kept in these empty cages on the cage rack for one hour and were subsequently returned to their home cages. Urine was collected from the bottom of the mouse cages using a P1000 pipette into sterile 1.7mL Eppendorf tubes. At least 100µL of urine is required to accurately measure urine specific gravity (Chad M. Vezina, personal communication), but 300µL is recommended. A pocket urine specific gravity refractometer was used to measure urine specific gravity (Atago PAL-10S, #4410), according to the manufacturer's instructions. All measurements were conducted on the day of urine collection at ambient room temperature in one sitting to avoid any fluctuations in temperature that may affect specific gravity measurements. Following the measurement of specific gravity, the urine was carefully pipetted off the refractometer and stored in a designated freezer box at -80°C.

A summary of urine specific gravity measurements is listed in Table 6.10. All urine specific gravity measurements are plotted in Figure 6.16. The urine specific gravity was not significantly different among male *Htr3a*-KO mice (p=0.1388, one-way ANOVA), nor female *Htr3a*-KO mice (p=0.9892, one-way ANOVA).

Table 6.10 Summary of urine specific gravity in *Htr3a*-KO adult mice

	Urine Specific Gravity (mean ± SEM)		
Genotype	**Male**	**Female**	**All Animals**
Htr3a+/+	1.0311 ± 0.0027	1.0292 ± 0.0014	1.0303 ± 0.0017
Htr3a+/-	1.0391 ± 0.0045	1.0296 ± 0.0041	1.0352 ± 0.0033
Htr3a-/-	1.0299 ± 0.0026	1.0298 ± 0.0008	1.0298 ± 0.0016
All Genotypes	1.0334 ± 0.0021	1.0295 ± 0.0014	

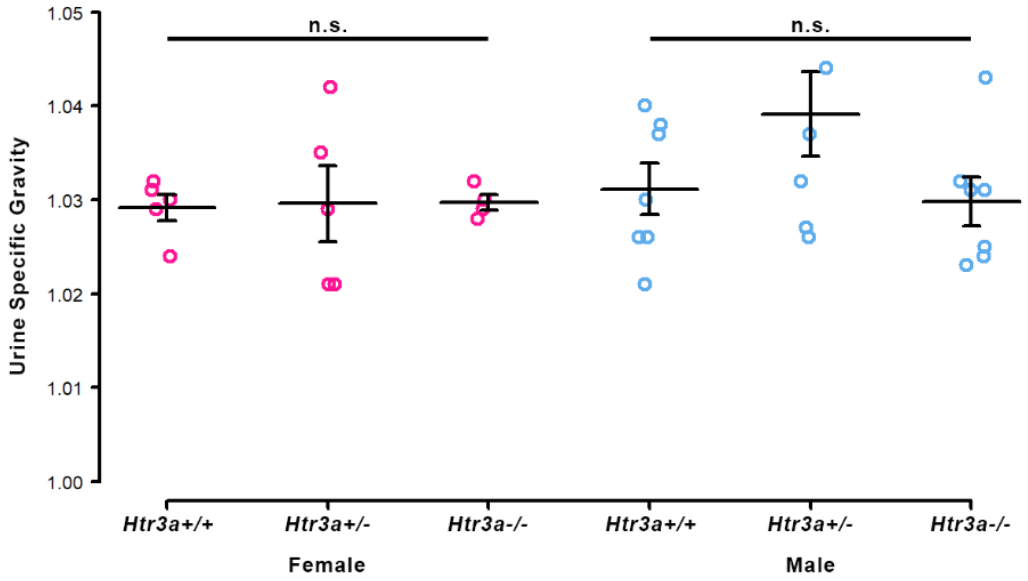

Figure 6.16 Assessment of urine specific gravity in *Htr3a* mutant adult mice. Each dot represents the urine specific gravity measurement of one animal. Female measurements are plotted in magenta on the left; male measurements are plotted in blue on the right. Black bars denote the mean ± SEM. n.s. = not statistically significant.

Given that neither urine specific gravity nor voided volume measured via anesthetized cystometry was significantly different among female mice (see Chapter III), the trending difference in void surface area observed in spontaneous void spot assays was likely due to experimental differences in data collection and analysis. Voiding in the VSA was measured over one hour and averaged over three days of trial, while urine specific gravity and cystometric measurements of void volume were analyzed once per animal. Additionally, void volume is more precisely measured via bladder cystometry than VSA.

Analysis of *Htr3a*-EGFP; *Htr3a*-KO phenotypes

To determine the consequences of 5-HT3A loss on neurodevelopment of bladder innervation, I had initially planned to employ the *Htr3a*-KO mouse line crossed with the *Htr3a*-EGFP transgenic reporter mouse line used in my gene expression analysis studies. Theoretically, the *Htr3a*-EGFP transgene is under the control of endogenous regulatory factors that govern *Htr3a* gene expression, which is independent of the *Htr3a* knockout allele. With *Htr3a*-EGFP/+; *Htr3a-/-* mice, I had intended to visualize cells that would normally express *Htr3a* and determine their outcome over fetal and postnatal development. The breeding strategy for obtaining *Htr3a*-EGFP; *Htr3a-/-* mice is schematized in Figure 6.17.

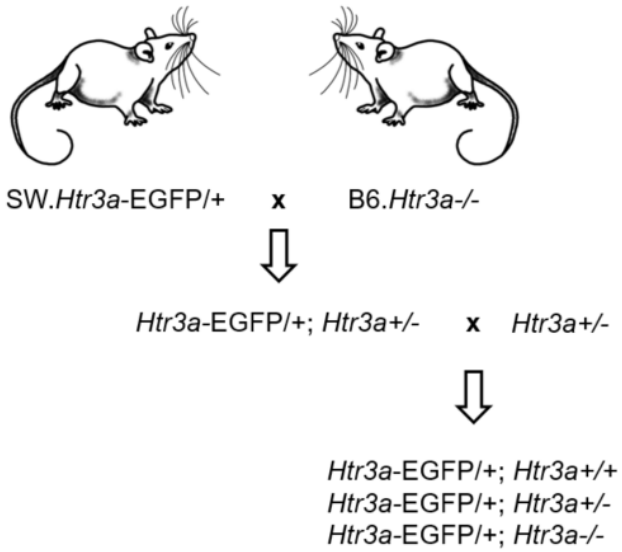

Figure 6.17 Breeding strategy to generate *Htr3a*-EGFP/+; *Htr3a*-KO animals. The *Htr3a*-EGFP transgenic reporter mice are maintained on a Swiss Webster background, while *Htr3a*-KO mice are maintained on a C57/BL6J background. Reporter mice were maintained as heterozygotes to avoid comparing fluorescence intensity levels between EGFP/EGFP and EGFP/+ mice. SW = Swiss Webster, B6 = C57BL/6J.

Despite the establishment of a large breeding program with this mice, no *Htr3a*-EGFP/+; *Htr3a-/-* animals survived to birth. Additionally, of 64 fetuses from these crosses collected, only

a single *Htr3a*-EGFP/+; *Htr3a-/-* animal survived to 14.5dpc. Dissection of embryos at 10.5dpc revealed that many homozygotes, and even some heterozygotes, died very early in embryonic development. Compared to a typically developing wild type 10.5dpc embryo (Figure 6.18, Panel A), the homozygous knockout animal appears severely deformed (Figure 6.18, Panel B).

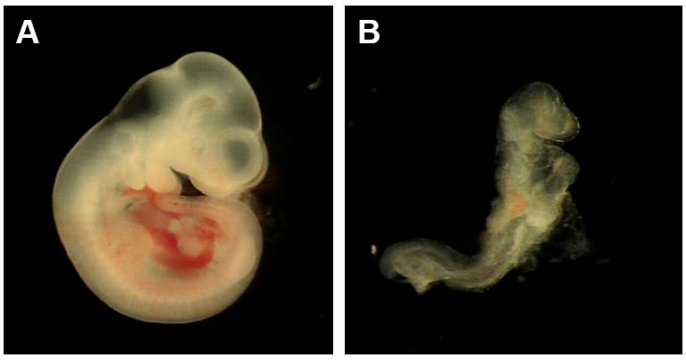

Figure 6.18 Representative 10.5dpc embryos from *Htr3a*-EGFP; *Htr3a*-KO crosses. (**A**) *Htr3a*-EGFP/+; *Htr3a+/+* embryo is typically developing and morphologically normal. (**B**) *Htr3a*-EGFP/+; *Htr3a-/-* embryo is severely deformed and appears to have died at approximately 8.5dpc during the process of turning.

Immunohistochemistry was conducted on the single *Htr3a*-EGFP/+; *Htr3a-/-* fetus that survived to age 14.5dpc. Staining for tyrosine hydroxylase (TH, adrenergic neurons, presumably sympathetic) and vesicular acetylcholine transporter (vAChT, cholinergic, presumably parasympathetic) in this sample and a wild-type littermate revealed a dramatic disturbance of proportions of these autonomic neuronal subtype markers (Figure 6.19). TH expression was significantly increased in the *Htr3a*-EGFP/+; *Htr3a-/-* pelvic ganglia compared to *Htr3a*-EGFP/+; *Htr3a+/+*. Additionally, expression of vAChT was markedly reduced in the mutant compared to wild type pelvic ganglia.

The extremely poor survival rate of *Htr3a*-EGFP/+; *Htr3a-/-* animals is likely due to a deleterious integration site of the *Htr3a*-EGFP transgene, and perhaps genetic modifiers present in the C57/BL6J background. Two observations support this notion: 1) animals from these

crosses lacking the *Htr3a*-EGFP transgene survived, with expected Mendelian proportions of the *Htr3a* knockout allele, and 2) my previous attempts at breeding the *Htr3a*-EGFP mouse line to homozygosity led to decreased birth rates of pups expressing the transgene. It is likely that the *Htr3a*-EGFP transgene was inserted into a region of the genome that does not require two normal alleles to function properly in an outbred Swiss Webster background, but this region in the C57/BL6J genome is particularly sensitive to genetic and structural integrity. Due to the low efficiency of obtaining *Htr3a*-EGFP/+;*Htr3a-/-* animals, I ultimately abandoned this research strategy and instead opted to cross *Htr3a*-KO animals in the absence of a transgenic reporter, and *Htr3a*-KO mice cross a *ChAT*-EGFP reporter (also maintained on a C57/BL6J genetic background) for better visualization of cholinergic pelvic ganglia neurons.

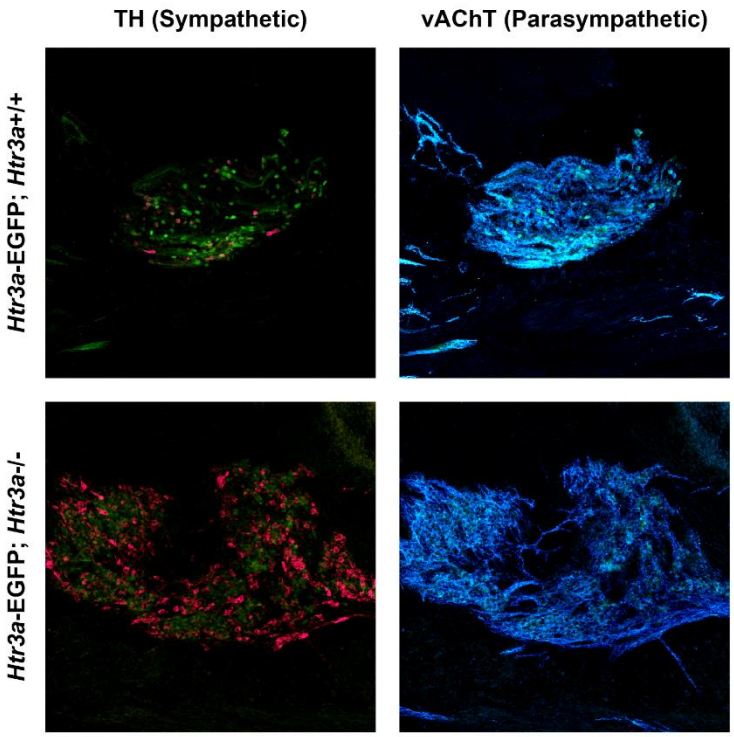

Figure 6.19 Autonomic neuronal subtype proportions in 14.5 dpc *Htr3a*-EGFP/+; *Htr3a*-KO mice. Expression of TH is substantially increased in mutant pelvic ganglia compared to wild type pelvic ganglia. Expression of vAChT is slightly reduced in mutant pelvic ganglia compared to wild type.

Characterization of *Htr3a*-Cre reporter mouse line

Previous work using the *Htr3a*-EGFP transgenic reporter mouse line revealed an early onset of expression of *Htr3a* in many neural crest derivatives and a subsequent loss of expression in a subset of cells later in development (see Chapter III). This dynamic pattern of gene expression raises the question of how these early *Htr3a*+ cells contribute to tissues later in development. To conduct fate mapping of *Htr3a*+ lineages, the Tg(*Htr3a*-Cre)NO152Gsat transgenic mouse line (hereafter *Htr3a*-Cre) was crossed with the B6.Cg-*Gt(ROSA)26Sor*$^{tm9(CAG-tdTomato)Hze}$/J (hereafter Rosa-tdTomato) transgenic reporter mouse line. Rosa-tdTomato mice were bred and maintained as homozygotes while the *Htr3a*-Cre mice were maintained as heterozygotes. Mice were anesthetized via isoflurane inhalation and euthanized via cervical dislocation. Fluorescence was visualized in sub-dissected tissues using a Leica M205 FA stereofluorescent microscope equipped with the mApp filter capable of detecting tdTomato fluorescence. Tissues in adult mice expressing *Htr3a*-Cre; Rosa-tdTomato+ cells are shown in Figure 6.20.

As expected, *Htr3a*-Cre transgene was observed in the majority of pelvic ganglia neurons (Figure 6.20, Panels A-A"). Co-staining with Hu C/D revealed that a few Hu C/D+ neurons did not express *Htr3a*-Cre; however, these cells were scarce. Quantification of Cre+; Hu C/D+ and Cre-; Hu C/D+ neurons must be conducted in the future to determine what proportion of pelvic ganglia neurons derive from the *Htr3a* lineage.

The lumbar dorsal root ganglia of Htr3a-Cre; Rosa-tdTomato mice harbor many Cre+ neurons (Figure 6.20, Panel B). This observation is not unexpected, given the pronounced, high levels of expression of Htr3a in fetal lumbosacral DRG (see Chapter III). Staining these DRG

sections with pan-neuronal Hu C/D revealed that the vast majority of DRG neurons express Htr3a-Cre with very few Cre-; Hu C/D+ cells.

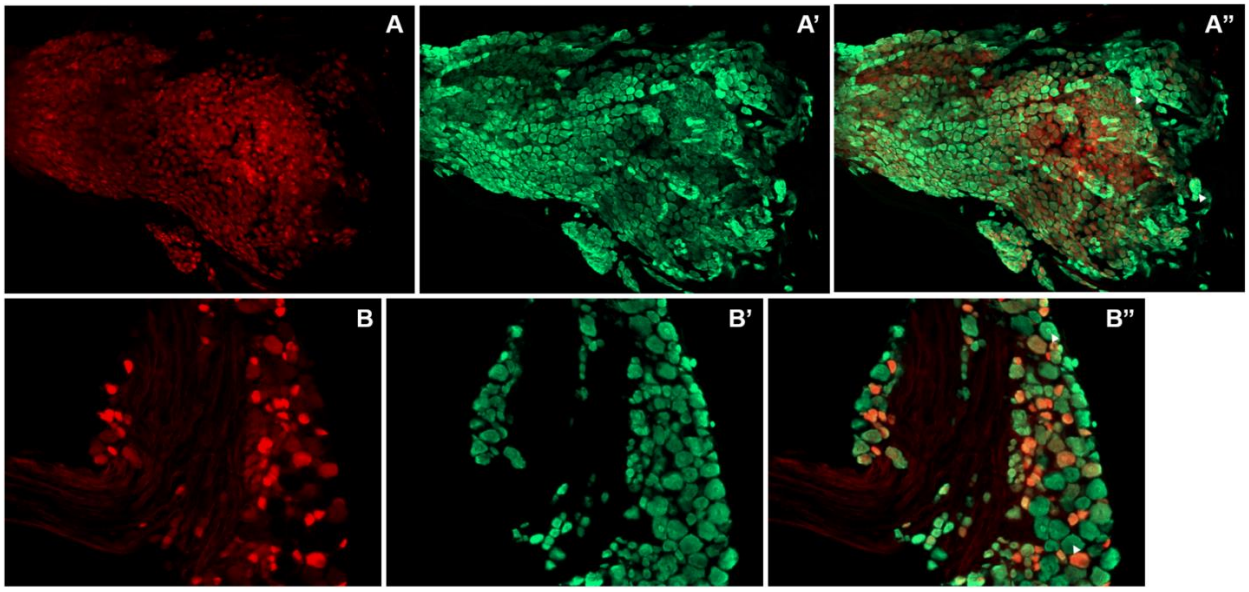

Figure 6.20 Distribution of *Htr3a*-Cre;Rosa-tdTomato lineages (red) in postnatal mice. Co-staining tissues with pan-neuronal marker Hu C/D (green) allows comparison of lineage-traced cells with neuronal populations. (**A-A"**) Whole mount pelvic ganglion from a P10 *Htr3a*-Cre;Rosa-tdTomato mouse. *Htr3a*-Cre labels the majority of Hu C/D+ pelvic ganglia neurons. White arrowheads denote Cre-;Hu+ cells. (**B-B"**) Cryosection of lumbar dorsal root ganglion from a P28 *Htr3a*-Cre;Rosa-tdTomato labels many sensory neurons. White arrowheads denote Cre-;Hu+ cells.

The enteric nervous system (ENS), which supplies autonomic innervation to the gastrointestinal system, also demonstrated strong and widespread expression of *Htr3a*-Cre (data not shown). The 5-HT3A receptor has been previously implicated in Irritable Bowel Syndrome, Diarrhea-Predominant (IBS-D) and Inflammatory Bowel Disease (IBD) (Camilleri and Boeckxstaens, 2017;Coates et al., 2017) and a variety of pharmacological agents that target this receptor are used to treat these two gastrointestinal diseases. However, 5-HT3A has not been studied in the context of ENS development. This area presents an intriguing avenue of future

research, especially for fellow members of the Southard-Smith laboratory who are focused on the molecular underpinnings of enteric neuronal development.

In addition to neuronal cell bodies, the Rosa-tdTomato fluorescent reporter also allows visualization of neuronal processes. The bladders from *Htr3a*-Cre; Rosa-tdTomato animals exhibit extensive innervation from Cre+ neurons, which is expected due to the broad expression of *Htr3a* in autonomic pelvic ganglia and sensory dorsal root ganglia that supply the lower urinary tract (Figure 6.21).

Htr3a-Cre; Rosa-tdTomato expression was not limited to neurons. The urothelium is a specialized epithelial layer that lines the interior of the bladder dome and urethra and acts to not only keep urine contained, but also to respond appropriately to irritants or pathogens. A variety of sensory receptors and ion channels, including members of the TRP family (Merrill et al., 2016), participate in the sensory functions of urothelial cells. Despite extensive study of the urothelium, so far only one study has reported expression of the 5-HT3A receptor in human urothelial cells (Imamura et al., 2015). Examination of the urothelium in *Htr3a*-Cre; Rosa-tdTomato mice revealed expression of *Htr3a*, which is consistent with *Htr3a*-EGFP transgene expression in the bladder neck urothelium of 14.5 dpc samples (Figure 6.21, Panels A and B).

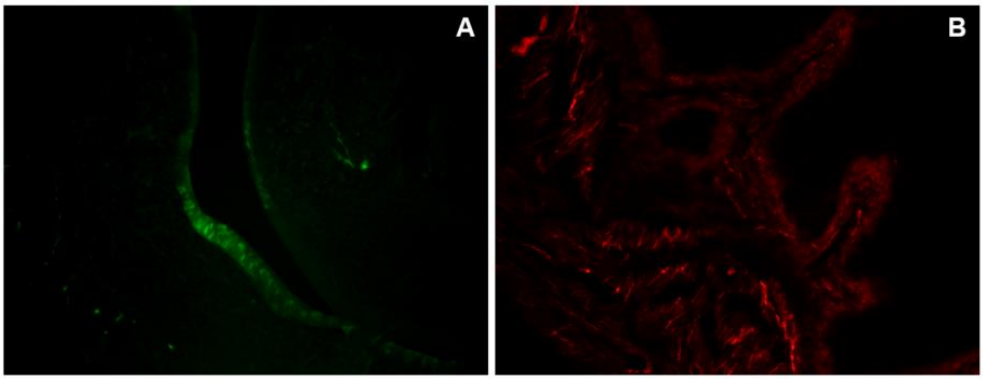

Figure 6.21 Distribution of *Htr3a*+ cells in the bladder. (**A**) Sagittal cryo-section of 14.5dpc *Htr3a*-EGFP bladder. *Htr3a*-EGFP transgene expression is strong in the urothelium of the bladder neck at this age. (**B**) Sagittal cryo-section of P28 *Htr3a*-Cre;Rosa-tdTomato bladder. *Htr3a*-Cre+ nerves are strongly labeled in bladder smooth muscle, as well as urothelial cells lining the bladder lumen.

References

Bjorling, D.E., Wang, Z., Vezina, C.M., Ricke, W.A., Keil, K.P., Yu, W., Guo, L., Zeidel, M.L., and Hill, W.G. (2015). Evaluation of voiding assays in mice: impact of genetic strains and sex. *Am J Physiol Renal Physiol* 308**,** F1369-1378. doi: 10.1152/ajprenal.00072.2015.

Camilleri, M., and Boeckxstaens, G. (2017). Dietary and pharmacological treatment of abdominal pain in IBS. *Gut* 66**,** 966-974.

Coates, M.D., Tekin, I., Vrana, K.E., and Mawe, G.M. (2017). Review article: the many potential roles of intestinal serotonin (5-hydroxytryptamine, 5-HT) signalling in inflammatory bowel disease. *Aliment Pharmacol Ther* 46**,** 569-580.

Desjardins, C., Maruniak, J.A., and Bronson, F.H. (1973). Social rank in house mice: differentiation revealed by ultraviolet visualization of urinary marking patterns. *Science* 182**,** 939-941.

Game`, X., Allard, J., Escourrou, G., Gourdy, P., Tack, I., Rischmann, P., Arnal, J.F., and Malavaud, B. (2008). Estradiol increases urethral tone through the local inhibition of neuronal nitric oxide synthase expression. *Am J Physiol Regul Integr Comp Physiol* 294**,** R851-857.

Girard, B.M., Peterson, A., Malley, S., and Vizzard, M.A. (2016). Accelerated onset of the vesicovesical reflex in postnatal NGF-OE mice and the role of neuropeptides. *Exp Neurol* 285**,** 110-125.

Hou, X.H., Hyun, M., Taranda, J., Huang, K.W., Todd, E., Feng, D., Atwater, E., Croney, D., Zeidel, M.L., Osten, P., and Sabatini, B.L. (2016). Central control circuit for context-dependent micturition. *Cell* 167**,** 73-86.

Imamura, T., Ishizuka, O., Ogawa, T., Minagawa, T., Ishikawa, M., Hiragata, S., Yokoyama, H., Nakazawa, M., Kurizaki, Y., and Nishizawa, O. (2015). Expression of 5-Hydroxytryptamine Receptors in Human Urinary Bladders with Benign Prostatic Hyperplasia. *Adv Ther* 32 Suppl 1**,** 29-37. doi: 10.1007/s12325-015-0242-0.

Keil, K.P., Abler, L.L., Altmann, H.M., Bushman, W., Marker, P.C., Li, L., Ricke, W.A., Bjorling, D.E., and Vezina, C.M. (2016). Influence of animal husbandry practices on void spot assay outcomes in C57BL/6J male mice. *Neurourol Urodyn* 35**,** 192-198. doi: 10.1002/nau.22692.

Malin, S.A., Davis, B.M., and Molliver, D.C. (2007). Production of dissociated sensory neuron cultures and considerations for their use in studying neuronal function and plasticity. *Nature Protocols* 2**,** 152-160.

Merrill, L., Gonzalez, E.J., Girard, B.M., and Vizzard, M.A. (2016). Receptors, channels, and signalling in the urothelial sensory system in the bladder. *Nat Rev Urol* 13**,** 193-204.

Mucignat-Caretta, C., Bondi, M., and Caretta, A. (2004). Endocrine status affects bladder size and postvoid residual urinary volume in mice. *Hormones and Behavior* 46**,** 11-18.

Potter, K.A., Simon, J.S., Velagapudi, B., and Capadona, J.R. (2012). Reduction of autofluorescence at the microelectrode-cortical tissue interface improves antibody detection. *J Neurosci Methods* 203**,** 96-105. doi: 10.1016/j.jneumeth.2011.09.024.

Yu, W., Ackert-Bicknell, C., Larigakis, J.D., Maciver, B., Steers, W.D., Churchill, G.A., Hill, W.G., and Zeidel, M.L. (2014). Spontaneous voiding by mice reveals strain-specific lower urinary tract function to be a quantitative genetic trait. *Am J Physiol Renal Physiol* 306**,** F1296-1307. doi: 10.1152/ajprenal.00074.2014.